

Journal Information

Maejo International Journal of Science and Technology (ISSN 1905-7873 © 2015), the international journal for preliminary communications in Science and Technology is the first peer-refereed scientific journal of Maejo University (www.mju.ac.th). Intended as a medium for communication, discussion, and rapid dissemination of important issues in Science and Technology, articles are published online in an open access format, which thereby gives authors the chance to communicate with a wide range of readers in an international community.

Publication Information

Three issues of MIJST are published per year (Jan.-April, May-Aug., Sept.-Dec.). Articles are available online and can be accessed free of charge at <http://www.mijst.mju.ac.th>. Printed and bound copies of each volume are produced and distributed to selected groups or individuals. This journal and the individual contributions contained in it are protected under the copyright by Maejo University.

Abstracting/Indexing Information

MIJST is covered and cited by Science Citation Index Expanded, SCOPUS, Journal Citation Reports/Science Edition, Zoological Record, Directory of Open Access Journals (DOAJ), CAB Abstracts, ProQuest, Google Scholar, EBSCO and ACI.

Contact Information

Editorial office: Maejo International Journal of Science and Technology (MIJST), 1st floor, Orchid Building, Maejo University, San Sai, Chiang Mai 50290, Thailand

Tel: +66-53-87-5532

E-mail: duang@mju.ac.th



MAEJO INTERNATIONAL JOURNAL OF SCIENCE AND TECHNOLOGY

Editor

Duang Buddhasukh, Maejo University, Thailand.

Associate Editors

Jatuphong Varith, Maejo University, Thailand.

Wasin Charentantanakul, Maejo University, Thailand.

Niwooti Whangchai, Maejo University, Thailand.

Morakot Sukchotiratana, Chiang Mai University, Thailand.

Nakorn Tippayawong, Chiang Mai University, Thailand.

Editorial Assistants

Jirawan Banditpuritat, Maejo University, Thailand.

Editorial Board

Assoc. Prof. Dr. Mohammad R. Alizadeh

Asst. Prof. Dr. V. Ananthaswamy

Dr. Serkan Araci

Emeritus Prof. Dr. Huseyin Bor

Emeritus Prof. John Bremner

Dr. Pei-Yi Chu, M.D.

Asst. Prof. Ekachai Chukeatirote

Prof. Richard L. Deming

Prof. Cynthia C. Divina

Asst. Prof. Dr. Mostafa Eslami

Prof. Mary Garson

Prof. Kate Grudpan

Dr. Soon Min Ho

Assoc. Prof. Dr. Duangrat Inthorn

Prof. Minoru Isobe

Prof. Dr. Sriman N. Iyengar

Asst. Prof. Dr. Dariusz Jakobczak

Prof. Dr. Prakash Naraian Kalla

Dr. Nakul Karkare

Prof. Kunimitsu Kaya

Prof. Dr. Margaret E. Kerr

Prof. Tanongkiat Kiatsirirot

Asst. Prof. Dr. Ignacy Kitowski

Asst. Prof. Dr. Andrzej Komosa

Prof. Dr. Monai Krairiksh

Asst. Prof. Dr. Pradeep Kumar

Asst. Prof. Dr. Sunil Kumar

Prof. Dr. T. Randall Lee

Asst. Prof. Ma. Dr. Elizabeth C.

Prof. Dr. Subrata Mallick

Asst. Prof. Dr. Vishnu Narayan Mishra

Prof. Amarendra N. Misra

Dr. Robert Molloy

Prof. Mohammad A. Mottaleb

Asst. Prof. Anand Nayyar

Engr.Obeta Nwachkwu

Assoc. Prof. Dr. Kaew Nualchawee

Prof. Dr. Yoko Oki

Prof. R. Ponalagusamy

Prof. Stephen G. Pyne

Dr. Khaled Nabih Rashed

Prof. Renato G. Reyes

Prof. Dr. Hidehiro Sakurai

Rice Research Institute of Iran, Guilan, Iran.

The Madura College, Tamil Nadu, India.

Hasan Kalyoncu University, Turkey.

P.O. Box 121, TR-06502 Bahcelievler, Ankara, Turkey.

University of Wollongong, NSW, Australia.

Changhua Christian Hospital, Taiwan, R.O.C.

Mae Fah Luang University, Chiang Rai, Thailand.

California State University Fullerton, Fullerton CA.

Central Luzon State University, Philippines.

University of Mazandaran, Babolsar, Iran.

The University of Queensland, Brisbane, Australia.

Chiang Mai University, Thailand.

INTI International University, Malaysia.

Mahidol University, Thailand.

Nagoya University, Japan.

VIT University, India.

Technical University of Koszalin, Poland.

University, Bikaner, Campus Jaipur, India.

York Hospital, PA, USA.

Tohoku University, Japan.

Worcester State College, Worcester, MA.

Chiang Mai University, Thailand.

State School of Higher Education in Chelm, Poland.

University of Maria-Curie Sklodowska, Poland.

King Mongkut's Institute of Technology Ladkrabang, Thailand.

Jaypee University of Information Technology, India.

National Institute of Technology, Jharkhand, India.

University of Houston, USA.

Central Luzon State University, Philippines.

Siksha O Anusandhan University, India.

Sardar Vallabhbhai National Institute of Technology, India.

Central University of Jharkhand, Ranchi, India.

Chiang Mai University, Thailand.

Northwest Missouri State University, USA.

KCL Institute of Management and Technology, India.

Enugu State University of Science and Technology, Nigeria.

Geoinformatics and Space Technology Development of Agency, Thailand.

Okayama University, Japan.

National Institute of Technology, India

University of Wollongong, Australia.

National Research Centre, Giza, Egypt.

Central Luzon State University, Philippines.

Institute for Molecular Science, Myodaiji, Japan.

Prof. Dr. Sung le Shim
Asst. Prof. Dr. Satish K. Singh
Prof. Paisarn Sithigorngul
Prof. S. Smys
Prof. Anupam Srivastav
Prof. Hari M. Srivastava
Prof. Maitree Suttajit
Prof. Dr. Asif Tanveer
Asst. Prof. Thanaphong Thanasaksiri
Asst. Prof. Narin Tongwittaya
Prof. Keshav D. Verma
Assoc. Prof. Malinee Wongnawa
Dr. Guo-Cheng Wu
Prof. Xiao-Jun Yang
Prof. Yudong Zhang
Prof. Zhihua Zhang
Asst. Prof. Dr. Rushan Ziatdinov
Dr. Mahdi Zowghi

University of Seoul, Korea.
Indian Institute of Information Technology, Allahabad, India.
Srinakharinwirot University, Thailand.
Karpagam College of Engineering, Coimbatore, India.
IFTM University, Moradabad, India.
University of Victoria, Victoria, Canada.
Naresuan University (Payao Campus), Thailand.
University of Agriculture Faisalabad, Pakistan.
Chiang Mai University, Thailand.
Maejo University, Thailand.
S.V. (P.G.) College, Aligarh, India.
Prince of Songkla University, Thailand.
Neijiang Noemal University, Sichuan, China.
China University of Mining and Technology, China.
Nanjing Normal University, China.
Beijing Normal University, China.
Keimyung University, Daegu, South Korea.
PWCS, Tehran, Iran.

Consultants

Asst. Prof. Chamnian Yosraj, Ph.D., President of Maejo University
Assoc. Prof. Thep Phongpanich, Ed. D., Former President of Maejo University
Assoc. Prof. Chalermchai Panyadee, Ph.D., Vice-President in Research of Maejo University

**MAEJO INTERNATIONAL JOURNAL
OF SCIENCE AND TECHNOLOGY**

*The International Journal for the Publication of Preliminary
Communications in Science and Technology*





MAEJO INTERNATIONAL JOURNAL OF SCIENCE AND TECHNOLOGY

Volume 9, Issue 2 (May - August 2015)

CONTENTS

Page

<i>Mohammad Homayoun, Ahmad Jalalian, Ali A. Besalatpour*, Ali Basirat and Inge Aalders</i>	136-146
Determining relationships between soil properties and plant distribution in a protected area in central Iran	
<i>Chalee Vorakulpipat*, Kittit Wongthavarawat, Kitiwat Limmongkol and Siwaruk Siwamogsatham</i>	147-155
WiMAX deployment: A report for a rural region of Thailand	
<i>Whaleeha Gudiño, Judith Márquez-Guzmán and Erick de la Barrera*</i>	156-164
Structural implications for nectar secretion by nectaries of three columnar cacti	
<i>Linlong Mu*, Richard J. Finno, Maosong Huang, Taesik Kim and Kristi Kern</i>	165-180
Defining the soil parameters for computing deformations caused by braced excavation	
<i>Khalida Inayat Noor and Nazar Khan*</i>	181-192
Some convolution properties of a subclass of p -valent functions	
<i>Mohd Nizam Ab Rahman*, Rosmaizura Mohd Zain, Afis Mohd Alias and Zulkifli Mohd Nopiah</i>	193-208
Statistical process control: Best practices in small and medium enterprises	
<i>Prateep Lueprasert, Pornkasem Jongpradist*, Kitcha Charoenpak, Pattanasak Chaipanna</i>	209-223
and Suchatvee Suwansawat Three dimensional finite element analysis for preliminary establishment of tunnel influence zone subject to pile loading	
<i>Abid Hussanan, Mohd Z. Salleh*, Ilyas Khan, Razman M. Tahar and Zulkhibri Ismail</i>	224-245
Soret effects on unsteady magnetohydrodynamic mixed- convection heat-and-mass-transfer flow in a porous medium with Newtonian heating	
<i>Serkan Araci*, Mehmet Acikgoz, Roberto B. Corcino and Cenap Özel</i>	246-254
An analogue of Eulerian polynomials related to L -type function	
<i>Hemen Dutta*</i>	255-264
Köthe-Toeplitz duals of some n -normed valued difference sequence spaces	
<i>Nednapis Vatanasuchart*, Pisut Butsuwan and Wassana Narasri</i>	265-277
Nutritional composition, in vitro starch digestibility and estimated glycemic index of three varieties of 'Kluai Namwa' banana (<i>Musa sapientum L.</i>) and its products	
<i>Nonglak Parinthawong*, Pennapar Tansian and Tanee Sreewongchai</i>	278-287
Genetic mapping of leaf blast resistance gene in landrace rice cultivar 'GS19769'	

**MAEJO INTERNATIONAL JOURNAL
OF SCIENCE AND TECHNOLOGY**

Volume 9, Issue 2 (May - August 2015)

Author Index

Author	Page	Author	Page
Aalders I.	136	Khan N.	181
Ab Rahman M. N.	193	Kim T.	165
Acikgoz M.	246	Limmongkol K.	147
Alias A. M.	193	Lueprasert P.	209
Araci S.	246	Márquez-Guzmán J.	156
Basirat A.	136	Mu L.	165
Besalatpour A. A.	136	Narasri W.	265
Butsuwan P.	265	Noor K. I.	181
Chaipanna P.	209	Nopiah Z. M.	193
Charoenpak K.	209	Özel C.	246
Corcino R. B.	246	Parinthawong N.	278
De la Barrera E.	156	Salleh M. Z.	224
Dutta H.	255	Siwamogsatham S.	147
Finno R. J.	165	Sreewongchai T.	278
Gudiño W.	156	Suwansawat S.	209
Homayoun M.	136	Tahar R. M.	224
Huang M.	165	Tansian P.	278
Hussanan A.	224	Vatanasuchart N.	265
Ismail Z.	224	Vorakulpipat C.	147
Jalalian A.	136	Wongthavarawat K.	147
Jongpradist P.	209	Zain R. M.	193
Kern K.	165		
Khan I.	224		

Instructions for Authors

A proper introductory e-mail page containing the title of the submitted article and certifying its originality should be sent to the editor (Duang Buddhasukh, e-mail: duang@mju.ac.th). The manuscript proper together with a list of suggested referees should be attached in separate files. The list should contain at least 5 referees with appropriate expertise. Three referees should be non-native from 3 different countries. Each referee's academic/professional position, scientific expertise, affiliation and e-mail address must be given. The referees should not be affiliated to the same university/institution as any of the authors, nor should any two referees come from the same university/institution. The editorial team, however, retain the sole right to decide whether or not the suggested referees are approached.

Failure to conform to the above instructions will result in non-consideration of the submission.

Please also ensure that English and style is properly edited before submission. UK style of spelling should be used. Authors who would like to consult a professional service can visit www.editage.com/?ref=referral, www.bioedit.co.uk (bioscience and medical papers), www.scribendi.com, www.letpub.com, www.papersconsulting.com, www.sticklerediting.com, Cambridge Proofreading (<http://proofreading.org/>), www.ProofreadingServices.com, www.horizonproofreading.org, Help.Plagtracker, www.ninjaessays.com/editing/, <http://bid4papers.com/editing-services.html>, www.enago.com, www.medscediting.com, www.manuscriptedit.com, <http://www.proofreadmyfile.com>, ProofreadMyDocument, www.24x7editing.com, www.tulyasys.com, www.regentediting.co.uk, www.editnpublish.com, www.sciencedocs.com or www.geediting.com.

Important : Manuscript with substandard English and style will not be considered.

Warning : Plagiarism (including self-plagiarism) may be checked for at *the last* stage of processing and, if detected, will result in a rejection and blacklisting.

Manuscript Preparation

Manuscripts must be prepared in English using a word processor. MS Word for Macintosh or Windows, and .doc or .rtf files are preferred. Manuscripts may be prepared with other software provided that the full document (with figures, schemes and tables inserted into the text) is exported to a MS Word format for submission. Times or Times New Roman font is preferred. The font size should be 12 pt and the line spacing 'at least 17 pt'. A4 paper size is used and margins must be 1.5 cm on top, 2.0 cm at the bottom and 2.0 cm on both left and right sides of the paper. Although our final output is in .pdf format, authors are asked NOT to send manuscripts in this format as editing them is much more complicated. Under the above settings, a manuscript submitted should not be longer than **15 pages** for a full paper or **20 pages** for a review paper.

A template file may be downloaded from the *Maejo Int. J. Sci. Technol.* homepage. ([DOWNLOAD HERE](#))

Authors' full mailing addresses, homepage addresses, phone and fax numbers, and e-mail addresses homepages can be included in the title page and these will be published in the manuscripts and the Table of Contents. The corresponding author should be clearly identified. It is the corresponding author's responsibility to ensure that all co-authors are aware of and approve of the contents of a submitted manuscript.

A brief (200 word maximum) Abstract should be provided. The use in the Abstract of numbers to identify compounds should be avoided unless these compounds are also identified by names.

A list of three to five keywords must be given and placed after the Abstract. Keywords may be single words or very short phrases.

Although variations in accord with contents of a manuscript are permissible, in general all papers should have the following sections: Introduction, Materials and Methods, Results and Discussion, Conclusions, Acknowledgments (if applicable) and References.

Authors are encouraged to prepare Figures and Schemes in colour. Full colour graphics will be published free of charge.

Tables and Figures should be inserted into the main text, and numbers and titles supplied for all Tables and Figures. All table columns should have an explanatory heading. To facilitate layout of large tables, smaller fonts may be used, but in no case should these be less than 10 pt in size. Authors should use the Table option of MS Word to create tables, rather than tabs, as tab-delimited columns are often difficult to format in .pdf for final output.

Figures, tables and schemes should also be placed in numerical order in the appropriate place within the main text. Numbers, titles and legends should be provided for all tables, schemes and figures. Chemical structures and reaction schemes should be drawn using an appropriate software package designed for this purpose. As a guideline, these should be drawn to a scale such that all the details and text are clearly legible when placed in the manuscript (i.e. text should be no smaller than 8-9 pt).

For bibliographic citations, the reference numbers should be placed in square brackets, i.e. [], and placed before the punctuation, for example [4] or [1-3], and all the references should be listed separately and as the last section at the end of the manuscript.

Format for References

Journal :

1. D. Buddhasukh, J. R. Cannon, B. W. Metcalf and A. J. Power, "Synthesis of 5-n-alkylresorcinol dimethyl ethers and related compounds *via* substituted thiophens", *Aust. J. Chem.*, **1971**, *24*, 2655-2664.

Text :

2. A. I. Vogel, "A Textbook of Practical Organic Chemistry", 3rd Edn., Longmans, London, **1956**, pp. 130-132.

Chapter in an edited text :

3. W. Leistriz, "Methods of bacterial reduction in spices", in "Spices: Flavor Chemistry and Antioxidant Properties" (Ed. S. J. Risch and C-T. Ito), American Chemical Society, Washington, DC, **1997**, Ch.2.

Thesis / Dissertation :

4. W. phutdhawong, "Isolation of glycosides by electrolytic decolourisation and synthesis of pentinomycin", *Ph.D. Thesis*, **2002**, Chiang Mai University, Thailand.

Patent :

5. K. Miwa, S. Maeda and Y. Murata, "Purification of stevioside by electrolysis", *Jpn. Kokai Tokkyo Koho 79 89,066* (**1979**).

Proceedings :

6. P. M. Sears, J. Peele, M. Lassauzet and P. Blackburn, "Use of antimicrobial proteins in the treatment of bovine mastitis", Proceedings of the 3rd International Mastitis Seminars, **1995**, Tel-Aviv, Israel, pp.17-18.

Websites :

7. S. Simon, "What is an odds ratio?", **2008**, <http://www.childrensmarcy.org/stats/definitions/or.htm> (Accessed: October 2011).

Manuscript Revision Time

Authors who are instructed to revise their manuscript should do so within **45** days. Otherwise the revised manuscript will be regarded as a new submission.

Manuscript Processing Time

As a result of a large number of submissions, there may be a long delay in the evaluation or publication of a paper. A duration of at least 6-8 months between submission and acceptance (or rejection) can normally be expected.

Maejo International Journal of Science and Technology

ISSN 1905-7873

Available online at www.mijst.mju.ac.th

Communication

Determining relationships between soil properties and plant distribution in a protected area in central Iran

Mohammad Homayoun¹, Ahmad Jalalian¹, Ali A. Besalatpour^{2,*}, Ali Basirat³ and Inge Aalders⁴

¹ Department of Soil Science, College of Agriculture, Islamic Azad University, Khorasgan (Isfahan) Branch, Isfahan, Iran

² Department of Soil Science, College of Agriculture, Vali-e-Asr University of Rafsanjan, Rafsanjan 7718897111, Iran

³ Natural Language and Text Processing Laboratory, School of Electrical and Computer Engineering, College of Engineering, University of Tehran, Tehran, Iran

⁴ The James Hutton Institute, Craigiebuckler, Aberdeen AB15 8QH, United Kingdom

* Corresponding author, e-mail: a_besalatpour@yahoo.com; a.besalatpour@vru.ac.ir

Received: 26 November 2014 / Accepted: 8 May 2015 / Published: 12 May 2015

Abstract: A hybrid algorithm specifically designed to work with optimised support vector machine with genetic algorithm (GA-SVM) was developed for determining the relationships between soil properties and plant distribution and vegetation cover densities in a protected area (Ghomeshlu, central Iran). The bulk density, porosity, silt, total nitrogen and chloride contents are the main essential factors (with a screen accuracy of 100%) for the establishment and growth of *Scariola*. For *Astragalus*, surface fragment content has the greatest influence, while available phosphorus was screened by the GA-SVM analysis as the factor with a closer relationship with *Anabasis* growth in the study sites. Particle density, aggregate stability, available magnesium and pH are the more important combination of soil properties affecting the coverage density of *Stipa*. Soil organic matter content, available phosphorus, total nitrogen, electrical conductivity, porosity and particle density have a closer relationship with the coverage density of *Noaea*. This study provides a strong basis for identifying habitat characteristics of vulnerable and/or endangered species in Iran.

Keywords: soil-plant relationships, endangered plant species, Iran, support vector machines

INTRODUCTION

Plants differ in their requirements and tolerance to site conditions created by soil and landscape characteristics [1]. Variations in soil resource levels and landscape features influence patterns in biodiversity and natural processes including soil-nutrient-water interactions [2]. In fact, soil characteristics (such as nutrients, salinity and moisture conditions) determine the resources available to plants. Therefore, the change in soil type and their spatial variation may affect the distribution of plant species [3]. In addition, plant community and soil conditions are influenced by landscape features including topography, landscape position, slope gradient and elevation [4]. Thus, it is important to understand the ecological relationship between soil variables and plant species in order to plan and execute a successful forest and rangeland restoration programme.

In several studies, traditional regression models, principal component analysis (PCA), cluster analysis and geostatistic analysis approaches have been employed to recognise the relationships between landscape feature, soil factors and vegetation distribution [1, 3, 5, 6]. Nevertheless, many of the methods have focused on controls over spatial variability in local scales (less than 2 km) and have not been recommended for large areas as various soils and environmental factors are involved and a large amount of samples are required to characterise the above-mentioned relationships [5].

In this study the potential use of optimised support vector machine (SVM) models with genetic algorithm (GA) for determining the relationships between soil properties and plant distribution and vegetation cover density in a protected area (Ghomeshlu, central Iran) is evaluated. SVMs are a promising machine learning method originally developed for a pattern recognition problem based on structural risk minimisation. SVMs are closely related to artificial neural networks (ANNs) and they can be divided into two categories: support vector classification (SVC) machines and support vector regression (SVR) machines [7-11]. Recently they have attracted greater interest in agricultural and biological engineering [7].

Conservation, sustainable management and possible restoration of endangered or vulnerable plantations in natural forests and rangelands require knowledge of the relationship between the distribution and regeneration of native species and the pattern of soil properties [1]. A major goal of this study is to understand the relationship between natural vegetation and soil as an environmental variable in the rangelands of the Ghomeshlu exclusion area, central Iran. The information obtained could increase the effectiveness of current restoration programmes, which aim to replace exotics with native species in this protected area. The native species restoration is thought to be more effective if plant species requirements are matched with soil and site characteristics in the area. Therefore, the specific objectives of our study are: (i) to investigate the relationship between the distribution of native plant species in these natural rangelands and soil characteristics and (ii) to evaluate the potential use of the hybrid support vector machine with genetic algorithm (GA-SVM) for this investigation. The hypothesis of the study is that the distribution of native species within the natural rangelands depends on the physical and chemical properties of the soil.

METHODS

Study Area

The study area is part of the Ghomeshlu exclusion area (32° 43' to 33° 2' N and 50° 59' to 51° 28' E) in Isfahan province, central Iran (Figure 1). The elevation ranges from 1687 m at the

western part of the study area to 2767 m on the southern part. The long-term average rainfall and temperature in the region are 165 mm and 11.5°C respectively. The zonal vegetation cover of the study region is mostly herbaceous vegetation which includes *Scariola* (*Scariola viminea*), *Anabasis* (*Anabasis aphylla*), *Stipa* (*Stipa barbata*), *Astragalus* (*Astragalus gummifer*) and *Noaea* (*Noaea mucronata*). These plant species are the dominant vegetation covering around 98% of the study area.

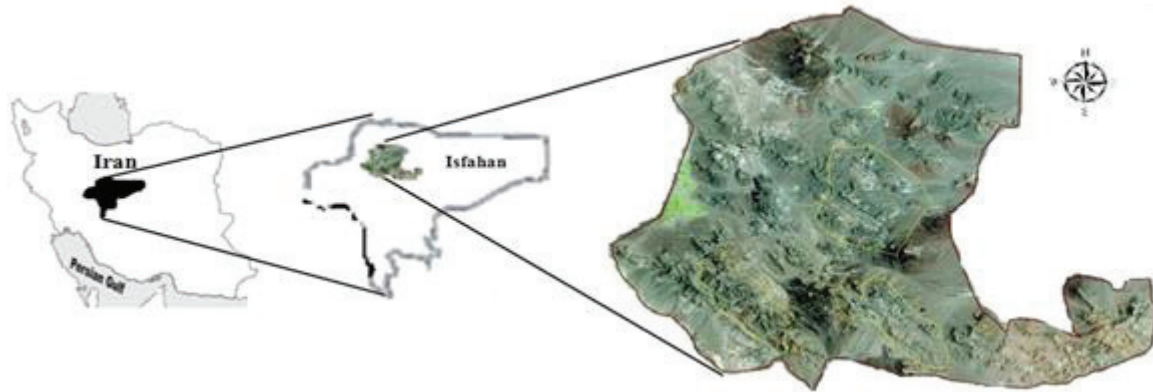


Figure 1. Location of the Ghomeshlu protected area in central Iran ($32^{\circ} 43' - 33^{\circ} 2' N$ and $50^{\circ} 59' - 51^{\circ} 28' E$)

Vegetation Investigation, Soil Sampling and Analysis

A stratified random sampling was designed using digital topography, soil, and land cover maps in the environment of ILWIS 3.4 software (ITC, University of Twente, Netherlands) to determine the investigation sites in the study area. A total of 59 sites were selected. At each of these sites, one homogeneous plot of 400 m² (20 m × 20 m) was chosen randomly for a detailed vegetation inventory. Within each plot, three quadrates (1 m × 1 m) on the diagonal line were randomly chosen for detailed inventory of herbaceous vegetation. In each plot all the individual herbs were identified and their layer coverage and height measured. Environmental variables such as altitude and landscape position and aspect were recorded for each plot.

Soil samples were obtained from three points in each quadrate at a depth of 0-30 cm. The three replicate samples were homogenised by hand. Large plant material (roots and shoots) and pebbles in each sample were separated and discarded. The soil samples were air-dried and sieved for the determination of soil properties. For aggregate stability assessment, separate soil samples were taken such that minimum structural deformation and/or destruction happened to the soil aggregates.

The soil samples were air-dried and ground to pass a 2-mm sieve. Soil organic matter (SOM) content was determined by the Walkley-Black method [12]. Soil pH and electrical conductivity (EC) were measured in saturated paste with a conductivity meter. Calcium carbonate equivalent (CCE) content was determined by the back-titration method [13]. Available phosphorus content (P_{ava}) was determined by a colorimetric method [14]. Total nitrogen was measured by the micro-Kjeldahl method [15]. Concentrations of available calcium (Ca_{ava}) and magnesium (Mg_{ava}) were determined by the methods described by Black [14]. Available potassium (K_{ava}) was measured using 1N ammonium acetate as the extractant [16], and cation exchangeable capacity (CEC) was determined using 1N sodium acetate [17].

Soil bulk density was measured by the core method [18] and soil particle density was predicted by the method described by Saxton et al. [19]. Percentages of clay, silt and sand particles were measured using the procedure described by Gee and Bauder [20]. The method of Kemper and Rosenau [21] was used to determine the mean weight diameter (MWD) of aggregates. The MWD (mm) of water-stable aggregates was calculated using the following equation:

$$MWD = \sum_{i=1}^n w_i \bar{X}_i \quad (1)$$

where \bar{X}_i is the arithmetic mean diameter of each size fraction (mm) and w_i is the proportion of the total weight of water-stable aggregates in the corresponding size fraction after deducting the weight of sand/gravel particles (upon dispersion and passing through the same sieve).

After measuring the soil parameters, descriptive statistics of the experimental data, i.e. mean, minimum, maximum, standard deviation (S.D.) and skewness, were determined using the SPSS statistical software (IBM, USA). The data set were then divided into two subsets of training and testing. The training subset was randomly chosen from 80% of the total set of the data and the remaining samples were used as the testing set.

Brief Description of SVM Technique

SVM is a type of learning machine which was first proposed by Vapnik [9]. It is based on the structure risk minimisation principle that seeks to minimise an upper bound of the generalisation error. A detailed description of SVM model can be found in the literature [7, 8, 9, 11]. Very briefly, suppose there is a training dataset (D) [9, 22]:

$$D = \{(x_i, y_i) | i = 1, 2, \dots, l\}, x_i \in R^n, y_i \in R \quad (2)$$

where x_i is the input value, y_i is the target value and i is the number of sample data. Let $f(x)$ define the estimated regression function:

$$f(x) = (w, x) + b \quad (3)$$

and let ξ_i^* define the slack variable:

$$\xi_i^* = \begin{cases} 0 & |f(x) - y_i| < \varepsilon \\ |f(x) - y_i| - \varepsilon & |f(x) - y_i| > \varepsilon \end{cases} \quad (4)$$

The dimension of w is the dimension of the feature space. With the slack variables (ξ_i and ξ_i^*), punishment coefficient (C) and insensitive loss (ε) based on the SVM theory, the original SVM optimum model in the feature space (ϕ) can be described as:

$$\min_{w, b, \xi_i, \xi_i^*} \phi = \frac{1}{2} \|w\|^2 + C \sum_{i=1}^l (\xi_i + \xi_i^*) \quad (5)$$

$$\begin{aligned} \text{subject to: } & y_i - (w \cdot x_i + b) \leq \varepsilon + \xi_i, \\ & (w \cdot x_i + b) - y_i \leq \varepsilon + \xi_i^*, \\ & \xi_i \geq 0, \xi_i^* \geq 0, i = 1, 2, \dots, l \end{aligned}$$

The dual optimisation model of the original SVM model can be obtained as follows:

$$\max_{a, a^*} w = -\frac{1}{2} \sum_{i=1}^l \sum_{j=1}^l (a_i - a_i^*) (a_j - a_j^*) \langle x_i, x_j \rangle + \sum [a_i (y_i - \varepsilon) - a_i^* (y_i + \varepsilon)] \quad (6)$$

subject to: $\sum_{i=1}^l (a_i - a_i^*) = 0$

$0 \leq a_i, a_i^* \leq C \quad i = 1, 2, \dots, l$

Based on this, w can be expressed as:

$w = \sum_{i=1}^l (a_i - a_i^*) x_i$ (7)

Thus, the regression estimation function can be expressed as:

$f(x) = \sum_{i=1}^l (a_i - a_i^*) K(x_i, x) + b$ (8)

where $K(x_i, x)$ is named the kernel function. A common example of kernel functions is the radial basis function [7, 8, 10, 22]:

$K(x_i, x) = \exp\left(-\frac{\|x_i - x\|^2}{2\sigma^2}\right)$ (9)

where σ is the kernel parameter.

Optimisation of SVM Parameters Using GA

The identification of optimal values for the SVM parameters (i.e. punishment coefficient (C) and insensitive parameter (ϵ)) is important for a good forecast and estimation performance [22].

The procedure of parameter optimisation we used for the SVM models can be described as follows:

Step 1: Initialising the parameters of SVM such as punishment coefficient C and insensitive parameter ϵ .

Step 2: Initialising the parameters of genetic algorithm including the parent population, maximum number of iteration and genetic operators (crossover and mutation values).

Step 3: Defining the fitness function.

Step 4: Calculating the fitness. If this value is acceptable according to the fitness, the population is the optimal solution. Otherwise, generate new population.

Step 5: Judge the condition for stop; if the new population meets the stopping criterion, then stop the iteration and this will be the optimal solution which represents the best parameters for SVM. Otherwise, generate new population and repeat from step 2.

Step 6: According to the optimised parameter of C and ϵ , the SVM model is established and is ready for the prediction. The schema of the hybrid GA-SVM model is presented in Figure 2.

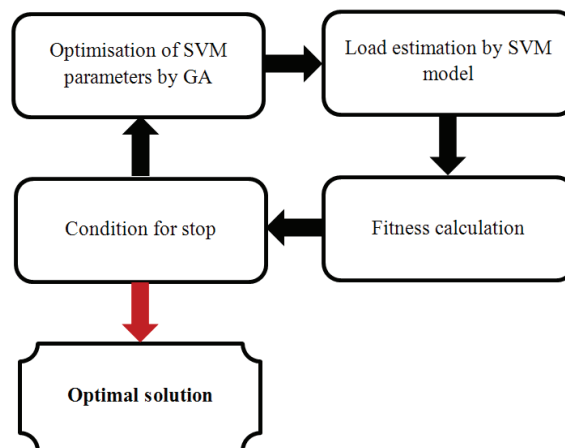


Figure 2. Diagram of GA-SVM model

RESULTS

Descriptive statistics of the measured soil properties including mean, minimum, maximum, standard deviation (SD) and skewness are presented in Table 1.

Table 1. Summary of statistics of measured soil properties

Soil property	Mean	Minimum	Maximum	S.D.	Skewness
Clay (%)	18.47	6.66	31.67	6.29	0.37
Silt (%)	30.93	7.5	52.5	10.04	-0.14
Sand (%)	50.59	20.83	77.50	13.74	0.14
pH	8.01	7.70	8.53	0.16	1.05
EC (dS m ⁻¹)	0.27	0.17	0.56	0.07	1.09
SOM (%)	0.25	0.0	0.67	0.15	0.77
CCE (%)	49.84	4.0	88.0	25.50	-0.08
TN (%)	0.08	0.01	0.15	0.03	-0.08
CEC (cmol kg ⁻¹ soil)	11.74	4.80	24.60	5.53	0.76
K _{ava} (mg kg ⁻¹)	356.94	151.01	626.10	128.42	0.35
Ca _{ava} (meq l ⁻¹)	1.84	0.80	2.80	0.64	-0.21
Mg _{ava} (meq l ⁻¹)	0.71	0.20	1.80	0.38	0.68
Na _{ava} (meq l ⁻¹)	0.21	0.05	1.11	0.25	0.28
P _{ava} (mg kg ⁻¹)	41.51	0.17	93.89	21.39	0.61
Cl ⁻ (meq l ⁻¹)	0.66	0.25	1.50	0.29	0.81
MWD (mm)	0.22	0.17	0.28	0.03	0.55
SF (%)	37.18	10.0	83.0	15.09	0.39
Por	0.42	0.36	0.49	0.03	-0.08
Inf (cm h ⁻¹)	1.19	0.34	4.24	0.82	1.39
PD (g cm ⁻³)	2.53	2.43	2.67	0.06	0.63
BD (g cm ⁻³)	1.45	1.32	1.62	0.08	0.21

Note: EC = electrical conductivity, SOM = soil organic matter content, CCE = calcium carbonate equivalent content, TN = total nitrogen, CEC = cation exchangeable capacity, K_{ava} = available potassium content, Ca_{ava} = available calcium content, Mg_{ava} = available magnesium content, Na_{ava} = available sodium content, P_{ava} = available phosphorus content, Cl⁻ = chloride content, MWD = mean weight diameter, SF = surface fragment content, Por = porosity, Inf = infiltration rate, PD = particle density, BD = bulk density, SD = standard deviation

The GA analysis has generated optimal values for the SVM parameters, i.e. punishment coefficient (C) and insensitive parameter (ϵ) (Table 2). Parameter C determines the trade-off between the model's complexity and the degree to which deviations larger than ϵ are tolerated. In the case that C is too large, the rate of accuracy of the estimation is high in the training phase, but may be low in the testing phase. If C is too small, the accuracy of the estimation is unsatisfactory, and the model is useless. The value of ϵ illustrates the anticipated value for sample data error. Large ϵ will reduce the reliability of results [22]. The SVM parameter results for both the constructed SVM model types (i.e. SVR and SVC models) seem to be satisfactory in terms of C and ϵ parameter values. The elegance of using the kernel function lies in the fact that one can deal with feature

spaces of arbitrary dimensionality without having to calculate the feature condition. Any function that satisfies the conditions can be used as the kernel function. In this study the radial basis function (Eq. 9) and the Gaussian kernel (i.e. $K(x,y)=exp(-(x-y)^2/\sigma^2)$) show satisfactory results.

Table 2. Optimal values of SVM parameters resulting from GA analysis

SVM model type	Plant studied	SVM parameter		
		Kernel type	Insensitive parameter (ϵ)	Punishment coefficient (C)
SVC	Scariola	RBF	0.24	46.47
	Stipa	RBF	0.33	70.29
	Astragalus	RBF	0.84	80.32
	Anabasis	RBF	0.80	112.45
	Noaea	RBF	0.45	76.59
SVR	Scariola	Gaussian	0.005	4.50
	Stipa	Gaussian	0.0	7.0
	Astragalus	Gaussian	0.005	15.50
	Anabasis	Gaussian	0.0	6.0
	Noaea	Gaussian	0.0	15.50

Note : SVC = support vector machines for classification, SVR = support vector machines for regression, RBF = radial basis function

The results of SVM classifications of soil variables that influence the establishment and growth of plant species in the study sites are depicted in Table 3. According to the SVC results, bulk density, porosity, silt, total nitrogen and chloride content are the main factors (with a screen accuracy of 100%) that account for the occurrence of Scariola in the study area. The CCE is the determinant parameter that affects the establishment and development of Stipa in the study sites. For Astragalus, surface fragment content has the greatest influence, while available phosphorus content is screened by the SVC analysis as the factor with the closest relationship with the occurrence and distribution of Anabasis. Soil bulk density is identified as the essential factor (with a screen accuracy of 80%) influencing Noaea occurrence.

Table 3. Soil variables influencing occurrence of investigated plant species according to SVC analysis

Plant	Characteristic	Accuracy (%)
Scariola	Silt, BD, Por, Cl ⁻ , TN	100
Stipa	CCE	80
Astragalus	SF	85
Anabasis	P _{ava}	80
Noaea	BD	80

Note: BD = bulk density, Por = porosity, Cl⁻ = chloride content, TN = total nitrogen, CCE = calcium carbonate equivalent content, SF = surface fragment content, P_{ava} = available phosphorus content

The application of SVR approach, which discerns and determines the main factors affecting the vegetation cover density and height, results in different findings (Table 4). The CEC, SOM, Na_{ava}, Mg_{ava}, pH, EC, infiltration rate and porosity are components influencing Scariola density while particle density, aggregate stability, Mg_{ava} and pH are, according to the SVR model, the more important combination of soil properties affecting Stipa occurrence. The combination of total nitrogen, Na_{ava} and surface fragment content has a close relationship with Astragalus vegetation cover density and height while the vegetation cover percentage and height of Anabasis are more related to the combination of CEC, Na_{ava}, CCE, Cl⁻, infiltration rate, clay content and bulk density. SOM, P_{ava}, total nitrogen, EC, porosity and particle density are the most important factors affecting Noaea presence.

Table 4. Soil variables influencing coverage density and height of investigated plant species according to SVR analysis

Plant	Characteristic	MSE
Scariola	CEC, SOM, Na _{ava} , Mg _{ava} , pH, EC, Inf, Por	0.076
Stipa	PD, MWD, pH, Mg _{ava}	0.008
Astragalus	TN, Na _{ava} , SF	0.133
Anabasis	CEC, CCE, Na _{ava} , Cl ⁻ , Inf, BD, Clay	0.032
Noaea	SOM, TN, P _{ava} , EC, Por, BD	0.047

Note: MSE = mean estimation error, CEC = cation exchangeable capacity, SOM = soil organic matter content, Na_{ava} = available sodium content, Mg_{ava} = available magnesium, EC = electrical conductivity, Inf = infiltration rate, Por = porosity, PD = particle density, MWD = mean weight diameter, TN = total nitrogen, SF = surface fragment content, CCE = calcium carbonate equivalent content, Cl⁻ = chloride content, BD = bulk density, P_{ava} = available phosphorus content

DISCUSSION

Soil characteristic spatial variations influence plant diversity and community features by affecting the movement and persistence of organisms, as well as the redistribution of organic matter and nutrients [23]. Especially in semi-arid terrestrial ecosystems, patchiness may play a critical role in maintaining ecosystem productivity by concentrating limited resources [24]. On the other hand, variations in plant type and landscape condition can affect soil characteristics and water interactions [2].

A strong relationship between soil available nitrogen, phosphorus and magnesium contents and the occurrence and distribution of plant species in the study site was observed, which is expected since they are generally considered essential plant nutrients. The SVC results suggest that bulk density, porosity and silt are the main factors accounting for the occurrence of Scariola. These are the main soil physical properties which affect the establishment and growth of plants by improving the structure and fertility of soil. The Stipa occurrence is most responsive to calcium carbonate content. Calcium carbonate in soil plays a considerable role in the creation of good structure. Together with soil pH, they are two important factors which determine plant-type distribution [25, 26]. According to the SVC analysis results, surface fragment content is the key factor for the occurrence, growth and development of Astragalus in the study area. It is well known that this species prefers mountainous and slightly eroded soil with surface fragment [27]. Its relatively deep and straight root system is well adapted to this condition. This species is a good

competitor species because it can absorb essential nutrients from the soil better than species with more shallow root systems [27]. The bulk density influences soil formation and aeration and thus may affect the *Noaea* occurrence in the study area. *Noaea* is a strong plant species which can handle challenging conditions of high bulk density and adverse aeration conditions [28].

Available phosphorus content is most important for the occurrence of *Anabasis*, which is a perennial plant that can grow in nutrition-poor soils, although phosphorus has an essential role in its growth and metabolism. Its root system is strong and penetrates down into the ground for several meters, thus enabling the plant to absorb phosphorus from both deep and shallow soils. The relationship between the abundance of *Anabasis* and clay content is due to the impact of clay particles on the soil moisture/aeration conditions and to the positive effect of clay on exchangeable nutrient contents. Higher amounts of clay generally indicate an improved soil nutrient status [1].

A positive correlation between pH and densities of *Scariola* and *Stipa* species indicates that in this study area pH levels affect the availability of essential plant nutrients and the spatial distribution of these species. A strong relationship between soil extractable sodium contents and *Scariola*, *Astragalus* and *Anabasis* species composition is unexpected since sodium is not generally considered as an essential plant nutrient. There is some evidence, however, that for potassium-deficient soils in particular, sodium may substitute for potassium [24]. This would indicate that the effect of potassium was being masked by sodium. The possible substitution of potassium by sodium requires further investigation [1].

Soil fertility and nutrient availability are closely connected to SOM content and its mineralisation. The extent of carbon mineralisation determines the release of soil nutrients and hence nutrient availability [3]. The actual soil water content, total water capacity, bulk density and porosity are also the main physical characteristics of soil that affect plant growth. These characteristics improve the soil structure and fertility, and consequently they affect growth, regeneration and establishment of plants. Therefore, the results of our work confirm that the investigated plant species have very different demands from their environment, which are important to consider when planning a restoration process in areas with very high spatial variability in soils.

CONCLUSIONS

The results in this study support the hypothesis that plans for the restoration of native plant communities can benefit from establishing the levels of soil variables. The SVC and SVR results indicated that, although some of the native species were not related specifically to any of the soil variables, other species responded to a varying set of variables. Therefore, soil properties should be considered when explaining and managing the variability in plant distribution and coverage density. The study also shows that there is a possibility of using GA-SVM approach in determining the relationships between soil properties and plant occurrence. However, further research in this area should be conducted and needs to be validated, especially for soils in different management systems.

REFERENCES

1. L. M. A. Omoro, R. Laiho, M. Starr and P. K. E. Pellikka, “Relationships between native tree species and soil properties in the indigenous forest fragments of the Eastern Arc Mountains of the Taita Hills, Kenya”, *For. Stud. China*, **2011**, 13, 198-210.
2. B. J. Fu, L. D. Chen, K. M. Ma, H. F. Zhou and J. Wang, “The relationships between land use and soil conditions in the hilly area of the loess plateau in northern Shaanxi, China”, *Catena*, **2000**, 39, 69-78.
3. B. J. Fu, S. L. Liu, K. M. Ma and Y. G. Zhou, “Relationships between soil characteristics, topography and plant diversity in a heterogeneous deciduous broad-leave d forest near Beijing, China”, *Plant Soil*, **2004**, 261, 47-54.
4. M. L. Silveria, N. B. Comerford, K. R. Reddy, J. Prengger and W. F. Debusk, “Soil properties as indicators of disturbance in forest ecosystems of Georgia, USA”, *Ecol. Indic.*, **2009**, 9, 740-747.
5. J.-T. Zhang and E. R. B. Oxley, “A comparison of three methods of multivariate analysis of upland grasslands in North Wales”, *J. Veg. Sci.*, **1994**, 5, 71-76.
6. V. D. Vasil’evskaya, V. Ya. Grigor’ev and E. A. Pogozheva, “Relationships between soil and vegetation characteristics of Tundra ecosystems and their use to assess soil resilience, degradation, and rehabilitation potentials”, *Eurasian Soil Sci.*, **2006**, 39, 314-323.
7. A. A. Besaltpour, M. A. Hajabbasi, S. Ayoubi, A. Gharipour and A. Y. Jazi, “Prediction of soil physical and mechanical properties using optimized support vector machines”, *Int. Agrophys.*, **2012**, 26, 109-115.
8. H. Li, Y. Liang and Q. Xu, “Support vector machines and its applications in chemistry”, *Chemo. Intell. Lab. Syst.*, **2009**, 95, 188-198.
9. V. N. Vapnik, “The Nature of Statistical Learning Theory”, Springer, New York, **1995**.
10. F. Melgani and L. Bruzzone, “Classification of hyperspectral remote sensing images with support vector machines”, *IEEE Trans. Geosci. Rem. Sens.*, **2004**, 42, 1778-1790.
11. N. Cristianini and J. Shawe-Taylor, “An Introduction to Support Vector Machines and Other Kernel-based Learning Methods”, Cambridge University Press, New York, **2000**.
12. D. W. Nelson and L. E. Sommers, “Total carbon, organic carbon and organic matter”, in “Methods of Soil Analysis: Part 2 – Chemical and Microbiological Properties” (Ed. A. L. Page, R. H. Miller and D. R. Keeney), 2nd Edn., American Society of Agronomy Inc. - Soil Science Society of America Inc., Madison, **1982**, Ch.29.
13. R. E. Nelson, “Carbonate and gypsum”, *ibid.*, Ch.11.
14. S. R. Olsen and L. E. Sommers, “Phosphorus”, *ibid.*, Ch.24.
15. J. M. Bremner and C. S. Mulvaney, “Nitrogen-total”, *ibid.*, Ch.31.
16. L. A. Richards (Ed.), “Diagnosis and Improvement of Saline and Alkali Soils”, U.S. Government Printing Office, Washington, D.C., **1954**.
17. J. D. Rhoades, “Cation exchange capacity”, in “Methods of Soil Analysis: Part 2 – Chemical and Microbiological Properties” (Ed. A. L. Page, R. H. Miller and D. R. Keeney), 2nd Edn., American Society of Agronomy Inc. - Soil Science Society of America Inc., Madison, **1982**, Ch.8.

18. G. R. Blake and K. H. Hartge, "Bulk density". in "Methods of Soil Analysis: Part 1 – Physical and Mineralogical Properties" (Ed. A. Klute), 2nd Edn., American Society of Agronomy Inc. - Soil Science Society of America Inc., Madison, **1986**, Ch.13.
19. K. E. Saxton, W. J. Rawls, J. S. Romberger and R. I. Papendick, "Estimating generalized soil-water characteristics from texture", *Soil Sci. Soc. Am. J.*, **1986**, 50, 1031-1036.
20. G. W. Gee and J. W. Bauder, "Particle-size analysis", in "Methods of Soil Analysis: Part 1 - Physical and Mineralogical Properties" (Ed. A. Klute), 2nd Edn., American Society of Agronomy Inc. - Soil Science Society of America Inc., Madison, Wisconsin, **1986**, Ch. 15.
21. W. D. Kemper and K. Rosenau, "Aggregate stability and size distribution", *ibid.*, Ch. 17.
22. N. Lu, J. Zhou, Y. He and Y. Liu, "Particle swarm optimization for parameter optimization of support vector machine model", Proceedings of 2nd International Conference on Intelligent Computation Technology and Automation, **2009**, Zhangjiajie, China, pp.283-286.
23. S. T. Pickett and M. L. Cadenasso, "Landscape ecology: Spatial heterogeneity in ecological systems", *Science*, **1995**, 269, 331-334.
24. J. C. R. Almeida, J.-P. Laclau, J. L. de Moraes Concalves, J. Ranger and L. Saint-André, "A positive growth response to NaCl applications in *Eucalyptus* plantations established on K-deficient soils", *For. Ecol. Manag.*, **2010**, 259, 1786-1795.
25. A. A. Besalatpour, S. Ayoubi, M. A. Hajabbasi, M. R. Mosaddeghi and R. Schulin, "Estimating wet soil aggregate stability from easily available properties in a highly mountainous watershed", *Catena*, **2013**, 111, 72-79.
26. J. G. Pausas and M. P. Austin, "Patterns of plant species richness in relation to different environments: An appraisal", *J. Veg. Sci.*, **2001**, 12, 153-166.
27. G. A. Dianati Tilaki, H. N. Nasrabad and J. Abdollahi, "Investigation of Relationship between Vegetation, Topography and Some Soil Physico-Chemical Characteristics in Nodoushan Rangelands of Yazd Province (Iran) ", *Int. J. Nat.. Resour. Marine Sci.*, **2011**, 1, 147-156.
28. A. A. Morsy, A. M. Youssef, H. A. M. Mosallam and A. M. Hashem, "Assessment of selected species along Al-Alamein-Alexandria international desert road, Egypt", *J. Appl. Sci. Res.*, **2008**, 4, 1276-1284.

Maejo International Journal of Science and Technology

ISSN 1905-7873

Available online at www.mijst.mju.ac.th

Report

WiMAX deployment: A report for a rural region of Thailand

Chalee Vorakulpipat^{*}, Kitti Wongthavarawat, Kitiwat Limmongkol and Siwaruk Siwamogsatham

National Electronics and Computer Technology Centre, 112 Thailand Science Park, Phahonyothin Road, Klong 1, Klong Luang, Pathumthani 12120, Thailand

^{*} Corresponding author, e-mail: chalee.vorakulpipat@nectec.or.th

Received: 12 May 2014 / Accepted: 29 May 2015 / Published: 5 June 2015

Abstract: We report on the deployment of WiMAX (worldwide interoperability for microwave access) in Mae Hong Son, a remote, rural and mountainous province in northern Thailand. WiMAX deployment is a means to enhance educational opportunities through technology. Three years after installation, we collected data from a wide range of stakeholders ranging from system administrators, teachers and students to government officials, who were potential beneficiaries of the new digital infrastructure. The results indicate that the WiMAX service can help improve the development of a rural area, in particular in the realm of education. Importantly, it can bridge the digital divide that exists between people in rural and city areas.

Keywords: Thailand, WiMAX, rural community, educational opportunities

INTRODUCTION

Since 2006 Thailand has adopted an aggressive approach to creating an information-oriented society. The National IT Policy Framework, IT2010 (2001-2010), aimed for the construction of a knowledge-based economy and society. This framework emphasised leveraging information technology (IT), development of IT human resources, and construction of information and telecommunication infrastructure. Like most other countries that have advanced their information and communication infrastructure, development in provincial cities in Thailand is quite slow; rural areas still lack access to telephones, the Internet and telecommunication infrastructure. As a result, the digital divide between urban and rural areas has widened, thus contributing to other disparities in

terms of economic opportunity, education and quality of life in recent years [1]. Rectification of the digital divide has thus become one of the highest priority for development in Thailand [2].

With support from Japan International Cooperation Agency (JICA) in the form of project equipment and from the National Broadcasting and Telecommunications Commission (NBTC) in the form of a trial frequency band, together with a Japanese advisory team and local agencies, the Worldwide Interoperability for Microwave Access (WiMAX) system was set up in the rural province of Mae Hong Son. Although the work entailed the implementation of a wireless communications system demonstration test, the goal was not simply for testing. It was anticipated that WiMAX would help improve the development of the area and that its deployment would be further extended into other rural provinces when the testing, establishing, disseminating and refining of the system for practical applications were completed.

It is important to realise the practical applications of a local wireless communications system and to enhance the IT knowledge for the local people so they can contribute to a local revitalisation. The WiMAX system was seen as having considerable potential for developing the rural and mountainous areas in Mae Hong Son. WiMAX is a technology that can provide an operator-independent telecoms service as long as the operator license is available locally [3]. WiMAX is faster than Wi-Fi and, more importantly, has a much greater fixed, nomadic and mobility coverage [4]. Rural areas frequently lack optical fibre or copper-wire infrastructure for broadband services, and providers are unwilling to install the necessary equipment for regions with low profit potential. Thus, many residents must do without broadband service. WiMAX can address this problem since a wireless infrastructure can be considerably cheaper and requires less time to set up compared with the traditional wired options [5].

In this paper we report on an impact survey conducted three years after the installation of WiMAX in Mae Hong Son province. We focus on two outputs: 1) actual usage of the WiMAX and development of local information technology infrastructure, and 2) economic development in terms of advancement of school curricula and online learning. Both quantitative and qualitative data were collected from three groups of stakeholders, i.e. system administrators, teachers and students, to gauge the impact of WiMAX on the rural community.

IT INFRASTRUCTURE IN RURAL COMMUNITIES

A viable IT infrastructure is vital for rural areas for the simple reason that people living in these areas are more isolated from the rest of the world and need technology to connect with others [6,7]. The uneven distribution of information and communications technology (ICT) access may mean that those who have no or limited access to this technology may be denied socio-economic opportunities such as social and economic equality, economic growth and access to innovations [8]. A study in South Korea identifies two factors influencing ICT use in rural areas: perceived usefulness for commerce and perceived entertainment value [9]. Since each developing economy exhibits different characteristics (in particular, problems and limitations), the goals of deploying ICT are diverse [10]. For example, in India the Communication Initiative Network 2000 [11] has focused on IT deployment for education purposes. The Warana Wired Village project [12] helps the villager gain access to information about agriculture, healthcare and education. In contrast, in Kenya, IT deployment has focused on improving agricultural practices [13]. Today, WiMAX receives growing acceptance and is a cost-effective method for delivering broadband internet service in rural and urban areas [14, 15].

Government and private initiatives can overcome the urban-rural digital divide by providing funds for investment and access to education [16]. Also, governments can provide subsidies and incentives to diffuse broadband to rural areas where people are still regarded as “broadband have-nots” [9]. Several countries have launched national broadband plans or frameworks involving ICT investment in rural areas [17, 18]. In summary, although investment in information technologies and infrastructure is not a panacea for all of the problems of developing countries, it is a proven enabler of economic development [8]. This is especially true for rural areas in developing or underdeveloped countries.

IT INFRASTRUCTURE AND DEVELOPMENT OF E-LEARNING PROJECT

The National Electronics and Computer Technology Centre (NECTEC), a Thai ICT research institution, and JICA, a Japanese government agency that assists economic and social growth in developing countries, initiated the ‘Project of human resource development through utilising the information technology for rural community vitalisation in the kingdom of Thailand’ in December 2007. The project aimed to realise the practical application of a local wireless communications system to enhance local vitalization and the specific deliverable was the deployment of WiMAX in Mae Hong Son province. After some delays, the WiMAX service and its supporting website were officially launched in Mae Hong Son on 28 March 2010.

In April 2009, before the start of the WiMAX project, baseline data were collected from local citizens residing in four areas within Mae Hong Son province: Muang, Mae Sariang, Pai and Kun Yuam. Questionnaires were hand-delivered to 17 local people in Muang, 16 in Mae Sariang, 9 in Pai and 2 in Kun Yuam. In total, all 44 questionnaires were returned and analysed. The major findings of the baseline survey (good points and problems) are summarised in Table 1.

Table 1. Major findings of baseline survey

Good Points	Problems
<p>Awareness</p> <ul style="list-style-type: none"> • Overall good awareness for the role that IT could play in improving education, economy and overall quality of life • Good awareness for the capabilities of Internet technology 	<p>Infrastructure (computers)</p> <ul style="list-style-type: none"> • Lack of computers and hardware infrastructure; budget for human development preventing people from accessing the Internet • Inadequate number of personal computers (PCs) in schools (20-50 computers per school, 200-500 students per school) <p>Infrastructure (electricity and communication)</p> <ul style="list-style-type: none"> • Slow and inconvenient internet access • Poor conditions of existing infrastructure such as unstable supply of electricity <p>Appropriate Use</p> <ul style="list-style-type: none"> • Lack of use of e-learning systems on a regular basis • Too much concern about misuse of IT such as access to inappropriate contents (e.g. pornography) <p>Personnel</p> <ul style="list-style-type: none"> • Limited personnel for training and maintenance

IMPLEMENTATION PHASE

WiMAX Installation

Over a one-year period, from January 2010 to January 2011, WiMAX base stations were installed in three districts of Mae Hong Son province: Muang, Pai and Mae Sariang. For each of the three sites, stakeholders were solicited from three sectors: schools and community colleges, government and local communities (Table 2). The survey focuses on a number of stakeholders in these sectors using stratified random sampling technique.

Table 2. Number of stakeholders by district

District	School	Government	Community	Total
Muang	9	8	2	19
Mae Sariang	12	3	1	16
Pai	6	3	1	10
Total	27	14	4	45

Personnel Training

Educating people correctly was a key success factor for achieving stated goals and managing the project in a systematic way. A training plan was created to maximise stakeholders' understanding of the technology. More than 20 training courses were offered throughout the areas from August 2009 to October 2011. Another role of the personnel was system support, so a system support structure was created and assigned to community members so that when a problem occurs they know how to fix it, and if they cannot fix it, they know where to go to find solutions.

Applications

LearnSquare is a Thai open source learning management system that was introduced in schools in March 2010 and allows users to design a content structure and create an online course. AcuConference is an application tool that supports video/audio conferencing. In this project this tool was mainly used for distance learning during project implementation.

POST-IMPLEMENTATION REPORT

Given this background, we conducted an impact survey over a three-year period (November 2010 - October 2013) following the installation of the WiMAX to gauge changes, outcomes and conditions in the rural communities. We contacted 45 local communities within the three districts: Muang, Mae Sariang and Pai. Kun Yuam was not contacted because while testing WiMAX, it was found that Kun Yuam was located too far from the WiMAX range to participate, the maximum range being five kilometers for this project. Thus, Kun Yuam was removed from the project. The objectives of this impact survey were: firstly, to collect and analyse data on the status of the current system, the users' training experience, and the actual e-learning content development and usage; and secondly, to identify the project success factors and ongoing issues that need to be addressed for further actions.

The project output after a series of infrastructure implementation and training courses with local people included the following:

- WiMAX system was up and running in 45 sites (schools, government offices and local communities) within Mae Hong Son province

- Technical knowledge about WiMAX system was transferred to local people, and they could monitor and maintain the system on their own or with minimal guidance from the project team.
- The number of developed e-learning contents that had been created by the 45 local sites increased substantially.

Three sets of questionnaires and an interview protocol were designed to collect data from the identified targets. Survey data were collected from 45 IT administrators from all 45 sites, 40 e-learning teachers and 117 'IT-Valley' students from eight schools. Questions were asked in the areas of system status (number of PCs, network conditions, internet access and usage, wireless access and electricity), system training and e-learning outcomes for both teachers and students. In addition to the questionnaire survey, we also ran two focus groups and conducted individual interviews with 48 stakeholders, consisting of system administrators, teachers, government officials and business owners, to identify key success factors of the project as well as concerns that needed to be addressed for further actions. The data collection was done via two field trips to Mae Hong Son. Results from the questionnaire survey, focus groups and interviews were then analysed to generate a list of possible impacts of the WiMAX service on the target sites, which later was validated through an internal brainstorming session involving researchers, teachers, local governors and the project's funding sponsor.

Three years after the WiMAX installation, the findings were presented in the following five categories: awareness, personnel, electricity and communication infrastructure, computer infrastructure, and appropriate use.

Awareness

After the implementation of the WiMAX service, the number of system administrators that were aware of wireless technology trainings held in their area increased from 2 to 25. It was also found that there were more wireless training instructors and that their wireless skills (design, installation, monitoring, maintenance and configuration) expanded. People gained more understanding of how WiMAX wireless technology could improve their everyday lives. For example, people now use mobile devices including laptops and smart phones to connect to the Internet on a regular basis.

Personnel

There was no significant change in the number of staff members (teachers, IT instructors or administrators). Most students had computer proficiency and could use resources on the Internet. Compared to the baseline data, school size actually increased slightly. This might be because people had more opportunities to get access to the Internet and the contents in the Internet could influence them to send their children to school. However, there was no change regarding the number of students that could use computers and the Internet. Although the number of personnel did not change, their IT skills were greatly improved. They could use computer software, applications and the Internet without assistance from IT experts. This could be because they had more opportunities to learn, given the availability of the Internet access and e-learning.

Electricity and Communications Infrastructure

Compared to the baseline data, there were more connections through the Communications Authority of Thailand, increasing from 8 sites in 2010 to 19 sites in 2013. The number of system administrators per site also increased, with many sites reporting more administrators than those in 2010. Also, a better management of the network was reported, with a decreasing number of sites that had no identification or authentication system, and more sites with such a system available for all users. More than half of the servers (27 out of 45) were housed in a locked facility.

Most uninterruptible power supplies last for about 5-13 minutes after a blackout. As noted earlier, electricity problems were prevalent in Mae Hong Son areas. Blackouts were frequent (except in Pai), usually lasting for up to 1 hour each day. Voltage instability came mostly in the form of voltage drops and voltage fluctuation. Compared to the baseline data, there was an important improvement in blackout problems, shifting from a daily occurrence down to a few times a week.

Computer Infrastructure

Compared to the baseline survey, there was an increase in the number of PCs in organisations that could connect to the Internet, a jump in wireless communication throughput from 1 Mbps to >5 Mbps, and a big improvement in PC and network conditions for teaching an IT curriculum. Almost all sites had a Wi-Fi connection and 30 out of 45 sites could get WiMAX communication up and running. The majority of sites had at least 2 access points covering most buildings at each site. Compared to the baseline data, the use of wireless communication significantly increased during the year 2010, with Wi-Fi increasing from 27 to 41 sites and WiMAX going from zero to 30 sites. In addition, there were marked increases in the number of wireless access points as well as wireless locations and buildings. Most of the sites (69%) had a connection speed of at least 1 Mbps. Also, most system administrators/teachers thought the actual PC and current network conditions were quite sufficient for teaching an IT curriculum. Compared to the baseline data, the length (hours) of Internet usage per day remained unchanged. However, many students accessed the Internet more frequently, from a few times a week to daily usage.

Appropriate Use

After the installation of WiMAX, teachers tried to teach a subject using e-learning contents, and more than half developed some e-learning content themselves. Many teachers helped train others to support teaching and helped their colleagues master IT curriculum items such as Media creation, Graphics, Computer and IT, and Internet usage. In addition, most of the teachers felt that the contents of the IT curriculum fitted their needs.

Most of the teachers who used LearnSquare used it about once a month. For those who did not use the application, their reasons were the associated materials being not suitable for their class, failed attempts to use the application, and lack of time/personnel. As site users gradually improved their understanding and cooperation, a change in awareness was observed, and comments shifted from asking: “why should we develop content?” to stating: “we want to create content if we have the time” and “we can’t develop them but we want to use them.” Eventually, there were more than 800 contents stored on the e-learning server. Since the introduction of AcuConference late in 2010, only few teachers taught a class using that application.

Half of the students reported having learned online. They also expressed an interest in e-learning and thought it could be useful or helpful. Most students liked to participate a project to develop an IT curriculum content. Since there were in the e-learning system contents that still needed updating, selected students were encouraged to help teachers and IT instructors to improve them. The baseline data showed that most students had never used e-learning contents (in general). Three years later, all the students used e-learning contents and e-learning tools on a regular basis. The available subjects were the same because the contents had not updated from the previous years.

DISCUSSION

Overall, the project did increase the connectivity of the rural communities to the rest of the country and the world beyond. According to our findings, WiMAX could address social issues in several ways including education and economic opportunities, although it also had its own problems.

Education

The WiMAX service for local communities had strong signals in the coverage areas and the mobile WiMAX dongles were well received by all users. Wireless communication technology and knowledge was transferred to local communities and made a difference in the educational mission and outcomes. The project also helped build a strong network for local personnel in the field of information technology and education even beyond the WiMAX context. For the first time, a platform was built to allow local teachers to utilise IT to create digital content and share it with both colleagues and students. The project significantly helped the IT-savvy teachers improve their e-learning skills. Also, although new to e-learning, students showed a strong interest in e-learning activities and such IT curricula as programming and image editing. Despite being introduced late in the project, WiMAX had great potential to save time and travel expenses for a province like Mae Hong Son. Several IT-oriented teachers conducted e-learning classes to offset the shortage of specialised teachers.

Opportunities

One of our expectations was to see an increase in the number of PCs connected to the Internet. In this project the introduction of WiMAX vitalised the rural communities, was well accepted and received good support from both the community and the local government. In Mae Hong Son case most of the region is mountainous, so people have to spend more time and money in travelling within or between the provinces. The videoconference application was thus well accepted by the local government staff, because it enabled them to hold meetings across districts.

Schools in Mae Hong Son tend to lack teachers and also have high teacher turnover rates. e-learning can therefore be used as a tool to strengthen education in the province. An increase in PCs with Internet access leads to increased access to information for lessons and network collaboration [6]. In this case the WiMAX service can bridge the digital divide between rural areas and downtown if it is adequately implemented, managed, maintained and made cost-effective [7].

Problems

One of the major complaints about the WiMAX service was that users were unable to freely access the Internet via the system. Since use of the system was limited to a few specific functions for academic purposes, sometimes users felt they might not choose to use WiMAX, if they had an

alternative connection. It is not surprising that users wanted access also to non-educational contents, especially for entertainment purposes, which might be blocked by the system. However, they could use their personal mobile phones or dial-up modems to access this content instead, although the cost of these connection methods was much higher while the connection speed was much lower and the users had to pay by themselves. We perceive this is not a long-term problem because users did not often use these connection methods. Also, the cost of connecting to the Internet using a smart phone (3G) decreases every year and the connection speed is always improving.

Time and motivation were issues for some local teachers. While many outstanding teachers were recognised and assigned as e-learning expert instructors, some were still not motivated enough to learn and create their e-learning content independently. Some teachers reported finding no content that would align with their needs. Also, at this stage of the project, LearnSquare was still used mainly by teachers to create contents and by students to download specified learning materials. Students must be encouraged to create e-learning contents themselves in the next stage of the project.

Another disadvantage was the limited selection of applications suited to rural areas. The applications were limited to educational items (e-learning, VoIP and TV conference) while a survey of wishes revealed that there was also a large demand for items related to e-health and e-tourism. Mae Hong Son's ex-governor and the tourism community strongly suggested using WiMAX service to promote the local tourism industry. It was apparent that not all demands for applications could be fulfilled.

CONCLUSIONS

This paper reports the impact of introducing WiMAX service to a rural province in northern Thailand. Importantly, the WiMAX service can bridge the digital divide that exists between people in rural and city areas. Hence education can be strengthened across the province regardless of geographical barriers. While this study addresses the adoption of a specific technology (WiMAX) in specific rural areas (Mae Hong Son), further studies on IT adoption in other rural areas using other technologies could be conducted in similar ways, using this project as a baseline work. However, distinctive characteristics of the local areas should be addressed before conducting future studies.

ACKNOWLEDGEMENTS

This project was wholly funded by Japan International Cooperation Agency (JICA) and National Electronics and Computer Technology Centre (NECTEC). We thank the National Broadcasting and Telecommunications Commission (NBTC) for providing technical support. We also thank Mae Hong Son Governor's Office, Mae Hong Son Community College, Mae Hong Son Primary Educational Service (Area 2) Office and Pai Wittayakarn School for their general support of this project.

REFERENCES

1. P. Sutharoj, "Wimax to bridge Mae Hong Song's digital divide", **2008**, <http://www.nationmultimedia.com/technology/Wimax-to-bridge-Mae-Hong-Song-s-digital-divide-30079946.html> (Accessed: May 2015).

2. P. Punyabukkana, S. Thanawastien and A. Jirachiefpattana, "Thailand's national digital divide strategic framework", Proceedings of International Cross-Disciplinary Conference on Web Accessibility, **2008**, Beijing, China, pp.97-100.
3. M. Norris and A. Golds, "Realising the WiMAX opportunity in the Middle East", Proceedings of WiMAX London 2007 Conference, **2007**, London, UK, pp.1-7.
4. K. Chaudhari, U. Dalal and R. Jha, "E-Governance in rural India: Need of broadband connectivity using wireless technology", *Wireless Eng. Technol.*, **2011**, 2, 212-220.
5. S. J. Vaughan-Nichols, "Achieving wireless broadband with WiMax", *Computer*, **2004**, 37, 10-13.
6. A. E. D. Andrade and C. Urquhart, "The value of extended networks: Social capital in an ICT intervention in rural Peru", *Inform. Technol. Devel.*, **2009**, 15, 108-132.
7. N. Gorla, "A Survey of rural e-government projects in India: Status and benefits", *Inform. Technol. Devel.*, **2009**, 15, 52-58.
8. M. W. L. Fong, "Digital divide: The case of developing countries", *Issues Inform. Sci. Inform. Technol.*, **2009**, 6, 471-478.
9. J. Moon, J. Park, G. H. Jung and Y. C. Choe, "The impact of IT use on migration intentions in rural communities" *Technol. Forecast. Social Change*, **2010**, 77, 1401-1411.
10. C. Vorakulpipat, S. Siwamogsatham, A. Kamolsook and P. Jamchudjai, "An empirical study of IT adoption in rural areas of Thailand", Proceedings of Portland International Conference on Management of Engineering and Technology, **2010**, Phuket, Thailand.
11. The Communication Initiative Network, "Information and communication technology in rural development", **2000**, <http://www.cominit.com/en/node/275663/307> (Accessed: May 2015).
12. e-Agriculture, "Warana Wired Village Project", **2007**, <http://www.e-agriculture.org/content/warana-wired-village-project> (Accessed: May 2015).
13. A. G. Muriithi, E. Bett and S. A. Ogaleh, "Information technology for agriculture and rural development in Africa: Experiences from Kenya", Proceedings of Conference on International Research on Food Security, Natural Resource Management and Rural Development, **2009**, Hamburg, Germany.
14. R. R. Dube and A. G. Dhanashetti, "Analysis of WiMax connectivity in rural and urban area using Okumura-Hata propagation model", *Int. J. Innov. Res. Devel.*, **2014**, 3, 311-314.
15. V. Krizanovic, D. Zagar, S. Rimac-Drlje and T. Svedek, "Business models and cost optimization of wireless rural broadband access implementation", Proceedings of 22nd International Conference on Software, Telecommunications and Computer Networks, **2014**, Split, Croatia, pp.170-174.
16. P. Preston, A. Cawley and M. Metykova, "Broadband and rural areas in the EU: From technology to applications and use", *Telecommun. Policy*, **2007**, 31, 389-400.
17. D. Espinoza and D. P. Reed, "Technology broadband roadmap for rural areas in the Andes and Amazon regions in Peru", **2015**, <http://ssrn.com/abstract=2588010> (Accessed: May 2015).
18. M. S. N. Mamba and N. Isabirye, "A framework to guide development through ICTs in rural areas in South Africa", *Inform. Technol. Devel.*, **2015**, 21, 135-150.

Full Paper

Structural implications for nectar secretion by nectaries of three columnar cacti

Whaleeha Gudiño^{1,2}, Judith Márquez-Guzmán³ and Erick de la Barrera^{1,*}

¹ Instituto de Investigaciones en Ecosistemas y Sustentabilidad, Universidad Nacional Autónoma de México, Morelia, Michoacán 58190, Mexico

² Posgrado en Ciencias Biológicas, Universidad Nacional Autónoma de México, Mexico City 04510, Mexico

³ Laboratorio de Desarrollo de Plantas, Departamento de Biología Comparada, Facultad de Ciencias, Universidad Nacional Autónoma de México, Mexico City 04510, Mexico

* Corresponding author, e-mail: delabarrera@unam.mx

Received: 7 July 2014 / Accepted: 1 June 2015 / Published: 5 June 2015

Abstract: Floral nectaries are essential for plant reproduction. Their position and shape are important because these factors determine the amount of nectar secreted and therefore the pollinators that are attracted. The main objective of this study is to determine the position, shape and macromorphology of floral nectaries for three columnar cacti, namely *Polaskia chende*, *P. chichipe* and *Stenocereus quevedonis*. By means of light microscopy, scanning electron microscopy and histochemical tests, the floral nectar-secreting structures were investigated. Different secreting structures were found for the three species, with *S. quevedonis* having the largest nectar secreting area consisting of stomates located at the base of the stem filaments (1.9 mm²). The nectar secretory pores of *P. chichipe* measured 0.93 mm², while the cuticular fissures of *P. chende* measured 0.8 mm². For the case of these three species, the surface available for nectar secretion appears to determine the volume of nectar secretion. The relationships between nectarial chamber size, total nectar volume secreted and size of secreting structure found for the three species suggest that the surface area available is the central influential variable that determines the volume of secreted nectar.

Keywords: floral morphology, Mexico, nectar, Pachycerae, reproductive ecophysiology, columnar cacti, *Polaskia chende*, *Polaskia chichipe*, *Stenocereus quevedonis*

INTRODUCTION

The floral nectary is an anatomical feature of angiosperms with great evolutionary and ecological relevance because nectar, an aqueous solution primarily containing sugars, can mediate pollination [1-3]. The structure is characterised by a specialised epidermis and parenchyma cells that synthesise, accumulate and release the nectar solution [4]. Anatomical studies have shed some light on the structural and functional traits of floral nectaries, but the actual mechanisms of nectar unloading remains unclear [5, 6]. In addition, their position in a flower can determine the nature of plant-pollinator interactions [7]. For instance, the flowers of *Dolichandra cynanchoides* and *Parabignonia chodatii* present nectaries on the outer or inner surface of the sepals that have no relation to pollination [8] while the positions of the nectaries of *Echinacea purpurea* and *Hymenaea stigonocarpa* do promote pollination [9, 10].

The nectar of the flowers of columnar cacti (Family: Cactaceae) can be the main source of water and nutrients for pollinator communities in arid and semi-arid environments of the New World [11]. This is especially important in Mexico, where the ensuing fruits of most species of the mentioned columnar cacti are consumed by humans [12]. Thus, an understanding of the reproductive biology of these plants can have economical implications, especially when considering that the impending climate change could result in phenological decouplings of pollinators and flowers [3] or a decline of pollinators as it appears to be occurring at present [13].

To advance our understanding of the mechanism of nectar secretion in the columnar cacti, we study the floral anatomy of three columnar cacti whose fruits are edible. In particular, we determine the position, shape and macromorphology for the floral nectaries of the sympatric and congeneric *Polaskia chende* and *P. chichipe* as well as of *Stenocereus quevedonis* in order to gain insight into the mechanism of nectar secretion in these species. To our knowledge, this research represents the first contribution towards the understanding of nectary morphology in the Pachycereae subfamily.

MATERIALS AND METHODS

Plant Material

Flowers of *Polaskia chende* (Rol.-Goss.) A.C. Gibson & K.E. Horak and *P. chichipe* (Rol.-Goss.) Backeb. were collected on 5 May 2010 from a natural population located in San Luis Atolotitlán, Puebla, in the Tehuacán-Cuicatlán Biosphere Reserve (18°10'43" N, 97°26'38" W). This is a semi-arid region spanning 10,000 km², with an average annual rainfall of 400 mm and an annual mean temperature of 21°C [14]. The flowering for these species occurs during late winter and spring [15]. From a similar latitude, flowers of *Stenocereus quevedonis* (J. G. Ortega) Buxb. were collected on 15 May 2010 from a natural population located in La Pitirera, Michoacán, in the Zicuirán-Infiernillo Biosphere Reserve (18°18'45.34" N, 101°52'37.76" W). Also a semi-arid region, Infiernillo spans 2,651 km², with an average annual rainfall of 500 mm and an annual mean temperature of 28°C [16]. The flowering for *S. quevedonis* occurs from January to May [17]. In all cases, the plants were identified following Anderson [18].

Anatomical Studies

The flowers, which were collected during anthesis, were fixed in formaldehyde: acetic acid: 96% ethanol: water (2:1:10:7) [19] and later examined with a stereo-microscope (Olympus SZX12, Japan) in order to locate the position of the nectaries.

Nectaries were dissected to conduct the anatomical studies described below. They were dehydrated in a graded series of ethanol (30, 50, 70, 85, 96 and 100%) for 2 hr in each step and finally in xylol for 40 min. before being embedded in paraplast paraffin. Longitudinal and transverse serial sections (9 μ m thick) were obtained with a microtome (Spencer 820, American Optical, USA). The sections were stained with either safranin - Fast Green, periodic acid Schiff's reagent (PAS reaction) or Lugol's solution to induce a histochemical reaction. The tissue samples were observed under a microscope (Micron 1.07, Westover Scientific, USA).

Structural Studies

Flower tissue samples were dehydrated in the ethanol series as described above but with repeating the absolute ethanol step three times to complete micromorphological observations of the nectar-secreting structures. The dehydrated samples were then placed in a critical-point drier (AutoSamDri 815, Tousimis, USA), coated with gold and examined under high-vacuum with a scanning electron microscope (JSM-6360-LV, Jeol, Japan). Magnifications utilised were $\times 40$, $\times 2,000$ and $\times 15,000$ for *P. chende*, $\times 50$, $\times 200$ and $\times 2,700$ for *P. chichipe*, and $\times 40$, $\times 500$, $\times 3,500$ for *S. quevedonis*.

Data Analyses

Statistical analyses were performed with SigmaStat (SPSS Science, Chicago, USA). Values of *p* are from pairwise Tukey's tests following one-way ANOVAs. Data are presented as mean \pm 1 S.E. (n = sample size).

RESULTS

The flowers of *Polaskia chende*, *P. chichipe* and *Stenocereus quevedonis* were bisexual with an inferior ovary (Figure 1). The secretory tissue was located in the area where the receptacle differentiates from the ovary. The receptacle and the base of the anther filaments fuse to form a nectarial chamber, which makes up a secretory ring around the style.

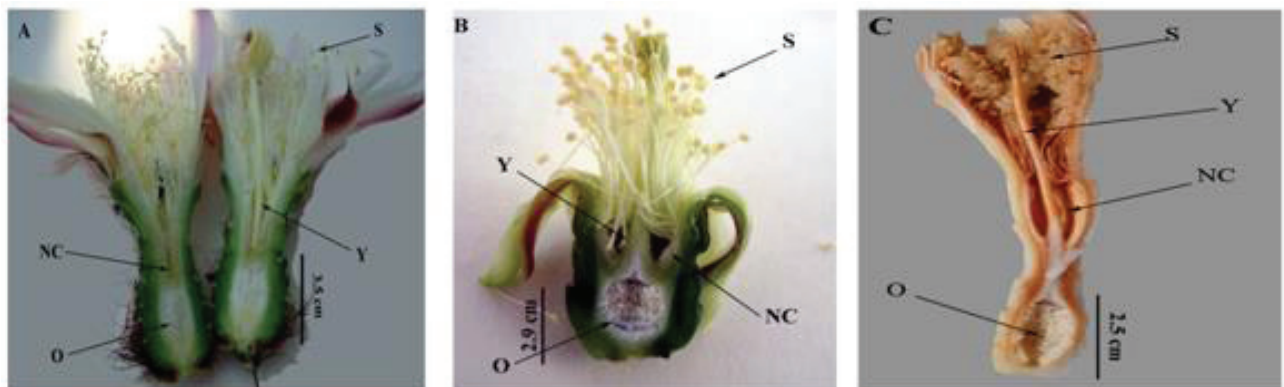


Figure 1. Floral anatomy for *Polaskia chende* (A), *Polaskia chichipe* (B) and *Stenocereus quevedonis* (C). For these three bisexual flowers, reproductive structures are labelled, i.e. nectariferous chamber (NC), ovary (O), stamens (S) and style (Y)

The secretory tissue is composed of cells that have a large nucleus, a distinguishable nucleolus and dense cytoplasm (Figures 2A, D, G). This tissue also presents vascular bundles with both xylem and phloem branches (Figures 2A-I). In turn, the epithelial cells possess fewer cellular components (Figures 2B, C, E, F, H, I). The epidermis is composed of a layer of cubical cells while the sub-epidermal tissue consists of a variable number of layers of parenchyma cells without a specific arrangement.

The Lugol's stain reveals a greater accumulation of starch within the cells of the secretory tissue than in the rest of the floral tissues for all three species (Figures 2B, E, H). However, the frequency of the starch-containing cells varies among species, with *S. quevedonis* having the highest content and *P. chende* the lowest (Table 1). A similar pattern was found with the PAS reaction that stains the insoluble polysaccharides of cell walls (Figures 2C, F, I).

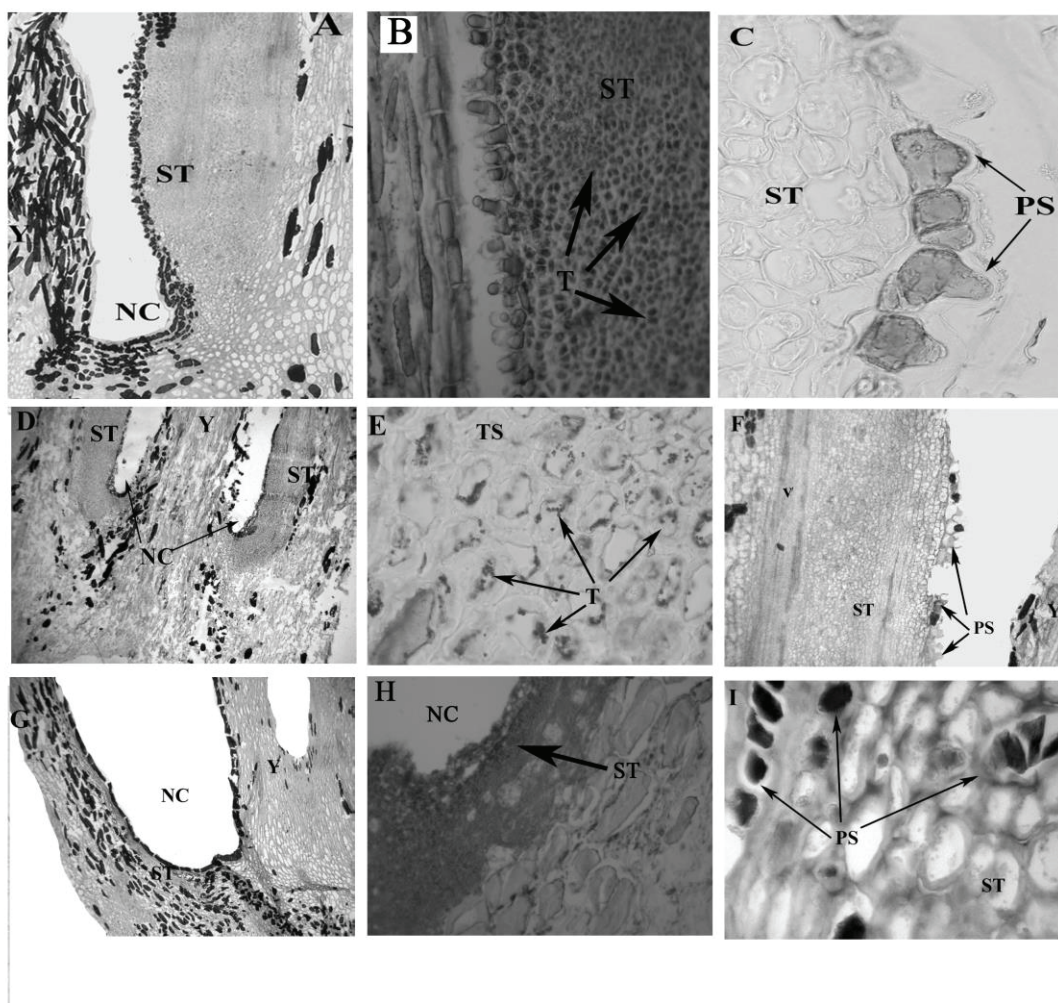


Figure 2. Nectary sections of *P. chende* (A, B, C), *P. chichipe* (D, E, F) and *S. quevedonis* (G, H, I). The structural features of the nectaries were identified with a safranin - Fast Green stain (A, D, G). Stored carbohydrates in the secretory tissue were identified with Lugol's solution (for starch: B, E, H) and with PAS reaction (for other insoluble polysaccharides: C, F, I). Structural features are nectariferous chamber (NC), insoluble polysaccharides (PS), stamens (S), nectar secretory tissue (ST), starch (T), style (Y) and vascular elements (V).

The cuticular fissures of *P. chende* (Figures 3A-C) have the smallest area for nectar secretion among the cacti considered. For this species the cuticle fissures contain a total nectar secretory surface of 0.0836 mm² (Table 2). The pores of *P. chichiipe* (Figures 3D-F) have the second largest secreting area (0.0936 mm²). For this species, the pores have a 12% greater area than the fissures of *P. chende*. The flowers of *S. quevedonis* have stomates connecting the nectaries to the nectariferous chamber (Figures 3G-I). For this species, the total secreting area is 1.976 mm² (Table 2), the largest among the species considered.

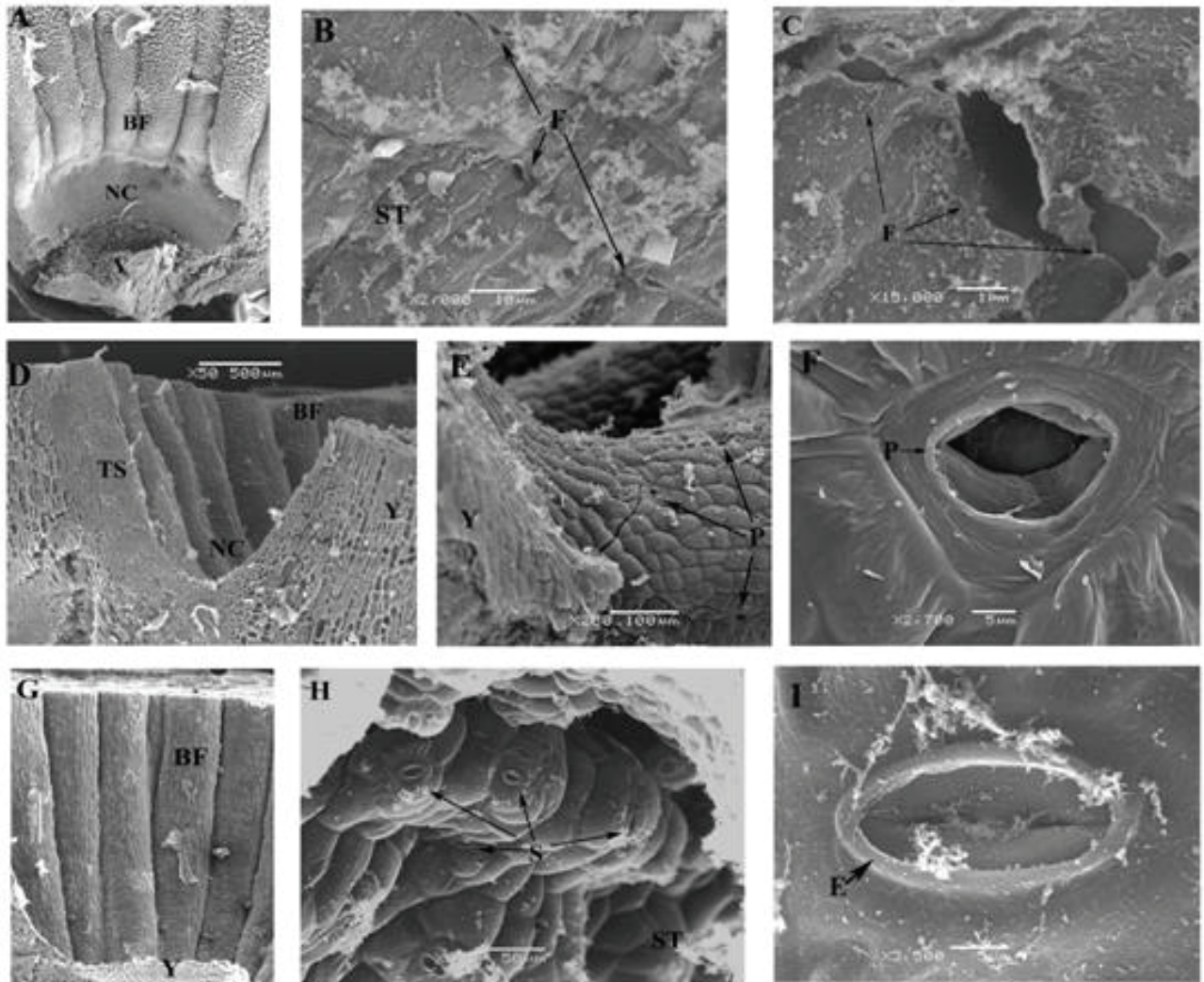


Figure 3. Micromorphological characteristics of the nectary secretory tissue in flowers of three columnar cacti. For *P. chende* (A, B, C), nectar is released through cuticle fractures (F); *P. chichiipe* (D, E, F) presents secretory pores (P); and *S. quevedonis* (G, H, I) has stomates (S). Light-coloured debris observed in the micrographs is solidified nectar. Other structural features identified for reference are: base of filaments (BF), nectariferous chamber (NC), nectar secretory tissue (ST) and style (Y).

Table 1. Anatomical characteristics of secretory tissue of three columnar cacti. Data are presented as mean \pm 1 S.E. (n = 5 flowers from different individuals). Different letters in each column indicate statistical differences ($p < 0.05$) from Tukey test following one way ANOVA.

Species	Number of cell layers	Cell wall thickness (μm)	Nucleus diameter (μm)	Percentage of cells with starch	Percentage of cells with polysaccharides
<i>Polaskia chende</i>	7 \pm 0.19 ^a	1.04 \pm 0.02 ^a	3.1 \pm 0.08 ^a	49 \pm 0.43 ^a	11.5 \pm 0.84 ^a
<i>Polaskia chichipe</i>	11 \pm 0.17 ^{ab}	0.94 \pm 0.03 ^b	1.9 \pm 0.08 ^b	74 \pm 1.07 ^{ab}	10.8 \pm 0.53 ^a
<i>Stenocereus quevedonis</i>	18 \pm 0.34 ^b	1.2 \pm 0.03 ^{ab}	2.36 \pm 0.13 ^c	91 \pm 0.48 ^b	12.6 \pm 0.94 ^a

Table 2. Frequency and size of secreting structures of three columnar cacti. Data are shown as mean \pm 1 S.E. (n = 2 fields of view for each one of 5 flowers or 0.1 mm² per flower). Different letters in each column indicate statistical differences ($p < 0.05$) from Tukey test following one way ANOVA.

Species	Secretory structure	Structure frequency	Maximum length (10 ⁻³ mm)	Minimum length (10 ⁻³ mm)	Structure area (10 ⁻⁵ mm ²)	Total secreting area (mm ²)
<i>Polaskia chende</i>	Fissures	37.7mm ⁻²	0.0025 \pm 0.15 ^a	0.00089 \pm 0.04 ^a	0.0022 \pm 0.19 ^a	0.0836 ^a
<i>Polaskia chichipe</i>	Pores	7.5 mm ⁻²	0.0112 \pm 0.22 ^b	0.0111 \pm 0.30 ^b	0.0117 \pm 0.48 ^b	0.0936 ^a
<i>Stenocereus quevedonis</i>	Stomates	10.4mm ⁻²	0.024 \pm 0.61 ^c	0.0096 \pm 0.13 ^b	0.1796 \pm 4.54 ^c	1.9756 ^b

DISCUSSION

The position of nectaries for the cacti considered here, along with field observations of pollinator activity, confirms that these nectaries are involved in plant reproduction [15]. For the case of columnar cacti in Mexico, the importance of the interaction with pollinators has been widely documented [11-17]. This is important considering that not all floral nectaries are involved in pollination, as is the case for some species in the Bignoniaceae from Argentina whose floral nectaries play a protective role against herbivores [9].

For the three species in this study, the nectar secretory tissue was found at the base of the anther filaments of their bisexual flowers. Such a pattern, known as a disk, is most prevalent among the middle and upper levels in the evolution of dicots [4, 8, 9, 20]. Solutes are delivered to the nectary tissue where they are stored as different polysaccharides, as observed here for the cells containing starch and other insoluble polysaccharides. The calcium oxalate crystals found near the vascular bundles in the nectaries of *S. quevedonis* are quite common in nectaries vascularised by phloem [11, 21].

The nectaries are easily distinguishable from the surrounding parenchyma for the three cacti. In particular, multiple cell layers of thickened cell wall and a conspicuous nucleus were observed. These anatomical characteristics of nectary cells have also been found for other species whose nectary cell walls are thicker than those of other floral tissues [4, 8, 21-25].

Whether the presence of thickened cell walls such as those found here for cactus nectaries enables the floral tissues to withstand the very high hydrostatic pressures resulting from water displacement in response to solute accumulation requires further investigation [1]. However,

hydrostatic pressures measured inside of storage cells can exceed 2 MPa while the normal turgor pressure for a cactus cell is in the order of 0.15 MPa [26, 27]. Concerning the conspicuously enlarged nuclei of the nectary tissue, a basic observation in cell biology is that a cell nucleus is only visible when it is undergoing intense metabolic activity, generally related to mitosis [28].

Based on the anatomical and macromorphological evidence gathered in the present work, the secreting of nectar to the nectariferous chamber occurs directly through fissures for *P. chende* while for *P. chichipe* and *S. quevedonis*, this occurs through pores and stomates respectively. This study documents nectar secretion through fissures and pores in the Cactaceae for the first time. For *Mammillaria san-angelensis*, *Opuntia tomentosa* and *Pereskia lychnidiflora*, the few cacti whose nectary structure has been studied, stomates release the nectar solution into the nectariferous chamber [24]. For female and male flowers of *Cucurbita pepo*, nectar secretion also occurs through stomates, although nectar release through cuticle fissures has also been observed [29]. For the three species in this study, nectaries are highly vascularised, similar to the case of *Mammillaria san-angelensis* and *Opuntia tomentosa* [24].

With respect to nectar secretion, a positive correlation between floral length and volume of nectar solution produced has been documented [23]. The species considered in this study appear to follow a similar pattern with nectar secretion responding to the total area of the secretory tissue. Thus, the nectarial chamber of *P. chichipe* yields 13 $\mu\text{L}/\text{day}$ and that of *P. chende* yields 9 $\mu\text{L}/\text{day}$, while the much larger nectarial chamber of *S. quevedonis* yields 2 mL day^{-1} [30].

The relationships found between nectarial chamber size, total nectar volume secreted, and size of secretory structures in *P. chende*, *P. chichipe* and *S. quevedonis* suggests that structural constraints contribute to the volume of nectar secretion. However, information about the structure and micromorphology of cactus nectaries remains scant.

CONCLUSIONS

The nectary location and secretory structure have been studied for three columnar cacti, namely *Polaskia chende*, *P. chichipe* and *Stenocereus quevedonis* by identifying a relationship between the nectary structure, the area of nectary chamber and the volume of nectar solution produced.

ACKNOWLEDGEMENTS

We thank the funding by UNAM's General Direction of Academic Personnel Affairs (Project PAPIIT-IN224910). We are grateful to Edgar Pérez Negrón and Omar Hernández for field assistance, Monica Karina Pérez Pacheco for laboratory assistance, and Yolanda Ornelas de Uribe for microscopy laboratory assistance at Electron Microscopy Laboratory, ICML-UNAM. W.G. thanks the National Council of Science and Technology (CONACyT) for a Graduate Studies Fellowship.

REFERENCES

1. E. de la Barrera and P. S. Nobel, "Nectar: Properties, floral aspects and speculation on origin", *Trends Plant Sci.*, **2004**, 9, 65-69.
2. P. K. Endress, "Diversity and Evolutionary Biology of Tropical Flowers", Cambridge University Press, London, **1994**, Ch.5.

3. E. de la Barrera, E. Pimienta-Barrios and J. E. Schondube, “Reproductive ecophysiology”, in “Perspectives in Biophysical Plant Ecophysiology: A Tribute to Park S. Nobel” (Eds. E. de la Barrera and W. K. Smith), Universidad Nacional Autónoma de México, Mexico City, **2009**, Ch.12.
4. A. Fahh, “Secretory tissues in vascular plants”, *New Phytol.*, **1988**, *108*, 229-257.
5. A. E. Vassilyev, “On the mechanisms of nectar secretion: Revisited”, *Ann. Bot.*, **2010**, *105*, 349-354.
6. M. Heil, “Nectar: Generation, regulation and ecological functions”, *Trends Plant Sci.*, **2011**, *16*, 191-200.
7. M. Nepi, “Nectary structure and ultrastructure”, in “Nectaries and Nectar” (Ed. S. W. Nicolson, M. Nepi and E. Pacini), Springer, Dordrecht, **2007**, Ch.3.
8. G. L. Rivera, “Nectarios extranupciales florales en especies de Bignoniaceae de Argentina”, *Darwiniana*, **2000**, *38*, 1-10.
9. T. J. Wist and A. R. Davis, “Floral nectar production and nectary anatomy and ultrastructure of *Echinacea purpurea* (Asteraceae)”, *Ann. Bot.*, **2006**, *97*, 177-193.
10. E. S. A. Paiva and S. R. Machado, “The floral nectary of *Hymenaea stigonocarpa* (Fabaceae, Caesalpinioideae): Structural aspects during floral development”, *Ann. Bot.*, **2008**, *101*, 125-133.
11. M. C. Arizmendi, A. Valiente-Banuet, A. Rojas-Martínez and P. Dávila-Aranda, “Columnar cacti and the diets of nectar-feeding bats”, in “Columnar Cacti and Their Mutualists: Evolution, Ecology and Conservation” (Ed. T. H. Fleming and A. Valiente-Banuet), Arizona University Press, Tucson, **2002**, Ch.13.
12. A. Valiente-Banuet, M. C. Arizmendi, A. Rojas-Martínez, A. Casas, C. Silva, H. Godínez and P. Dávila-Aranda, “Biotic interactions and population dynamics of columnar cacti”, in “Columnar Cacti and Their Mutualists: Evolution, Ecology and Conservation” (Ed. T. H. Fleming and A. Valiente-Banuet), Arizona University Press, Tucson, **2002**, Ch.11.
13. S. Kluser and P. Peduzzi, “Global Pollinator Decline: A Literature Review”, United Nations Environment Programme, Geneva, **2007**.
14. P. A. Dávila, M. C. Arizmendi, A. Valiente-Banuet, J. L. Villaseñor, A. Casas and R. Lira, “Biological diversity in the Tehuacán-Cuicatlán Valley, Mexico”, *Biodiv. Conservat.*, **2002**, *11*, 421-442.
15. W. Gudiño, A. Casas, A. Valiente-Banuet, R. Orozco-Martínez and E. de la Barrera, “Climate and microenvironmental parameters affecting anthesis and nectar secretion for *Polaskia chende* and *P. chichipe*, endemic columnar cacti from the Tehuacán Valley, Puebla”, *J. Prof. Assoc. Cactus Devel.*, **2011**, *13*, 88-101.
16. Comisión Nacional de Áreas Naturales Protegidas, “Justificatory Study for the Establishment of the Biosphere Reserve Zicuirán Infiernillo” (in Spanish), Comisión Nacional de Áreas Protegidas, México City, **2006**.
17. A. G. Rodríguez-Oceguera, A. Casas, Y. Herreras-Diego and E. Pérez-Negrón, “Effect of habitat disturbance on pollination biology of the columnar cactus *Stenocereu quevedonis* at landscape-level in central Mexico”, *Plant Biol.*, **2013**, *15*, 573-582.
18. E. A. Anderson, “The Cactus Family”, Timber Press, Portland, **2002**.

19. M. de López-Curto, J. Márquez-Guzmán and G. Murguía-Sánchez, “Techniques for the Study of Angiosperm Development” (in Spanish), Universidad Nacional Autónoma de México, Mexico City, **2005**.
20. E. Pacini, M. Nepi and J. L. Vesprini, “Nectar biodiversity: A short review”, *Plant Syst. Evol.*, **2003**, 238, 7-21.
21. L. T. Durkee, “The ultrastructure of floral and extrafloral nectaries”, in “The Biology of Nectaries” (Ed. B. Bentley and T. S. Elias), Columbia University Press, New York, **1983**, Ch.1.
22. I. G. Varassin, D. S. Penneys and F. A. Michelangeli, “Comparative anatomy and morphology of nectar-producing Melastomataceae”, *Ann. Bot.*, **2008**, 102, 899-909.
23. L. Galetto and G. Bernardello, “Floral nectaries, nectar production dynamics and chemical composition in six *Ipomea* species (Convolvulaceae) in relation to pollinators”, *Ann. Bot.*, **2004**, 94, 269-280.
24. O. A. Montero-Alfaro, “Localización e histoquímica de nectarios florales en cactáceas”, *B.S. Thesis*, **2004**, Universidad Nacional Autónoma de México, Mexico.
25. M. Stpiczńska, K. L. Davies and A. Gregg, “Comparative account of nectary structure in *Hexisea imbricata* (Lindl.) Rchb.f. (Orchidaceae)”, *Ann. Bot.*, **2005**, 95, 749-756.
26. G. Goldstein and P. S. Nobel, “Changes in osmotic pressure and mucilage during low-temperature acclimation of *Opuntia ficus-indica*”, *Plant Physiol.*, **1991**, 97, 954-961.
27. D. B. Fisher and C. E. Cash-Clark, “Sieve tube unloading and post-phloem transport of fluorescent tracers and proteins injected into sieve tubes via severed aphid stylets”, *Plant Physiol.*, **2000**, 123, 125-138.
28. H. Lodish, A. Berk, S. L. Zipursky, P. Matsudaira, D. Baltimore and J. Darnell, “Molecular Cell Biology”, 6th Edn., H. Freeman and Co., New York, **2008**, Ch.18.
29. M. Nepi, E. Pacini and M. T. M. Willemse, “Nectary biology of *Cucurbita pepo*: Ecophysiological aspects”, *Acta Bot. Neerland.*, **1996**, 45, 41-54.
30. W. Gudiño, unpublished observations.

© 2015 by Maejo University, San Sai, Chiang Mai, 50290 Thailand. Reproduction is permitted for noncommercial purposes.

Full Paper

Defining the soil parameters for computing deformations caused by braced excavation

Linlong Mu^{1,2,3,*}, Richard J. Finno³, Maosong Huang^{1,2}, Taesik Kim⁴ and Kristi Kern³

¹ Department of Geotechnical Engineering, Tongji University, Shanghai, 200092, China

² Key Laboratory of Geotechnical and Underground Engineering of Ministry of Education, Tongji University, Shanghai, 200092, China

³ Department of Civil and Environment Engineering, Northwestern University, Evanston, IL, 60201, USA

⁴ Department of Civil Engineering, Hongik University, Seoul, Korea

* Corresponding author, e-mail: mulinlong@tongji.edu.cn

Received: 31 March 2014 / Accepted: 22 June 2015 / Published: 26 June 2015

Abstract: Evaluation of the soil response is required to estimate the potential building damage caused by excavations. Using proper soil parameters is a key ingredient when computing soil responses, assuming the model represents the actual soil response in a reasonable way. Soil parameters are usually identified from laboratory experiments performed on tube samples or from *in situ* tests, but large uncertainties are associated with these methods for most projects. Inverse analysis is a quantitative technique that allows one to select parameters to fit the responses of soil from both laboratory tests and field observations. The technique is applied to results of both the laboratory experiments on block and thin-walled tube samples and the field performance data, all of which were collected from an excavation made through Chicago clays. The results of computed soil responses based on the hardening soil (HS) model and the hardening soil with small strain (HSS) model found in the computer code Plaxis are compared to illustrate the problems that are likely to be encountered in practical application of finite element simulations. Guidance is provided for selecting the parameters from laboratory tests to compute the field responses for braced excavation loadings.

Keywords: braced excavation, soil parameters, finite element, small strain, stress probing test

INTRODUCTOIN

Many projects in geotechnical practice require a relatively accurate computation of ground deformations. For example, ground deformations are required when evaluating the damage potential arising from construction-induced deformations of structures and utilities surrounding deep supported excavations. It is generally recognised that the modelling of soil behaviour at small strain levels is required to estimate the excavation-induced ground settlement adjacent to excavations [1-5]. In many urban areas, buildings adjacent to excavations are supported by deep foundations. To estimate the potential damage to these foundations, it is also important to estimate soil movements below the ground surface. Considering the complex conditions around excavations, the finite element method (FEM) is commonly used to compute wall deflections and the distribution of ground movements. The use of an appropriate soil model and attendant parameters are the key ingredients for computing soil responses in these situations. Laboratory experiments are commonly used to select the soil parameters for design, but they are affected by sample quality and details of experiments, especially when the strain is small. Because of these inherent uncertainties, it is useful to understand the relationship between parameters based on both laboratory experiments and field observations.

The soil around an excavation is subjected to a variety of stress paths [6-8]. In general, the soil in front of a retaining wall is subjected to extension, whereas the soil behind a retaining wall is subjected to reduced compression. While it is the goal of a well-formulated constitutive model to represent the soil behaviour for all loading paths, this is rarely realised in practice. For a given soil model, the parameters based on laboratory experiments for these paths may differ, and these in turn may differ from those found from the best fit of various aspects of field performance data. Thus, it is useful to evaluate the difference in soil parameters based on these types of data, particularly in terms of models commonly used in practice. However, the inverse analysis is currently only used to calibrate the soil parameters of a soil model that did not consider the small strain behaviour based on field performance data.

In this paper inverse analysis is used to identify soil parameters for the hardening soil (HS) model and the hardening soil with small strain (HSS) model based on triaxial test results on specimens cut from thin-walled tube and block samples and on field performance data from the excavation at the Block 37 project in Chicago, IL, USA. The Block 37 project was a top-down construction project completed in an urban environment. The excavation commenced in 2007 and was completed in 2008. The models were chosen because they are found in a commonly used commercial finite element code and represent current practice in many areas. The relationship between the soil stiffness obtained from laboratory experiments and field observations is discussed in light of the different stress paths and strain levels aimed at defining the triaxial stress test most suited to calibrate the soil parameters that are most relevant to the simulation of an excavation system while considering the small strain behaviour of the soil.

PROCEDURE

Inverse Analysis

Inverse analysis techniques have been applied to geotechnical engineering problems and found to be useful for quantifying parameters and updating performance computations [9-11]. Herein, inverse analyses were used to find proper stiffness parameters for the HSS and HS models based on both triaxial test data and lateral movements measured during excavation. The inverse

analysis based on a gradient method was conducted by coupling the optimisation toolbox in the mathematical code Matlab with the finite element code Plaxis 9.0. Because Plaxis is a closed program, we can only input and output the data through the interface of the program. A macro program was written to read the calibration results from Matlab, which were then written into Plaxis through the interface of Plaxis. Next, the analysis results of the Plaxis program, which were subsequently written into Matlab, were also read by the macro program through the interface of Plaxis. The method used to find the best fit between the computed and observed values is defined by a weighted least-square objective function, $F(\mathbf{b})$:

$$F(\mathbf{b}) = [\mathbf{y} - \mathbf{y}'(\mathbf{b})]^T \boldsymbol{\omega} [\mathbf{y} - \mathbf{y}'(\mathbf{b})] \quad (1)$$

where \mathbf{b} is a vector containing values of the number of parameters to be estimated, \mathbf{y} is the vector of the observations being matched by the regression, $\mathbf{y}'(\mathbf{b})$ is the vector of the computed values that correspond to the observations and $\boldsymbol{\omega}$ is the weight matrix. As Calvello [11] described, the weighting is used to reduce the influence of observations that are less reliable and increase the influence of observations that are more reliable. In this work a diagonal weight matrix is used. The weight of every observation, ω_{ii} , is equal to the inverse of its error variance $\omega_{ii} = \frac{1}{\sigma_i^2}$. When analysing the triaxial test results, the standard deviation, σ_i , is

$$\sigma_i = \frac{\varepsilon_i}{1.96} \quad (2)$$

where ε_i is the measurement error of the observations (stress, pore pressure and volumetric strain) in the laboratory tests. In the excavation analysis using inclinometer data as observations, $\sigma_i = 0.0001d_i$, where d_i is the distance from the bottom of the inclinometer casing.

The objective function values $F(\mathbf{b})$ quantitatively describe how well the computed results based on the optimised parameters fit the test results. A lower $F(\mathbf{b})$ value indicates a better fit.

Soil Model

The behaviour of the HSS model is determined by 13 parameters: ϕ (friction angle), c (cohesion), R_f (failure ratio), Ψ (dilatancy angle), ν_{ur} (Poisson's ratio), K_0 (static earth pressure coefficient at rest), OCR (over-consolidation ratio), E_{50}^{ref} (secant stiffness in standard drained triaxial test), E_{oed}^{ref} (tangent stiffness for primary odometer loading), E_{ur}^{ref} (unloading-reloading stiffness), m (power for stress-level dependency of stiffness), G_0^{ref} (reference shear modulus at very small strains) and $\gamma_{0.7}$ (shear strain at which the secant shear modulus is equal to $0.772G_0$). The details of the parameters and model formulation are described by Schanz et al. [12] and Benz et al. [13]. Note that G_0^{ref} and $\gamma_{0.7}$ are added to define the small strain behaviour [13] and other eleven parameters are the same as those used to define the behaviour according to the HS model [12].

Of the 13 parameters, ϕ , c and R_f are the Mohr-Coulomb failure criteria parameters [12, 14]. The stiffness of the soil is determined in the HSS model by E_{50}^{ref} , E_{oed}^{ref} , E_{ur}^{ref} , m , G_0^{ref} and $\gamma_{0.7}$. E_{oed}^{ref} and E_{ur}^{ref} are computed as 0.7 and 3 times E_{50}^{ref} respectively. The dilatancy angle, Ψ , is individually defined in the HS and HSS models. Although the dilatancy angle is usually zero for normal to lightly over-consolidated soil, it is optimised herein as a check. G_0^{ref} can be computed as follows:

$$G_0^{ref} = G_0 \left(\frac{c \cos \phi - \sigma'_3 \sin \phi}{c \cos \phi + p^{ref} \sin \phi} \right)^{-m} \quad (3)$$

where σ'_3 is the horizontal effective stress, p^{ref} is the reference stress and G_0 is shear modulus at very small strains that can be computed by:

$$G_0 = \rho v^2 \quad (4)$$

where ρ is the density of the soil and v is shear wave propagation velocity through soil medium. This velocity can be evaluated from bender element tests in the laboratory. A bender element consists of two piezoceramic plates bonded together in parallel with a brass electrode plate in between. They are typically mounted on the base and top of the soil specimen as miniature cantilever beams. When excited by an input voltage, the source bender element bends, emitting a shear wave which travels through the soil specimen at shear wave velocity. The wave motion causes the receiver element to mechanically vibrate, which results in a voltage signal that is captured by a high-speed digital acquisition system. The shear wave velocity is calculated by determining the travel time of the shear wave between the tips of the source and receiver elements. In the field this velocity can be obtained by performing seismic cone penetration test (SCPT) that is equipped with a velocity geophone to measure shear wave propagation velocity. Both the bender element tests and SCPT were conducted to evaluate the shear wave propagation velocity at the site. The details of the tests were described by Kim [15].

One cannot use the inverse analysis to simultaneously compute the soil responses by optimising all 13 parameters. Thus, it is necessary to judiciously select the parameters to be optimised. As Calvello and Finno [16] showed for the HS model, the failure parameter, ϕ , and the stiffness parameters, m and E_{50}^{ref} , have the most impact on the computed values of lateral deformations measured close to a support wall of an excavation, based on the values of composite-scaled sensitivity. They also noted that m and E_{50}^{ref} are highly correlated parameters, and because one cannot simultaneously optimise parameters that have high correlation, E_{50}^{ref} was selected for optimisation because it is directly proportional to the soil stiffness. Details can be found in the work of Calvello and Finno [16]. Because this paper considers an excavation with relatively small deformations, which is a very practical application, the failure parameters were not optimised in the inverse analysis presented herein.

As seen in Figure 1, the shear wave velocities based on bender element tests on block samples reconsolidated against the *in situ* vertical effective stress with a 36-hour period of drained creep agree reasonably well with the shear wave velocities measured in the field using SCPT. (Detailed results of the tests can be found in Kim's work [15].) As such, G_0^{ref} is relatively well-defined in the laboratory and *in situ* for these clays and can be used to represent the maximum stiffness of the soil. Herein, the value of G_0^{ref} calculated from the bender element test results was used in the inverse analysis. Thus, three individual parameters, E_{50}^{ref} , Ψ and $\gamma_{0.7}$, were chosen for optimisation based on the triaxial test results. The remaining parameters were set to reasonable values based on site-specific data and parameters obtained from the inverse analysis of the Chicago State excavation project [11].

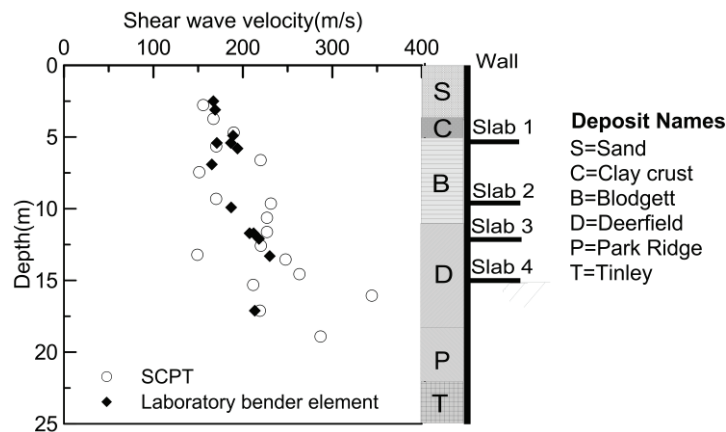


Figure 1. Measured shear wave velocity based on SCPT and bender element tests

CASE STUDY

Block 37 Project

The case study analysed herein is the Block 37 project located in downtown Chicago [17]. The excavation was approximately 110 m long and 110 m wide and was made through compressible soft-to-medium-stiff glacial clay to a depth of 15 m using a partial top-down construction technique. An existing freight tunnel was approximately 3 m away from the excavation near the retaining wall. A reinforced concrete-slurry wall and four concrete slabs were installed to laterally support the excavation.

The subsurface soil profile of Block 37 is shown in Figure 2. The geology and typical geotechnical characteristics of these deposits were presented by Finno and Chung [18]. The groundwater level was at a depth of 4 m below ground surface. The interior of the excavation was potholed to remove the old shallow foundations and then refilled prior to excavation. Inclinerometers were installed around the perimeter to record the slurry wall and the soil movements behind the wall, as shown in Figure 3.

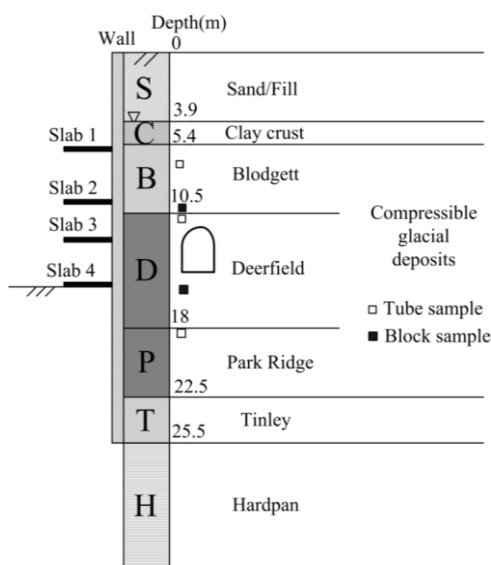


Figure 2. Soil profile of Block 37

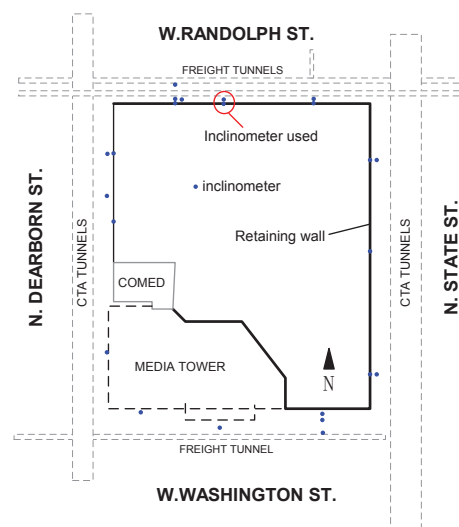


Figure 3. Inclinerometer locations around Block 37

Triaxial Testing Program

Thin-walled, 71-mm-diameter tube samples and hand-cut block samples were obtained from the compressible glacial deposits at the site at the depths shown in Figure 2. Triaxial experiments were conducted at Northwestern University using specimens cut from the tube samples and block samples. Complete details of the experimental program can be found in the work of Kim [15]. The specimens were K_0 -consolidated to *in situ* stresses and then subjected to an approximately 36-hr drained creep period under constant effective stress until the axial strain was less than 0.001%/hr. Thereafter, the specimens were sheared along one of the stress paths in Figure 4, which shows a plot of the mean effective stress, p' , against the deviator stress, q , with p' and q defined as:

$$p' = (\sigma'_a + 2\sigma'_r) / 3 \quad (5)$$

$$q = \sigma'_a - \sigma'_r \quad (6)$$

where σ'_a is the effective axial stress and σ'_r is the effective radial stress. From Figure 4, undrained TC and RTE tests were conducted on both the specimens from tube samples and those cut from blocks, while drained CMS, CMSE and CQU tests were conducted on specimens cut from blocks.

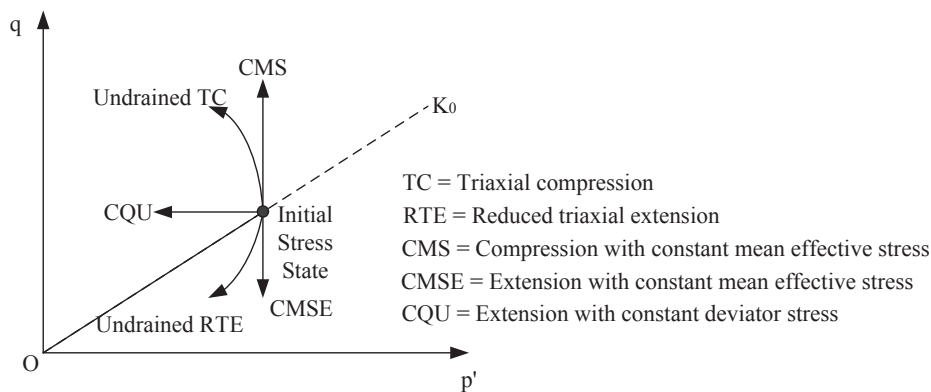


Figure 4. Stress probing paths of laboratorial triaxial tests

The internal deformations were measured using a pair of subminiature linear variable differential transformers mounted on the side of the specimen with a spring-loaded caliper placed around the centre of the specimen. The internal measurement system could resolve as small as 0.002% of axial strains, which is approximately the lower limit of small strain behaviour, as defined by Atkinson et al. [19]. Bender elements were incorporated into the system to allow the determination of G_0 , as noted previously.

Figure 5 summarises the stress-strain responses obtained from the triaxial tests of samples from all three strata. These results form the basis of the laboratory observations used to quantitatively optimise the soil parameters. Both drained and undrained results are shown. The specimens were cut from blocks obtained in the softer Blodgett and Deerfield strata. Thin-walled tube samples were obtained from all three strata. The data plotted at this scale illustrate that the block specimens yielded stiffer and stronger responses than that of the tube specimens.

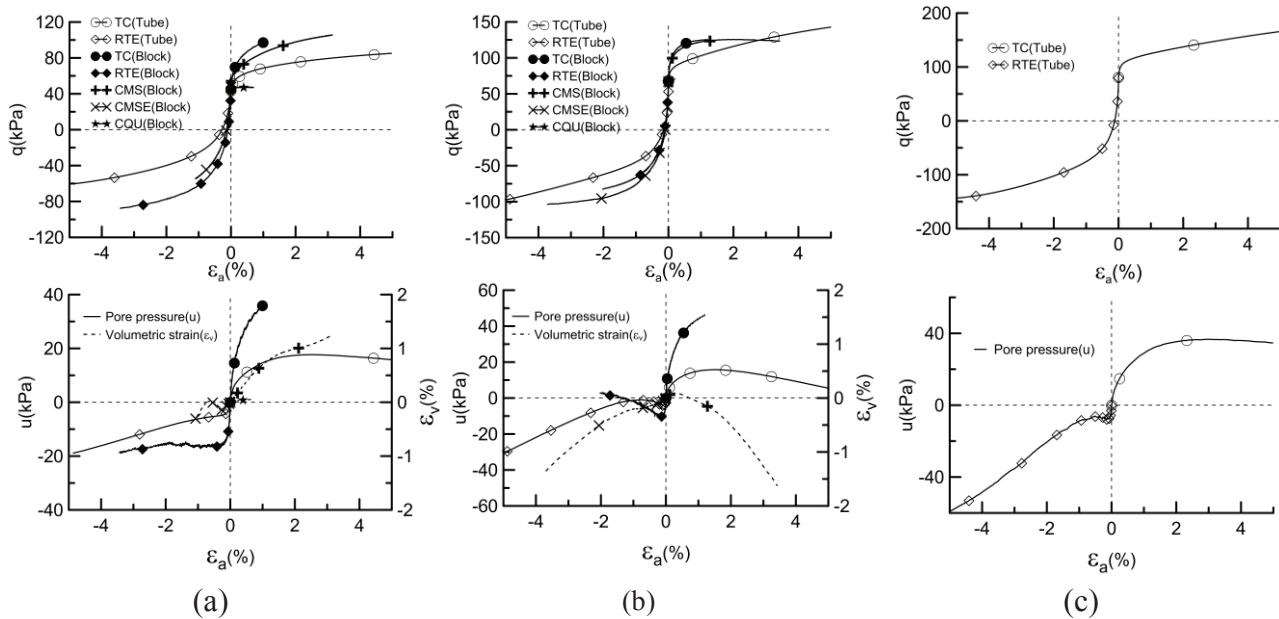


Figure 5. Results of triaxial tests: (a) Blodgett; (b) Deerfield; (c) Park Ridge

Observed Lateral Deformation Adjacent to Block 37 Excavation

The excavation process at Block 37 project was divided into five stages, as summarised in Table 1. The data from an inclinometer located 1 m behind the wall were typical of the responses during the excavation and were used as observations for the inverse analysis. This inclinometer was located near the centre of the north wall of the excavation where essentially no end restraints existed. Hence the behaviour at this location was plane strain and was simulated as such. Figure 6 shows the lateral ground deformations that developed immediately behind the wall during the excavation. As seen from the results, it is important to consider potholing in the simulation of the excavation because as much as 10 mm of wall deformation was induced by the potholing and refilling. Most of the subsequent deformations occurred during the first stage, when a 6.2-m cut was made prior to the placing of any lateral support.

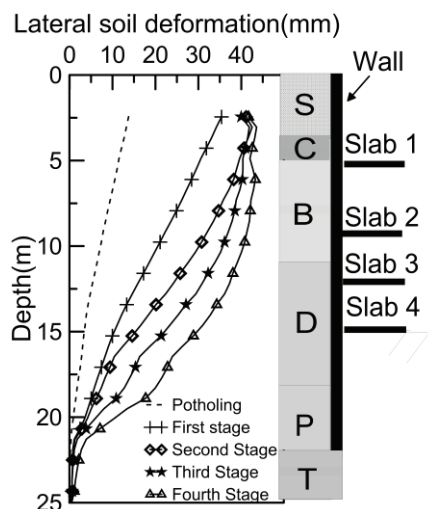


Figure 6. Measured lateral deformations of the soil 1 m behind the wall

Table 1. FEM simulation phases and activations of Block 37

Stage	Phase	Activation
0	1	Freight tunnel installation
	2	Consolidation
	3	Wall installation
	4	Resetting displacements
	5	Potholing
	6	Refilling
1	7	Dewatering and excavating to 6.2 m
	8	B1 slab installation
2	9	Dewatering and excavating to 9.8 m
	10	B2 slab installation
3	11	Dewatering and excavating to 12.2 m
	12	B3 slab installation
4	13	Dewatering and excavating to 15 m
	14	B4 slab installation

The lateral support was provided by reinforced concrete slabs which were attached to the wall with a moment-resisting connection. Thus, the slabs might pull the wall into the excavation after they were poured due to shrinkage or creep of the concrete since these slabs were firmly connected to the wall as soon as they were placed. Consequently, the deformation recorded at stage 1 was more likely to represent that which was induced by the excavation than those at the other stages since shrinkage or creep of the concrete was likely to induce additional deformations during the excavation process.

CALIBRATION OF SOIL MODEL

Inverse Analysis of Triaxial Data

To optimise the parameters for the triaxial test results, the principal stress differences and excess pore water pressures versus the axial strain were selected as observations for the undrained tests, while the principal stress differences and volumetric strain versus the axial strain were chosen as observations for the drained tests. The number of points that served as observations varied depending on the strain to failure and the model type. For the HSS model, the curves were discretised for the inverse analysis by considering one observation point every 0.005% of the axial strain between 0.001-0.1%, every 0.05% between 0.1-1%, and every 0.5% between 1% and failure strain. Only the data where axial strains were larger than 0.5% were used to optimise the HS parameters because the model does not have the capability to replicate very small strain behaviour. Because of the different numbers of data points used for the various tests, the computed objective function in equation (1) was normalised by the number of data points used in each optimisation ($F'(b)$) as a means to easily evaluate the relative fit.

The values of the HS parameters used to start the optimisation were those found by Calvello [11], based on the field performance of a Chicago State excavation project located approximately 1 km from Block 37 site. In addition to these same initial parameters, G_0^{ref} was calculated by equations (3) and (4), and $\gamma_{0.7}$ was set at 0.001%.

To illustrate the best fits obtained from the optimisation, Figure 7 shows the computed and measured stress-strain responses of the undrained TC and RTE tests and the drained CMS and CMSE tests of the Blodgett specimens at a conventional scale. The computed results are those based on the optimised parameters of the HSS model for each test. Also shown next to each curve are the values of the normalised objective function, $F'(b)$. The HSS model is found to be limited in its capacity to represent the responses of excess pore pressure in the RTE tests, given the poor fit and large $F'(b)$ value. In contrast, the other results are well represented by the HSS model using the optimised parameters. The results of simulations for specimens from the other two strata also exhibit the same trends.

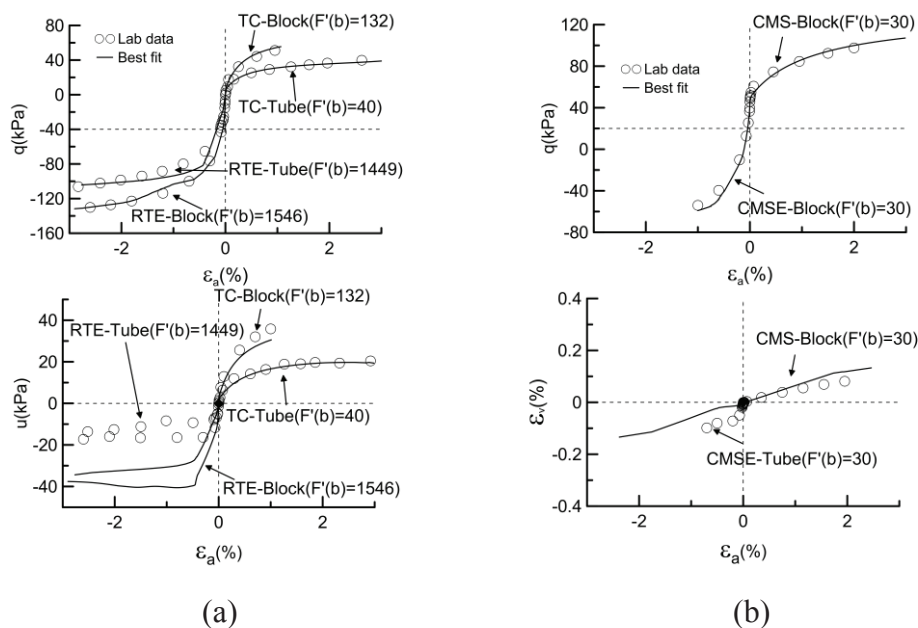


Figure 7. Comparison of best fit responses to laboratory responses of triaxial test for Blodgett specimens: (a) q - ϵ_a and u - ϵ_a curves of undrained TC and RTE; (b) q - ϵ_a and ϵ_v - ϵ_a curves of drained CMS and CMSE

To better illustrate the small strain variations, Figure 8 shows the results of the same tests in Figure 7, but they are plotted as normalised secant shear stiffness versus the log of shear strain. The shear strain is defined as $2(\epsilon_a - \epsilon_r)/3$, where ϵ_a is the axial strain and ϵ_r is the radial strain. The secant shear stiffness is normalised by the G_0 value determined from the bender element tests performed at the end of consolidation and from the drained creep in each test. As indicated in Figure 8, the initial stiffness based on the on-specimen instrumentation from the extension tests was larger than that from the triaxial compression tests. The initial stiffness of the extension tests was much closer to that measured from the bender elements, which is consistent with the results reported in many references [20-22]. Kung et al. [21] and Finno and Cho [22] indicated that the smaller values in the compression results are likely to arise from insufficient strain accuracy of capturing the elastic behaviour of the soil. Note that the differences in the maximum values of G_{sec}/G_0 between those measured from extension tests and compression tests using block samples were smaller than those based on the tube sample results. This result is a direct measure of the better sample quality obtained from the blocks when compared to the tube samples.

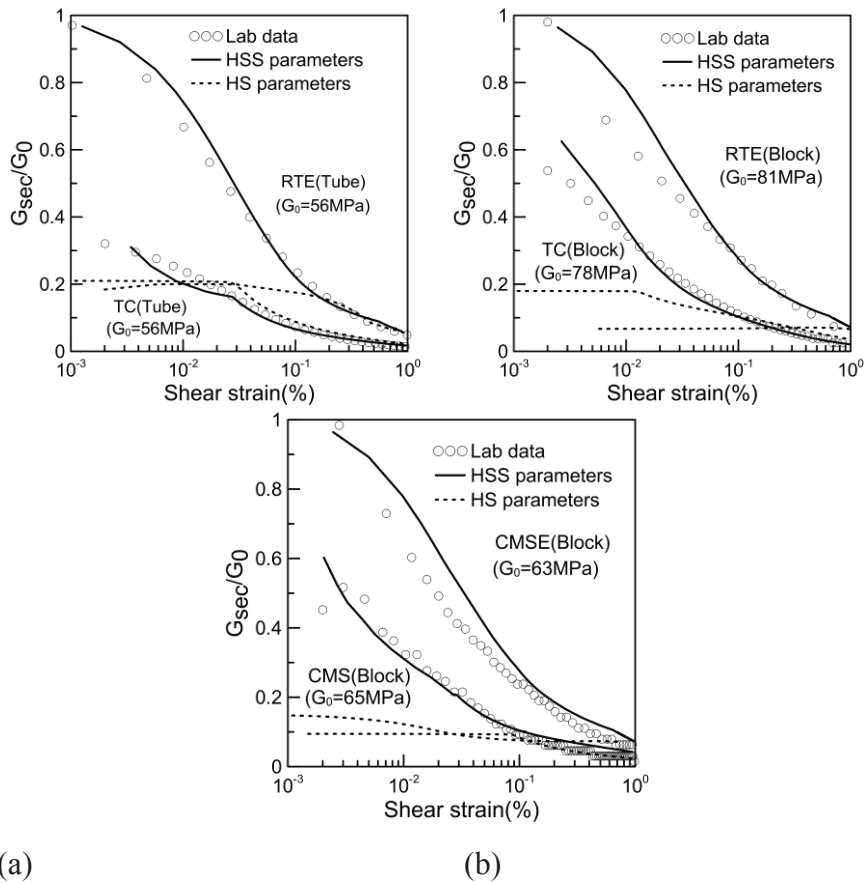


Figure 8. Comparison of computed (with optimised parameters) and measured stiffness-strain responses at small strain level for Blodgett specimens: (a) TC and RTE (tube sample); (b) TC and RTE (block sample); (c) CMS and CMSE

In the TC (block) test the soil stiffness at the small strain level was closer to that in the field than that based on the TC (tube) results; the value of $\gamma_{0.7}$ based on RTE tests for Chicago clay [15] was found to be in the order of 0.01% while $\gamma_{0.7}$ was smaller than 0.001% in the TC tests. This latter value could not be measured in the laboratory using the internal instrumentation used in this study. In any case, after optimisation, the HSS model can represent the responses reasonably well. Table 2 summarises the values of the optimised HSS and HS parameters and the normalised objective function values for each of the triaxial tests. As presented in Figure 7 and Table 2, an $F'(b)$ value smaller than approximately 150 indicates a reasonable fit. As illustrated with the Blodgett data, the HSS model, even using optimised parameters, cannot represent the soil behaviour in the RTE and CQU modes of shearing for any of the specimens ($F'(b) > 1000$).

Table 2. Optimised HSS and HS parameters for triaxial tests

Sample	Test	HSS model					HS model		
		ψ	$E_{50}^{ref} (kPa)$	$\gamma_{0.7}$	$F'(b)$	$\gamma_{0.7}(Lab)^2$	ψ	$E_{50}^{ref} (kPa)$	$F'(b)$
Blodgett Tube	TC	1	8700	4.21E-06	40	<1.00E-6	0.2	7900	230
	RTE	10	3600	7.32E-05	1449	7.00E-5	13	3800	2102
Blodgett Block	TC	0.2	7800	1.21E-05	132	<1.00E-6	0.1	8600	423
	RTE	2.3	3600	7.56E-05	1546	7.00E-5	6	3200	1870
	CMS	0.8	5900	2.48E-05	30	<1.00E-6	0	5100	100
	CMSE	0.1	2900	3.97E-05	30	8.00E-5	1	3200	121
	CQU	1.2	4000	1.13E-04	1025	-	7	7600	46
Deerfield Tube	TC	3.4	10800	3.70E-06	41	<1.00E-6	2.5	14000	131
	RTE	0.4	3000	6.74E-05	374	8.00E-5	20	3400	2456
Deerfield Block	TC	0.1	7800	1.36E-05	142	1.00E-6	0.1	11000	170
	RTE	0.4	3400	5.82E-05	3715	1.00E-4	1	3800	4121
	CMS	0.5	5400	1.35E-05	55	3.00E-6	0	11000	111
	CMSE	0.7	3300	7.84E-05	36	1.00E-4	0.1	3200	143
	CQU	0.7	1900	2.34E-04	7271	-	-	-	-
Park Ridge Tube	TC	0.8	8500	5.91E-06	47	<1.00E-6	2.6	5600	67
	RTE	9	4000	7.40E-05	2582	8.00E-5	10	4300	4234

Note: 1) $p^{ref}=100$ kPa; 2) $\gamma_{0.7}(Lab)$ refers to $\gamma_{0.7}$ estimated from laboratory tests.

It can be recalled that the three individual parameters, E_{50}^{ref} , Ψ and $\gamma_{0.7}$, were optimised for each triaxial result. The values of Ψ are usually smaller than 1, which is consistent with the Chicago clay being lightly overconsolidated. Exceptions include the RTE data for the Blodgett (tube sample) and the Park Ridge specimens. The overestimation of Ψ in the RTE tests arises from the poor fit of the excess pore pressures.

The values of E_{50}^{ref} from the TC tests are similar to Cavello’s results [11], based on drained TC tests. These values are approximately 2 to 3 times the value of E_{50}^{ref} determined from the extension tests. The reason for this apparent discrepancy is illustrated in Figure 9, which shows the computed stress-strain results from the simulations of the TC and RTE tests following two pre-shear stress paths, K_0 consolidation (K_0) and isotropic consolidation (I). The optimised parameters from the TC (block) Blodgett specimen were used for all four simulations, as shown in Figure 9. Normally, in the HS and HSS models, E_{50}^{ref} is defined based on isotropically consolidated drained TC tests. After isotropic consolidation, E_{50}^{ref} is used to calculate the soil responses in both I-TC and I-RTE test simulations because both paths are “loading” paths. One can note the same value of stiffness in both modes of shear for the isotropic consolidation results. In contrast, after K_0 consolidation, whereas E_{50}^{ref} is used to calculate the soil response in a K_0 -TC (loading) path, E_{ur}^{ref} is used to calculate the soil response in the K_0 -RTE (unloading) path. When optimising parameters based on the K_0 -RTE test results, E_{ur}^{ref} , defined as $3E_{50}^{ref}$, is really the operative stiffness because of the unloading in the test. Thus, the optimised E_{50}^{ref} based on the analysed extension tests should be one-third of the E_{50}^{ref} from the compression tests. The optimized E_{50}^{ref} values from the extension

tests presented in Table 2 generally are one-half to one-third of those based on the compression tests. Thus, one should not use extension tests to find the E_{50}^{ref} values using this optimisation method.

A comparison between the optimised and observed $\gamma_{0.7}$ values is also presented in Table 2. The values of $\gamma_{0.7}$ obtained from inverse analysis are similar to the experimental $\gamma_{0.7}$ values for the extension tests, which provided the entire modulus reduction curve. The $\gamma_{0.7}$ values for the TC tests cannot be extracted from the data in Figure 8, but those obtained from the inverse analysis suggest that they are smaller than 0.0001%, which, again, is too small to be measured with the internal instrumentation. This trend arises because the G_0 parameters in the HSS model were taken from bender element results rather than the maximum value of shear stiffness from the internal instrumentation. Because the HSS model does not allow for a different value of $\gamma_{0.7}$ based on the direction of loading or, more specifically, based on recent stress history [22], this type of response was not replicated in the model.

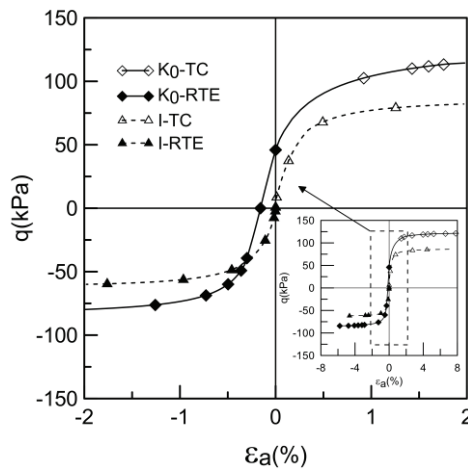


Figure 9. Plot of q versus ε_a : simulations of the TC and RTE tests using Blodgett TC (block) parameters in Table 2

Finally, as presented in Table 2, the optimised values of E_{50}^{ref} are not the same for the HS and HSS models. Apparently, one should use caution if the HS-based stiffness values are used directly with the two small strain parameters in the HSS model.

Inverse Analysis of Braced Excavation

Table 1 summarises the simulation phases in Plaxis defined to represent the major construction activities during the excavation of Block 37. Details of the simulation can be found in the work of Kern [17]. An interface was modelled between the wall and the soil. Freight tunnel construction (see Figure 2) and potholing were simulated to reflect the effects of these activities on the soil stresses before excavation began. Unfortunately, it was difficult to simulate the potholing properly when the potholes were excavated in the field to unknown dimensions. Site photographs provided approximate dimensions of these activities along the north wall. To minimise the errors related to the potholing simulation and the shrinkage and creep of concrete in the floor slab that provided lateral support, the incremental deformation induced by excavation at stage 1 was used as observations in the inverse analysis to optimise the soil parameters. Herein, the incremental deformation at stage 1 minus the deformation measured at the potholing stage was defined as

deformation at stage 1'. The inclinometer data obtained within the Blodgett, Deerfield and Park Ridge layers were used to optimise the parameters for those deposits.

The Blodgett, Deerfield and Park Ridge layers were modelled as both HS and HSS materials, and the remaining strata were modelled as HS materials. The soil stiffness parameters E_{50}^{ref} and $\gamma_{0.7}$ were optimised in the inverse analysis of the excavation. The initial small strain parameters, $\gamma_{0.7}$, for each layer were estimated based on the inverse analysis of laboratory tests with the lowest value of $F'(b)$.

Figure 10 illustrates a comparison of the computed deformations and the observed deformations, where the former are based on the optimised HSS and HS parameters. As expected, the computed deformations based on the optimised parameters agree well with the measured deformations at the first stage. The optimised HSS and HS parameters are used to compute the wall deformations at the final excavation stage. Figure 10 also shows that the computed wall deformations at the final excavation stage using optimised HSS parameters are as much as 10 mm smaller than the measured deformations above the bottom of the excavation. However, below the bottom of the excavation, the computed deformations are much more consistent with the measured ones. This discrepancy is likely to be due to the shrinkage and creep of the concrete slab, which was not considered in the simulation of the excavation [17]. The calculated wall deformation using the HS model is smaller than the measured deformation both below and above the bottom of the excavation because the stiffness of the soil was overestimated to fit the deformation at the first stage when the deformations were relatively small and the ground strains were very small. The advantage of using a model with small strains is clear because of its capabilities to allow for use of the appropriate stiffness for a wider range of strains.

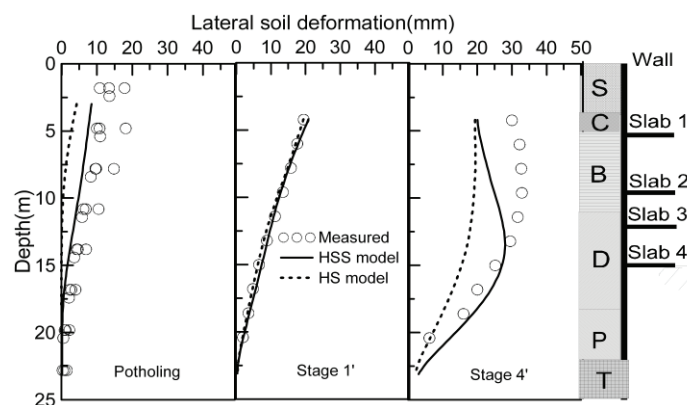


Figure 10. Comparison of computed and measured lateral soil deformations using optimised parameters

Table 3 presents the optimised parameters based on the inclinometer data from the excavation at stage 1'. The values of E_{50}^{ref} optimised from the inclinometer data using the HSS model are close to those optimised based on undrained TC results of the block samples of the Blodgett and Deerfield strata. The optimised E_{50}^{ref} values for the HS model are larger than those for the HSS model. This difference is expected when the deformation is relatively small because the full range of stiffness is not considered in the HS model and a higher value is required to result in a smaller deformation.

Table 3. Optimised parameters for HSS and HS models based on data from excavation

	HSS model		HS model
	$E_{50}^{ref} (kPa)$	$\gamma_{0.7}$	$E_{50}^{ref} (kPa)$
Blodgett	8200	7.64×10^{-5}	10000
Deerfield	7600	6.56×10^{-5}	14000
Park Ridge	12700	7.21×10^{-5}	32000

Note: $p^{ref} = 100 \text{ kPa}$

The optimised values of $\gamma_{0.7}$ are close to those optimised based on the extension tests. The reasons for this similarity might be the insufficient strain accuracy to capture the elastic behaviour of soil in compression tests [21, 22] and also the chance that the soil in front the retaining wall, which was subjected to extension, may dominate the lateral wall deformation. Usually, when the properties of a laboratory sample are more similar to those of the sample in the field, a better sample quality is indicated. It can be recalled that the only difference between TC (block) and TC (tube) is the quality of the sample, while $\gamma_{0.7}$ from TC (block) is closer to $\gamma_{0.7}$ obtained from the *in situ* data, which indicates that the quality of the block sample is better than that of the tube sample. Figure 11 indicates that the soil deformations are strongly influenced by $\gamma_{0.7}$: the deformations decrease when $\gamma_{0.7}$ increases. Therefore, the small strain behaviour of the soil surrounding the excavation must be considered when one calculates soil deformations induced by the excavation.

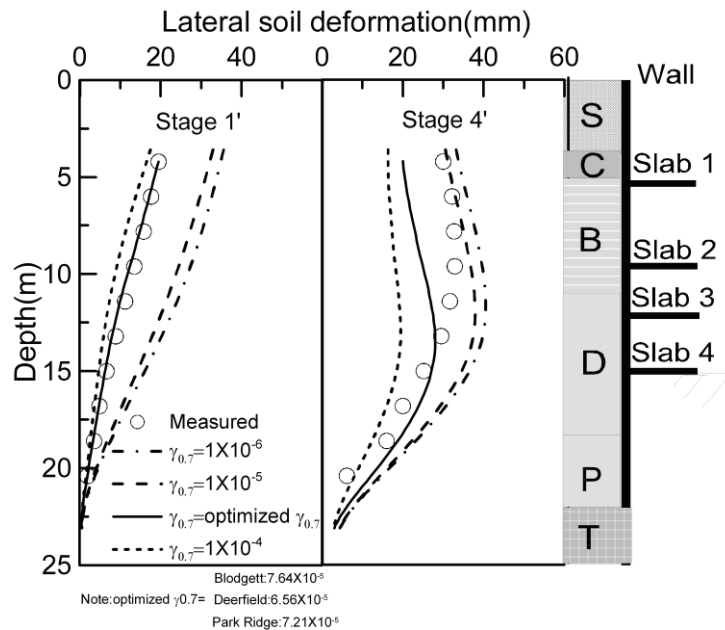


Figure 11. Computed lateral soil movement induced by excavation using different $\gamma_{0.7}$ values

CONCLUSIONS

Based on the results of the laboratory experiments, field observations and numerical simulations for the excavation of Block 37 through compressible Chicago glacial clays, the following conclusions can be drawn:

- (1) The HS and HSS models cannot describe the soil responses following different stress paths using a unique set of soil parameters. In particular, neither model can simulate the stress-strain responses from the CQU tests or the excess pore pressure responses of the RTE tests. In general,

with the use of proper parameters, the HSS model better represents the soil responses than does the HS model, both in the field and in the laboratory, especially at relatively small strain levels.

(2) The values of $\gamma_{0.7}$ optimised based on TC (block), compared with $\gamma_{0.7}$ optimised based on TC (tube), are closer to those optimised based on the *in situ* data, which reflects the higher quality of the block samples compared to the tube samples.

(3) The soil stiffness at small strain levels significantly influences the soil deformations induced by excavation, at least for the deformation levels encountered at Block 37 site, which is consistent with the observations of other researchers regarding the importance of small strain non-linearity.

(4) For the HSS and HS models, the values of E_{50}^{ref} optimised based on field performance data produce similar results to those obtained from the optimisation based on the TC results from block specimens. For the HSS model, $\gamma_{0.7}$ optimised based on performance data produces similar results to those obtained from $\gamma_{0.7}$ optimised based on RTE results.

(5) The optimised values of E_{50}^{ref} for the same stress path in the laboratory are not the same for the HS and HSS models. One should not use stiffness parameters derived from the HS model in the HSS model without evaluating the computed responses in light of the effects of the two small strain parameters

ACKNOWLEDGMENTS

The financial support for this work was provided by the National Science Fund of China through Grant No. 51208378 and by the National Science Foundation of USA through Grant No. CMMI-0928184.

REFERENCES

1. B. Simpson, N. J. O’Riordan and D. D. Croft, “A computer model for the analysis of ground movements in London clay”, *Géotechnique*, **1979**, 29, 149-175.
2. J. B. Burland, “The stiffness of soils at small strain”, *Can. Geotech. J.*, **1989**, 26, 499-516.
3. A. J. Whittle, Y. M. A. Hashash and R. V. Whitman, “Analysis of deep excavation in Boston”, *J. Geotech. Eng.*, **1993**, 119, 69-90.
4. S. E. Stallebras and R. N. Taylor, “The development and evaluation of a constitutive model for the prediction of ground movements in overconsolidated clay”, *Géotechnique*, **1997**, 47, 235-253.
5. L. C. Jen, “The design and performance of deep excavations in clay”, *PhD Thesis*, **1998**, Massachusetts Institute of Technology, USA.
6. R. J. Finno, I. S. Harahap and P. J. Sabatini, “Analysis of braced excavations with coupled finite element formulations”, *Comput. Geotech.*, **1991**, 12, 91-114.
7. C. W. W. Ng, “Stress paths in relation to deep excavations”, *J. Geotech. Geoenviron. Eng.*, **1999**, 125, 357-363.
8. Y. M. A. Hashash and A. J. Whittle, “Mechanisms of load transfer and arching for braced excavations in clay”, *J. Geotech. Geoenviron. Eng.*, **2002**, 128, 187-197.
9. C. Rechea, S. Lefvasseur and R. J. Finno, “Inverse analysis techniques for parameter identification in simulation of excavation support systems”, *Comput. Geotech.*, **2008**, 35, 331-345.

10. R. J. Finno and M. Calvello, "Supported excavations: Observational method and inverse modeling", *J. Geotech. Geoenviron. Eng.*, **2005**, *131*, 826-836.
11. M. Calvello, "Inverse analysis of a supported excavation through Chicago glacial clays", *PhD Thesis*, **2002**, Northwestern University, USA.
12. T. Schanz, P. A. Vermeer and P. G. Bonnier, "The hardening soil model--formulation and verification", Proceedings of Plaxis Symposium--Beyond 2000 on Computational Geotechnics, **1999**, Amsterdam, Netherlands, pp.281-296.
13. T. Benz, R. Schwab and P. Vermeer, "Small-strain stiffness in geotechnical analyses", *Bautechnik*, **2009**, *86*, 16-27.
14. J. F. Labuz and A. Zang, "Mohr-Coulomb failure criterion", *Rock Mech. Rock Eng.*, **2012**, *45*, 975-979.
15. T. Kim, "Incrementally nonlinear responses of soft Chicago glacial clays", *PhD Thesis*, **2011**, Northwestern University, USA.
16. M. Calvello and R. J. Finno, "Selecting parameters to optimize in model calibration by inverse analysis", *Comput. Geotech.*, **2004**, *31*, 410-424.
17. K. Kern, "Analysis of pseudo top-down construction in Chicago", *Master Thesis*, **2011**, Northwestern University, USA.
18. R. J. Finno and C. K. Chung, "Stress-strain-strength responses of compressible Chicago glacial clays", *J. Geotech. Eng.*, **1992**, *118*, 1607-1625.
19. J. H. Atkinson, D. Richardson and S. E. Stallebrass, "Effect of recent stress history on the stiffness of overconsolidated soil", *Géotechnique*, **1990**, *40*, 531-540.
20. R. J. Jardine, "Some observations on the kinematic nature of soil stiffness", *Soils Found.*, **1992**, *32*, 111-124.
21. G. T. C. Kung, C. Y. Ou and C. H. Juang, "Modeling small-strain behavior of Taipei clays for finite element analysis of braced excavations", *Comput. Geotech.*, **2009**, *36*, 304-319.
22. R. J. Finno and W. J. Cho, "Recent stress-history effects on compressible Chicago glacial clays", *J. Geotech. Geoenviron. Eng.*, **2011**, *137*, 197-207.

© 2015 by Maejo University, San Sai, Chiang Mai, 50290 Thailand. Reproduction is permitted for noncommercial purposes.

Full Paper

Some convolution properties of a subclass of p -valent functions

Khalida Inayat Noor and Nazar Khan *

Department of Mathematics COMSATS, Institute of Information Technology, Park Road Islamabad, Pakistan

* Corresponding author, e-mail: nazarmaths@gmail.com

Received: 15 January 2014 / Accepted: 24 June 2015 / Published: 3 July 2015

Abstract: In this paper we introduce and study a new subclass R_p of p -valent functions that are analytic in the open unit disk $E = \{z: |z| < 1\}$. Some interesting results by using convolution technique for this subclass R_p are obtained. Also, we point out some known consequences of our main results.

Keywords: analytic functions, p -valent functions, p -valently starlike functions, p -valently convex functions, convolution

INTRODUCTION

Let $A(p)$ denote the class of functions

$$f(z) = z^p + \sum_{n=1}^{\infty} a_{n+p} z^{n+p} \quad (p \in N = \{1, 2, \dots\}), \quad (1)$$

which are analytic and p -valent in the open unit disk $E = \{z: |z| < 1\}$. A function $f(z) \in A(p)$ is said to be p -valently starlike of order α ($0 \leq \alpha < p$) in E if and only if

$$\operatorname{Re} \left(\frac{zf'(z)}{f(z)} \right) > \alpha \quad (z \in E).$$

We denote the class of all p -valent starlike functions of order α by $S_p^*(\alpha)$. Further, a function $f(z) \in A(p)$ is said to be p -valently convex of order α ($0 \leq \alpha < p$) in E if and only if

$$\operatorname{Re} \left(1 + \frac{zf''(z)}{f'(z)} \right) > \alpha \quad (z \in E).$$

We denote by $C_p(\alpha)$ the subclass of $A(p)$, consisting of all p -valently convex functions of order α in E . It follows from the definition that if $f(z)$ is p -valently convex function, then $zf'(z)$ is p -valently starlike in E . The classes $S_p^*(\alpha)$ and $C_p(\alpha)$ were first introduced by Owa [1].

It is easy to see that $S_p^*(0) = S_p^*$ and $C_p(0) = C_p$ are, respectively, the classes of p -valently starlike and p -valently convex functions in E . We also note that $S_p^* = S^*$ and $C_1 = C$ are, respectively, the well-known classes of starlike and convex functions in E .

We say that a function

$$h(z) = 1 + \sum_{n=1}^{\infty} c_n z^n \quad (z \in E)$$

belongs to the class $P(\alpha)$ if $h(z)$ satisfies the following condition

$$Reh(z) > \alpha, \quad 0 \leq \alpha < 1 \quad (z \in E).$$

Let $f(z), g(z) \in A(p)$, where $f(z)$ is given by (1) and $g(z)$ is defined by

$$g(z) = z^p + \sum_{n=1}^{\infty} b_{n+p} z^{n+p} \quad (z \in E).$$

Then the Hadamard product (or convolution) $f * g$ of the functions $f(z)$ and $g(z)$ is defined by

$$(f * g)(z) = z^p + \sum_{n=1}^{\infty} a_{n+p} b_{n+p} z^{n+p} = (g * f)(z).$$

In recent years many interesting subclasses of analytic multivalent functions associated with the linear operator and their many special cases were investigated by, for example Liu [2] and Sokol et al. [3], and also by Arif et al. [4, 5] and others [e.g. 6-8] using convolution technique.

We now define the following:

Definition 1. A function $f(z)$ given by (1) is said to belong to the class R_p if

$$Re \left(\frac{f^{(p)}(z) + z f^{(p+1)}(z)}{p!} \right) > 0 \quad (z \in E, p \in N = \{1, 2, \dots\}), \quad (2)$$

where $f^{(p)}(z)$ is the p th derivative of $f(z)$.

As a special case, the class $R_1=R$ was studied by Singh and Singh [9] in 1989. Using essentially their technique and that of Lashin [10], we prove the main results for the class R_p , which is the main motivation of this paper.

PRELIMINARY RESULTS

Lemma 1 [11]. Let $\{d_n\}_0^{\infty}$ be a convex null sequence. Then the function

$$q(z) = \frac{d_0}{2} + \sum_{n=1}^{\infty} d_n z^n$$

is analytic in E and $Re q(z) > 0 \quad (z \in E)$.

Lemma 2 [12]. If $N(z)$ and $D(z)$ are analytic in E , $N(0) = D(0) = 0$, $D(z)$ is starlike in E and

$$Re \left(\frac{N'(z)}{D'(z)} \right) > 0, \quad \text{then} \quad Re \left(\frac{N(z)}{D(z)} \right) > 0 \quad (z \in E).$$

Lemma 3 [9]. If $h(z)$ is analytic in E , $h(0) = 1$ and $Reh(z) > \frac{1}{2} \quad (z \in E)$, then for any function F analytic in E , the function $h * F$ takes values in the convex hull of the image of E under F .

Lemma 4 [13]. Let $\beta < 1$. If the function $h(z)$ is analytic in E , with $h(0) = 1$, and

$$Re \left(h(z) + zh'(z) \right) > \beta \quad (z \in E).$$

Then

$$Reh(z) > (2\beta - 1) + 2(1 - \beta)\ln 2 \quad (z \in E).$$

The result is sharp.

Lemma 5 [14]. For $\alpha \leq 1$ and $\beta \leq 1$,

$$P(\alpha) * P(\beta) \subset P(\delta), \quad \delta = 1 - 2(1 - \alpha)(1 - \beta).$$

The result is sharp.

MAIN RESULTS

Theorem 1. Let $f(z) \in R_p$; then

$$Re \left(\frac{f^{(p)}(z)}{p!} \right) > -1 + 2\log 2 \quad (z \in E).$$

The constant $-1 + 2\log 2$ cannot be replaced by any larger one.

Proof. Let $f(z) \in R_p$; then we have

$$Re \left(\frac{f^{(p)}(z) + z f^{(p+1)}(z)}{p!} \right) > 0 \quad (z \in E),$$

which can be written as

$$Re \left(1 + \sum_{n=1}^{\infty} \frac{(p+n)!(n+1)}{p!n!} a_{p+n} z^n \right) > 0 \quad (z \in E), \tag{3}$$

or equivalently,

$$Re \left(1 + \frac{1}{2} \sum_{n=1}^{\infty} \frac{(p+n)!(n+1)}{p!n!} a_{p+n} z^n \right) > \frac{1}{2} \quad (z \in E). \tag{4}$$

Consider the function

$$h(z) = 1 + 2 \sum_{n=1}^{\infty} \frac{1}{n+1} z^n. \tag{5}$$

Clearly, $h(z)$ is analytic in E , $h(0) = 1$ and

$$\begin{aligned} Reh(z) &= Re \left(1 - \frac{2}{z} \{z + \log(1 - z)\} \right) \\ &> -1 + 2\log 2 \quad [15]. \end{aligned} \tag{6}$$

From (4) and (5) we obtain

$$\frac{f^{(p)}(z)}{p!} = \left(1 + \frac{1}{2} \sum_{n=1}^{\infty} \frac{(p+n)!(n+1)}{p!n!} a_{p+n} z^n \right) * \left(1 + 2 \sum_{n=1}^{\infty} \frac{1}{n+1} z^n \right),$$

from which it follows, in view of (4), (6) and Lemma 3, that

$$Re \left(\frac{f^{(p)}(z)}{p!} \right) > -1 + 2\log 2 \quad (z \in E).$$

The constant $-1 + 2\log 2$ cannot be replaced by any larger one, which follows from the fact that the function f_1 defined by $\frac{z f_1^{(p)}(z)}{p!} = -z - 2\log(1 - z)$ is in the class R_p .

Corollary 1 [9]. If $f(z) \in R$, then

$$Ref'(z) > -1 + 2\log 2 = 0.39... \quad (z \in E).$$

The constant $-1 + 2\log 2$ cannot be replaced by any larger one.

Theorem 2. Let $f(z) \in R_p$, then

$$Re \left(\frac{f^{(p-1)}(z)}{z} \right) > \frac{p!}{2} \quad (z \in E).$$

Proof. Since the sequence $\{d_n\}_0^\infty$ defined by $d_0 = 1, d_n = \frac{2}{(n+1)^2}, n \geq 1$ is a convex null sequence, using Lemma 1 we have

$$Re \left(1 + 2 \sum_{n=1}^{\infty} \frac{1}{(n+1)^2} z^n \right) > \frac{1}{2} \quad (z \in E). \tag{7}$$

We can write

$$\frac{f^{(p-1)}(z)}{p!z} = \left(1 + \frac{1}{2} \sum_{n=1}^{\infty} \frac{(p+n)!(n+1)}{p!n!} a_{p+n} z^n \right) * \left(1 + 2 \sum_{n=1}^{\infty} \frac{1}{(n+1)^2} z^n \right).$$

From (4), (7) and Lemma 3, we have the required result.

Theorem 3. Let $f(z) \in R_p$, then for every $n \geq 1$, the n^{th} partial sum of $f(z)$ satisfies $Re S_n^{(p)}(z, f) > 0, z \in E$ and hence $S_n(z, f)$ is p -valent in E .

Proof. From (3) and (5) we can write

$$\frac{S_n^{(p)}(z, f)}{p!} = \left(1 + \sum_{n=1}^{\infty} \frac{(p+n)!(n+1)}{p!n!} a_{p+n} z^n \right) * \left(1 + \sum_{n=1}^{\infty} \frac{1}{(n+1)} z^n \right). \tag{8}$$

Putting $z = re^{i\theta}$, $0 \leq r \leq 1$, $0 \leq \theta \leq \pi$, and using the minimum principle for harmonic functions with the result in the literature[16], we have

$$\begin{aligned} Re \left(1 + \sum_{n=1}^k \frac{z^n}{n+1} \right) &= Re \left(1 + \sum_{n=1}^k \frac{r^n e^{in\theta}}{n+1} \right) \\ &= Re \left(1 + \sum_{n=1}^k \frac{r^n}{n+1} (\cos n\theta + i \sin n\theta) \right) \\ &= 1 + \sum_{n=1}^k \frac{r^n}{n+1} \cos n\theta \quad (0 \leq \theta \leq \pi) \\ &= 1 + \sum_{n=1}^k \frac{\cos n\theta}{n+1} \geq \frac{1}{2}. \end{aligned} \tag{9}$$

Using (3), (8), (9) and Lemma 3, we deduce that $Re \left(S_n^{(p)}(z, f) \right) > 0, z \in E$. From the result given [17], we see that $S_n(z, f)$ is p -valent in E for every $n \geq 1$. If $p = 1$, then Theorem 2 and Theorem 3 were proved [9].

Theorem 4. If $f(z) \in A(p)$ and

$$Re \left(\frac{f^{(p)}(z) + z f^{(p+1)}(z)}{p!} \right) > -\frac{1}{4} \quad (z \in E), \tag{10}$$

then $f(z) \in S_p^*(p-1)$.

Proof. Let $f(z) \in A(p)$ given by(1). It follows from the hypothesis of the theorem that

$$Re \left(1 + \frac{2}{5} \sum_{n=1}^{\infty} \frac{(p+n)!(n+1)}{p!n!} a_{p+n} z^n \right) > \frac{1}{2} \quad (z \in E). \tag{11}$$

Also, the sequence $\{d_n\}_0^{\infty}$, where $d_0 = 1$ and $d_n = \frac{5}{2} \frac{1}{(n+1)^2}, n \geq 1$, is a convex null sequence such as

$$Re \left(1 + \frac{5}{2} \sum_{n=1}^{\infty} \frac{1}{(n+1)^2} z^n \right) > \frac{1}{2} \quad (z \in E). \tag{12}$$

From (11), (12) and Lemma 1, we obtain

$$\begin{aligned} Re \left(\frac{f^{(p-1)}(z)}{p!z} \right) &= Re \left(1 + \frac{2}{5} \sum_{n=1}^{\infty} \frac{(p+n)!(n+1)}{p!n!} a_{p+n} z^n \right) * \left(1 + \frac{5}{2} \sum_{n=1}^{\infty} \frac{1}{(n+1)^2} z^n \right) \\ &> \frac{1}{2} \quad (z \in E). \end{aligned} \tag{13}$$

Now we define a function $w(z)$ by

$$w(z) = \frac{z f^{(p)}(z) - f^{(p-1)}(z)}{z f^{(p)}(z) + f^{(p-1)}(z)},$$

which can be written as

$$\frac{zf^{(p)}(z)}{f^{(p-1)}(z)} = \frac{1+w(z)}{1-w(z)} \quad (z \in E). \tag{14}$$

Clearly, $w(0) = 0$. Since $f(z)$ is p -valent in E , we have $w(z) \neq 1$ in E . From (14) we obtain

$$\frac{f^{(p)}(z)+zf^{(p+1)}(z)}{p!} = \frac{f^{(p-1)}(z)}{p!z} \left(\left(\frac{1+w(z)}{1-w(z)} \right)^2 + \frac{2zw'(z)}{(1-w(z))^2} \right). \tag{15}$$

We claim that $|w(z)| < 1$ in E . If this is not true, then there exists a point $z_0 \in E$ such that

$$\max_{|z| \leq |z_0|} |w(z)| = |w(z_0)| = 1.$$

Then from the result given [18], we have

$$zw'(z_0) = kw(z_0), \text{ where } k \geq 1, w(z_0) = e^{i\theta}, 0 < \theta < 2\pi.$$

Putting $z = z_0$ in (15), we obtain

$$\begin{aligned} \operatorname{Re} \left(\frac{f^{(p)}(z_0)+z_0f^{(p+1)}(z_0)}{p!} \right) &= \operatorname{Re} \left(\frac{f^{(p-1)}(z_0)}{p!z_0} \left(\left(\frac{1+e^{i\theta}}{1-e^{i\theta}} \right)^2 + \frac{2ke^{i\theta}}{(1-e^{i\theta})^2} \right) \right) \\ &\leq -\frac{\cos\theta+1+k}{\cos\theta-1} \operatorname{Re} \left(\frac{f^{(p-1)}(z_0)}{z_0} \right) \\ &\leq -\frac{k}{2} \operatorname{Re} \left(\frac{f^{(p-1)}(z_0)}{z_0} \right) \\ &\leq -\frac{1}{4}. \end{aligned} \tag{16}$$

Since $k \geq 1$ and from (13), $\operatorname{Re} \left(\frac{f^{(p-1)}(z)}{p!z} \right) > \frac{1}{2}$, $z \in E$. Inequality (16) contradicts inequality (10); thus, $|w(z)| < 1$ in E . Equation (14) then implies that $f(z) \in S_p^*(p-1)$ [19].

Using the Alexander type relation, we obtain the following corollary.

Corollary 2. If $g(z) \in A(p)$ and

$$\operatorname{Re} \left(\frac{g^{(p)}(z)+3zg^{(p+1)}(z)+z^2g^{(p+2)}(z)}{p!} \right) > -\frac{1}{4} \quad (z \in E),$$

then $g(z) \in C_p(p-1)$.

Corollary 3 [9]. If $f(z) \in A$ and let

$$\operatorname{Re}(f'(z) + zf''(z)) > -\frac{1}{4} \quad (z \in E),$$

then $f(z) \in S^*$.

Our next result shows that the class R_p is closed with respect to Hadamard product.

Theorem 5. If $f(z)$ and $g(z)$ belong to the class R_p and

$$h^{(p-1)}(z) = f^{(p-1)}(z) * g^{(p-1)}(z),$$

then $h(z)$ also belongs to the class R_p .

Proof. Since

$$h^{(p-1)}(z) = f^{(p-1)}(z) * g^{(p-1)}(z),$$

it follows that

$$zh^{(p)}(z) = zf^{(p)}(z) * g^{(p-1)}(z).$$

A simple computation gives

$$\operatorname{Re} \left(\frac{h^{(p)}(z)+zh^{(p+1)}(z)}{p!} \right) = \operatorname{Re} \left(\left(\frac{f^{(p)}(z)+zf^{(p+1)}(z)}{p!} \right) * \left(\frac{g^{(p-1)}(z)}{p!z} \right) \right). \tag{17}$$

From (17), using (1), (13) and Lemma 3, we have the desired result.

Corollary 4 [9]. If $f(z) = z + \sum_{n=2}^{\infty} a_n z^n$ and $g(z) = z + \sum_{n=2}^{\infty} b_n z^n$ belong to R , then their Hadamard product

$$h(z) = (f * g)(z)$$

also belongs to R .

From the proof of Theorem 5, it is clear that the following more general result holds.

Theorem 6. If $f(z) \in R_p$, $g(z) \in A(p)$ and $Re\left(\frac{g^{(p-1)}(z)}{p!z}\right) > \frac{1}{2}$, $z \in E$, then

$$f^{(p-1)}(z) * g^{(p-1)}(z)$$

also belongs to the class R_p .

Theorem 7. Let $f(z) \in R_p$. Then $Re(f^{(p)}(z)) > 0$, $z \in E$ and hence $f(z)$ is p -valent in E .

Proof. Using the result given [17] and applying Lemma 2 with $N(z) = \frac{zf^{(p)}(z)}{p!}$ and $D(z) = z$ proves Theorem 7. If $p = 1$, then Theorem 7 was proved earlier [20].

Ruscheweyh and Small [21] have proved that the class C is closed with respect to Hadamard product. In what follows we prove that the Hadamard product of functions of the class R_p belongs to the class $C_p(\alpha)$.

Theorem 8. If $f(z)$ and $g(z)$ belong to R_p and

$$h^{(p-1)}(z) = f^{(p-1)}(z) * g^{(p-1)}(z),$$

then $h(z) \in C_p(p - 1)$.

Proof. In view of Corollary 3, it is sufficient to show that

$$Re\left(\frac{h^{(p)}(z) + 3zh^{(p+1)}(z) + z^2h^{(p+2)}(z)}{p!}\right) > -\frac{1}{4} \quad (z \in E).$$

Equivalently, this can be written as

$$Re\left(1 + \sum_{n=1}^{\infty} (n+1) \left(\frac{(n+p)!}{n!p!}\right)^2 a_{n+p} b_{n+p} z^n\right) > -\frac{1}{4} \quad (z \in E). \tag{18}$$

Since $f(z), g(z) \in R_p$, we have

$$Re\left(1 + \frac{1}{2} \sum_{n=1}^{\infty} \frac{(n+p)!(n+1)}{p!n!} a_{n+p} z^n\right) > \frac{1}{2} \quad (z \in E),$$

and

$$Re\left(1 + \frac{1}{2} \sum_{n=1}^{\infty} \frac{(n+p)!(n+1)}{p!n!} b_{n+p} z^n\right) > \frac{1}{2} \quad (z \in E).$$

Using Lemma 3, we obtain

$$Re\left(1 + \frac{1}{4} \sum_{n=1}^{\infty} (n+1)^2 \left(\frac{(n+p)!}{n!p!}\right)^2 a_{n+p} b_{n+p} z^n\right) > \frac{1}{2} \quad (z \in E). \tag{19}$$

Consider the function

$$h(z) = \left(1 + 4 \sum_{n=1}^{\infty} \frac{1}{n+1} z^n\right). \tag{20}$$

Clearly, $h(z)$ is analytic in E , $h(0) = 1$ and

$$\begin{aligned} Re\left(1 + 4 \sum_{n=1}^{\infty} \frac{1}{n+1} z^n\right) &= Re\left(-3 - \frac{4}{2} \log(1-z)\right) \\ &> -3 + 4 \log 2 \text{ [15]} \\ &> -\frac{1}{4} \quad (z \in E). \end{aligned} \tag{21}$$

From (19) and (20), we can write

$$\begin{aligned} & \left(1 + \sum_{n=1}^{\infty} (n+1) \left(\frac{(n+p)!}{n!p!}\right)^2 a_{n+p} b_{n+p} z^n\right) \\ &= \left(1 + \frac{1}{4} \sum_{n=1}^{\infty} (n+1)^2 \left(\frac{(n+p)!}{n!p!}\right)^2 a_{n+p} b_{n+p} z^n\right) * \left(1 + 4 \sum_{n=1}^{\infty} \frac{1}{n+1} z^n\right). \end{aligned} \tag{22}$$

Using (19), (21), (22) and Lemma 3, we see that (18) holds for all $z \in E$. This completes the proof.

Corollary 5 [9]. If $f(z) = z + \sum_{n=2}^{\infty} a_n z^n$ and $g(z) = z + \sum_{n=2}^{\infty} b_n z^n$ belong to R , then

$$h(z) = (f * g)(z) \in C.$$

We now define the integral operator $F(z)$ as follows. Let $f(z) \in A(p)$; then

$$\begin{aligned} \frac{F^{(p-1)}(z)}{p!} &= \frac{c+1}{z^c} \int_0^z t^{c-1} \left(\frac{f^{(p-1)}(t)}{p!}\right) dt, \quad (c > -p, p \in N = \{1, 2, \dots\}). \\ &= z + \sum_{n=1}^{\infty} \frac{(c+1)(n+p)!}{(n+c+1)(n+1)!p!} a_{n+p} z^{n+1}. \end{aligned} \tag{23}$$

For $p=1$, the operator defined in (23) is a generalised form of operator by Bernardi [22]. A comprehensive study of operators with applications can be found in the literature [23-30].

Theorem 9. Let $f(z) \in R_p$ and

$$\frac{F^{(p-1)}(z)}{p!} = \frac{c+1}{z^c} \int_0^z t^{c-1} \left(\frac{f^{(p-1)}(t)}{p!}\right) dt \quad (z \in E). \tag{24}$$

Then $F(z) \in R_p$.

Proof. Let

$$\frac{F^{(p)}(z) + zF^{(p+1)}(z)}{p!} = h(z).$$

Then $h(z)$ is analytic in E and $h(0) = 1$.

From (24), we have

$$\left(\frac{z^c F^{(p-1)}(z)}{p!}\right)' = (c+1)z^{c-1} \frac{f^{(p-1)}(z)}{p!}.$$

A simple computation gives us:

$$Re \left(h(z) + \frac{zh'(z)}{c+1} \right) = Re \left(\frac{f^{(p)}(z) + z f^{(p+1)}(z)}{p!} \right).$$

From the hypothesis of Theorem 9 with the result given [31], we have

$$Re \left(\frac{F^{(p)}(z) + zF^{(p+1)}(z)}{p!} \right) > 0 \quad (z \in E).$$

This completes the proof. It is easy to see that if $0 \leq \lambda \leq 1$, and $f(z)$ and $g(z)$ are in R_p , then $G(z) = \lambda g(z) + (1 - \lambda)f(z)$ is also in R_p . This shows that the class R_p is a convex set.

Theorem 10. Let $f(z), g(z) \in A(p)$ and $\alpha, \beta < 1$. If

$$\frac{f^{(p)}(z)}{p!} \in P(\alpha), \quad \frac{g^{(p)}(z)}{p!} \in P(\beta),$$

and

$$\phi^{(p-1)}(z) = f^{(p-1)}(z) * g^{(p-1)}(z),$$

then $\phi(z) \in S_p^*(p-1)$, provided that

$$(1 - \alpha)(1 - \beta) < \frac{3}{8(\ln 2 - 1)^2 + 4}. \tag{25}$$

Proof. Using the given hypothesis on $f(z)$ and $g(z)$ and Lemma 5, we have

$$\begin{aligned} \operatorname{Re} \left(\frac{f^{(p)}(z)}{p!} * \frac{g^{(p)}(z)}{p!} \right) &= \operatorname{Re} \left(\frac{\phi^{(p)}(z) + z\phi^{(p+1)}(z)}{p!} \right) \\ &> 1 - 2(1 - \alpha)(1 - \beta). \end{aligned} \tag{26}$$

By using Lemma 4, from (26) we have

$$\operatorname{Re} \left(\frac{\phi^{(p)}(z)}{p!} \right) > 1 + 4(1 - \alpha)(1 - \beta)(\ln 2 - 1) \quad (z \in E),$$

or equivalently, this can be written as

$$\operatorname{Re} \left(\frac{\phi^{(p-1)}(z)}{p!z} + z \left(\frac{\phi^{(p-1)}(z)}{p!z} \right)' \right) > 1 + 4(1 - \alpha)(1 - \beta)(\ln 2 - 1) \quad (z \in E). \tag{27}$$

Using Lemma 4, (27) becomes

$$\operatorname{Re} \left(\frac{\phi^{(p-1)}(z)}{p!z} \right) > 1 - 8(1 - \alpha)(1 - \beta)(\ln 2 - 1)^2.$$

Suppose

$$h(z) = \frac{z\phi^{(p)}(z)}{\phi^{(p-1)}(z)} \quad \text{and} \quad q(z) = \frac{\phi^{(p-1)}(z)}{z}.$$

Then $h(z)$ is analytic in E , $h(0) = 1$ and

$$\operatorname{Re} q(z) > 1 - 8(1 - \alpha)(1 - \beta)(\ln 2 - 1)^2. \tag{28}$$

A simple computation gives us:

$$\begin{aligned} \phi^{(p)}(z) + z\phi^{(p+1)}(z) &= q(z)(h^2(z) + zh'(z)) \\ &= \Psi(h(z), zh'(z), z). \end{aligned} \tag{29}$$

By taking $u = h(z)$ and $v = zh'(z)$, $\Psi(u, v; z) = q(z)(u^2 + v)$. From (25) and (29) we have

$$\operatorname{Re} \left(\Psi(h(z), zh'(z), z) \right) > 1 - 2(1 - \alpha)(1 - \beta) \quad (z \in E).$$

Now for real $x, y \leq -\frac{1}{2}(1 + x^2)$, we have

$$\begin{aligned} \operatorname{Re}(\Psi(ix, y, z)) &= (-x^2 + y)\operatorname{Re} q(z) \\ &\leq -\frac{1}{2}(1 + 3x^2)\operatorname{Re} q(z) \\ &\leq -\frac{1}{2}\operatorname{Re} q(z) \quad (z \in E). \end{aligned} \tag{30}$$

From (28) and (30) we obtain

$$\operatorname{Re}(\Psi(ix, y, z)) \leq 1 - 2(1 - \alpha)(1 - \beta), \quad \text{for all } z \in E.$$

By using the results given [19, 31], we have $\phi(z) \in S_p^*(p - 1)$ ($z \in E$).

Corollary 6. Let $f(z), g(z) \in A(p)$ and $\alpha, \beta < 1$. If

$$\frac{f^{(p)}(z)}{p!} \in P(\alpha), \quad \frac{g^{(p)}(z)}{p!} \in P(\beta),$$

and

$$\psi^{(p-1)}(z) = \int_0^z \frac{(f^{(p-1)} + g^{(p-1)})(t)}{t} dt,$$

then $\psi(z) \in C_p(p - 1)$, provided that

$$(1 - \alpha)(1 - \beta) < \frac{3}{8(\ln 2 - 1)^2 + 4}.$$

The proof is simple by taking $z\psi^{(p)}(z) = \phi^{(p-1)}(z)$.

Theorem 11. Let $f(z), g(z), h(z) \in A(p)$, $\alpha, \beta, \gamma < 1$. If

$$\frac{f^{(p)}(z)}{p!} \in P(\alpha), \frac{g^{(p)}(z)}{p!} \in P(\beta), \frac{h^{(p)}(z)}{p!} \in P(\gamma),$$

and

$$\phi^{(p-1)}(z) = (f^{(p-1)} * g^{(p-1)} * h^{(p-1)})(z),$$

then $\phi(z) \in S_p^*(p-1)$, provided that

$$(1-\alpha)(1-\beta)(1-\gamma) < \frac{3}{\{8(\ln 2-1)^2+4\}(-4)(\ln 2-1)}.$$

Proof. By the hypotheses on f, g and h and Lemma 5, we obtain

$$\begin{aligned} \operatorname{Re} \left(\frac{K^{(p)}(z)}{p!} * \frac{h^{(p)}(z)}{p!} \right) &= \operatorname{Re} \left(\frac{\phi^{(p)}(z) + z\phi^{(p+1)}(z)}{p!} \right) \\ &> 1 - 2(1-\alpha_1)(1-\beta), \end{aligned} \tag{31}$$

where $K^{(p-1)}(z) = (f^{(p-1)} * g^{(p-1)})(z)$ and $\operatorname{Re} \frac{K^{(p)}(z)}{p!} > \alpha_1, \alpha_1 = 1 + 4(1-\alpha)(1-\beta)(\ln 2 - 1)$.

From (31), together with Lemma 4, we have

$$\operatorname{Re} \left(\frac{\phi^{(p)}(z)}{p!} \right) > 1 - 16(1-\alpha)(1-\beta)(1-\gamma)(\ln 2 - 1)^2 \quad (z \in E),$$

Using the same technique similar to that of Theorem 10, we obtain the required result.

Corollary 7. Let $f(z), g(z), h(z) \in A(p)$, $\alpha, \beta, \gamma < 1$. If

$$\frac{f^{(p)}(z)}{p!} \in P(\alpha), \frac{g^{(p)}(z)}{p!} \in P(\beta), \frac{h^{(p)}(z)}{p!} \in P(\gamma),$$

and

$$\phi^{(p-1)}(z) = (f^{(p-1)} * g^{(p-1)} * h^{(p-1)})(z),$$

Then $\phi(z) \in C_p(p-1)$, provided that

$$(1-\alpha)(1-\beta)(1-\gamma) < \frac{3}{16(\ln 2-1)^2+8}.$$

For proving $\phi(z) \in C_p(p-1)$, it is sufficient to show that

$$\zeta^{(p-1)}(z) = z\phi^{(p)}(z) \in S_p^*(p-1).$$

By the hypotheses on $f(z), g(z)$ and $h(z)$ and Lemma 5, we obtain

$$\begin{aligned} \operatorname{Re} \left(\frac{(f^{(p)} * g^{(p)} * h^{(p)})(z)}{p!} \right) &= \operatorname{Re} \left(\frac{\zeta^{(p)}(z) + z\zeta^{(p+1)}(z)}{p!} \right) \\ &> 1 - 4(1-\alpha)(1-\beta)(1-\gamma), \end{aligned}$$

and the proof is completed similarly to that of Theorem 10. If $p = 1$, then Theorem 10 and Corollary 7 were given [10].

Theorem 12. Let $f_1(z), f_2(z), \dots, f_n(z) \in A(p)$, $\alpha_1, \alpha_2, \dots, \alpha_n < 1$. If

$$\frac{f_1^{(p)}(z)}{p!} \in P(\alpha_1), \frac{f_2^{(p)}(z)}{p!} \in P(\alpha_2), \dots, \frac{f_n^{(p)}(z)}{p!} \in P(\alpha_n),$$

and

$$\tau^{(p-1)}(z) = (f_1^{(p-1)} * f_2^{(p-1)} * \dots * f_n^{(p-1)})(z), \tag{32}$$

then $\tau(z) \in S_p^*(p-1)$, provided that

$$(1 - \alpha_1)(1 - \alpha_2) \dots (1 - \alpha_n) < \frac{3}{\{8(\ln 2 - 1)^2 + 4\} \{(-4)(\ln 2 - 1)\}^{n-2}}, \quad n \geq 2. \quad (33)$$

Proof. For proving the above Theorem, we use the principle of mathematical induction. For $n = 2$, we have proved Theorem 10; thus, (32) holds for $n = 2$. Suppose that (32) holds true for $n = k$; that is,

$$\tau^{(p-1)}(z) = (f_1^{(p-1)} * f_2^{(p-1)} * \dots * f_k^{(p-1)})(z),$$

then $\tau(z) \in S_p^*(p - 1)$, provided that inequality (33) is satisfied.

We have to prove that (32) holds true for $n = k + 1$. For this, consider

$$\tau^{(p-1)}(z) = (f_1^{(p-1)} * f_2^{(p-1)} * \dots * f_{k+1}^{(p-1)})(z).$$

Now using the given hypothesis on $f_j(z)$, $j = 1, 2, \dots, k$ and Lemma 5, we have

$$\begin{aligned} \operatorname{Re} \left(\frac{M^{(p)}(z)}{p!} * \frac{f_{k+1}^{(p)}(z)}{p!} \right) &= \operatorname{Re} \left(\frac{\tau^{(p)}(z) + z\tau^{(p+1)}(z)}{p!} \right) \\ &> 1 - 2(1 - \alpha^*)(1 - \alpha_{k+1}), \end{aligned} \quad (34)$$

where $M^{(p-1)}(z) = (f_1^{(p-1)} * f_2^{(p-1)} * \dots * f_k^{(p-1)})$ and

$$\operatorname{Re} \frac{M^{(p)}(z)}{p!} > \alpha^*, \quad \alpha^* = 1 + 4(1 - \alpha_1)(1 - \alpha_2) \dots (1 - \alpha_k)(\ln 2 - 1)^{k-1}(-4)^{k-2}.$$

By using Lemma 4, from (34) we have

$$\operatorname{Re} \frac{\tau^{(p)}(z)}{p!} > 1 + 4(1 - \alpha_1)(1 - \alpha_2) \dots (1 - \alpha_k)(\ln 2 - 1)^k(-4)^{k-1}, \quad z \in E, \quad k \geq 2. \quad (35)$$

Applying Lemma 4, (35) can be written as

$$\operatorname{Re} \frac{\tau^{(p-1)}(z)}{zp!} > 1 - 8(1 - \alpha^*)(1 - \alpha_{k+1}).$$

Now with the same procedure used in Theorem 10, we have $\tau(z) \in S_p^*(p - 1)$, provided that

$$(1 - \alpha_1)(1 - \alpha_2) \dots (1 - \alpha_k)(1 - \alpha_{k+1}) < \frac{3}{\{8(\ln 2 - 1)^2 + 4\} \{(-4)(\ln 2 - 1)\}^{k-1}}.$$

Therefore, the result is true for $n = k + 1$ and hence by using mathematical induction, (32) holds true for all $n \geq 2$. This completes the proof.

ACKNOWLEDGEMENTS

The authors would like to thank Dr. S. M. Junaid Zaidi, rector of Comsats Institute of Information Technology, for providing excellent research facilities. This research was carried out under the Higher Education Commission project grant no. NRPU No. 20-1966/R&D/11-2553. The authors are also grateful to the referees for their helpful comments and suggestions which improved the presentation of the paper.

REFERENCES

1. S. Owa, "On certain classes of p-valent functions with negative coefficients", *Simon Stevin.*, **1985**, 59, 385-402.
2. J. L. Liu, "Certain convolution properties of multivalent analytic functions associated with a linear operator", *General Math.*, **2009**, 17, 41-52.
3. J. Sokol, J. Dziok and M. K. Aouf, "On certain classes of meromorphically p-valent starlike and p-valent quasi-convex functions", *Tamkang J. Math.*, **2013**, 44, 261-269.

4. M. Arif, "Sufficiency criteria for a class of p-valent analytic functions of complex order", *Abst. Appl. Anal.*, **2013**, doi: 10.1155/2013/517296.
5. M. Raza, M. Arif and M. Darus, "Fekete-Szego inequality for a subclass of p-valent analytic functions", *J. Appl. Math.*, **2013**, 2013, Art.ID 127615.
6. S. Hussain, N. Anjum and I. Z. Cheema, "Certain classes of multivalent functions related with a linear operator", *Acta. Uni. Apul.*, **2011**, 28, 367-377.
7. Z. Shareef, S. Hussain and M. Darus, "Convolution operators in the geometric functions theory", *J. Ineq. Appl.*, **2012**, doi: 10.1186/1029-242X-2012-213.
8. J. Sokol, "Classes of multivalent functions associated with a convolution operator", *Comput. Math. Appl.*, **2010**, 60, 1343-1350.
9. R. Singh and S. Singh, "Convolution properties of a class of starlike functions", *Proc. Amer. Math. Soc.*, **1989**, 106, 145-152.
10. A. Y. Lashin, "Some convolution properties of analytic functions", *Appl. Math. Lett.*, **2005**, 18, 135-138.
11. L. Fejer, "Uber die positivitat von summen, die nach trigonometrischen order Legendreschen funktionen fortschreiten", *Acta Litt. Ac. Sci. Szeged*, **1925**, 2, 75-86.
12. R. J. Libera, "Some classes of regular univalent functions", *Proc. Amer. Math. Soc.*, **1965**, 16, 755-758.
13. L. Yi and S. Ding, "A new criterion for starlike functions", *Int. J. Math. Math. Sci.*, **1996**, 19, 613-614.
14. S. Ponnusamy and V. Singh, "Convolution properties of some classes of analytic functions", *J. Math. Sci.*, **1998**, 89, 1008-1020.
15. M. S. Robertson, "An extremal problem for functions with positive real part", *Michigan Math. J.*, **1964**, 11, 327-335.
16. W. Rogosinski and G. Szego, "Uber die abschimlte von potenzreihen die in ernein kreise be schrankt bleiben", *Math. Z.*, **1928**, 28, 73-94.
17. S. Ozaki, "On the theory of multivalent functions", *Sci. Rep. Tokyo Bunrika Daigaku A.*, **1935**, 40, 167-188.
18. I. S. Jack, "Functions starlike and convex of order α ", *J. London Math. Soc.*, **1971**, s2-3, 469-474.
19. M. Nunokawa, S. Owa, T. Sekine, R. Yamakawa, H. Saitoh and J. Nishiwaki, "On certain multivalent functions", *Int. J. Math. Math. Sci.*, **2007**, 2007, Art. ID 72393.
20. P. N. Chichra, "New subclasses of the class of close-to-convex functions", *Proc. Amer. Math. Soc.*, **1977**, 62, 37-43.
21. S. Ruscheweyh and T. Sheil-Small, "Hadamard products of schlicht functions and the Polya-Schoenberg conjecture", *Comm. Math. Helv.*, **1973**, 48, 119-135.
22. S. D. Bernardi, "Convex and starlike univalent functions", *Trans. Amer. Math. Soc.*, **1969**, 135, 429-446.
23. B. C. Carlson and D. B. Shaffer, "Starlike and prestarlike hypergeometric functions", *SIAM J. Math. Anal.*, **1984**, 15, 737-745.

24. N. E. Cho, O. S. Kwon and H. M. Srivastava, "Inclusion relationships and argument properties for certain subclasses of multivalent functions associated with a family of linear operators", *J. Math. Anal. Appl.*, **2004**, 292, 470-483.
25. J. Dziok and H. M. Srivastava, "Classes of analytic functions associated with the generalized hypergeometric function", *Appl. Math. Comput.*, **1999**, 103, 1-13.
26. J. L. Liu and H. M. Srivastava, "A linear operator and associated families of meromorphically multivalent functions", *J. Math. Anal. Appl.*, **2001**, 259, 566-581.
27. K. I. Noor, "Some classes of p-valent analytic functions defined by certain integral operator", *Appl. Math. Comput.*, **2004**, 157, 835-840.
28. K. I. Noor, "On new classes of integral operators", *J. Natur. Geom.*, **1999**, 16, 71-80.
29. K. I. Noor and M. A. Noor, "On integral operators", *J. Math. Anal. Appl.*, **1999**, 238, 341-352.
30. J. Sokol, K. I. Noor and H. M. Srivastava, "A family of convolution operators for multivalent analytic functions", *Eur. J. Pure Appl. Math.*, **2012**, 5, 469-479.
31. D. J. Hallenbeck and S. Ruscheweyh, "Subordination by convex functions", *Proc. Amer. Math. Soc.*, **1975**, 52, 191-195.

© 2015 by Maejo University, San Sai, Chiang Mai, 50290 Thailand. Reproduction is permitted for noncommercial purposes.

Report

Statistical process control: Best practices in small and medium enterprises

Mohd Nizam Ab Rahman^{1, *}, **Rosmaizura Mohd Zain**², **Afis Mohd Alias**¹ and **Zulkifli Mohd Nopiah**³

¹ Department of Mechanical and Materials Engineering, Faculty of Engineering and Built Environment, Universiti Kebangsaan Malaysia, 43600 Bangi, Selangor, Malaysia

² Faculty of Entrepreneurship and Business, Universiti Malaysia Kelantan, Pengkalan Chepa, 16100 Kota Bharu, Kelantan, Malaysia

³ Unit of Fundamental Engineering Studies, Faculty of Engineering and Built Environment, Universiti Kebangsaan Malaysia, 43600 Bangi, Selangor, Malaysia

* Corresponding author, e-mail: mnizam@eng.ukm.my; mnizam@ukm.edu.my

Received: 22 February 2014 / Accepted: 24 June 2015 / Published: 27 July 2015

Abstract: Many developing countries have started to focus on quality in manufacturing industries including small and medium enterprises (SMEs) in Malaysia. Statistical Process Control (SPC) is one of the quality improvement practices companies employ to ensure the reliability of their products, thus increasing customer satisfaction. This paper aims to present the recent development of a computer-based SPC system to be used by operators or shop-floor workers to perform simple data analysis, as well as to enhance the efficiency of the improved process. Ideas and information concerning system development are generated through an in-depth case study at ten SME companies, featuring interviews, questionnaires and observation. The system, namely small and medium enterprises - statistical process control (SMEs-SPC), tends to focus on particular data sets, simple statistical operations and user groups. The findings show that the SMEs-SPC system is highly practical for quality data management and data analysis and has advantages over the manual SPC. Furthermore, it is suitable for users with a limited understanding of SPC and/or statistical background, highlighting the importance of SPC.

Keywords: statistical process control (SPC), small and medium enterprises (SMEs), system development

INTRODUCTION

Small and medium enterprises (SMEs) have become an important sector for the growth of any country as they are the life blood of modern economy [1] and also contribute to innovation [2, 3]. SMEs have been known to be a catalyst for economic growth as they are a major source of income and employment and consequently result in poverty reduction [4, 5]. Rahman et al. [6] argue that SMEs play a vital role in gaining a competitive advantage. Moreover, SMEs play a major role in total economic development both in developing and developed countries [7]. Generally, the long-term goals for SMEs are to maintain business competitiveness and to bring continuous profit. One of the fundamental ways of achieving this goal is the elimination or reduction of failure or waste including reworking, scrap, warranty claims, inspection tests, etc.

Statistical process control (SPC) is one of the quality control activities implemented to improve quality assurance programmes and Total Quality Management (TQM) practices through a process of monitoring, managing and analysing process performance [8, 9]. According to Gerard et al. [10], SPC is a method that has been used in industry since 1920 and approximately 80 per cent of companies have implemented SPC [11]. In practical terms, SPC is a statistical procedure that uses several control charts to detect any malfunction of a production process that could result in a poor-quality product [12]. Moreover, SPC can help to improve quality and productivity by reducing variations in a process [13]. To survive in a competitive market, all companies need to engage in SPC to ensure continual improvement.

Castagliola et al. [14] note that SPC is applied to assist practitioners in monitoring and controlling processes in manufacturing lines by detecting and removing assignable (special) causes of variation. Sharma and Kharub [15] emphasize that the process variation is the main course of quality problems that affect the process performance of SMEs. According to Bevilacqua et al. [16], SPC allows corrective action to be taken in a timely manner once a process has been identified as not meeting specifications. Previously, SPC has been implemented in numerous types of domain: the software industry [11], the health care sector [17], electrics and electronics [18], engineering, industrial and environmental applications [19], the production sector [20], the food industry [21, 22], the general service sector [23, 24] and the chemical industry [25]. It has also expanded to other non-manufacturing sectors including education and banking [26]. According to Abdolshah et al. [27], traditional quality concepts such as statistical quality control, SPC, zero defects and total quality management are crucial to companies in gaining a competitive advantage.

Moreover, SPC helps production employees to improve the quality of processes in their work environment. Statistical methods such as the 'seven basic tools of quality' offer valuable approaches that can be learned by everyone in an organisation [6]. Utley and May [28] note that quality control researchers first began to study the problem of monitoring and control related to variable data over 60 years ago. Since then, manufacturing disciplines have benefited from SPC tools in relation to decision making. For example, control charts and process capability measures aid in identifying the level of stability and performance of processes [16, 29]. According to MacCarthy and Wasusri [30], control charts are a powerful tool used in process control and improvement to manufacturing businesses. As pointed out by Yang and Yang [31] and Xue et al. [32], the main use of charts is to establish whether a process is in a controlled state, as well as to maintain the ongoing process during a production run. The use of control charts was first introduced by Shewhart in the 1920s and is commonly applied in large-scale manufacturing operations to trace special causes of variation present in processes [29, 33, 34]. Control charts make it possible to

distinguish between special causes and common causes in manufacturing processes. However, White et al. [35] contend that control charts are intended to detect process change, not to improve or ensure product quality. MacCarthy and Wasusri [30] note that there is a need for user-friendly statistical SPC packages enabling companies to remain competitive in the business environment.

RESEARCH MOTIVATION AND OBJECTIVES

In keeping with recent developments, the manufacturing field has had to adopt advanced technology systems due to customer demand for low prices and the fast delivery of products [36]. Moreover, according to Caldeira and Ward [37], many SMEs need to implement new business approaches and adapt to new technologies to confront the changing global market. In a recent study conducted by Marri et al. [38], SMEs prefer to select advanced manufacturing technology and computer-integrated manufacturing systems as effective tools for reducing operating costs and improving manufacturing efficiency. Accordingly, existing computer software is frequently used in quality control to analyse industrial problems by assessing data quality, for example by means of SPC software packages. Das et al. [39] believe that the latest developments in software offer various additional statistical functions and advances in graphical display. Groeneveld [40] points to SAS, SPSS and Minitab as being the most widely used and effective statistical software packages in the academic, business and government sectors. Many extensive SPC software packages are widely available, such as STATPACK and spreadsheets which are used in firms engaged in plastics production and the manufacture of drinking bottles, and also by other companies to monitor the quality problem efficiently [41]. Nevertheless, such software involves understanding of commands which are not easy to learn, especially for users with little statistical knowledge. Thus, a systematic approach to the problem is needed, whether through educational programmes or practical training in SPC methods.

As Castagliola et al. [14] and Jiao et al. [42] point out, the development of SPC through an online quality information system allows users to input data sets using the database, thus enabling them to disseminate problems and generate calculations using sample statistics and charts automatically, as well as share the system and information in real time. Computer-based SPC, or e-SPC, is widely used in organisations [13].

Currently, the development of online quality information system in SMEs is affected by the high costs of running such applications. According to Robson [43] and Hanif et al. [44], there are many basic statistical calculations and tools intentionally built into Microsoft Excel to perform a wide range of analyses as well as convert data into graphical figures such as pie charts, histograms and normal distribution. However, using Microsoft Excel also requires skill and training to understand the function names and syntax for each statistical operation [45]. Antony et al. [46] recognise that most organisations tend to develop control charts by using spreadsheet software or computer-based systems. However, several manufacturing firms continue to use a manual SPC approach (paper-based control chart) and the traditional SPC has a number of limitations such as the fact that few quality faults are detectable, there is the risk of human error and it is time-consuming [47]. According to Ahmed and Hassan [48], few manufacturing companies are able to use statistical tools effectively, and lack of education and training on how to use SPC hinders them from effectively applying the SPC tools and technique [20]. Up to this point, they continue to lag behind in the application of quality tools to quality improvements. Furthermore, there are few and limited SPC software programmes that can be effectively and appropriately used in the context of the

constraints faced by SMEs, such as operators' skills level as well as other issues faced specifically by Malaysian SMEs.

Therefore, this study highlights specific tools associated with the SPC system development and covers several basic methods such as variable control charts, histograms and process capabilities. A previous study provided a presentation of the case study of companies and covered several significant areas such as the background of the companies, general aspects of SPC implementation, and problems with the SPC software and barriers to its use by associated companies [7]. This paper specifically explores the conception of a complete small and medium enterprises-statistical process control (SMEs-SPC) system and the validation methods employed to strengthen the usability of this tool. One key feature of the SMEs-SPC is the use of an online monitoring system for interaction between shop-floor workers and upper management, enabling them to engage in problem solving together. This is considered one of the core contributions of the research.

DEVELOPMENT OF SMEs-SPC SYSTEM

A case-study research typically involves a small number of cases which are not necessarily representative of the larger population [49]. In the first phase of the research, the case studies were conducted in 10 SME manufacturing companies located in Selangor, Malaysia. The types of industry involved were the automotive industry and the manufacturing of electronics, medical disposal devices, computer components, plastics and chemicals. The collection of ideas, information and data for the system development was undertaken through in-depth interviews, open-ended questionnaires and non-participation observation. A well-designed questionnaire was given to key personnel to seek further information concerning SPC practices. In the second phase, an in-depth case study of a selected automotive company was conducted to develop the proposed system, focusing on process characteristics, collection of existing quality data, process control sheets (paper-based control charts) and user groups involved in the process. The design and development of the SPC system also drew on consultations regarding company requirements and suggestions from academics. The last phase of the study focused on the validation of the system including assessment of the complete system in the selected company and other SME types compatible with the use of this system.

Conceptually, the SMEs-SPC system is integrated through a client database server with a graphic user interface using Visual Basic. All tools and object models in Visual Basic are used to access the database server. Based on the data stored in the database, Visual Basic is employed to compute or perform statistical calculations. The user interface provides the user with an intuitive graphic tool to analyse data through control charts and histograms. According to Rao [50], the database server known as MySQL (Structured Query Language) is supported by the administrative software to manage the entire database server, enabling functions such as browsing and dropping database objects, creating tables, and viewing, renaming, exporting and importing databases. Developing the SPC system through a main server application allows many users to use the same software, share the same data sets and share knowledge about capabilities, control limits, graphs and out-of-control events simultaneously. For example, users at the production site in the quality control division and in the top management can all interface with the system to share information and make instant decisions concerning problems with quality.

Figure 1 shows the schematic diagram of the operation of the system, illustrating the link between (a) the database server, (b) the administrative application assigned to manage the database and (c) the user workstations. The data on quality processes and on variability are not only used to identify the variation in the processes, but can enable the end users to compare the stability of performance across different times, values and processes.

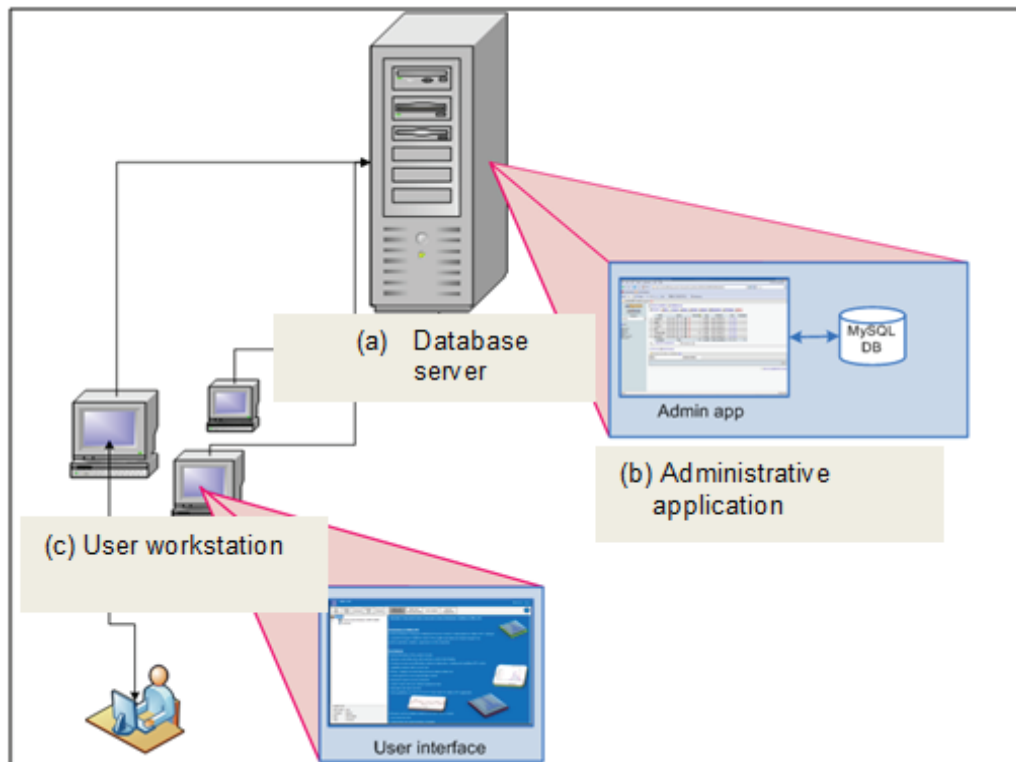


Figure 1. Operation system of SMEs-SPC

The details of data flow are shown in Figure 2. The design for SMEs is simple, unlike other commercial statistical software which tends to be complex. As can be seen from Figure 2, the administrative software relates to the generation of data input and typically uses six categories of table, viz. information of user, company name, folder name, characteristics of process and product, sample size (k) and frequency of subgroup (f), to differentiate data values and add variable information, as well as to assist in computing statistical operations. Under the administrative software, the SPC data processing manages the user's information and specific parameters to be used, such as process characteristics, type of control chart, sample size, time, date of entry, as well as classified user-defined control limits based on the respective table. Moreover, the SPC data processing organises data storage and finally passes results to the information system of SPC for the generation of graphs and process capability statistics, underpinned by statistical formulae.

FINDINGS AND ANALYSIS

The findings and analysis of this paper comprise three main aspects: first, the implementation of SPC in 10 companies; second, the development of the SMEs-SPC system; and third, the validation of SMEs-SPC by respondents from SMEs to meet user requirements.

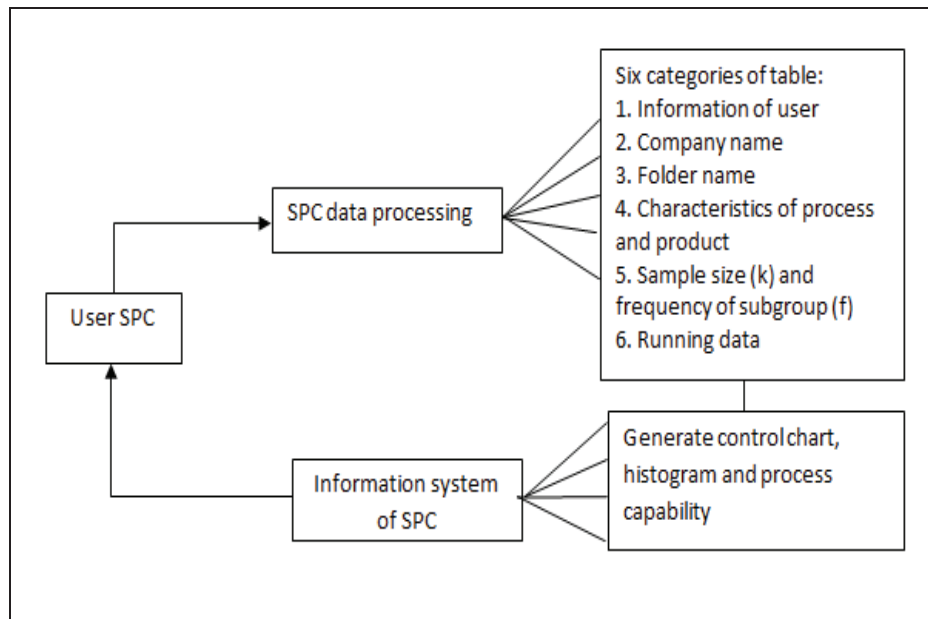


Figure 2. Data flow diagram

The case-study approach adopted could differentiate between the case companies in relation to the level of SPC adoption, type of SPC software, and problems and advantages of the application. It also identified the input and requirements of SMEs to develop the SPC tool. The initial results (Table 1) revealed that only five companies - A, B, E, G and I - fully utilised the SPC software or SPC system. Companies C and J were using manual methods (paper-based control charts) and companies D, F and H developed control charts or graphs using Microsoft Excel. Of those companies that fully implemented SPC, only companies E and G used an online SPC system to monitor process control. Company G was closest to implementing an ideally effective SPC application; hence it greatly enhanced the process performance, reduced customer complaints to the minimum level, and reduced time, paper consumption and human error throughout its processes. Companies C and J (automotive industries) were found to have many deficiencies and problems in SPC implementation amongst shop-floor workers; the application of SPC at company C and J were subjected to certain limitations such as human error and effects of delays in relation to data measurement, data entry, chart plotting and calculation of control limits.

Our previous study [6, 7] identified typical problems associated with using SPC and the barriers that may prevent Malaysian SMEs from adopting the SPC software or systems effectively. One of these are that the implementation of SPC systems is more difficult in SMEs than in other firms because smaller companies are not able to afford high-technology systems (hardware, software, networking and security) due to the high costs involved. Thus, some companies continue to use simple control charts based on paper (manual method). As already mentioned, a number of key problems were also found in the first phase of the study, such as the lack of efficiency in quality data management, the inconsistent formatting and the inability to disseminate information on time. Other barriers to the effective implementation of SPC are the lack of commitment and support from top management and the lack of awareness of SPC as a powerful problem-solving technique. Furthermore, the lack of training and education is also a major factor in the failure of SPC implementation.

Table 1. Companies in the case study and types of SPC software/system used

Company	Type of company	Type of SPC software/system
A	Automotive	Minitab
B	Medical devices	SPC XL 2000
C	Automotive	Manual
D	Plastics	Microsoft Excel
E	Electronics	e-SPC
F	Chemicals	Microsoft Excel
G	Automotive and electronics (computer components)	Online SPC database
H	Automotive	Microsoft Excel
I	Automotive and electronics	QC calculation
J	Automotive	Manual

Based on the above, SPC implementation can be considered to be at a moderate level in Malaysian SMEs. The first phase of the study ended with the selection of company J to collaborate in developing the system. Based on this collaboration, it was apparent that the system developed would have to be simple to operate and offer ease of use for low-level workers. The development of the SMEs-SPC aimed to address the problems and drawbacks of other systems and approaches identified in the first phase of study. Thus, the system was designed to make use of graphics and employ buttons to access key features rather than requiring the users to do so manually. For users, it is easier use buttons to generate calculations, graphs and reports. For example, they can set their own control limit values and select control chart rules to suit the company requirements. As mentioned earlier, this system is intended to be used by a wide range of users at different levels in the SMEs. Thus, the users are given a simple introduction to the system, its key features, objectives and application of X-bar (average) and R (range) charts, X-bar and s (standard deviation) charts, and histograms, as shown in Figure 3. Moreover, the system contains several novel features and provides guidance and information aided by the ‘help’ button, as shown in Figure 4. These guidelines make use of a few key concepts in statistics to facilitate the understanding necessary to use the system.

The graphic interface provided in the system is one of its advantages in performing systematic calculations. Figures 5-8 address certain features available to the user, expressed in each interface. First, the user is requested to complete some information to register as a means of protecting confidential data, as shown in Figure 5. When first using the system, the user should input raw data or quality data into the system to have statistical analyses performed quickly and the recorded data will be displayed in a data table as illustrated in Figure 6.

According to Taylor and Shouls [51], SPC comprises control chart rules which identify an out-of-control condition through an abnormal pattern. In some cases the system employs colour coding (either red or yellow) to signal an out-of-control condition based on control chart rules and provides feedback on any event by suggesting action disseminated via email. This aspect is of great importance in providing information on problems at the site in real time. The results (graphs and limit calculations) are then displayed in either a text or image form as shown in Figure 7. This should identify whether the variation that has occurred is in control or out of control. The system also performs calculations to determine the process capability. Figure 8 illustrates the overall performance report, which includes control charts, histograms and capability studies, which can be saved as an electronic file and printed for reference.

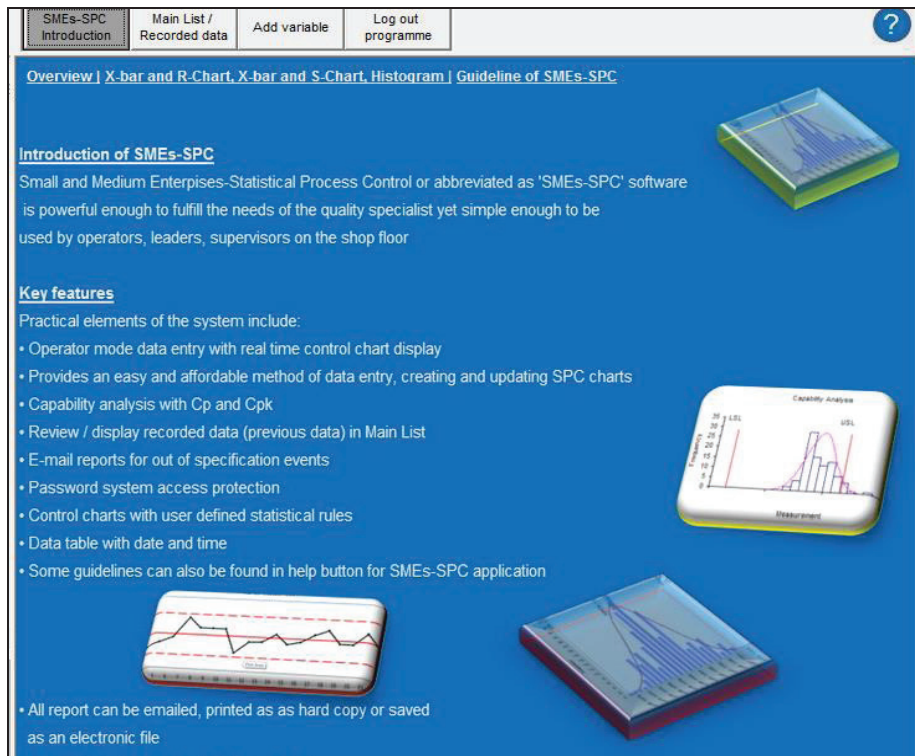


Figure 3. Introduction to SMEs-SPC

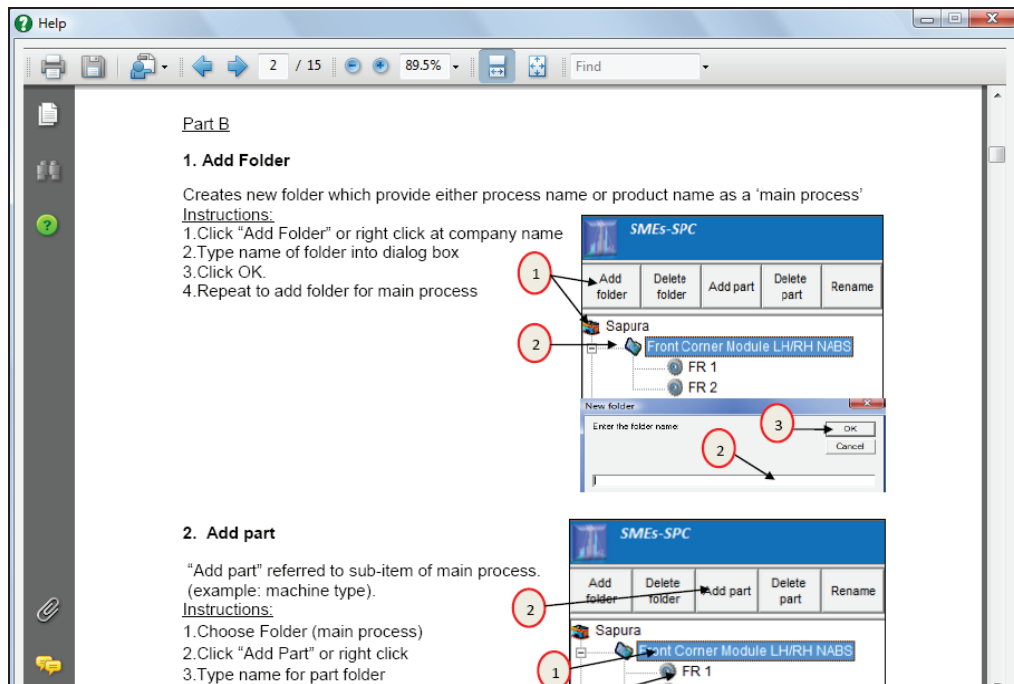


Figure 4. Guidelines (help) for using SMEs-SPC system

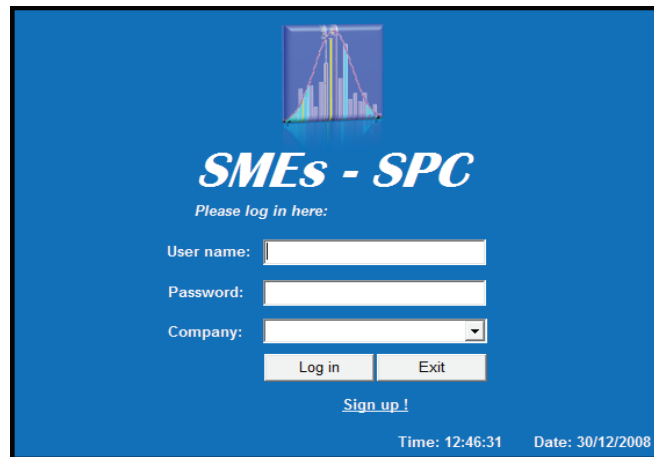


Figure 5. User registration

Add variable		Proces name: FRONT CORNER MODULE LH/RH NABS								Part Code: FR 1				
Variable		Data entry			View data				Variable calculation and graph					
View data Feb 2008														
* Subprocess name:		Press wheel brake to knuckle						Shift:		A				
* Characteristic process:		Press load						No of (k):		23				
* Unit of measurement:		kN						Month:		Feb				
* Product specification:		USL: 3263.000		LSL: 920.000		Year:		2008						
* Sample size (n):		3						View data						
Samples no	No (k)	1	2	3	4	5	6	7	8					
(n)	Date	01/02/2008	02/02/2008	03/02/2008	04/02/2008	05/02/2008	06/02/2008	07/02/2008	08/02/2008	09/02/2008				
1					05:37 AM	05:38 AM	05:38 AM	05:39 AM	05:40 AM	05				
					zura	zura	zura	zura	zura					
					1041.000	1621.000	1242.000	1232.000	1422.000	14				
2					A	A	A	A	A					
					Edit	Edit	Edit	Edit	Edit					
					05:37 AM	05:38 AM	05:38 AM	05:39 AM	05:40 AM	05				
3					zura	zura	zura	zura	zura					
					1262.000	1340.000	1136.000	1601.000	1262.000	10				
					A	A	A	A	A					
					Edit	Edit	Edit	Edit	Edit					
					05:37 AM	05:38 AM	05:38 AM	05:39 AM	05:40 AM	05				
					zura	zura	zura	zura	zura					
					Value	1026.000	1124.000	1782.000	1431.000	1621.000	1041.000	1421.000	1341.000	10
					Shift	A	A	A	A	A	A	A		
					Action	Edit	Edit	Edit	Edit	Edit	Edit	Edit		

Figure 6. Example of data entry and data table

Another important feature of this system is that, unlike commercial software, it is not based on a spreadsheet or tabular format and does not require functions or syntax to conduct statistical calculations. Also, the instructions given using the help button are user friendly and easy to understand at all levels. The results of SPC data processing based on structured query language are placed into result tables using standard formatting and labelling. Figure 9 illustrates the result table processed by means of the structured query language database in company J. The result tables are stored in the main process folder (Figure 9a) and the part folder (Figure 9b) and show the running data, i.e. specifications, target, data values and other aspects (Figure 9c). Another enhancement in this system is the possibility of creating final reports that contain image files and results in text.

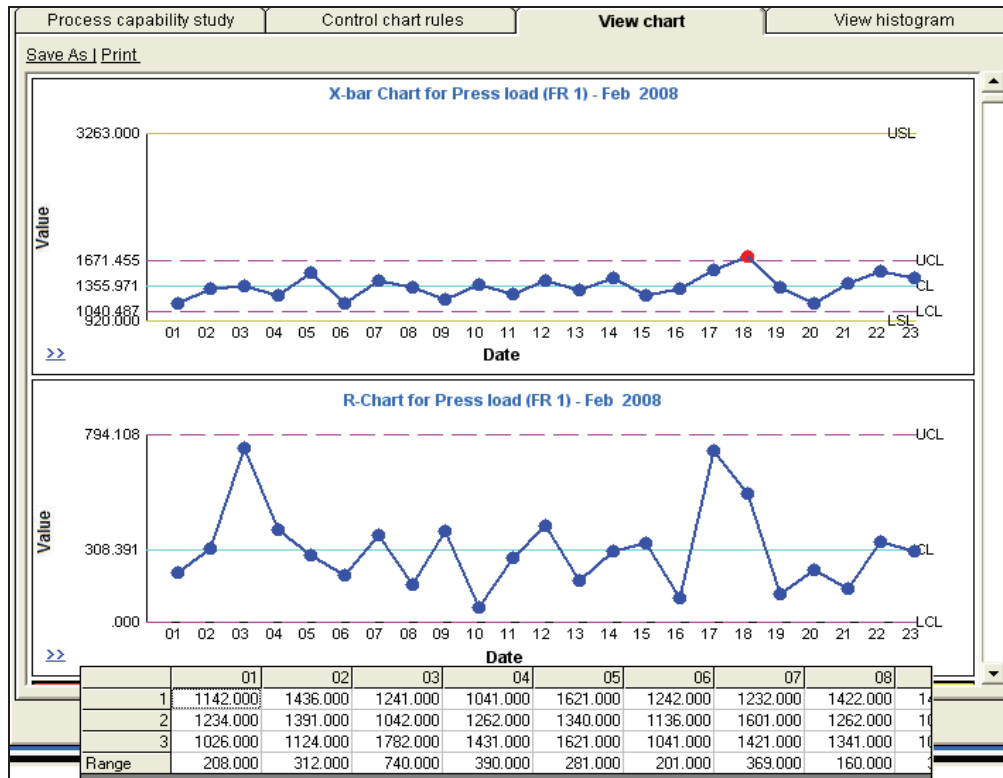


Figure 7. Example of control charts

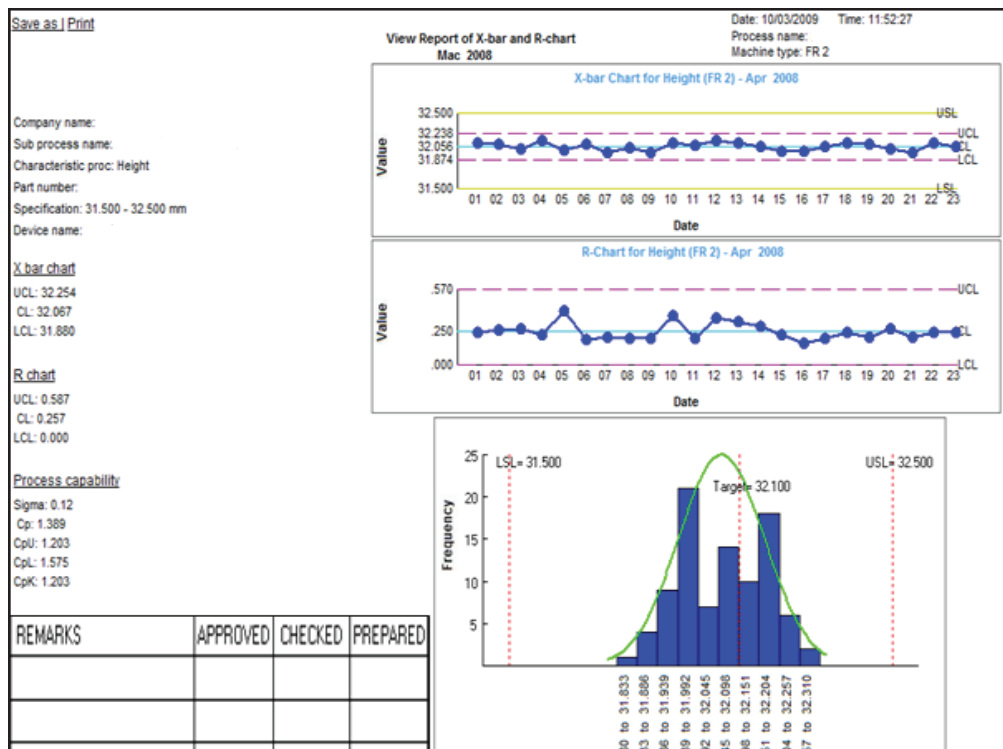


Figure 8. Example of monthly report

FolderID	Name	Operator	CompanyID	Status	DeleteBy	DelDate
18	TEST1	zura	4	1		0000-00-00

(a) Main process folder

CompanyID	Value	Date	Time	EnteredBy	Shift	n_index
4	1234	2008-12-01	06:39:00	zura	A	1
4	1245	2008-12-01	06:39:00	zura	A	2
4	1235	2008-12-01	06:40:00	zura	A	3
4	1124	2008-12-02	06:40:00	zura	A	1
4	1256	2008-12-02	06:40:00	zura	A	2
4	1567	2008-12-02	06:40:00	zura	A	3
4	2100	2008-12-03	06:42:00	zura	A	1
4	2300	2008-12-03	06:42:00	zura	A	2

(b) Part folder

PartID	PartNo	Target	CpkTarget	Date	Operator	CompanyID
6	825763/64	0	1.33	2008-12-10	zura	4
7	825763/64	0	1	2009-01-08	zura	4
8	825763/64	0	0	2009-01-08	zura	4

(c) Running data

Figure 9. Example of result tables

Based on our research, the calculations and SPC operations required by SMEs are relatively basic, e.g. control charts (X bar-R charts and X bar-s charts), histograms and process capability indices. A report on the process performance is presented in such a way that it allows users to provide progress reports to customers each month. It should be noted that this interface application only enables users of the SMEs-SPC system to conduct simple statistical analyses. The plotted X-bar and range charts based on the data from company J are shown in Figure 10 (analysed by the SMEs-SPC system) and Figure 11 (validated by Minitab software). This demonstrates that the results and graphs generated by SMEs-SPC are similar to those derived from Minitab software. An important issue is the way in which the statistical operations are calculated: the SMEs-SPC system uses three decimal places whereas the Minitab software uses four decimal places. However, results of the calculations performed using SMEs-SPC approximate almost exactly those shown in the Minitab figures.

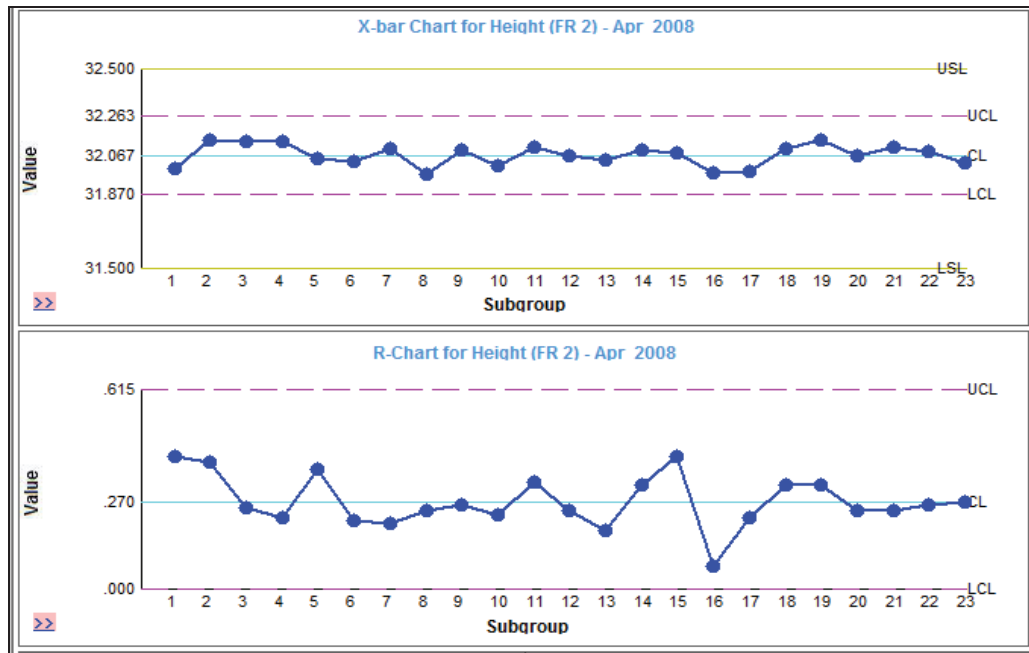


Figure 10. X-bar chart and range chart results for knuckle and brake disc height by SMEs-SPC

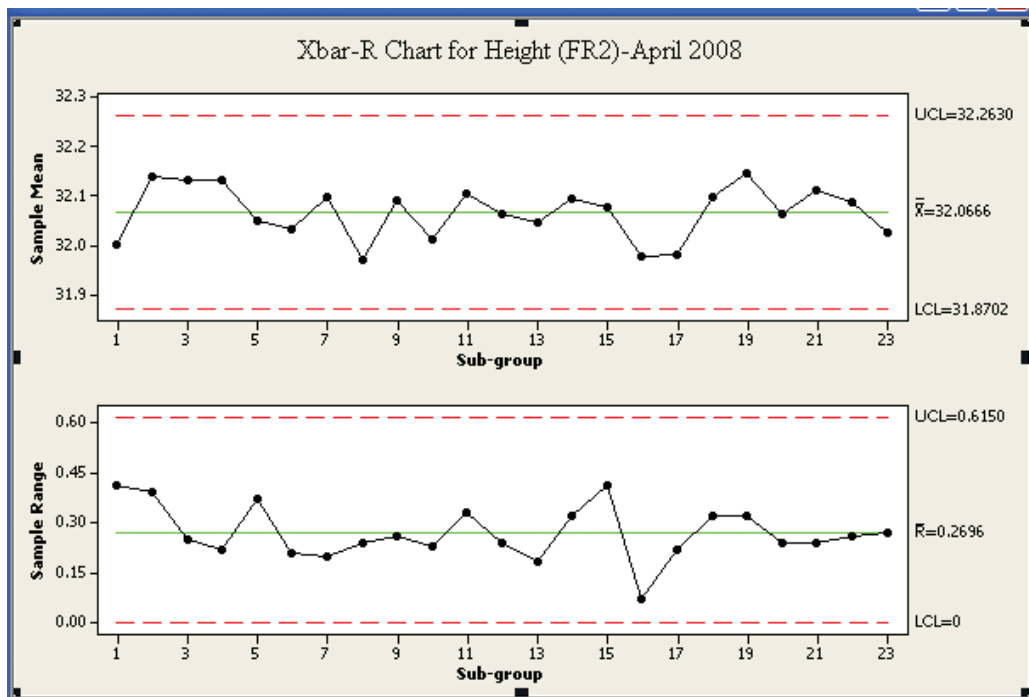


Figure 11. X-bar chart and range chart results for knuckle and brake disc height by Minitab software

The final stage in the development process was the assessment of the SMEs-SPC system by respondents from company J and other SMEs. According to the final reviews by respondents after completing the development phase, this system is suitable for application in automotive companies and provides education in SPC starting from a basis of little statistical training. The SMEs-SPC allows users to share the system, data and information with flexibility in time and space. The graphic interface provided in this system is sufficiently simple to allow a quick and easy analysis,

which can facilitate timely and correct decisions in solving quality problems. The respondents from other SMEs found the basic analytic tools very encouraging, considering that they would allow those from different educational backgrounds to participate in the process of analysis. They believed that the system as a whole would be highly practical for application in production sites. Nevertheless, to increase the sensitivity of analyses and prevent any inconsistencies in the results derived by other SMEs, as well as to ensure that the system would fulfil the need of multiple users, it was considered that flexibility, usability and applicability should be addressed with greater rigour. Table 2 shows the specifications for the SMEs-SPC system that is compliant with the main requirements of company J and other SMEs.

Table 2. SMEs-SPC specifications in compliance with SMEs' requirements

Type: X-bar and R charts	•
User-friendly operation and multiple users	•
Suitability for low-level education	•
Systematic data storage	•
Automatic generation of graphs	•
Automatic calculation of process capabilities	•
Automatic data retrieval and update	•
Ease of checking recorded data processes	•
Recorded information and quality data characteristics based on process, machine, product name, etc.	•
Rapid analysis of data	•
Presentation of complete report	•

CONCLUSIONS

The introduction of the SMEs-SPC system as a tool would greatly enhance the SPC in SMEs. The use of this latest system is expected to assist in overcoming common quality problems and should thus be supported by upper management levels.

ACKNOWLEDGEMENTS

The authors thank the Ministry of Education and the National University of Malaysia for their support in providing research funding for the projects entitled “Nurturing SMEs through the application of SME-on-STAT as a green ICT tool for quality and productivity improvement” (Knowledge Transfer Programme Grant PHI-2014-002), and “Development of SME-on-STAT for productivity and quality performance measures” (Grant PRGS/1/2014/TK01/UKM/02/1).

REFERENCES

1. A. Ghobadian and D. N. Gallear, “Total quality management in SMEs”, *Omega Int. J. Manag. Sci.*, **1996**, 24, 83-106.
2. Z. J. Acs, R. Morck, J. M. Shaver and B. Yeung, “The internationalization of small and medium-sized enterprises: A policy perspective”, *Small Bus. Econ.*, **1997**, 9, 7-20.
3. J. P. Antony and S. Bhattacharyya, “Measuring organizational performance and organizational excellence of SMEs - Part 1: A conceptual framework”, *Measur. Bus. Excell.*, **2010**, 14, 3-11.

4. T. Beck and A. Demirgüç-Kunt, "SMEs, Growth, and Poverty - Do pro-SME policies work?", **2004**, http://siteresources.worldbank.org/DEC/600659-1109953265771/20487449/beck_demirguc_viewpoint-sme.pdf (Accessed: May 2015).
5. M. Ayyagari, T. Beck and A. Demirgüç-Kunt, "Small and medium enterprises across the globe", *Small Bus. Econ.*, **2007**, 29, 415-434.
6. M. N. A. Rahman, R. M. Zain, Z. M. Nopiah, J. A. Ghani, B. M. Deros, N. Mohamad and A. R. Ismail, "Statistical process control in SMEs: A case study", Proceedings of 4th WSEAS/IASME International Conference on Dynamical Systems and Control, **2008**, Corfu, Greece, pp.145-152.
7. M. N. A. Rahman, R. M. Zain, J. A. Ghani, Z. M. Nopiah, R. I. Ahmad and S. A. Rahman, "Barriers to implementing an online SPC system in Malaysian automotive manufacturing companies", *Eur. J. Sci. Res.*, **2009**, 30, 315-325.
8. B. G. Dale, "Managing Quality", 2nd Edn., Prentice-Hall Inc., Eaglewood Cliffs (N. J.), **1994**.
9. R. J. M. M. Does, W. A. J. Schippers and A. Trip, "A framework for implementation of statistical process control", *Int. J. Qual. Sci.*, **1997**, 2, 181-198.
10. K. Gerard, J-P. Grandhay, V. Marchesi, P. Aletti, F. Husson, A. Noel and H. Kafrouni, "Feasibility study of using statistical process control to optimize quality assurance in radiotherapy", *J. Qual. Maint. Eng.*, **2009**, 15, 331-343.
11. R. Mahanti and J. R. Evans, "Critical success factors for implementing statistical process control in the software industry", *Benchmark. Int. J.*, **2012**, 19, 374-394.
12. R. S. Russell and B. W. Taylor III, "Operations Management", 4th Edn., Prentice-Hall Education Inc., Upper Saddle River (NJ), **2003**.
13. W. W. C. Chung, K. C. M. Wong and P. T. K. Soon, "An ANN-based DSS system for quality assurance in production network", *J. Manuf. Technol. Manag.*, **2007**, 18, 836-857.
14. P. Castagliola, G. Celano and S. Fichera, "Economic-statistical design of an S EWMA control chart for monitoring process variability", *J. Qual. Maint. Eng.*, **2007**, 13, 304-320.
15. R. Sharma and M. Kharub, "Attaining competitive positioning through SPC - An experimental investigation from SME", *Measur. Bus. Excell.*, **2014**, 18, 86-103.
16. M. Bevilacqua, F. E. Ciarapica, G. Giacchetta and B. Marchetti, "Implementation of a quality procedure based on the Delphi method and the ISO/TS 16949:2009 in the production of stainless steel tubes for automotive exhaust systems", *Int. J. Qual. Reliabil. Manag.*, **2011**, 28, 841-866.
17. S. Giligan and M. Walters, "Quality improvements in hospital flow may lead to a reduction in mortality", *Clin. Gov. Int. J.*, **2008**, 13, 26-34.
18. K. A. Salzman, "Statistical process control implementation for GaAs integrated circuit fabrication", Proceedings of 14th Annual IEEE Gallium Arsenide Integrated Circuit Symposium, **1992**, Miami Beach (FL), USA, pp.217-220.
19. G. Cartwright and B. Hogg, "Measuring processes for profit", *TQM Mag.*, **1996**, 8, 26-30.
20. Y. M. Awaj, A. P. Singh and W. Y. Amedie, "Quality improvement using statistical process control tools in glass bottles manufacturing company", *Int. J. Qual. Res.*, **2013**, 7, 107-126.
21. N. P. Grigg and L. Walls, "The use of statistical process control in food packing: Preliminary findings and future research agenda", *Br. Food J.*, **1999**, 101, 763-784.

22. S. A. H. Lim, J. Antony and S. Albliwi, "Statistical process control (SPC) in the food industry - A systematic review and future research agenda", *Trends Food Sci. Technol.*, **2014**, 37, 137-151.
23. T. H. Law, R. S. R. Umar and S. V. Wong, "The Malaysian government's road accident death reduction target for the year 2010", *IATSS Res.*, **2005**, 29, 42-49.
24. N. Kureshi, F. Qureshi and A. Sajid, "Current health of quality management practices in service sector SME: A case study of Pakistan", *TQM J.*, **2010**, 22, 317-329.
25. S. S. Chaudry and J. R. Higbie, "Practical implementation of statistical process control in a chemical industry", *Int. J. Qual. Reliabil. Manag.*, **1989**, 6, 37-48.
26. A. Hassan, M. S. N. Baksh and A. M. Shaharoun, "Issues in quality engineering research", *Int. J. Qual. Reliabil. Manag.*, **2000**, 17, 858-875.
27. M. Abdolshah, R. M. Yusuff, M. Ismail and T. S. Hong, "Overcoming the challenges of implementing six sigma in service industries", Proceedings of International Conference on Information Management and Engineering, **2009**, Kuala Lumpur, Malaysia, pp.191-195.
28. J. S. Utley and J. G. May, "Monitoring service quality with residual control charts", *Manag. Serv. Qual. Int. J.*, **2009**, 19, 162-178.
29. M. Xie and T. N. Goh, "Statistical technique for quality", *TQM Mag.*, **1999**, 11, 238-242.
30. B. L. MacCarthy and T. Wasusri, "A review of non-standard applications of statistical process control (SPC) charts", *Int. J. Qual. Reliabil. Manag.*, **2002**, 19, 295-320.
31. S-F. Yang and C-M. Yang, "Economic statistical process control for over-adjusted process mean", *Int. J. Qual. Reliabil. Manag.*, **2004**, 21, 412-424.
32. L. Xue, J. Xu and Y. Liu, "Economic-statistical design of variable sampling intervals EWMA charts under non-normality", *Asian J. Qual.*, **2010**, 11, 277-287.
33. S. E. A. Hamza, "Monitoring and controlling design process using control charts and process sigma", *Bus. Process Manag. J.*, **2009**, 15, 358-370.
34. G. C. Kim and M. J. Schniederjans, "Use of short-run statistical process control techniques: A comparison of U.S. and Japanese manufacturing", *Am. J. Bus.*, **2000**, 15, 21-30.
35. E. M. White, M. Kaighobadi and T. J. Wharton, "Process goal charts for quality improvement programmes", *Int. J. Qual. Reliabil. Manag.*, **1994**, 11, 26-40.
36. G. S. Dangayach and S. G. Deshmukh, "Advanced manufacturing technology implementation: Evidence from Indian small and medium enterprises (SMEs)", *J. Manuf. Technol. Manag.*, **2005**, 16, 483-496.
37. M. M. Caldeira and J. M. Ward, "Using resource-based theory to interpret the successful adoption and use of information systems and technology in manufacturing small and medium-sized enterprises", *Eur. J. Inf. Syst.*, **2003**, 12, 127-141.
38. H. B. Marri, A. Gunasekaran and B. Kobu, "Implementation of computer-integrated manufacturing in small and medium enterprises", *Indust. Commer. Train.*, **2003**, 35, 151-157.
39. S. R. Das, U. Yaylaciçegi and C. Canel, "Using ISO 90003 for software 'design and development' in large virtual teams", *Indust. Manag. Data Syst.*, **2008**, 108, 775-793.
40. R. A. Groeneveld, "Introductory Statistical Methods: An Integrated Approach Using Minitab", PWS-KENT Publication, Boston, **1988**.
41. C. Hewson, P. O'Sullivan and K. Stenning, "Training needs associated with statistical process control", *Train. Qual.*, **1996**, 4, 32-36.

42. R. J. Jiao, S. Pokharel, A. Kumar and L. Zhang, "Development of an online quality information system for e-manufacturing", *J. Manuf. Technol. Manag.*, **2007**, 18, 36-53.
43. A. Robson, "Statistical analysis with a spreadsheet: A comparison of software", *Logist. Inf. Manag.*, **1994**, 7, 12-17.
44. A. S. Hanif, N. M. Salleh, N. Ubaidullah, K. A. Shamsuddin and R. Mailok, "Teknologi komputer", Penerbit Universiti Pendidikan Sultan Idris, Tanjung Malim (Malaysia), **2005**.
45. J. K. West and P. S. Mann, "Excel Manual to Accompany Introductory Statistics", 5th Edn., Wiley, Hoboken (NJ), **2004**.
46. J. Antony, A. Balbontin and T. Taner, "Key ingredients for the effective implementation of statistical process control", *Work Study*, **2000**, 49, 242-247.
47. X. Pan, "Computer-aided SPC and cybernetic view on quality control", *Int. J. Qual. Reliabil. Manag.*, **2006**, 23, 1192-1203.
48. S. Ahmed and M. Hassan, "Survey and case investigations on the application of quality management tools and techniques in SMIs", *Int. J. Qual. Reliabil. Manag.*, **2003**, 20, 795-826.
49. R. K. Yin, "Case Study Research: Design and Methods", 2nd Edn., Sage Publications, London, **1994**.
50. S. Rao, "Database-driven Web sites: A case study with software in biotechnology and bioengineering", *Electron. Libr.*, **2004**, 22, 357-361.
51. J. R. A. Taylor and S. Shouls, "Transforming access: The role of data within service improvement to transform access to services", *Clin. Govern. Int. J.*, **2008**, 13, 8-18.

© 2015 by Maejo University, San Sai, Chiang Mai, 50290 Thailand. Reproduction is permitted for noncommercial purposes.

Maejo International Journal of Science and Technology

ISSN 1905-7873

Available online at www.mijst.mju.ac.th

Full Paper

Three dimensional finite element analysis for preliminary establishment of tunnel influence zone subject to pile loading

Prateep Lueprasert¹, Pornkasem Jongpradist^{2,*}, Kitcha Charoenpak³, Pattanasak Chaipanna⁴
and Suchatvee Suwansawat¹

¹ Department of Civil Engineering, King Mongkut's Institute of Technology Ladkrabang, Ladkrabang District, Bangkok, Thailand

² Department of Civil Engineering, Faculty of Engineering, King Mongkut's University of Technology Thonburi, Trungkru District, Bangkok, Thailand

³ Department of Highways, Ministry of Transport, Thailand

⁴ Department of Civil Engineering, Faculty of Industrial and Technology, Rajamangala University of Technology Isan, Sakonnakhon Campus, Sakonnakhon, Thailand

* Corresponding author, e-mail: pornkasem.jon@kmutt.ac.th

Received: 25 April 2014 / Accepted: 1 July 2015 / Published: 28 July 2015

Abstract: Urban development often involves the construction of infrastructures that require deep foundations or piles. Due to the existence of tunnels, the need to construct deep foundations in close proximity contributes to possible damage to the tunnels and operational safety concern. The concept of influence zones has been proposed as restrictive guidelines for construction adjacent to underground tunnels. However, the current influence zones are based on the conventional assumption of soil failure due to tunnelling rather than on an understanding of the pile-tunnel interaction. This paper thus analyses the impacts of piles under loading on the subway tunnel of the Mass Rapid Transit Authority of Thailand in Bangkok using the 3D finite element method. The analyses are carried out to investigate factors in tunnel deformations. The results show that the significant factors are the relative position of the pile tip with respect to the tunnel position as well as the soil type where the tunnel is located. In addition, this paper tentatively proposes a new influence zone for pile construction adjacent to the existing tunnel.

Keywords: tunnel influence zone, tunnel deformation, finite element method, pile foundation, tunnel distortion

INTRODUCTION

Underground tunnelling is regarded as an effective means to overcome the problem of limited space in major cities. Underneath most metropolises are tunnels for transportation, water, electricity and gas. Generally, tunnels are lined underground along the major roads to avoid being under the buildings. Due to urbanisation and traffic congestion, more new infrastructures are constructed to meet the demands, e.g. flyovers, elevated trains and tall buildings, all of which require deep foundations. In several instances, the piles of these new structures are inevitably close to existing tunnels. Thus, the movement of the piles under loading would induce a certain degree of impact on the tunnels. An assessment of the impact of piles under loading on the stability and integrity of the tunnels is necessary. The assessment is typically carried out in two steps. The first step is to evaluate the potential impact of the pile foundation for a design modification of the pile position. At present, this is carried out by defining the influence zone of the tunnel in combination with certain criteria. An influence zone refers to an area of land where future developments or construction activities to be undertaken could result in the imposition of additional load on the tunnel structure or affect an operational system [1]. If the possible impact is serious, the second step of assessment is necessary, in which the design must be modified or a detailed assessment must be carried out.

Tunnel owners have used restrictive guidelines for new constructions adjacent to the tunnels. The guidelines could include one or more influence zones or a minimum clearance between structures, maximum allowable tunnel deformation, and stress changes in tunnel lining. Figure 1 illustrates tunnel influence zones for the new construction of the Land Transport Authority (LTA) [1] and the Mass Rapid Transit Authority (MRTA) [2]. An influence zone was conventionally assumed from the ideal shear plane from the model test first proposed by Morton and King [3]. The influence zone is thus assumed from the shear plane of the ground due to tunnelling, rather than from the impact of a new construction on the existing tunnel. The zone is applied to all construction types but is proved to be inappropriate for piles. In addition, the restrictive guidelines were established based on experiences rather than on the theoretical understanding of the pile-tunnel interaction. According to the load transfer mechanism of pile, only the soil surrounding the pile perimeter and at the pile tip moves. Thus, the tunnel influence zone subject to pile under loading should be smaller than that assumed by the shear failure plane. A better and more specific tunnel influence zone affected by nearby piles is therefore necessary for an efficient issuance of construction permits of pile-supported structures in an area near the existing tunnel.

Several researches have attempted to understand the mechanisms of soil–tunnel–pile interactions. However, they mostly focused on the influence of tunnelling on nearby existing buildings and foundations, for examples the field observation [4], the full-scaled test [5], the physical modelling [6] and the numerical modelling [6-9]. With regard to the influence of nearby constructions on existing tunnels, there are few studies. Examples are the construction of a deep open excavation for an office block on the underlying tunnel complex in Prague-Czech Republic [10] and a multi-storey commercial building in Toronto [11].

Studies on the effects of pile loading on existing tunnels are even more limited even though the issue has been recognised since 1951 in London [12]. Schoroeder et al. [13] performed a numerical analysis on the interaction between pile rows supporting a 15-storey building and a tunnel. The study examined the influence of pile rows loading on the existing tunnel and the effects

in terms of tunnel distortions and global movements in relation to the loading of bored piles in the vicinity. The analysis results were used to determine a specific clearance between the pile rows and the tunnel. However, the limitations of the study were that the soil was homogeneous, the pile length was identical, and the pile tip position was much lower than that of the tunnel. In some situations where the foundations of a bridge approach or small buildings are constructed adjacent to the tunnel, e.g. as shown in Figure 2, the position of pile tips is close to that of the tunnel.

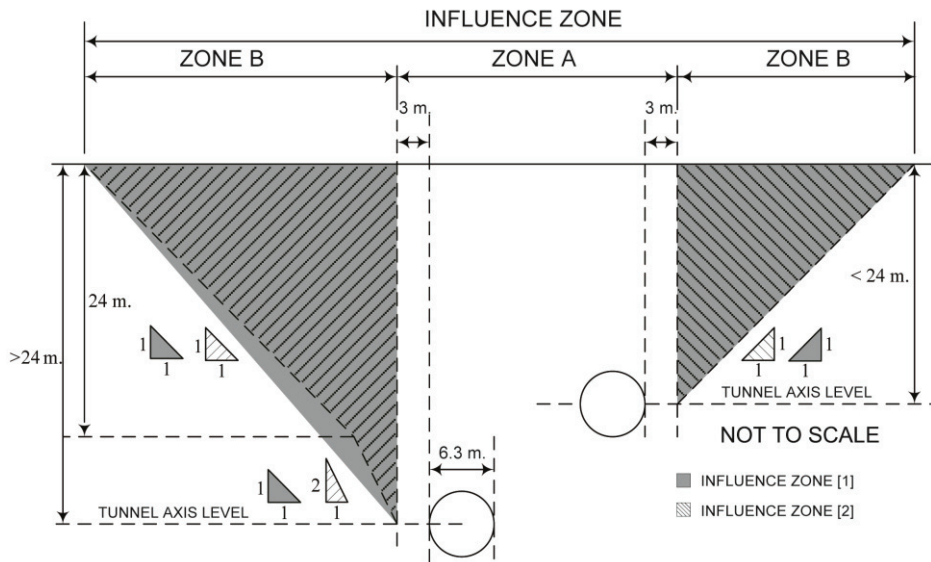


Figure 1. Tunnel influence zone utilised in current practice

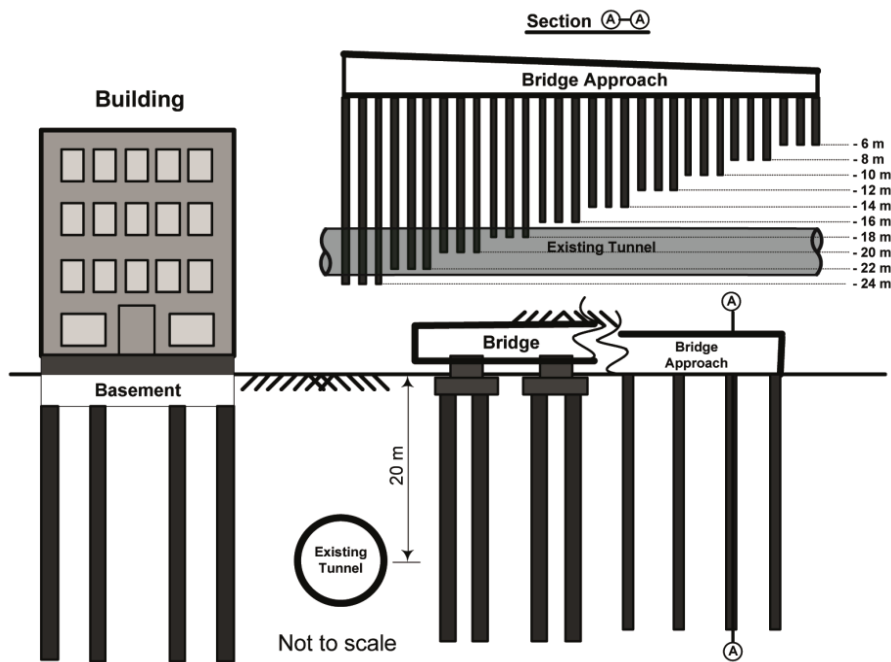


Figure 2. Pile foundations adjacent to existing tunnel

Studies on the impact of construction of urban tunnels on adjacent existing pile foundations indicate that the position of the pile tip in relation to the tunnel horizontal axis is the key issue of this problem [7, 14]. Recent research which numerically investigated the effect of pile loading adjacent to an existing tunnel also indicates that the clearance between the pile and the tunnel as well as the relative position between the pile tip and the tunnel is important [15]. Unlike the other previous studies, however, this study failed to investigate the effects of pile loading on the existing tunnel.

This present study numerically investigates the effects of the pile tip position in relation to the tunnel horizontal axis and of the nearby bored pile loading on the tunnel in multi-layer soil. The influence zone is then proposed. This research focuses on the Mass Rapid Transit (MRT) tunnel and on Bangkok subsoil. The analysis results in terms of tunnel deformations, i.e. changes of tunnel diameter in both vertical and horizontal directions, are presented. The evaluation of structural safety of the tunnel lining is, however, outside the scope of this research.

ANALYSIS METHOD

The response of tunnel lining when subjected to pile loading, particularly in a single pile case, is principally a three-dimensional problem. The simulation of the effects of adjacent piles under loading on the tunnel was performed by means of a three-dimensional simulation using the finite element program ABAQUS [16].

The analysis consists of two categories: single pile and pile row under loading. The first category is to investigate the significance of pile tip position relative to the tunnel and of soil stratum in which the tunnel is located. The geometric parameters in the analysis are depicted in Figure 3. The existing tunnel diameter, D_T , of 6.3 m and the depth, L_T , of 20 m below the ground surface are fixed throughout the study. The position of the tip of the bored piles with the diameter of 1 m is varied over a range of 0.20-1.80 L_T to investigate its impact. As shown in Figure 4, four cases of ground conditions in relation to the tunnel position are considered.

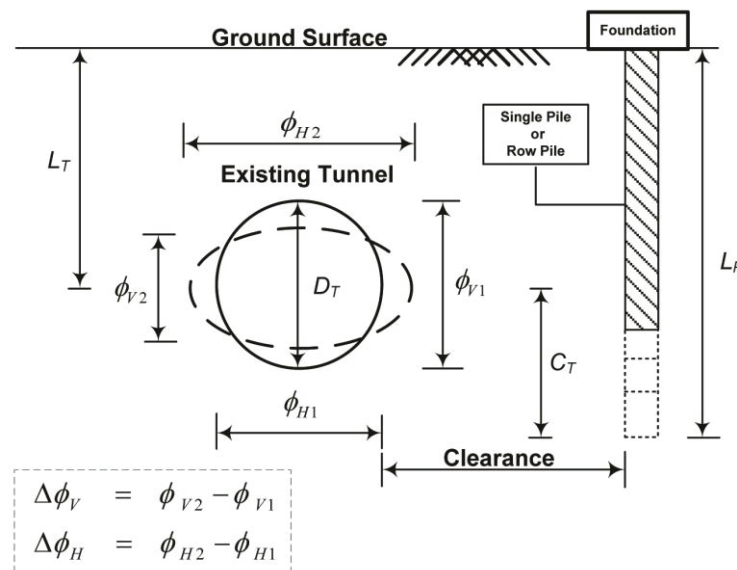


Figure 3. Illustration of piles under loading adjacent to an existing tunnel (D_T = tunnel diameter; L_T = tunnel depth; L_P = pile tip; C_T = vertical distance from centre of tunnel to pile tip; ϕ_H and ϕ_V = tunnel deformations)

Based on the soil profiles along the tunnel alignment and from the tunnel transition part to the ground level maintenance centre, the subsoil condition was varied to account for soft clay and stiff clay as shown in Figure 4. The piles were wished-in-place at the beginning of analysis. In the analysis the piles were loaded to their working load, which depends on the pile length and soil condition, using a safety factor of 2.5 of their ultimate capacity, which was calculated based on the alpha method [17]. From past experiences of a construction project in the UK, where the bored pile was successfully located at a distance of 3 m from the tunnel [18], a maximum clearance of 3.5 m (approximately $0.6 D_T$) is adopted in this study.

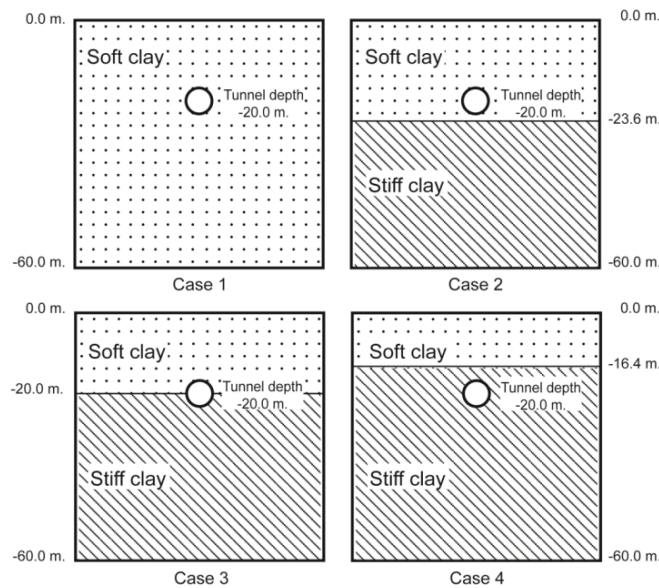


Figure 4. Soil profiles in this study

Finite Element Mesh

The soil and piles were discretised into hexahedral (or brick) elements with a suitable aspect ratio. The shell elements were used to represent the tunnel lining. For the region of greater interest, finer discretisation mesh is used to obtain accurate solutions, especially in the tunnel lining and the zone between pile and tunnel. A tied interaction was assigned to the soil-pile and soil-lining interfaces to prevent the relative displacement of adjacent nodes on the interfaces.

Figure 5 shows examples of the analytical meshes for single-pile and pile-row problems. For the single-pile case, the dimension of the mesh is 50 m in the longitudinal direction, 60 m in the vertical direction and 80 m in the transverse direction. The mesh dimension of the pile row is similar to that of the single pile but with a thickness (in longitudinal direction) of 2.0 m. The pile is located on one side of the tunnel.

Constitutive Model

The concrete bored pile and lining were assumed to be linearly elastic. The thickness of the lining is 0.30 m. The inner and outer diameters of the lining are thus 5.70 m and 6.30 m respectively. For the soil, several recently developed advanced models such as the hardening soil [19] can reproduce the behaviour of soil under loading with a higher degree of satisfaction. However, the Mohr-Coulomb model [16] is commonly used in current engineering practice due to its simplicity,

with only five parameters being required. In this study the observed values for the determination of influence zone are the changes in tunnel diameter. Therefore, the Mohr-Coulomb model is considered appropriate. The model parameters can be readily obtained from the literature [20, 21]. The parameters used in the analysis, including lateral earth pressure (k_0), undrained and drained Young's modulus (E_u, E'), undrained and drained shear strengths (C_u, C'), angle of friction (ϕ), unit weight of soil (γ), permeability (k) and specific gravity (GS), are garnered and listed in Tables 1 and 2. Note that the parameters for the hardening soil model for Bangkok subsoil can also be found in prior researches [e.g. 7, 22].

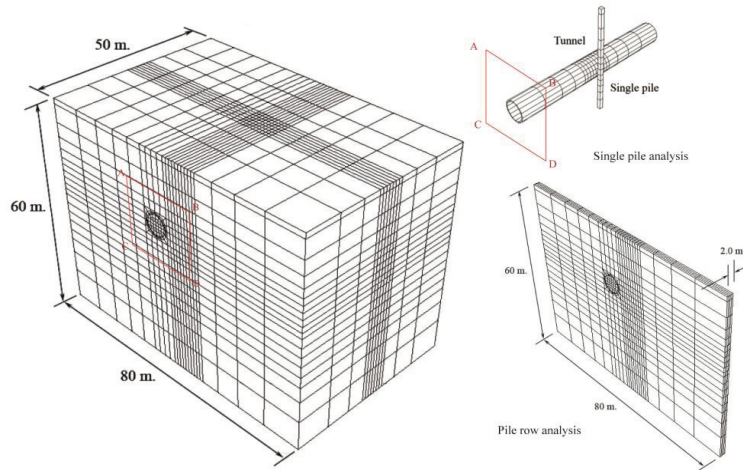


Figure 5. Finite element meshes for single-pile and pile-row cases

Table 1. Material properties of tunnel lining and bored pile [20]

Young modulus of concrete (E) (kN/m ²)	Poisson's ratio of concrete (ν_c)	Unit weight of concrete (γ_c) (kN/m ³)
3.1×10^7	0.20	24

Table 2. Geotechnical design parameters in MRT Project [20, 21]

Soil stratum	Material model	k_0	E_u	E'	Poisson's ratio	C_u	C'	ϕ	γ	k	GS
Weathered crust	Elastic	0.60	13500	10800	0.33	-	5	25	18	0.08	2.70
Soft clay	MC	0.75	6250	5000	0.33	20	5	20	16.5	0.0004	2.75
1 st Stiff clay	MC	0.85	66000	52800	0.33	120	5	26	20.5	0.0009	2.75
1 st Dense sand	MC	0.80	-	110000	0.25	-	0	36	20	0.08	2.65
2 nd Stiff clay	MC	0.80	82500	66000	0.30	120	5	26	20	0.0002	2.65
2 nd Dense sand	MC	0.80	-	150000	0.25	-	0	36	20	0.08	2.70

Note: MC = Mohr Coulomb; unit of E_u, E', C_u, C' in kN/m², γ in kN/m³ and k in m/day

k_0 = lateral earth pressure; E_u and E' = undrained and drained Young's modulus; C_u and C' = undrained and drained shear strengths; ϕ = angle of friction; γ = unit weight of soil; k = permeability; GS = specific gravity

Analysis Conditions

In the initial condition, the initial distributions of vertical effective stress and horizontal effective stress were controlled by the given soil unit weights and the coefficient of earth pressure at rest, k_o , for all strata. The bulk unit weight and k_o of each soil layer were adopted from the MRT tunnel project [23].

The displacement boundary condition was for performing the simulation in this study. The side and bottom boundaries were sufficiently extended from the area of greatest change in the model to avoid the boundary effect and minimise significant impacts on the analysis results.

In the finite element model, the front and rear sides of the mesh were restrained against lateral movements but allowed for free vertical movement. Thus, no movement perpendicular to these sides was expected. Since the bottom of the mesh was fixed, there were no vertical and horizontal movements. These conditions were applied to all finite element meshes throughout the study.

Each analysis was performed in 2 stages. The first involved the construction of the tunnel, which was modelled by consecutively removing the soil elements situated in the excavation zone and activating the tunnel lining with simultaneous application of pressure on the tunnel face to stabilise the excavation face. The second stage was the application of the pile axial loading, which was the design working load to a wished-in-place concrete pile. The undrained analysis was considered.

ANALYSIS RESULTS

Single Pile

Figure 6 illustrates the changes in tunnel diameters in vertical and horizontal directions for the single-pile case with a clearance of 0.5 m. The changes in tunnel diameter are normalised by the tunnel diameter (D_T) and plotted against the normalised depth of pile tip, L_p/L_T , for different cases (i.e. soil types). The normalised depth of tunnel position to tunnel diameter, C_T/D_T , is also provided in the y-axis on the right side. The negative and positive signs of magnitude in the x-axis denote a shortening and widening of the tunnel diameter respectively. It is clear from the Figure that, with identical clearance, the depth of the pile tip position relative to the tunnel has a strong influence on the tunnel deformations. The distribution patterns of changes in tunnel diameter in both vertical ($\Delta\phi_V$) and horizontal ($\Delta\phi_H$) directions are very similar for all analysis cases. The tunnel deformations become large when the pile tip is situated in the range of $2D_T$ above and $2D_T$ underneath the tunnel axis. Note that the pile in each case (with different length and soil profile) is loaded with different working load. However, the magnitude of tunnel deformation is extremely large for the tunnel in soft clay despite the smallest working load (for the same pile length), whereas it becomes small for the tunnel in stiff clay. The pile tip position that induces the maximum change in tunnel diameter is the point above the tunnel crown by $0.5-1D_T$. With regard to the pile tip position which induces the maximum tunnel deformation, it is found that this position is higher in stiffer soil than in softer soil. The maximum deformation occurs when the pile tip is embedded in the soft clay layer. The deformation rapidly decreases when the pile tip reaches the stiff clay layer underneath.

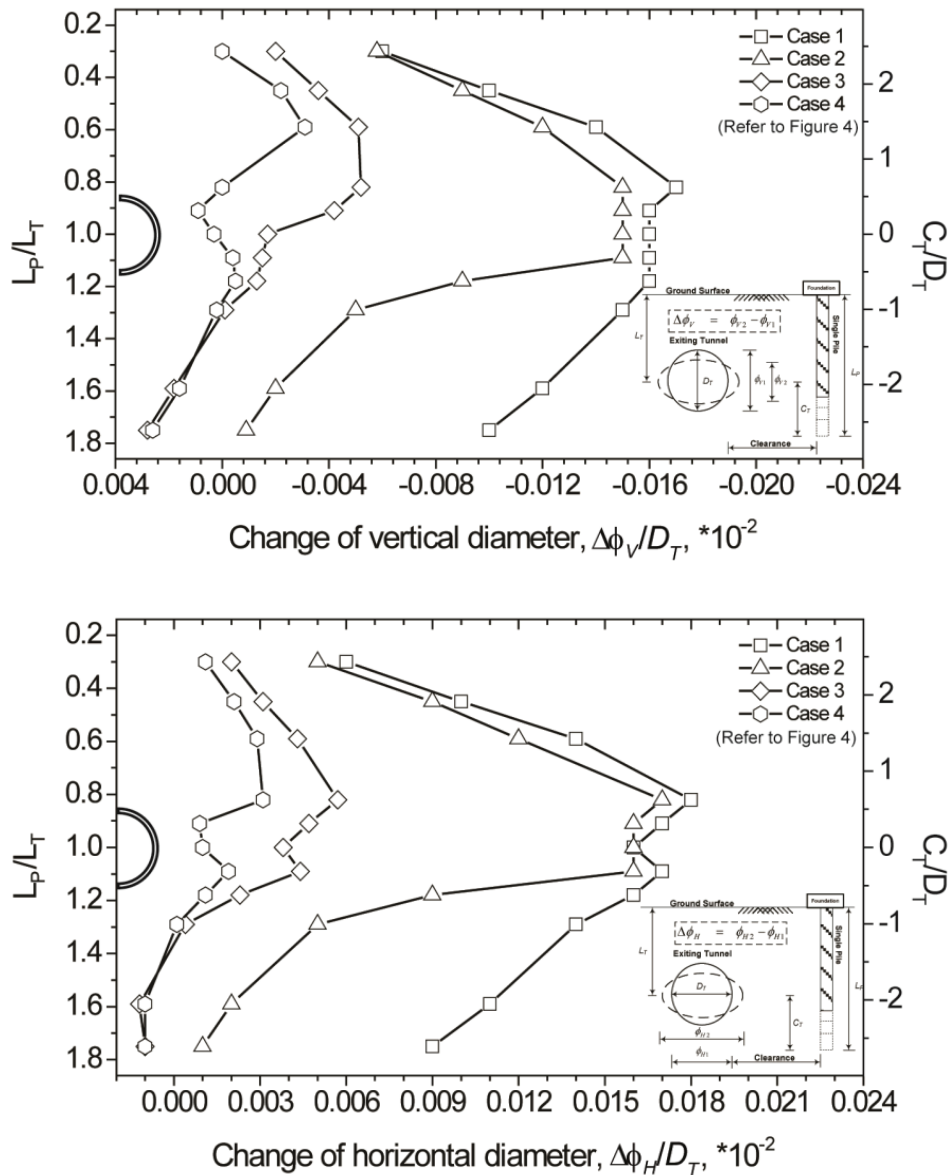


Figure 6. Impact of pile tip position relative to the tunnel and in relation to soil profile on the change in tunnel diameter for single pile (clearance = 0.5 m)

The tunnel-pile interaction behaviour can be determined by interpreting the numerical results. When a pile is loaded, the force is transmitted to the soil along the shaft and around the pile tip. This leads to an increase in stresses in soil. Simultaneously, the pile moves downward and causes the soil surrounding the pile to move. The soil movement interacts with the nearby existing tunnel and induces additional forces, stresses and displacements or distortion of the tunnel. The tunnel deformations by the pile tip located in soft clay are thus large due to large movements of the soil, as illustrated in Figure 7, which shows the distortion shapes by the same magnitude factor in the four cases of soil profile. The non-symmetric nature of the tunnel deformation can be observed. The tunnel diameter is reduced in the vertical direction and increased in the horizontal direction in all cases.

The preliminary results of this part confirm that the position of the pile tip relative to the tunnel and the soil type in which the tunnel is located have a significant impact on the tunnel

deformation. In engineering practice the tunnel deformation induced by a pile row or pile group is regularly encountered and is more severe due to more load concentrations. Thus, further investigation is carried out in the next section.

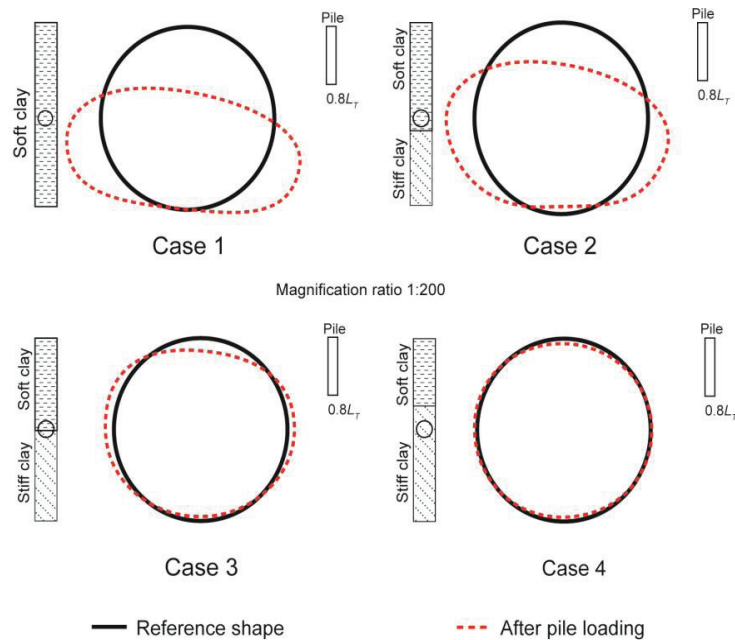


Figure 7. Tunnel distortions caused by pile under loading with the same pile tip position and clearance for four different cases of soil profile

Pile Row

Figure 8 illustrates the changes in tunnel diameter in the vertical ($\Delta\phi_V$) and horizontal ($\Delta\phi_H$) directions for the first case of soil profile (i.e. tunnel in soft clay) at various values of pile tip position and clearance. As seen in the Figure, the magnitude of $\Delta\phi_V$ and $\Delta\phi_H$ decreases when the clearance increases. The negative values indicate the shortening of tunnel diameter. For ease of understanding, absolute values are considered, so an ‘increase’ means that the absolute value becomes larger regardless of the sign. For the zone above the tunnel axis, $\Delta\phi_V$ increases with lower pile tip position. The increase rate of $\Delta\phi_V$ drastically changes when the pile tip position reaches approximately $2D_T$ (positive: above tunnel axis) and the maximum value occurs at a depth of about $0.80L_T$ (for the clearance of 0.50 m and 1.50 m) before slightly decreasing with increasing pile length. When the pile tip is extended below the tunnel axis, $\Delta\phi_V$ gradually increases again. At the clearance of 3.50 m, $\Delta\phi_V$ continues increasing with deeper pile tip position. The maximum $\Delta\phi_V$ occurs when the pile tip (for all three cases of clearance) is at about $1.1L_T$. As the pile length increases, thereby extending its tip below $1.1L_T$, $\Delta\phi_V$ decreases significantly. The decrease rate of $\Delta\phi_V$ approaches zero when the pile tip reaches about $-2D_T$ (negative: beneath tunnel axis). To recap, $\Delta\phi_V$ becomes large when the pile tip is situated in the range of $2D_T$ above and $2D_T$ underneath the tunnel axis. For $\Delta\phi_H$, a similar tendency to that of $\Delta\phi_V$ can be observed and the magnitude is also similar. The area with large $\Delta\phi_H$, therefore, covers the range of $2D_T$ above and $2D_T$ underneath the tunnel axis as well.

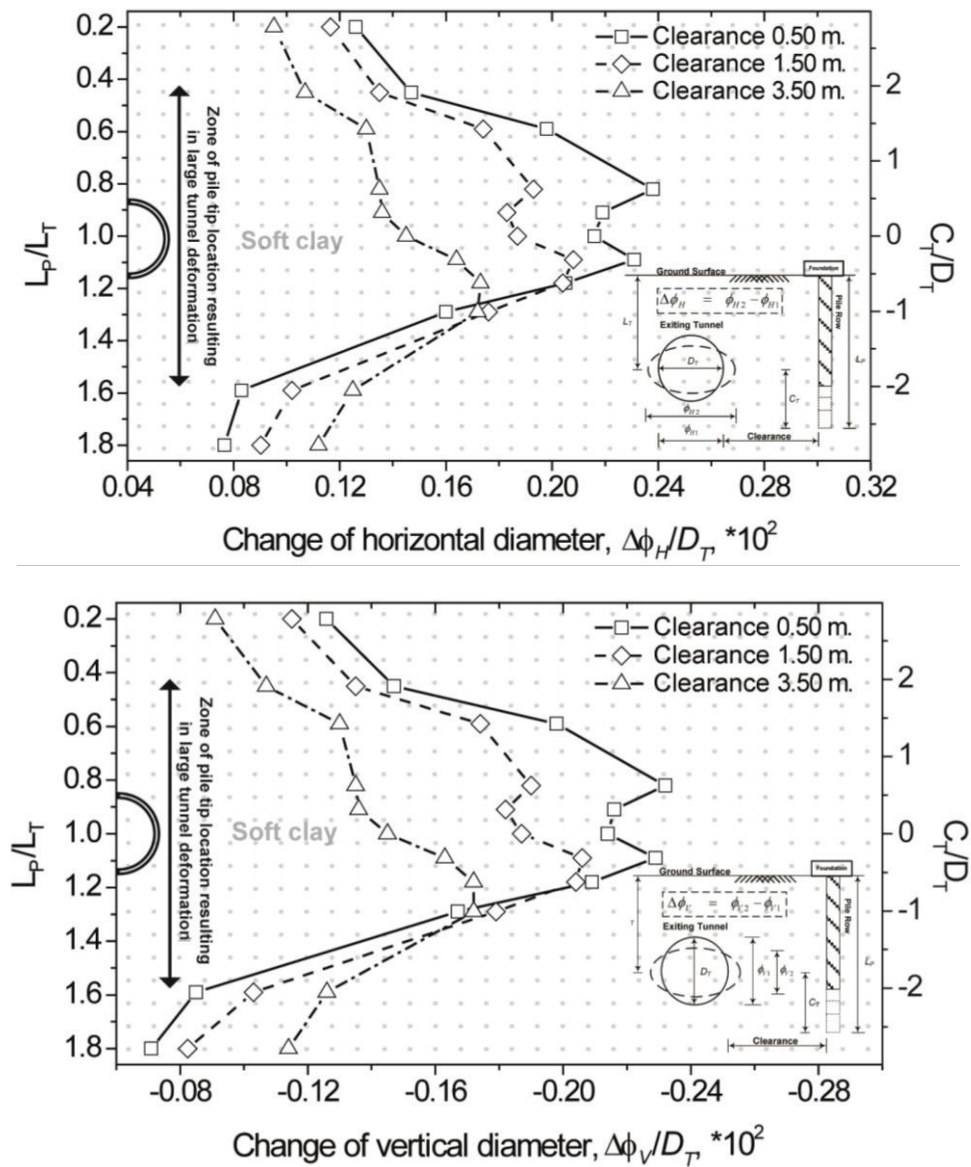


Figure 8. Impact of pile tip position relative to tunnel axis on the changes in tunnel diameter for tunnel in soft clay layer (case 1, Figure 4)

Investigating the three other cases of soil profile reveals that both the trend and magnitude of $\Delta\phi_V$ and $\Delta\phi_H$ are almost identical to one another, so only $\Delta\phi_V$ is shown for the three other cases. Figure 9 shows $\Delta\phi_V$ as a function of pile tip position for the tunnel in case 2 (Figure 4). Generally, the results are similar to case 1, where the tunnel is in soft clay, although the maximum values are lower. Besides, the level of pile tip at which $\Delta\phi_V$ rapidly decreases with increasing pile length is at the border between soft and stiff clays. Beneath this level, the rate of decrease for $\Delta\phi_V$ becomes noticeable. This implies that the existence of stiff layer underneath the tunnel could account for smaller tunnel deformations and a narrower influence zone. The zone with large tunnel deformations appears to cover a range from $2D_T$ above the tunnel axis to the border between soft and stiff clays, which is $0.5D_T$.

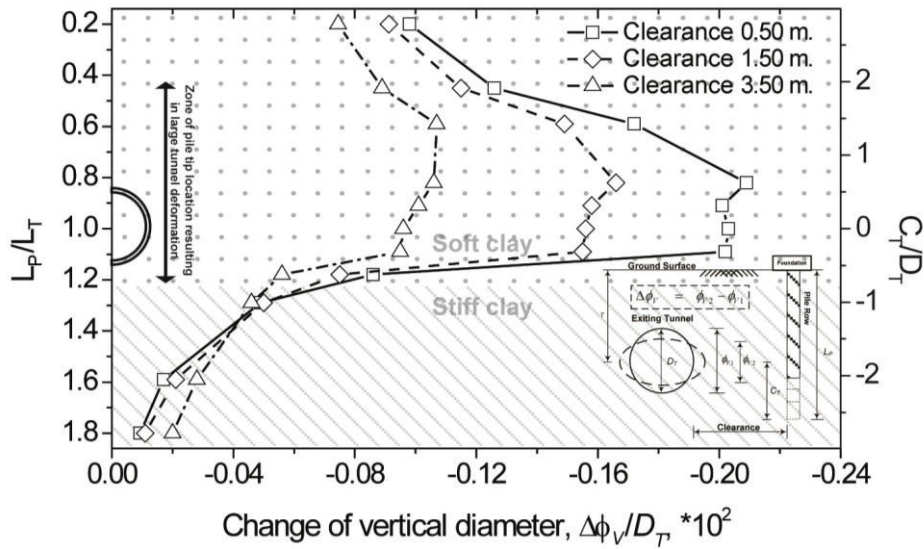


Figure 9. Changes in tunnel diameter in vertical direction subject to pile row loading with various pile tip positions for tunnel in case 2 (Figure 4)

The results for tunnel located between soft clay and stiff clay layers (case 3, Figure 4) are presented in Figure 10. The border between soft and stiff clays is set at the tunnel axis. For all three values of clearance, the values of $\Delta\phi_V$ are smaller than those from the two previous cases. In comparison to the previous cases, the maximum values are significantly smaller and occur when the pile tip is in soft clay at a higher level. Similar to case 2, the level of pile tip at which $\Delta\phi_V$ suddenly decreases with increasing pile length is at the border between soft and stiff clays. However, when the pile tip is extended below this level, which is stiff clay, $\Delta\phi_V$ slightly increases again for a certain depth before it gradually decreases with increasing pile length. This is probably because at that depth the piles have a larger working load (due to end bearing capacity) and their tips are at the same level as the tunnel axis.

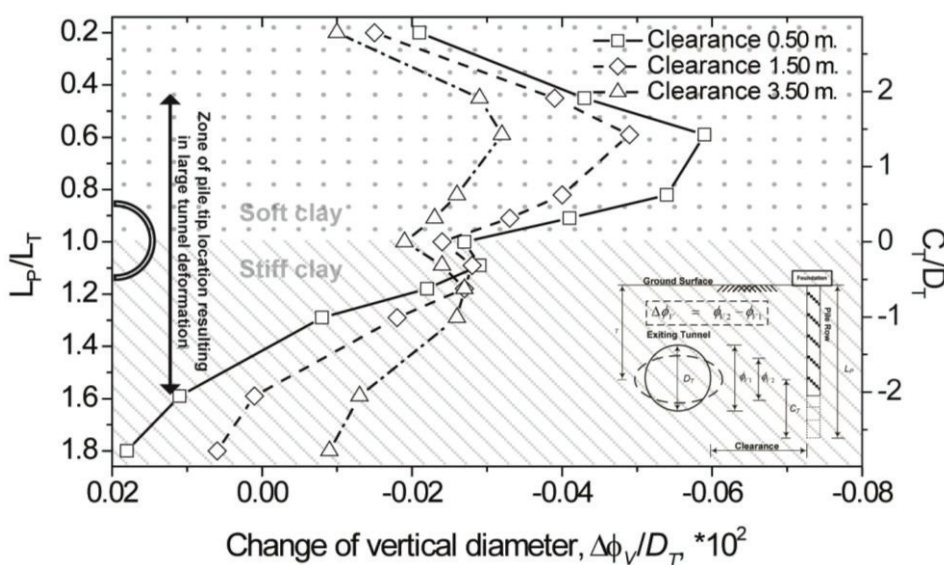


Figure 10. Changes in tunnel diameter in vertical direction subject to pile row loading with various pile tip positions for tunnel located between soft and stiff clays (case 3, Figure 4)

Figure 11 depicts the results for the case of the tunnel constructed in stiff clay (case 4, Figure 4). The tunnel deformations as well as their maximum values are smallest among the four cases in this study. The tunnel in stiff soil is thus safer than that in soft soil due to smaller soil movements in the tunnel vicinity. The maximum values still occur when the pile tip is in soft clay even with a small working load. Therefore, caution should be exercised in the construction of the bearing unit pile adjacent to the tunnel. When the pile tip is near the tunnel in stiff clay, $\Delta\phi_V$ increases again with a relatively higher value and longer range (compared to the previous case) after a large decrease at the clay border.

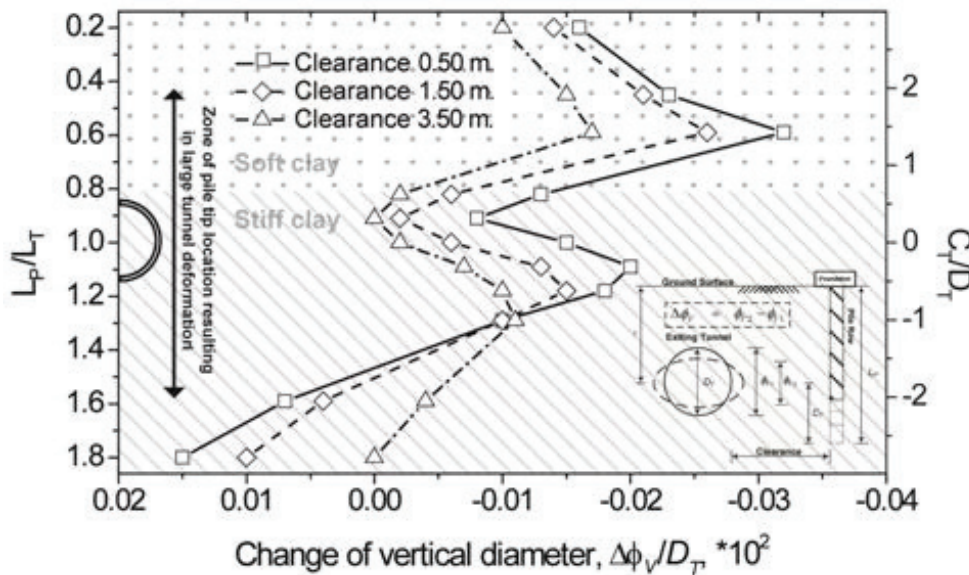


Figure 11. Changes in tunnel diameter in vertical direction due to pile row loading with various pile tip positions for tunnel in stiff clay layer (case 4, Figure 4)

The numerical results have confirmed that the deformations of an existing tunnel caused by a pile-row loading are similar to those caused by a single-pile loading, although the magnitude of the deformations in the former case is larger than in the latter. The deformations of the tunnel constructed in soft clay are much larger than in stiff clay and a large tunnel deformation occurs when the pile tip is close to the tunnel. The tunnel influence zone subject to nearby bored pile loading should therefore be determined by taking into account the relative position between the pile tip and the tunnel. The drastic changes of tunnel deformation are noticeable between about $2D_T$ above and $2D_T$ below the tunnel axis or down to the stiff layer, depending on the ground conditions, as listed in Table 3. For the horizontal clearance, a value of $0.6D_T$ (approximately 3.5 m) from the tunnel surface seems to be sufficient. A new influence zone for the existing tunnel subject to nearby piles can then be proposed as shown in Figure 12. By comparison with the previously used influence zones, the developed zone obtained in this study (shaded rectangular area in Figure 12) is much smaller. This increases the likelihood of new construction projects in the area near the tunnel alignment. However, the proposed influence zone is specified based on one specific tunnel (i.e. that of the MRTA) and one pile size (1 m). A broader set of data is required to enhance its reliability.

Table 3. Significant influence zone from pile-row analyses

Soil stratum	Significant influence zone	
	Change of vertical diameter	Change of horizontal diameter
Case 1	$2D_T - (-2D_T)$	$2D_T - (-2D_T)$
Case 2	$2D_T - (-0.5D_T)$	$2D_T - (-0.5D_T)$
Case 3	$2D_T - (-1D_T)$	$2D_T - (-1D_T)$
Case 4	$2D_T - (-1D_T)$	$2D_T - (-1D_T)$

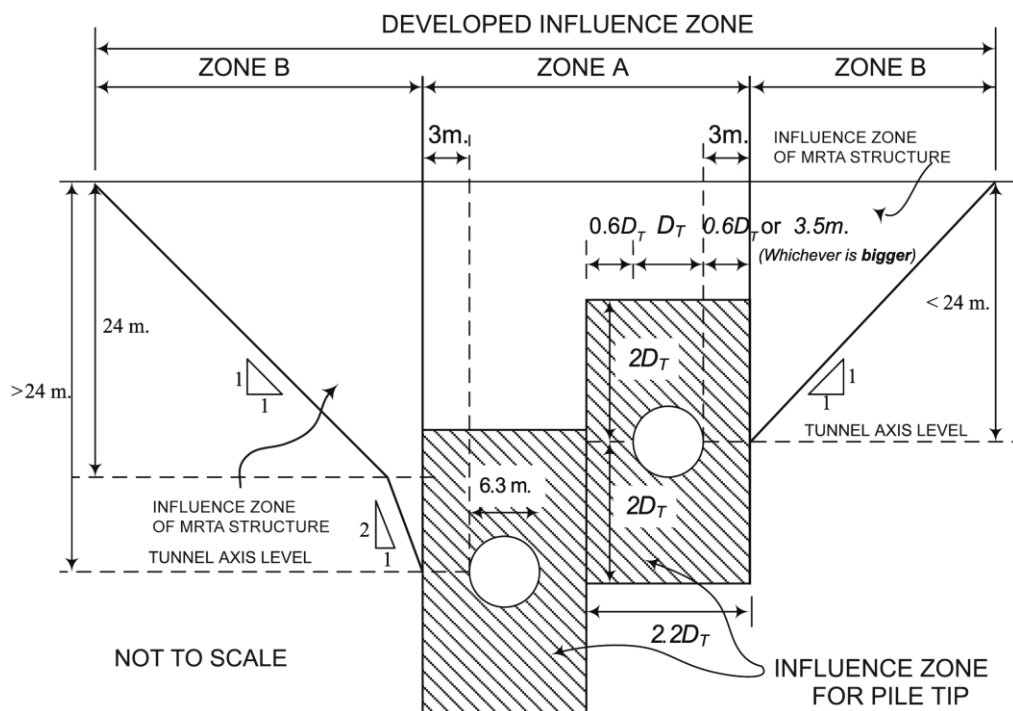


Figure 12. Developed tunnel influence zone from nearby pile tip position

CONCLUSIONS

The position of pile tip in relation to the tunnel axis and the soil type in which the tunnel is situated have a significant impact on deformations of the existing tunnel. The numerically generated data and the consideration of the relative position of the pile tip can suggest a new influence zone.

The following observations have been made from the study:

- 1) The tunnel deformations become drastically large when the pile tip is situated in a specific range, depending on the soil type in which the tunnel is situated. However, the ranges for the four different soil types hardly alter.
- 2) It is reasonable to recommend the range of $2D_T$ above and $2D_T$ underneath the tunnel centre as the influence zone.
- 3) For the horizontal clearance, the value of $0.6D_T$ from tunnel surface seems to be sufficient.
- 4) By considering the lining deformation induced by the movement of soil surrounding the pile, the proposed influence zone is much smaller than the existing zone in which all construction activities are taken into consideration. The smaller zone increases the possibility of new construction projects in the area near the tunnel alignment.

However, as more complex behaviours in engineering practice are excluded from this study, future research that includes other relevant parameters, e.g. tunnel diameter, thickness of lining and pile size, is necessary for a more refined and more realistic tunnel influence zone. Moreover, further study on the correlation between pile settlement, pile force distribution and soil stress distribution around pile with lining deformation should enhance the understanding of this soil-structure interaction problem.

ACKNOWLEDGEMENTS

The financial support provided by the Office of the Higher Education Commission under the Higher Education Research Promotion and National Research University (NRU) Project of Thailand is gratefully acknowledged. The first author would also like to extend his appreciation for the research funding from the Thailand Research Fund (TRF) and 1D2 Group Co. Ltd. under Grant PHD56I0057.

REFERENCES

1. Land Transport Authority, "Code of Practice for Railway Protection", Development and Building Control Department, Singapore, **2004**.
2. Mass Rapid Transit Authority of Thailand, "Restrictive Guideline for Protection Zone in Blue Line Project", Engineering Specifications for MRT Tunnels, Bangkok, **2009** (in Thai).
3. J. D. Morton and K. H. King, "Effects of tunneling on the bearing capacity and settlement of piled foundation", Proceedings of 2nd International Symposium on Tunnelling, **1979**, London, Great Britain, pp.57-68.
4. R. J. Mair, R. N. Taylor and A. Bracegirdle, "Subsurface settlement profiles above tunnels in clays", *Geotechnique*, **1993**, 43, 315-320.
5. D. Selemetas, J. R. Standing and R. J. Mair, "The response of full-scale piles to tunneling", Proceedings of 5th International Symposium TC28 on Geotechnical Aspects of Underground Construction in Soft Ground, **2005**, Amsterdam, Netherlands, pp.763-769.
6. Y. J. Lee and R. H. Bassett, "Influence zones for 2D pile-soil-tunnelling interaction based on model test and numerical analysis", *Tunn. Undergr. Space Technol.*, **2007**, 22, 325-342.
7. P. Jongpradist, T. Kaewsri, A. Sawatparnich, S. Suwansawat, S. Youwai, W. Kongkitkul and J. Sunitsakul, "Development of tunneling influence zones for adjacent pile foundations by numerical analyses", *Tunn. Undergr. Space Technol.*, **2013**, 34, 96-109.
8. P. Kitiyodom, T. Matsumoto and K. Kawaguchi, "A simplified analysis method for piled raft foundations subjected to ground movements induced by tunnelling", *Int. J. Numer. Anal. Meth. Geomech.*, **2005**, 29, 1485-1507.
9. H. Y. Liu, J. C. Small and J. P. Carter, "Full 3D modelling for effects of tunnelling on existing support systems in the Sydney region" *Tunn. Undergr. Space Technol.*, **2008**, 23, 399-420.
10. M. Dolezalova, "Tunnel complex unloaded by a deep excavation", *Comput. Geotech.*, **2001**, 28, 469-493.
11. M. Abdel-Meguid, R. K. Rowe and K. Y. Lo, "3D effects of surface construction over existing subway tunnels", *Int. J. Geomech.*, **2002**, 2, 447-469.
12. E. O. Measor and D. H. New, "The design and construction of the Royal Festival Hall, South Bank", *J. Inst. Civil Eng.*, **1951**, 36, 241-305.

13. F. C. Schroeder, D. M. Potts and T. I. Addenbrooke, “The influence of pile group loading on existing tunnels”, *Geotechnique*, **2004**, 54, 351-362.
14. H. Mroueh and I. Shahrour, “Three-dimensional finite element analysis of the interaction between tunneling and pile foundations”, *Int. J. Numer. Anal. Meth. Geomech.*, **2002**, 26, 217-230.
15. S. Arunkumar and R. Ayothiraman, “Effect of vertically loaded pile on existing urban tunnel in clay”, Proceedings of Indian Geotechnical Conference, **2010**, Mumbai, India, pp.751-754.
16. Simulia, “ABAQUS Analysis User's Manual, Version 6.3-1”, Dassault Systèmes Simulia Corp, Providence (RI), **2008**.
17. A. W. Skempton, “Cast in-situ bored piles in London Clay”, *Geotechnique*, **1959**, 9, 153-173.
18. I. Chudleigh, K. G. Higgins, H. D. St John, D. M. Pott and F. C. Schroeder, “Pile-tunnel interaction problems”, Proceedings of Tunnel Construction and Piling, **1999**, London, Great Britain, pp.172-185.
19. T. Schanz, P. A. Vermeer and P. G. Bonnier, “The hardening soil model: Formulation and verification”, Proceedings of PLAXIS symposium on “Beyond 2000 in Computational Geotechnics”, **1999**, Rotterdam, Netherlands, pp.281-296.
20. S. Timpong, “Analysis of ground movements in Bangkok MRT Blue Line project”, *Master Thesis*, **2002**, Asian Institute of Technology, Thailand.
21. C. T. Tseng, “Three dimension simulation of EPB shield tunneling in Bangkok soft ground”, *Master Thesis*, **2000**, Asian Institute of Technology, Thailand.
22. C. Surasak, S. Likitlersuang, D. Wanatowski, A. Balasubramanim, E. Oh and H. Guan, “Stiffness and strength parameters for hardening soil model of soft and stiff Bangkok clays”, *Soils Found.*, **2012**, 52, 682-697.
23. R. E. Prust, J. Davies and S. Hu, “Pressuremeter Investigation for Mass Rapid Transit in Bangkok, Thailand”, *Transport. Res. Rec. J. Transport. Res. Board*, **2005**, 1928, 207-217.

Full Paper

Soret effects on unsteady magnetohydrodynamic mixed-convection heat-and-mass-transfer flow in a porous medium with Newtonian heating

Abid Hussanan¹, Mohd Z. Salleh^{1,*}, Ilyas Khan², Razman M. Tahar³ and Zulkhibri Ismail¹

¹ Applied and Industrial Mathematics Research Group, Faculty of Industrial Science and Technology, Universiti Malaysia Pahang, Lebuhraya Tun Razak, 26300 UMP Kuantan, Pahang, Malaysia

² College of Engineering, Majmaah University, P.O. Box 66, Majmaah 11952, Saudi Arabia

³ Faculty of Industrial Management, Universiti Malaysia Pahang, Lebuhraya Tun Razak, 26300 UMP Kuantan, Pahang, Malaysia

* Corresponding author, e-mail: zukikuj@yahoo.com

Received: 31 May 2014 / Accepted: 4 August 2015 / Published: 5 August 2015

Abstract: Soret effects on unsteady mixed-convection heat-and-mass-transfer flow over an oscillating vertical plate embedded in a porous medium with Newtonian heating in the presence of magnetic field are studied. The governing equations, along with imposed initial and boundary conditions, are first converted into the dimensionless form and then solved using the Laplace transform technique. The numerical results for fluid velocity, temperature and concentration are graphically shown, whereas the skin friction, Nusselt number and Sherwood number are presented in tabular forms. It is observed that the fluid velocity and concentration increase with increasing values of Soret number. The conjugate parameter of Newtonian heating increases the temperature as well as the concentration and velocity distributions. It is also found that the rates of the heat-and-mass transfer increase as the conjugate parameter increases.

Keywords: Soret effects, magnetohydrodynamic flow, heat-and-mass-transfer flow, porous medium, Newtonian heating

INTRODUCTION

Recently the study of magnetohydrodynamic (MHD) flow, together with heat-and-mass transfer, has received the attention of a large number of researchers because of its diverse

applications in many branches of science and technology as well in industry. Some of the important applications are found in stellar and solar structures, cooling of nuclear reactors, interstellar matter, liquid metal fluid, power generation system, radio propagation, aero dynamics and electromagnetic material processing [1-3]. Suneetha et al. [4], for instance, studied the MHD heat-and-mass transfer flow past a vertical plate with variable surface temperature by considering the heat due to viscous dissipation. The effects of thermal radiation and chemical reaction on MHD free-convection flow past a semi-infinite inclined porous plate with variable surface temperature and concentration were studied by Uddin and Kumar [5]. The same problem was considered by Muthucumaraswamy and Valliammal [6] for an exponentially accelerated infinite vertical plate without thermal radiation effect. Recently, Nandkeolyar et al. [7] obtained an exact solution of unsteady MHD free-convection heat-and-mass-transfer flow in a heat absorbing fluid with ramped wall temperature.

On the other hand, the problem of MHD mixed-convection flow through porous media has been the subject of considerable research activity in recent years because of its several important applications such as those involving heat removal from nuclear fuel debris, drug permeation through human skin, oil flow through porous rock and filtration of solids from liquids [8, 9]. Beg et al. [10] presented exact solutions for unsteady MHD heat transfer in a semi-infinite porous medium with thermal radiation flux. In the same year, Reddy et al. [11] extended the work of Beg et al. [10] by taking into account the periodic wall temperature. The effects of thermal radiation on MHD free-convection flow through a porous medium with variable boundary conditions were investigated by Kishore et al. [12]. The effects of slip condition on the unsteady MHD flow of a viscoelastic fluid in a porous channel were analysed by Farhad et al. [13]. Recently, the influence of thermal radiation and chemical reaction on MHD heat-and-mass-transfer flow embedded in a porous medium with variable suction was studied by Ahmed and Das [14].

In all the above studies, the thermal-diffusion (Soret) effect was neglected. Thermal diffusion of great significance for isotope separation and for making a mixture of gases with very light molecular weights (H_2 , He) and medium molecular weights (N_2 , air) [15]. Due to the importance of thermal-diffusion effect, a number of researchers have studied it for different fluids. Ahmed [16], for instance, made an exact analysis of the thermal-diffusion effect on combined heat-and-mass-transfer Hartmann flow through a channel bounded by two infinite horizontal isothermal parallel plates. The Soret-driven, free-convection heat-and-mass-transfer flow of a non-Newtonian liquid past a vertical plate in a thermally stratified porous medium was studied by Narayana et al. [17]. Farhad et al. [18] found analytical solutions of MHD heat-and-mass-transfer flow past a vertical plate embedded in a porous medium in the presence of Soret and chemical effects. The influence of Soret effect on the unsteady motion of MHD mixed-convection flow of a viscoelastic fluid over an infinite vertical plate in the presence of a heat source was investigated by Jha et al. [19]. Sharma et al. [20] studied the Soret and Dufour effects on unsteady MHD mixed-convection flow with heat source and Ohmic dissipation. Recently, MHD heat-and-mass-transfer flow over a vertical plate in a porous medium under the influence of Dufour and Soret effects was discussed by Vedavathi et al. [21].

The mixed convection flows with combined heat-and-mass transfer past an oscillating vertical plate are usually modelled by considering the ramped wall temperature, variable surface temperature or constant surface heat-flux boundary conditions [22-24]. However, in many practical situations where the heat transfer from the surface is proportional to the local surface temperature, the above conditions fail to work and the Newtonian heating condition is needed. Merkin [25]

initiated the idea of Newtonian heating in his pioneering work on natural convection boundary flow passing through a vertical surface. Applications of Newtonian heating are found in many important engineering applications, e.g. in heat exchangers where bounding surfaces absorb heat by solar radiation and in conjugate heat transfer around fins. Considering the importance of Newtonian heating condition, many authors have used it in their convective heat-transfer problems and obtained the solutions either numerically [26-30] or analytically [31-38]. The main objective of the present study is to investigate the thermal-diffusion effect on unsteady MHD mixed-convection heat-and-mass-transfer flow past an oscillating vertical plate through a porous medium with Newtonian heating, where the heat transfer from the surface is proportional to the local surface temperature. The governing equations are solved using Laplace transform technique and the expressions for velocity, temperature and concentration are obtained in terms of exponential and complementary error functions. The corresponding expressions for skin friction, Nusselt number and Sherwood number are also evaluated.

MATHEMATICAL FORMULATION

Consider the unsteady mixed convection flow of a viscous incompressible fluid through a porous medium bounded by an infinite oscillating vertical plate. The x' -axis is taken along the vertical plate and y' -axis normal to it. The magnetic field B_0 of uniform strength is applied normal to the plate and the induced magnetic field is considered to be negligible. Initially, for time $t' \leq 0$, both the plate and fluid are at rest with constant temperature T_∞ and concentration C_∞ . At time $t' = 0^+$, the plate starts an oscillatory motion in its plane with velocity V :

$$V = U_0 \cos(\omega' t') \mathbf{i}; t' > 0, \tag{1}$$

where \mathbf{i} is the unit vector in the flow direction, U_0 is the amplitude of the plate oscillations and ω' is the frequency of oscillation. At the same time, the heat transfer from the plate to the fluid is proportional to the local surface temperature T' and the concentration near the plate is raised from C_∞ to C_w . The geometry of the problem is shown in Figure 1.

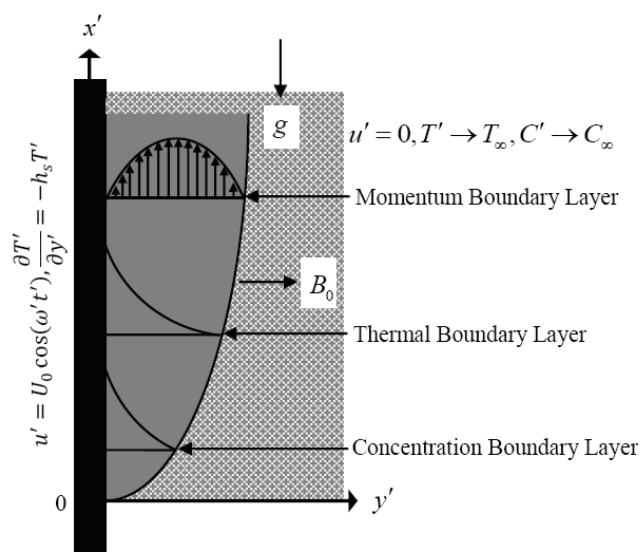


Figure 1. Physical sketch of different boundary layers in a porous medium under the effect of magnetic field, together with the corresponding Cartesian coordinates

Under the Boussinesq's approximation [39], the governing equations of free convection flow can be written as:

$$\frac{\partial u'}{\partial t'} = \nu \frac{\partial^2 u'}{\partial y'^2} - \frac{\sigma B_0^2}{\rho} u' - \frac{\nu \phi}{k_1} u' + g\beta(T' - T_\infty) + g\beta^*(C' - C_\infty), \quad (2)$$

$$\rho C_p \frac{\partial T'}{\partial t'} = k \frac{\partial^2 T'}{\partial y'^2} - \frac{\partial q_r}{\partial y'}, \quad (3)$$

$$\frac{\partial C'}{\partial t'} = D \frac{\partial^2 C'}{\partial y'^2} + \frac{DK_T}{T_m} \frac{\partial^2 T'}{\partial y'^2}, \quad (4)$$

where u' is the axial velocity, t' the time, ρ the fluid density, ν the kinematic viscosity, σ the electric conductivity of the fluid, ϕ the porosity, k_1 the permeability, g the acceleration due to gravity, β the volumetric coefficient of thermal expansion, β^* the volumetric coefficient of mass expansion, C_p the heat capacity at constant pressure, T' the temperature of the fluid, k the thermal conductivity, q_r the radiative flux along the y' -axis, C' the species concentration in the fluid, C_∞ the species concentration far away from the plate, K_T the thermal diffusion ratio, T_∞ the ambient temperature, T_m the mean fluid temperature and D the mass diffusivity.

The corresponding initial and boundary conditions are

$$t' \leq 0 : u' = 0, T' = T_\infty, C' = C_\infty \text{ for all } y' \geq 0, \quad (5)$$

$$t' > 0 : u' = U_0 \cos(\omega t'), \frac{\partial T'}{\partial y'} = -h_s T', C' = C_w \text{ at } y' = 0, \quad (6)$$

$$u' \rightarrow 0, T' \rightarrow T_\infty, C' \rightarrow C_\infty \text{ as } y' \rightarrow \infty, \quad (7)$$

where h_s is the heat transfer coefficient, and C_∞ and C_w are the species concentrations near and far away from the plate respectively. Using the Rosseland approximation [40], equation (3) modifies to:

$$\rho C_p \frac{\partial T'}{\partial t'} = k \left(1 + \frac{16\sigma^* T_\infty^3}{3kk^*} \right) \frac{\partial^2 T'}{\partial y'^2}. \quad (8)$$

Introducing the following non-dimensional variables,

$$y = \frac{y' U_0}{\nu}, t = \frac{t' U_0^2}{\nu}, u = \frac{u'}{U_0}, \theta = \frac{T' - T_\infty}{T_\infty}, C = \frac{C' - C_\infty}{C_w - C_\infty}, \omega = \frac{\omega' \nu}{U_0^2},$$

into equations (2), (4) and (8), we obtain

$$\frac{\partial u}{\partial t} = \frac{\partial^2 u}{\partial y^2} - M^2 u - \frac{1}{K} u + Gr\theta + GmC, \quad (9)$$

$$Pr \frac{\partial \theta}{\partial t} = (1 + R) \frac{\partial^2 \theta}{\partial y^2}, \quad (10)$$

$$\frac{\partial C}{\partial t} = \frac{1}{Sc} \frac{\partial^2 C}{\partial y^2} + Sr \frac{\partial^2 \theta}{\partial y^2}, \quad (11)$$

where

$$Gr = \frac{\nu g \beta T_\infty}{U_0^3}, Gm = \frac{\nu g \beta^* (C_w - C_\infty)}{U_0^3}, M^2 = \frac{\nu \sigma B_0^2}{\rho U_0^2}, \frac{1}{K} = \frac{\nu^2 \phi}{k_1 U_0^2},$$

$$Pr = \frac{\mu C_p}{k}, R = \frac{16 \sigma^* T_\infty^3}{3 k k^*}, Sc = \frac{\nu}{D}, Sr = \frac{DK_T T_\infty}{\nu T_m (C_w - C_\infty)},$$

are the Grashof number, modified Grashof number, magnetic parameter, porosity parameter, Prandtl number, radiation parameter, Schmidt number and Soret number respectively. The corresponding initial and boundary conditions in non-dimensional forms are:

$$t \leq 0 : u = 0, \theta = 0, C = 0 \text{ for all } y \geq 0, \tag{12}$$

$$t > 0 : u = \cos(\omega t), \frac{\partial \theta}{\partial y} = -\gamma(1 + \theta), C = 1 \text{ at } y = 0, \tag{13}$$

$$u \rightarrow 0, \theta \rightarrow 0, C \rightarrow 0 \text{ as } y \rightarrow \infty. \tag{14}$$

Here, $\gamma = h_s \nu / U_0$ is the conjugate parameter for Newtonian heating. It is important to note that equation (13) gives $\theta = 0$ when $\gamma = 0$, corresponding to $h_s = 0$ and consequently, in this case no heating from the plate exists [27, 33].

METHOD OF SOLUTIONS

Applying the Laplace transform with respect to time t to the system of equations (9) to (14), we obtain the following solutions in the transformed (y, q) plane:

$$\begin{aligned} \bar{u}(y, q) = & \frac{1}{2(q + i\omega)} e^{-y\sqrt{q+L}} + \frac{1}{2(q - i\omega)} e^{-y\sqrt{q+L}} + \frac{ac}{q^2(\sqrt{q} - c)} e^{-y\sqrt{q+L}} \\ & - \frac{cdh}{q^2(\sqrt{q} - c)} e^{-y\sqrt{q+L}} + \frac{bch}{q^2(\sqrt{q} - c)} e^{-y\sqrt{q+L}} + \frac{b}{q^2} e^{-y\sqrt{q+L}} \\ & - \frac{ac}{q^2(\sqrt{q} - c)} e^{-y\sqrt{q Pr_{eff}}} + \frac{cdh}{q^2(\sqrt{q} - c)} e^{-y\sqrt{q Pr_{eff}}} - \frac{b}{q^2} e^{-y\sqrt{q Sc}} \\ & - \frac{bch}{q^2(\sqrt{q} - c)} e^{-y\sqrt{q Sc}}, \end{aligned} \tag{15}$$

$$\bar{\theta}(y, q) = \frac{c}{q(\sqrt{q} - c)} e^{-y\sqrt{q Pr_{eff}}}, \tag{16}$$

$$\bar{C}(y, q) = \frac{1}{q} e^{-y\sqrt{q Sc}} + \frac{ch}{q(\sqrt{q} - c)} e^{-y\sqrt{q Sc}} - \frac{ch}{q(\sqrt{q} - c)} e^{-y\sqrt{q Pr_{eff}}}, \tag{17}$$

where $\bar{u}(y, q) = \int_0^\infty e^{-qt} u(y, t) dt$, $\bar{\theta}(y, q) = \int_0^\infty e^{-qt} \theta(y, t) dt$ and $\bar{C}(y, q) = \int_0^\infty e^{-qt} C(y, t) dt$ denote the

Laplace transforms of $u(y, t)$, $\theta(y, t)$ and $C(y, t)$ respectively, and $a = \frac{Gr}{Pr_{eff} - 1}$, $b = \frac{Gm}{Sc - 1}$,

$c = \frac{\gamma}{\sqrt{Pr_{eff}}}$, $d = \frac{Gm}{Pr_{eff} - 1}$, $h = \frac{Sc Sr Pr_{eff}}{Pr_{eff} - 1}$, $L = M^2 + \frac{1}{K}$ and $Pr_{eff} = \frac{Pr}{1 + R}$ (Pr_{eff} = the effective Prandtl

number) [40]. The inverse Laplace transform of equations (15) to (17) yields:

$$\theta(y,t) = e^{(c^2t-yc\sqrt{\text{Pr}_{\text{eff}}})} \operatorname{erfc}\left(\frac{y}{2}\sqrt{\frac{\text{Pr}_{\text{eff}}}{t}} - c\sqrt{t}\right) - \operatorname{erfc}\left(\frac{y}{2}\sqrt{\frac{\text{Pr}_{\text{eff}}}{t}}\right), \tag{18}$$

$$C(y,t) = \operatorname{erfc}\left(\frac{y}{2}\sqrt{\frac{Sc}{t}}\right) + h \left[e^{(c^2t-yc\sqrt{Sc})} \operatorname{erfc}\left(\frac{y}{2}\sqrt{\frac{Sc}{t}} - c\sqrt{t}\right) - \operatorname{erfc}\left(\frac{y}{2}\sqrt{\frac{Sc}{t}}\right) \right] - h \left[e^{(c^2t-yc\sqrt{\text{Pr}_{\text{eff}}})} \operatorname{erfc}\left(\frac{y}{2}\sqrt{\frac{\text{Pr}_{\text{eff}}}{t}} - c\sqrt{t}\right) - \operatorname{erfc}\left(\frac{y}{2}\sqrt{\frac{\text{Pr}_{\text{eff}}}{t}}\right) \right], \tag{19}$$

$$u(y,t) = \frac{1}{4} e^{-i\omega t} \left[e^{-y\sqrt{L-i\omega}} \operatorname{erfc}\left(\frac{y}{2\sqrt{t}} - \sqrt{(L-i\omega)t}\right) + e^{y\sqrt{L-i\omega}} \operatorname{erfc}\left(\frac{y}{2\sqrt{t}} + \sqrt{(L-i\omega)t}\right) \right] + \frac{1}{4} e^{i\omega t} \left[e^{-y\sqrt{L+i\omega}} \operatorname{erfc}\left(\frac{y}{2\sqrt{t}} - \sqrt{(L+i\omega)t}\right) + e^{y\sqrt{L+i\omega}} \operatorname{erfc}\left(\frac{y}{2\sqrt{t}} + \sqrt{(L+i\omega)t}\right) \right] + \frac{(dh-a)}{c^2} \left[e^{(c^2t-yc\sqrt{\text{Pr}_{\text{eff}}})} \operatorname{erfc}\left(\frac{y}{2}\sqrt{\frac{\text{Pr}_{\text{eff}}}{t}} - c\sqrt{t}\right) - \operatorname{erfc}\left(\frac{y}{2}\sqrt{\frac{\text{Pr}_{\text{eff}}}{t}}\right) \right] - \frac{(dh-a)}{c} \left[2\sqrt{\frac{t}{\pi}} e^{-\frac{y^2 \text{Pr}_{\text{eff}}}{4t}} - y\sqrt{\text{Pr}_{\text{eff}}} \operatorname{erfc}\left(\frac{y}{2}\sqrt{\frac{\text{Pr}_{\text{eff}}}{t}}\right) \right] - (dh-a) \left[\left(\frac{y^2 \text{Pr}_{\text{eff}}}{2} + t\right) \operatorname{erfc}\left(\frac{y}{2}\sqrt{\frac{\text{Pr}_{\text{eff}}}{t}}\right) - y\sqrt{\text{Pr}_{\text{eff}}} \sqrt{\frac{t}{\pi}} e^{-\frac{y^2 \text{Pr}_{\text{eff}}}{4t}} \right] - \frac{bh}{c^2} \left[e^{(c^2t-yc\sqrt{Sc})} \operatorname{erfc}\left(\frac{y}{2}\sqrt{\frac{Sc}{t}} - c\sqrt{t}\right) - \operatorname{erfc}\left(\frac{y}{2}\sqrt{\frac{Sc}{t}}\right) \right] + \frac{bh}{c} \left[2\sqrt{\frac{t}{\pi}} e^{-\frac{y^2 Sc}{4t}} - y\sqrt{Sc} \operatorname{erfc}\left(\frac{y}{2}\sqrt{\frac{Sc}{t}}\right) \right] + b(h-1) \left[\left(\frac{y^2 Sc}{2} + t\right) \operatorname{erfc}\left(\frac{y}{2}\sqrt{\frac{Sc}{t}}\right) - y\sqrt{Sc} \sqrt{\frac{t}{\pi}} e^{-\frac{y^2 Sc}{4t}} \right] + \frac{bt}{2} \left[e^{-y\sqrt{L}} \operatorname{erfc}\left(\frac{y}{2\sqrt{t}} - \sqrt{Lt}\right) + e^{y\sqrt{L}} \operatorname{erfc}\left(\frac{y}{2\sqrt{t}} + \sqrt{Lt}\right) \right] - \frac{yb}{4\sqrt{L}} \left[e^{-y\sqrt{L}} \operatorname{erfc}\left(\frac{y}{2\sqrt{t}} - \sqrt{Lt}\right) - e^{y\sqrt{L}} \operatorname{erfc}\left(\frac{y}{2\sqrt{t}} + \sqrt{Lt}\right) \right] + c(a-dh+bh) \int_0^t \left[\frac{1}{\sqrt{\pi(t-s)}} + ce^{c^2(t-s)} \operatorname{erfc}(-c\sqrt{t-s}) \right] \times \left[\left(\frac{s}{2} - \frac{y}{4\sqrt{L}}\right) e^{-y\sqrt{L}} \operatorname{erfc}\left(\frac{y}{2\sqrt{s}} - \sqrt{Ls}\right) + \left(\frac{s}{2} + \frac{y}{4\sqrt{L}}\right) e^{y\sqrt{L}} \operatorname{erfc}\left(\frac{y}{2\sqrt{s}} + \sqrt{Ls}\right) \right] ds. \tag{20}$$

where $\operatorname{erfc}(\cdot)$ represents the complementary error function.

Note that the above solutions for concentration and velocity given by equations (19) and (20) are only valid for $\text{Pr}_{\text{eff}} \neq 1$ and $Sc \neq 1$. Moreover, the other solutions are:

1) When $Pr_{eff} = 1$ and $Sc \neq 1$,

$$C(y,t) = \operatorname{erfc}\left(\frac{y}{2}\sqrt{\frac{Sc}{t}}\right) - \frac{ScSr}{(Sc-1)} \left[e^{(\gamma^2 t - y\gamma\sqrt{Sc})} \operatorname{erfc}\left(\frac{y}{2}\sqrt{\frac{Sc}{t}} - \gamma\sqrt{t}\right) - \operatorname{erfc}\left(\frac{y}{2}\sqrt{\frac{Sc}{t}}\right) \right] + \frac{ScSr}{(Sc-1)} \left[e^{(\gamma^2 t - y\gamma)} \operatorname{erfc}\left(\frac{y}{2\sqrt{t}} - c\sqrt{t}\right) - \operatorname{erfc}\left(\frac{y}{2\sqrt{t}}\right) \right], \tag{21}$$

$$u(y,t) = \frac{1}{4} e^{-i\omega t} \left[e^{-y\sqrt{L-i\omega}} \operatorname{erfc}\left(\frac{y}{2\sqrt{t}} - \sqrt{(L-i\omega)t}\right) + e^{y\sqrt{L-i\omega}} \operatorname{erfc}\left(\frac{y}{2\sqrt{t}} + \sqrt{(L-i\omega)t}\right) \right] + \frac{1}{4} e^{i\omega t} \left[e^{-y\sqrt{L+i\omega}} \operatorname{erfc}\left(\frac{y}{2\sqrt{t}} - \sqrt{(L+i\omega)t}\right) + e^{y\sqrt{L+i\omega}} \operatorname{erfc}\left(\frac{y}{2\sqrt{t}} + \sqrt{(L+i\omega)t}\right) \right] + \left(\frac{Gr + bScSr}{L}\right) \left[e^{(\gamma^2 t - y\gamma)} \operatorname{erfc}\left(\frac{y}{2\sqrt{t}} - \gamma\sqrt{t}\right) - \operatorname{erfc}\left(\frac{y}{2\sqrt{t}}\right) \right] + \frac{bScSr}{\gamma^2(Sc-1)} \left[e^{(\gamma^2 t - y\gamma\sqrt{Sc})} \operatorname{erfc}\left(\frac{y}{2}\sqrt{\frac{Sc}{t}} - \gamma\sqrt{t}\right) - \operatorname{erfc}\left(\frac{y}{2}\sqrt{\frac{Sc}{t}}\right) \right] - \frac{bScSr}{\gamma(Sc-1)} \left[2\sqrt{\frac{t}{\pi}} e^{-\frac{y^2 Sc}{4t}} - y\sqrt{Sc} \operatorname{erfc}\left(\frac{y}{2}\sqrt{\frac{Sc}{t}}\right) \right] - \frac{bScSr}{(Sc-1)} \left[\left(\frac{y^2 Sc}{2} + t\right) \operatorname{erfc}\left(\frac{y}{2}\sqrt{\frac{Sc}{t}}\right) - y\sqrt{Sc} \sqrt{\frac{t}{\pi}} e^{-\frac{y^2 Sc}{4t}} \right] - b \left[\left(\frac{y^2 Sc}{2} + t\right) \operatorname{erfc}\left(\frac{y}{2}\sqrt{\frac{Sc}{t}}\right) - y\sqrt{Sc} \sqrt{\frac{t}{\pi}} e^{-\frac{y^2 Sc}{4t}} \right] + \frac{bt}{2} \left[e^{-y\sqrt{L}} \operatorname{erfc}\left(\frac{y}{2\sqrt{t}} - \sqrt{Lt}\right) + e^{y\sqrt{L}} \operatorname{erfc}\left(\frac{y}{2\sqrt{t}} + \sqrt{Lt}\right) \right] - \frac{yb}{4\sqrt{L}} \left[e^{-y\sqrt{L}} \operatorname{erfc}\left(\frac{y}{2\sqrt{t}} - \sqrt{Lt}\right) - e^{y\sqrt{L}} \operatorname{erfc}\left(\frac{y}{2\sqrt{t}} + \sqrt{Lt}\right) \right] - \frac{\gamma bScSr}{(Sc-1)} \int_0^t \left[\frac{1}{\sqrt{\pi(t-s)}} + \gamma e^{\gamma^2(t-s)} \operatorname{erfc}(-\gamma\sqrt{t-s}) \right] \times \left[\left(\frac{s}{2} - \frac{y}{4\sqrt{L}}\right) e^{-y\sqrt{L}} \operatorname{erfc}\left(\frac{y}{2\sqrt{s}} - \sqrt{Ls}\right) + \left(\frac{s}{2} + \frac{y}{4\sqrt{L}}\right) e^{y\sqrt{L}} \operatorname{erfc}\left(\frac{y}{2\sqrt{s}} + \sqrt{Ls}\right) \right] ds. \tag{22}$$

2) When $Pr_{eff} \neq 1$ and $Sc = 1$,

$$C(y,t) = \operatorname{erfc}\left(\frac{y}{2\sqrt{t}}\right) - \frac{Pr_{eff} Sr}{(Pr_{eff}-1)} \left[e^{(c^2 t - yc\sqrt{Pr_{eff}})} \operatorname{erfc}\left(\frac{y}{2}\sqrt{\frac{Pr_{eff}}{t}} - c\sqrt{t}\right) - \operatorname{erfc}\left(\frac{y}{2}\sqrt{\frac{Pr_{eff}}{t}}\right) \right] + \frac{Pr_{eff} Sr}{(Pr_{eff}-1)} \left[e^{(c^2 t - yc)} \operatorname{erfc}\left(\frac{y}{2\sqrt{t}} - c\sqrt{t}\right) - \operatorname{erfc}\left(\frac{y}{2\sqrt{t}}\right) \right], \tag{23}$$

$$\begin{aligned}
 u(y,t) = & \frac{1}{4} e^{-i\omega t} \left[e^{-y\sqrt{L-i\omega}} \operatorname{erfc} \left(\frac{y}{2\sqrt{t}} - \sqrt{(L-i\omega)t} \right) + e^{y\sqrt{L-i\omega}} \operatorname{erfc} \left(\frac{y}{2\sqrt{t}} + \sqrt{(L-i\omega)t} \right) \right] \\
 & + \frac{1}{4} e^{i\omega t} \left[e^{-y\sqrt{L+i\omega}} \operatorname{erfc} \left(\frac{y}{2\sqrt{t}} - \sqrt{(L+i\omega)t} \right) + e^{y\sqrt{L+i\omega}} \operatorname{erfc} \left(\frac{y}{2\sqrt{t}} + \sqrt{(L+i\omega)t} \right) \right] \\
 & - \frac{Gm}{L} \left[e^{-y\sqrt{L}} \operatorname{erfc} \left(\frac{y}{2\sqrt{t}} - \sqrt{Lt} \right) + e^{y\sqrt{L}} \operatorname{erfc} \left(\frac{y}{2\sqrt{t}} + \sqrt{Lt} \right) - \operatorname{erfc} \left(\frac{y}{2\sqrt{t}} \right) \right] \\
 & - \frac{Gr}{L} \left[e^{(c^2t-y)c} \operatorname{erfc} \left(\frac{y}{2\sqrt{t}} - c\sqrt{t} \right) - \operatorname{erfc} \left(\frac{y}{2\sqrt{t}} \right) \right] \\
 & - \frac{1}{c^3} \left(a + \frac{dh}{Sc} \right) \left[e^{(c^2t-y)c\sqrt{\operatorname{Pr}_{\text{eff}}}} \operatorname{erfc} \left(\frac{y}{2} \sqrt{\frac{\operatorname{Pr}_{\text{eff}}}{t}} - c\sqrt{t} \right) - \operatorname{erfc} \left(\frac{y}{2} \sqrt{\frac{\operatorname{Pr}_{\text{eff}}}{t}} \right) \right] \\
 & + \frac{1}{c^2} \left(a + \frac{dh}{Sc} \right) \left[2\sqrt{\frac{t}{\pi}} e^{-\frac{y^2 \operatorname{Pr}_{\text{eff}}}{4t}} - y\sqrt{\operatorname{Pr}_{\text{eff}}} \operatorname{erfc} \left(\frac{y}{2} \sqrt{\frac{\operatorname{Pr}_{\text{eff}}}{t}} \right) \right] \\
 & + \frac{1}{c} \left(a + \frac{dh}{Sc} \right) \left[\left(\frac{y^2 \operatorname{Pr}_{\text{eff}}}{2} + t \right) \operatorname{erfc} \left(\frac{y}{2} \sqrt{\frac{\operatorname{Pr}_{\text{eff}}}{t}} \right) - y\sqrt{\operatorname{Pr}_{\text{eff}}} \sqrt{\frac{t}{\pi}} e^{-\frac{y^2 \operatorname{Pr}_{\text{eff}}}{4t}} \right] \\
 & + \frac{Gr}{2\pi L} \int_0^t \left[\frac{yc}{s^{3/2} \sqrt{(t-s)}} e^{-\left(Ls + \frac{y^2}{4s} \right)} \right] ds - \frac{Gr}{2\sqrt{\pi} L} \int_0^t \left[\frac{yc^2}{s^{3/2}} e^{-\left(Ls + \frac{y^2}{4s} \right)} \right] ds \\
 & + ac \left(1 + \frac{h}{Sc} \right) \int_0^t \left[\frac{1}{\sqrt{\pi(t-s)}} + ce^{c^2(t-s)} \operatorname{erfc} \left(-c\sqrt{t-s} \right) \right] \\
 & \times \left[\left(\frac{s}{2} - \frac{y}{4\sqrt{L}} \right) e^{-y\sqrt{L}} \operatorname{erfc} \left(\frac{y}{2\sqrt{s}} - \sqrt{Ls} \right) + \left(\frac{s}{2} + \frac{y}{4\sqrt{L}} \right) e^{y\sqrt{L}} \operatorname{erfc} \left(\frac{y}{2\sqrt{s}} + \sqrt{Ls} \right) \right] ds.
 \end{aligned} \tag{24}$$

3) When $\operatorname{Pr}_{\text{eff}} = 1$ and $Sc = 1$,

$$C(y,t) = \operatorname{erfc} \left(\frac{y}{2\sqrt{t}} \right), \tag{25}$$

$$\begin{aligned}
 u(y,t) = & \frac{1}{4} e^{-i\omega t} \left[e^{-y\sqrt{L-i\omega}} \operatorname{erfc} \left(\frac{y}{2\sqrt{t}} - \sqrt{(L-i\omega)t} \right) + e^{y\sqrt{L-i\omega}} \operatorname{erfc} \left(\frac{y}{2\sqrt{t}} + \sqrt{(L-i\omega)t} \right) \right] \\
 & + \frac{1}{4} e^{i\omega t} \left[e^{-y\sqrt{L+i\omega}} \operatorname{erfc} \left(\frac{y}{2\sqrt{t}} - \sqrt{(L+i\omega)t} \right) + e^{y\sqrt{L+i\omega}} \operatorname{erfc} \left(\frac{y}{2\sqrt{t}} + \sqrt{(L+i\omega)t} \right) \right] \\
 & - \frac{Gm}{2L} \left[e^{-y\sqrt{L}} \operatorname{erfc} \left(\frac{y}{2\sqrt{t}} - \sqrt{Lt} \right) + e^{y\sqrt{L}} \operatorname{erfc} \left(\frac{y}{2\sqrt{t}} + \sqrt{Lt} \right) - 2\operatorname{erfc} \left(\frac{y}{2\sqrt{t}} \right) \right] \\
 & + \frac{Gr}{L} \left[e^{(\gamma^2t-y\gamma)} \operatorname{erfc} \left(\frac{y}{2\sqrt{t}} - \gamma\sqrt{t} \right) - \operatorname{erfc} \left(\frac{y}{2\sqrt{t}} \right) \right] \\
 & - \frac{Gr}{2\pi L} \int_0^t \left[\frac{y\gamma}{s^{3/2} \sqrt{(t-s)}} e^{-\left(Ls + \frac{y^2}{4s} \right)} \right] ds + \frac{Gr}{2\sqrt{\pi} L} \int_0^t \left[\frac{y\gamma^2}{s^{3/2}} e^{-\left(Ls + \frac{y^2}{4s} \right)} \right] ds.
 \end{aligned} \tag{26}$$

The dimensionless expression for skin friction evaluated from equation (20) is given by

$$\begin{aligned} \tau &= \frac{\tau'}{\rho U_0^2} = -\frac{\partial u}{\partial y} \Big|_{y=0}, \\ &= \frac{1}{2} \sqrt{L-i\omega} e^{-i\omega t} \left[1 - \operatorname{erfc}(\sqrt{(L-i\omega)t}) \right] + \frac{1}{2} \sqrt{L+i\omega} e^{i\omega t} \left[1 - \operatorname{erfc}(\sqrt{(L+i\omega)t}) \right] \\ &\quad + \left(\frac{a-dh}{c} \right) \sqrt{\operatorname{Pr}_{\text{eff}}} \left[1 + e^{c^2 t} \left(-2 + \operatorname{erfc}(c\sqrt{t}) \right) \right] + 2(a-dh) \sqrt{\operatorname{Pr}_{\text{eff}}} \sqrt{\frac{t}{\pi}} \\ &\quad + \left(\frac{bh}{c} \right) \sqrt{Sc} \left[1 + e^{c^2 t} \left(-2 + \operatorname{erfc}(c\sqrt{t}) \right) \right] + 2b(a+h) \sqrt{Sc} \sqrt{\frac{t}{\pi}} \\ &\quad + bt\sqrt{L} \left[1 - \operatorname{erfc}(\sqrt{Lt}) \right] + \frac{b}{2L} \left[1 - \operatorname{erfc}(\sqrt{Lt}) \right] + \frac{1}{\sqrt{\pi t}} e^{-Lt} \\ &\quad - c(a-dh+bh) \int_0^t \left[\frac{1}{\sqrt{\pi(t-s)}} + c e^{c^2(t-s)} \operatorname{erfc}(-c\sqrt{t-s}) \right] \\ &\quad \times \left[\sqrt{\frac{s}{\pi}} e^{-Ls} + \frac{(1+2Ls)}{2\sqrt{L}} \operatorname{erf}(\sqrt{Ls}) \right] ds, \end{aligned} \tag{27}$$

where τ' is the dimensional skin friction. The dimensionless expression of the Nusselt number is given by

$$\begin{aligned} \text{Nu} &= -\frac{\nu}{U_0(T' - T_\infty)} \frac{\partial T'}{\partial y'} \Big|_{y'=0} = \frac{1}{\theta(0,t)} + 1, \\ &= c\sqrt{\operatorname{Pr}_{\text{eff}}} \left(1 + \frac{1}{e^{c^2 t} [1 + \operatorname{erf}(c\sqrt{t})] - 1} \right). \end{aligned} \tag{28}$$

The dimensionless expression of the Sherwood number is given by

$$\begin{aligned} \text{Sh} &= -\frac{\partial C}{\partial y} \Big|_{y=0}, \\ &= \sqrt{\frac{Sc}{\pi t}} + h(\sqrt{\operatorname{Pr}_{\text{eff}}} - \sqrt{Sc}) c e^{c^2 t} \left[-2 + \operatorname{erfc}(c\sqrt{t}) \right]. \end{aligned} \tag{29}$$

LIMITING CASES

In the Absence of Thermal-Diffusion Effect

In the absence of thermal-diffusion effect, which numerically corresponds to $Sr = 0$, the equations (19) and (20) reduce to:

$$C(y,t) = \operatorname{erfc} \left(\frac{y}{2} \sqrt{\frac{Sc}{t}} \right), \tag{30}$$

$$\begin{aligned}
 u(y,t) = & \frac{1}{4} e^{-i\omega t} \left[e^{-y\sqrt{L-i\omega}} \operatorname{erfc} \left(\frac{y}{2\sqrt{t}} - \sqrt{(L-i\omega)t} \right) + e^{y\sqrt{L-i\omega}} \operatorname{erfc} \left(\frac{y}{2\sqrt{t}} + \sqrt{(L-i\omega)t} \right) \right] \\
 & + \frac{1}{4} e^{i\omega t} \left[e^{-y\sqrt{L+i\omega}} \operatorname{erfc} \left(\frac{y}{2\sqrt{t}} - \sqrt{(L+i\omega)t} \right) + e^{y\sqrt{L+i\omega}} \operatorname{erfc} \left(\frac{y}{2\sqrt{t}} + \sqrt{(L+i\omega)t} \right) \right] \\
 & - \frac{a}{c^2} \left[e^{(c^2 t - y c \sqrt{\operatorname{Pr}_{\text{eff}}})} \operatorname{erfc} \left(\frac{y}{2} \sqrt{\frac{\operatorname{Pr}_{\text{eff}}}{t}} - c\sqrt{t} \right) - \operatorname{erfc} \left(\frac{y}{2} \sqrt{\frac{\operatorname{Pr}_{\text{eff}}}{t}} \right) \right] \\
 & + \frac{a}{c} \left[2\sqrt{\frac{t}{\pi}} e^{-\frac{y^2 \operatorname{Pr}_{\text{eff}}}{4t}} - y\sqrt{\operatorname{Pr}_{\text{eff}}} \operatorname{erfc} \left(\frac{y}{2} \sqrt{\frac{\operatorname{Pr}_{\text{eff}}}{t}} \right) \right] \\
 & + a \left[\left(\frac{y^2 \operatorname{Pr}_{\text{eff}}}{2} + t \right) \operatorname{erfc} \left(\frac{y}{2} \sqrt{\frac{\operatorname{Pr}_{\text{eff}}}{t}} \right) - y\sqrt{\operatorname{Pr}_{\text{eff}}} \sqrt{\frac{t}{\pi}} e^{-\frac{y^2 \operatorname{Pr}_{\text{eff}}}{4t}} \right] \\
 & - b \left[\left(\frac{y^2 Sc}{2} + t \right) \operatorname{erfc} \left(\frac{y}{2} \sqrt{\frac{Sc}{t}} \right) - y\sqrt{Sc} \sqrt{\frac{t}{\pi}} e^{-\frac{y^2 Sc}{4t}} \right] \\
 & + \frac{bt}{2} \left[e^{-y\sqrt{L}} \operatorname{erfc} \left(\frac{y}{2\sqrt{t}} - \sqrt{Lt} \right) + e^{y\sqrt{L}} \operatorname{erfc} \left(\frac{y}{2\sqrt{t}} + \sqrt{Lt} \right) \right] \\
 & - \frac{yb}{4\sqrt{L}} \left[e^{-y\sqrt{L}} \operatorname{erfc} \left(\frac{y}{2\sqrt{t}} - \sqrt{Lt} \right) - e^{y\sqrt{L}} \operatorname{erfc} \left(\frac{y}{2\sqrt{t}} + \sqrt{Lt} \right) \right] \\
 & + ac \int_0^t \left[\frac{1}{\sqrt{\pi(t-s)}} + ce^{c^2(t-s)} \operatorname{erfc}(-c\sqrt{t-s}) \right] \\
 & \times \left[\left(\frac{s}{2} - \frac{y}{4\sqrt{L}} \right) e^{-y\sqrt{L}} \operatorname{erfc} \left(\frac{y}{2\sqrt{s}} - \sqrt{Ls} \right) + \left(\frac{s}{2} + \frac{y}{4\sqrt{L}} \right) e^{y\sqrt{L}} \operatorname{erfc} \left(\frac{y}{2\sqrt{s}} + \sqrt{Ls} \right) \right] ds, \tag{31}
 \end{aligned}$$

the known solutions of Hussanan et al. [33] (see equations (20) and (22)). In addition, if we take $L = \omega = 0$ and $\gamma = 1$, the solutions for temperature (18) and velocity (31) reduce to that obtained by Narahari and Nayan [34] (see equations (14) and (15)).

In the Absence of Mass Diffusion

In the absence of mass diffusion the solution for velocity given in equation (20) reduces to:

$$\begin{aligned}
 u(y,t) = & \frac{1}{4} e^{-i\omega t} \left[e^{-y\sqrt{L-i\omega}} \operatorname{erfc} \left(\frac{y}{2\sqrt{t}} - \sqrt{(L-i\omega)t} \right) + e^{y\sqrt{L-i\omega}} \operatorname{erfc} \left(\frac{y}{2\sqrt{t}} + \sqrt{(L-i\omega)t} \right) \right] \\
 & + \frac{1}{4} e^{i\omega t} \left[e^{-y\sqrt{L+i\omega}} \operatorname{erfc} \left(\frac{y}{2\sqrt{t}} - \sqrt{(L+i\omega)t} \right) + e^{y\sqrt{L+i\omega}} \operatorname{erfc} \left(\frac{y}{2\sqrt{t}} + \sqrt{(L+i\omega)t} \right) \right] \\
 & - \frac{a}{c^2} \left[e^{(c^2 t - y c \sqrt{\operatorname{Pr}_{\text{eff}}})} \operatorname{erfc} \left(\frac{y}{2} \sqrt{\frac{\operatorname{Pr}_{\text{eff}}}{t}} - c\sqrt{t} \right) - \operatorname{erfc} \left(\frac{y}{2} \sqrt{\frac{\operatorname{Pr}_{\text{eff}}}{t}} \right) \right] \\
 & + \frac{a}{c} \left[2\sqrt{\frac{t}{\pi}} e^{-\frac{y^2 \operatorname{Pr}_{\text{eff}}}{4t}} - y\sqrt{\operatorname{Pr}_{\text{eff}}} \operatorname{erfc} \left(\frac{y}{2} \sqrt{\frac{\operatorname{Pr}_{\text{eff}}}{t}} \right) \right]
 \end{aligned}$$

$$\begin{aligned}
 &+a \left[\left(\frac{y^2 \text{Pr}_{\text{eff}}}{2} + t \right) \text{erfc} \left(\frac{y}{2} \sqrt{\frac{\text{Pr}_{\text{eff}}}{t}} \right) - y \sqrt{\text{Pr}_{\text{eff}}} \sqrt{\frac{t}{\pi}} e^{-\frac{y^2 \text{Pr}_{\text{eff}}}{4t}} \right] \\
 &+ac \int_0^t \left[\frac{1}{\sqrt{\pi(t-s)}} + ce^{c^2(t-s)} \text{erfc}(-c\sqrt{t-s}) \right] \\
 &\times \left[\left(\frac{s}{2} - \frac{y}{4\sqrt{L}} \right) e^{-y\sqrt{L}} \text{erfc} \left(\frac{y}{2\sqrt{s}} - \sqrt{Ls} \right) + \left(\frac{s}{2} + \frac{y}{4\sqrt{L}} \right) e^{y\sqrt{L}} \text{erfc} \left(\frac{y}{2\sqrt{s}} + \sqrt{Ls} \right) \right] ds,
 \end{aligned} \tag{32}$$

the known solution obtained by Hussanan et al. [35] (see equation (17)).

GRAPHICAL RESULTS AND DISCUSSION

We have solved the problem of unsteady MHD mixed convection flow in a porous medium past an oscillating vertical plate with constant mass diffusion and Newtonian heating in the presence of Soret and thermal radiation effects. Now it is very important to study the effects of all the parameters involved in the problem, i.e. Prandtl number (*Pr*), Grashof number (*Gr*), modified Grashof number (*Gm*), radiation parameter (*R*), magnetic parameter (*M*), porosity parameter (*K*), Schmidt number (*Sc*), Soret number (*Sr*), conjugate parameter (*γ*), time (*t*) and phase angle (*ωt*). Numerical results for velocity, temperature and concentration profiles are plotted in Figures 2-22, whereas skin friction, Nusselt number and Sherwood number are given in Tables 1-3.

The graph of the fluid velocity for different values of *Pr* are shown in Figure 2. From this Figure, it is observed that the velocity decreases with increasing values of *Pr* and velocity for electrolytic solution (*Pr*=1.0) is greater than that for vapour (*Pr*=3.0), water (*Pr*=7.0) and engine oil (*Pr*=100) in that order. Physically, a fluid with a large Prandtl number has high viscosity and small thermal conductivity, which makes the fluid thick and hence causes a decrease in velocity of the fluid. The effects of *Gr* and *Gm* on velocity profiles are examined in Figures 3 and 4. The velocity increases as *Gr* and *Gm* are increased, because an increase in both of these parameters means increasing thermal and mass buoyancy effects, which gives rise to an increase in the induced flow. Further, from these Figures, it is noticed that the Grashof number and modified Grashof number do not have any influence as the fluid moves away from the bounding surface.

The fluid velocity profiles are shown in Figure 5 for different values of *R*. It is found that the velocity increases with increasing values of *R* in the presence of thermal radiation (*R*=2,3,4) as well as in the case of pure convection (*R*=0). This is expected because higher radiation occurs when the temperature is higher and as a result the velocity increases. Effects of the magnetic parameter (*M*) on velocity are shown in Figure 6. Physically, *M*=0 means that there is no magnetic effect and the flow is purely hydrodynamic. It is found from this Figure that the velocity decreases with increasing value of *M*. This is expected as the application of the transverse magnetic field always results in a resistance-type force called Lorentz force. This force is similar in nature to a drag force, and upon increasing the values of *M* the drag force increases and tends to resist the fluid flow, thus reducing the fluid motion significantly. In order to visualise the velocity field in a porous medium, the profiles of velocity are illustrated in Figure 7 for different values of *K*, as the other flow parameters are kept fixed. It is observed that the velocity increases with an increase in *K*. This result may be explained by the fact that the presence of a porous medium decreases the resistance to flow and hence enhances the fluid motion. So it is confirmed from this graph that porosity has an important role in the present analysis.

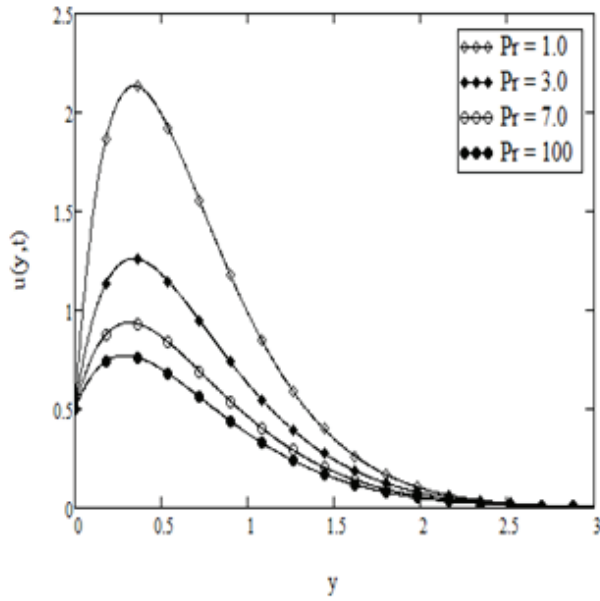


Figure 2. Velocity profiles for different values of Pr , when $Gr = 5, Gm = 2, R = 0.5, M = 2, K = 0.5, Sc = 0.62, Sr = 2, \gamma = 1, t = 0.4, \omega t = \frac{\pi}{3}$

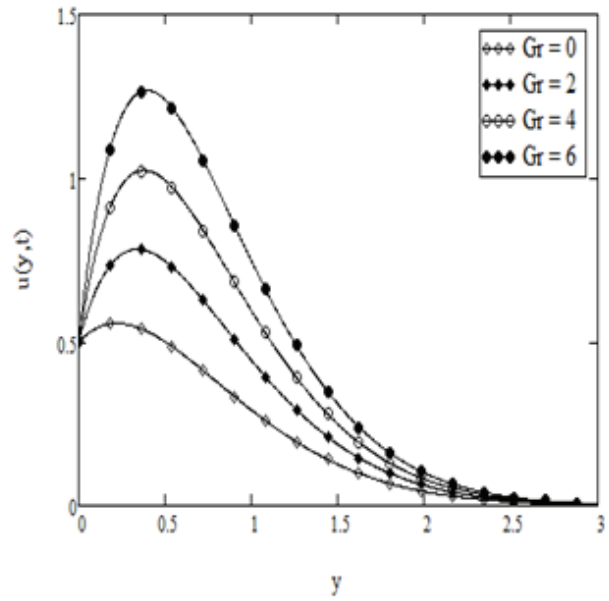


Figure 3. Velocity profiles for different values of Gr , when $Pr = 1, Gm = 2, R = 0.5, M = 0.2, K = 2, Sc = 0.62, Sr = 2, \gamma = 1, t = 0.4, \omega t = \frac{\pi}{3}$

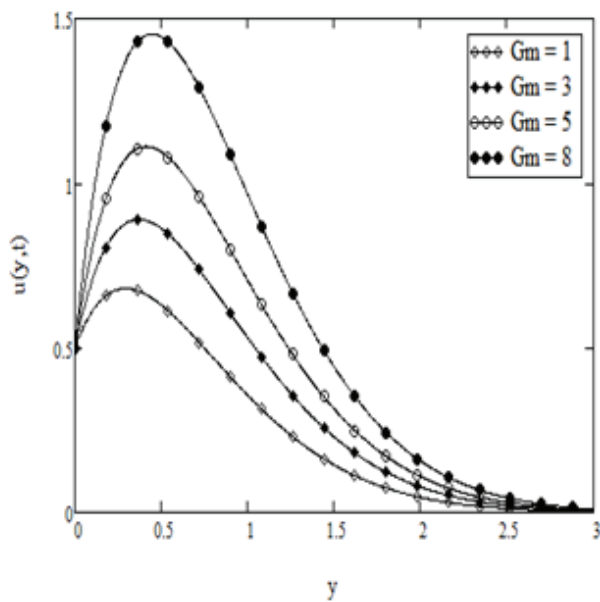


Figure 4. Velocity profiles for different values of Gm , when $Pr = 1, Gr = 2, R = 0.5, M = 0.2, K = 2, Sc = 0.62, Sr = 2, \gamma = 1, t = 0.4, \omega t = \frac{\pi}{3}$

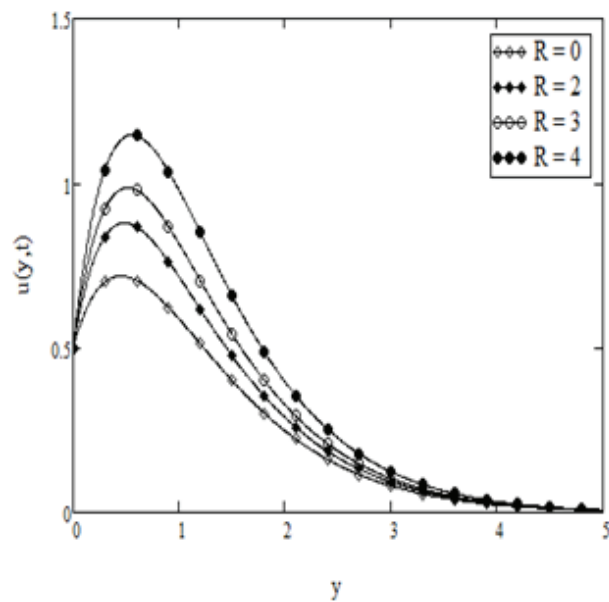


Figure 5. Velocity profiles for different values of R , when $Pr = 7, Gr = 5, Gm = 2, M = 0.2, K = 2, Sc = 0.22, Sr = 2, \gamma = 1, t = 0.5, \omega t = \frac{\pi}{3}$

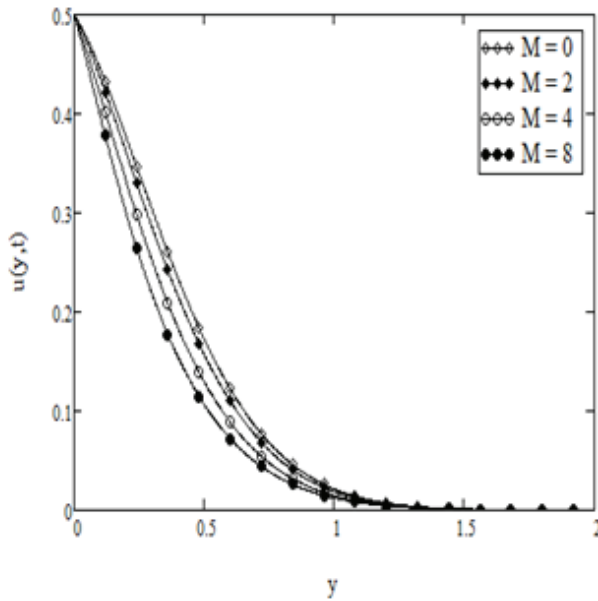


Figure 6. Velocity profiles for different values of M , when $Pr = 3, Gr = 3, Gm = 2, Sc = 0.62, R = 0.5, K = 0.5, Sr = 0.2, \gamma = 1, t = 0.1, \omega t = \frac{\pi}{3}$

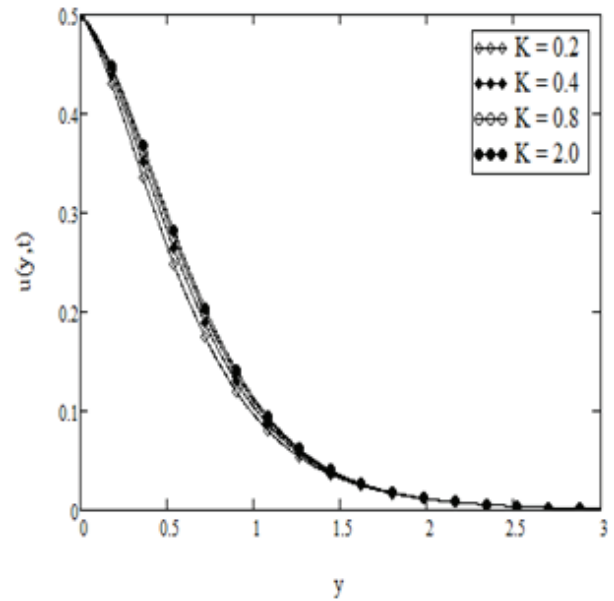


Figure 7. Velocity profiles for different values of K , when $Pr = 1, Gr = 2, Gm = 1, Sc = 0.22, R = 0.5, M = 0.2, Sr = 2, \gamma = 0.5, t = 0.2, \omega t = \frac{\pi}{3}$

The effects of Sc on the velocity profiles are shown in Figure 8. It is observed that an increase in Sc results in a decrease of velocity. Figure 9 shows that the fluid velocity increases with an increase in Sr . In Figure 10 the velocity profiles are illustrated for different values of γ ; as the conjugate parameter increases, the fluid density decreases and the momentum-boundary-layer thickness increases, and finally the fluid velocity increases. From Figure 11, the fluid velocity increases with an increase in t . The velocity profiles for different values of ωt are shown in Figure 12. It is observed that the velocity shows an oscillatory behaviour: near the plate it is maximum and decreases with increasing distance from the plate, finally approaching zero as $y \rightarrow \infty$. It is clearly seen from this Figure that the velocity satisfies the given boundary conditions (13) and (14), which shows the accuracy of our results.

The effects of Prandtl number (Pr) on the fluid temperature are shown in Figure 13, which shows that the temperature decreases with an increase in Pr . Physically, this is due to the fact that with increasing Pr , the thermal conductivity of the fluid decreases and the viscosity of the fluid increases, and as a result the thermal boundary layer decreases. On the other hand, the buoyancy that results from the thermal expansion of the fluid adjacent to the surface causes the development of a rising boundary layer. Consequently, it is found from a comparison of Figure 2 and Figure 13 that the momentum boundary layer is thicker than the thermal boundary layer because the buoyant fluid layer causes macroscopic motion in the thicker fluid layer due to high viscosity.

The behaviour of the radiation parameter (R) on temperature profiles are shown in Figure 14, where $R = 0$ indicates no thermal radiation. It is observed that the temperature increases with an increase in R . This is due to the fact that the effect of thermal radiation is to increase the thermal-boundary-layer thickness with an increase in the value of the radiation parameter R . From Figure 15, it is found that as the conjugate parameter (γ) increases, so does the thickness of the thermal boundary layer and as a result the temperature of the plate increases. The effects of time (t) on the

temperature (Figure 16) are quite identical to those on the velocity profiles, and it is observed from all the temperature profiles that the temperature is maximum near the plate and decreases away from the plate and finally approaches zero as $y \rightarrow \infty$.

The variations in the concentration field for different values of Pr and R are shown in Figures 17 and 18. An increase in Pr decreases the concentration field, but an increase in R increases the concentration field. Further, it is found from these Figures that the effects of Pr and R on the concentration field is similar to those on the velocity. Figure 19 illustrates the effects of Schmidt number (Sc) on the concentration field: an increase in the value of Sc makes the concentration boundary layer thick and hence the concentration field decreases. The effects of Sr on the concentration field are shown in Figure 20: the concentration increases with increasing value of Sr . From Figure 21, similar effects of the conjugate parameter (γ) on the concentration are found. The effects of time (t) on the concentration field (Figure 22) are similar to those on the velocity and temperature fields plotted in Figures 11 and 16 respectively.

The numerical values of skin friction, Nusselt number and Sherwood number for various parameters of interest are presented in Tables 1-3. The skin friction (τ) decreases with increasing t , R , Gm , Sc , Gr , K , γ and ωt , while it increases as Pr , Sr and M are increased (Table 1). The Nusselt number (Nu) increases with an increase in either Pr or γ , while the reverse effects are observed for t and R (Table 2). From Table 3, it is observed that the Sherwood number (Sh) increases with increasing value of Pr , Sc , Sr and γ , while it decreases with an increase in t and R .

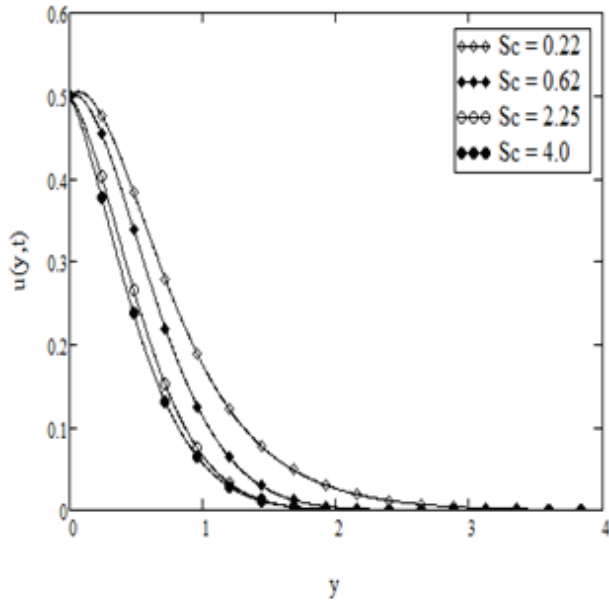


Figure 8. Velocity profiles for different values of Sc , when $Pr = 3, Gr = 8, Gm = 2, R = 0.5,$

$$M = 0.2, K = 3, Sr = 2, \gamma = 0.2, t = 0.2, \omega t = \frac{\pi}{3}$$

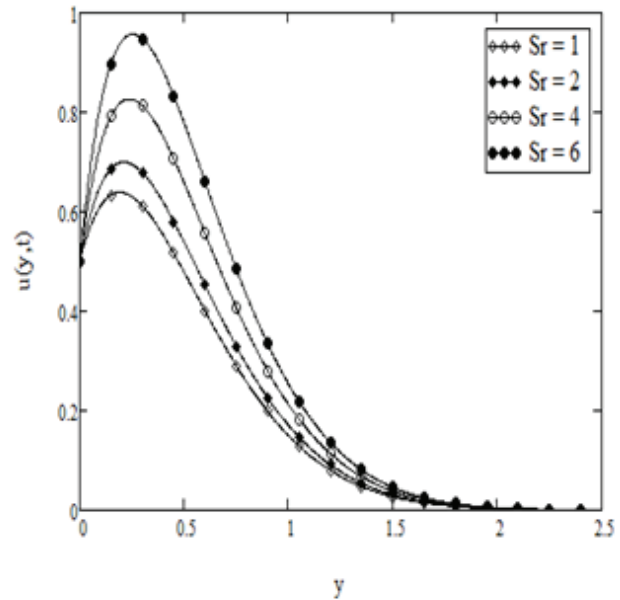


Figure 9. Velocity profiles for different values of Sr , when $Pr = 3, Gr = 5, Gm = 3, Sc = 0.78,$

$$R = 0.5, M = 0.2, K = 0.5, \gamma = 1, t = 0.2, \omega t = \frac{\pi}{3}$$

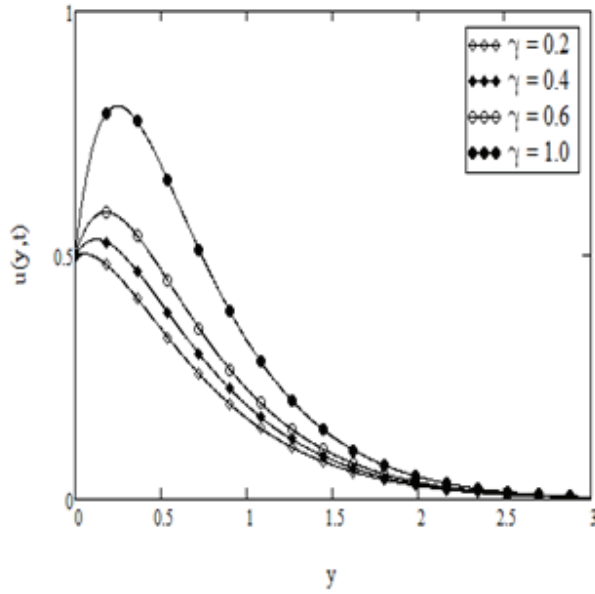


Figure 10. Velocity profiles for different values of γ , when $Pr = 1, Gr = 5, Gm = 2, R = 3, M = 2, K = 0.2, Sc = 0.22, Sr = 0.5, t = 0.2, \omega t = \frac{\pi}{2}$

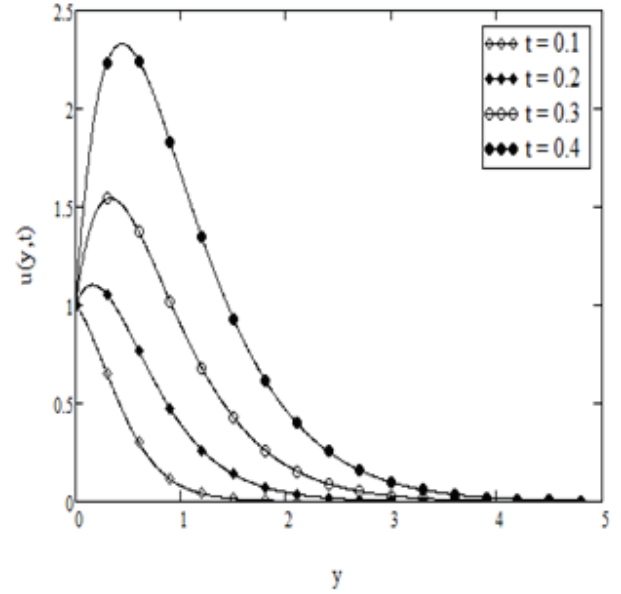


Figure 11. Velocity profiles for different values of t , when $Pr = 1, Gr = 3, Gm = 2, R = 3, K = 2, M = 0.2, Sc = 0.22, Sr = 0.5, \gamma = 1, \omega t = 0$

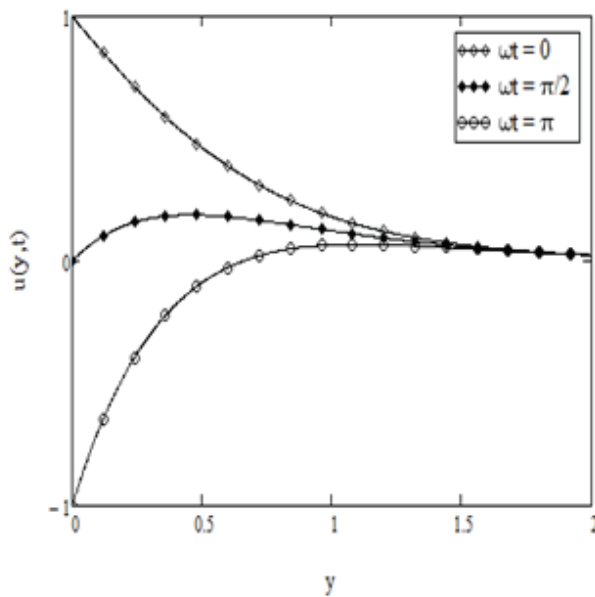


Figure 12. Velocity profiles for different values of ωt , when $Pr = 7, Gr = 3, Gm = 2, R = 0.2, M = 0.5, K = 0.2, Sc = 0.22, Sr = 2, \gamma = 0.1, t = 0.2$

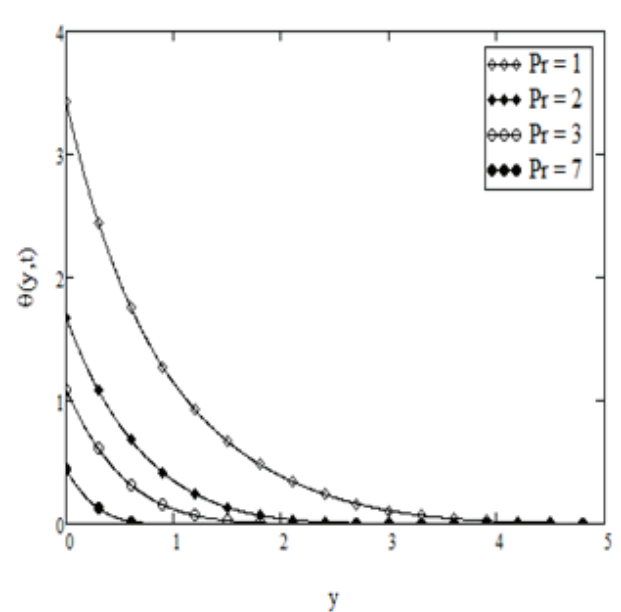


Figure 13. Temperature profiles for different values of Pr , when $t = 0.2, R = 3$ and $\gamma = 1$

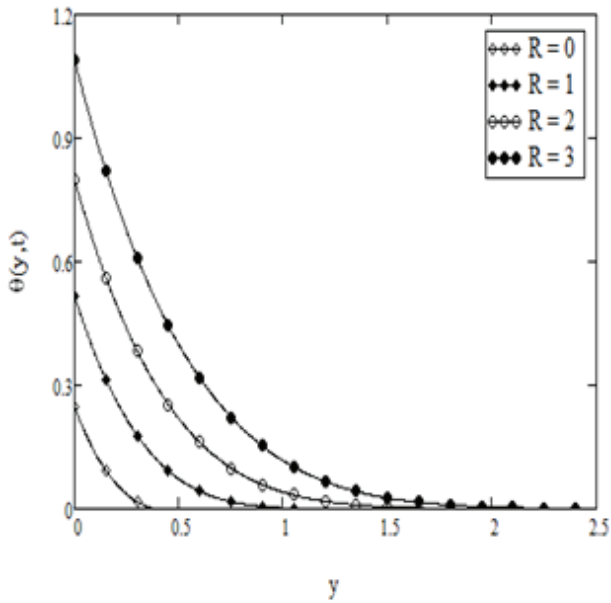


Figure 14. Temperature profiles for different values of R , when $t = 0.2, Pr = 3$ and $\gamma = 1$

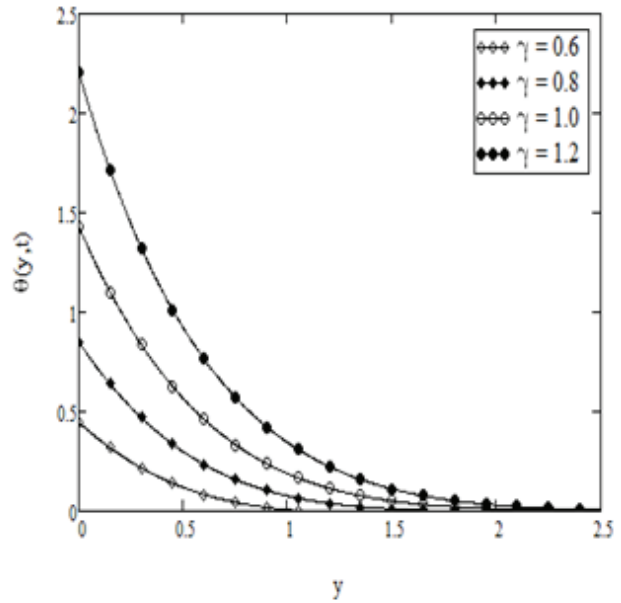


Figure 15. Temperature profiles for different values of γ , when $t = 0.4, Pr = 3$ and $R = 2$

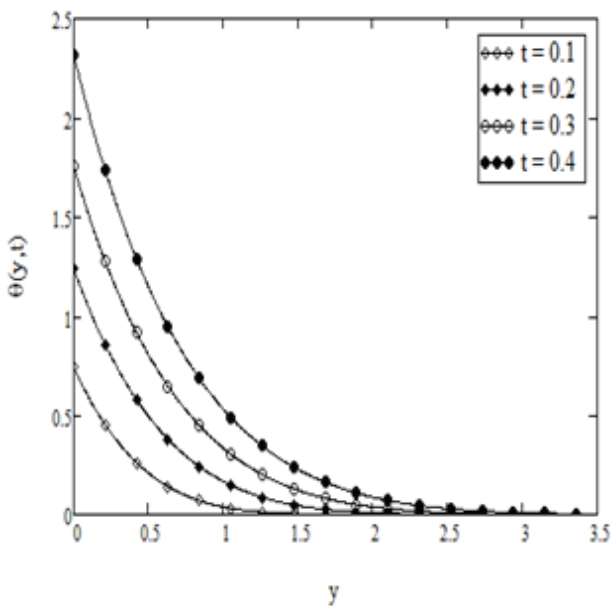


Figure 16. Temperature profiles for different values of t , when $R = 0.5, Pr = 1$ and $\gamma = 1$

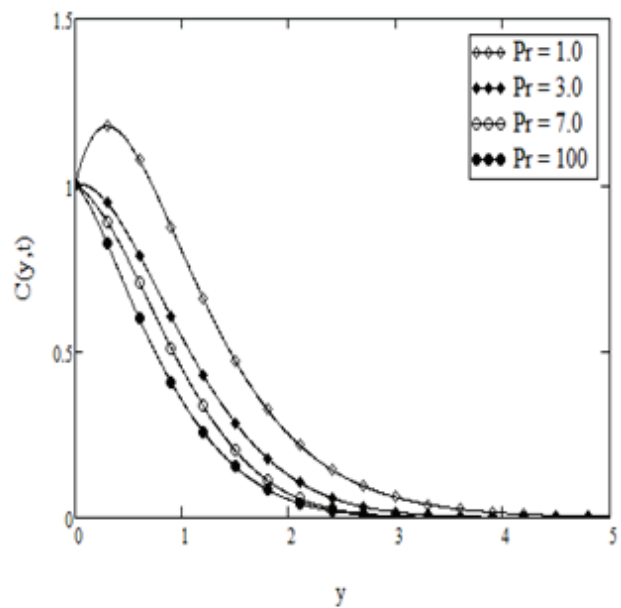


Figure 17. Concentration profiles for different values of Pr , when $t = 0.5, R = 3, Sc = 0.94, Sr = 0.5$ and $\gamma = 1$

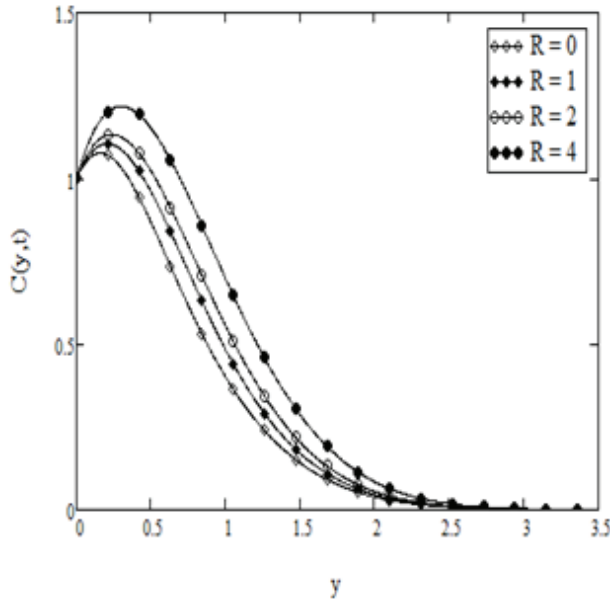


Figure 18. Concentration profiles for different values of R , when $t = 0.4, Pr = 7, Sc = 0.94, Sr = 2$ and $\gamma = 1$

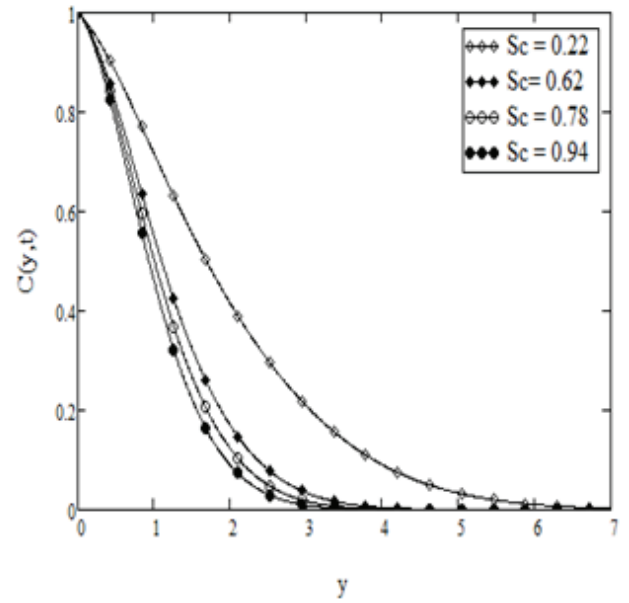


Figure 19. Concentration profiles for different values of Sc , when $t = 0.6, R = 0.8, Pr = 7, Sr = 0.5$ and $\gamma = 1$

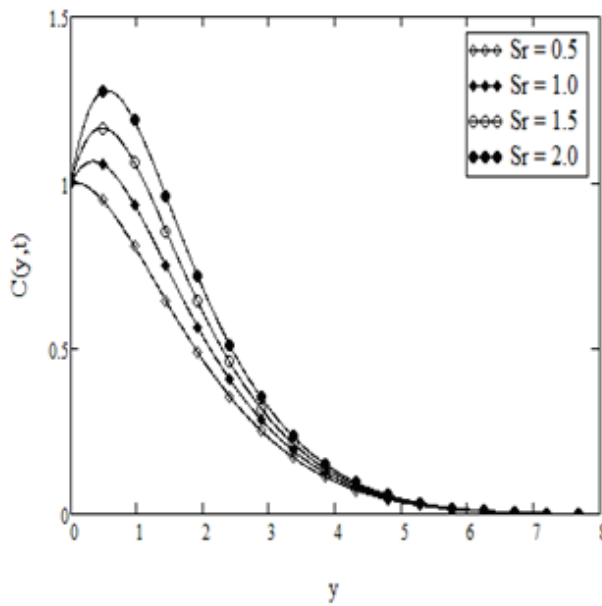


Figure 20. Concentration profiles for different values of Sr , when $t = 0.6, R = 3, Pr = 7, Sc = 0.5$ and $\gamma = 1$

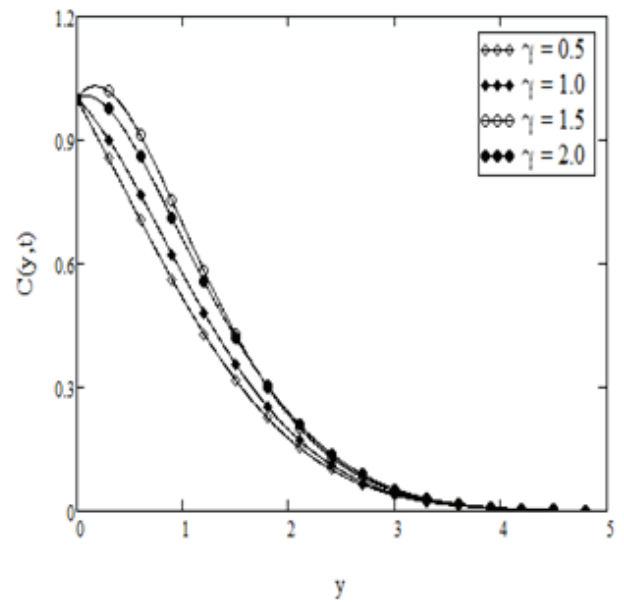


Figure 21. Concentration profiles for different values of γ , when $t = 0.8, R = 3, Pr = 7, Sc = 0.78$ and $Sr = 0.2$

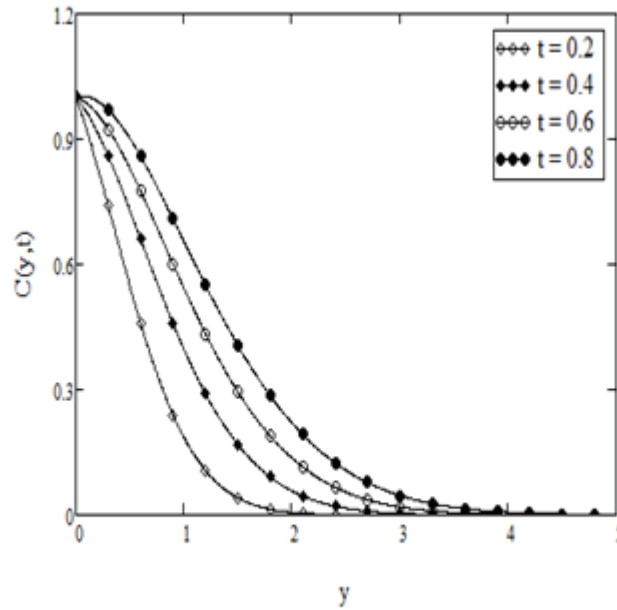


Figure 22. Concentration profiles for different values of t , when $R = 2, Pr = 7, Sc = 0.78, Sr = 0.5$ and $\gamma = 1$

Table 1. Skin friction variations

t	R	Pr	Gr	Gm	Sc	Sr	M	K	γ	ω	τ
0.1	2	0.71	3	2	0.22	0.5	0.5	0.2	1.0	$\pi/2$	2.949
0.2	2	0.71	3	2	0.22	0.5	0.5	0.2	1.0	$\pi/2$	0.637
0.1	4	0.71	3	2	0.22	0.5	0.5	0.2	1.0	$\pi/2$	0.984
0.1	2	1.0	3	2	0.22	0.5	0.5	0.2	1.0	$\pi/2$	4.683
0.1	2	0.71	4	2	0.22	0.5	0.5	0.2	1.0	$\pi/2$	3.481
0.1	2	0.71	3	3	0.22	0.5	0.5	0.2	1.0	$\pi/2$	2.861
0.1	2	0.71	3	2	0.62	0.5	0.5	0.2	1.0	$\pi/2$	2.771
0.1	2	0.71	3	2	0.22	1.0	0.5	0.2	1.0	$\pi/2$	2.923
0.1	2	0.71	3	2	0.22	0.5	1.0	0.2	1.0	$\pi/2$	3.080
0.1	2	0.71	3	2	0.22	0.5	0.5	0.4	1.0	$\pi/2$	2.429
0.1	2	0.71	3	2	0.22	0.5	0.5	0.2	1.5	$\pi/2$	0.322
0.1	2	0.71	3	2	0.22	0.5	0.5	0.2	1.0	π	2.757

Table 2. Nusselt number variations

t	R	Pr	γ	Nu
0.2	2	0.71	1	1.3119
0.4	2	0.71	1	1.1054
0.2	4	0.71	1	1.1471
0.2	2	1.0	1	1.4659
0.2	2	0.71	2	2.0347

Table 3. Sherwood number variations

t	R	Pr	Sc	Sr	γ	Sh
0.2	2	0.71	0.22	0.5	1	0.5931
0.4	2	0.71	0.22	0.5	1	0.4205
0.2	4	0.71	0.22	0.5	1	0.5876
0.2	2	1.0	0.22	0.5	1	0.6024
0.2	2	0.71	0.62	0.5	1	0.9229
0.2	2	0.71	0.22	1.0	1	0.5946
0.2	2	0.71	0.22	0.5	2	0.5998

CONCLUSIONS

Exact solutions of magnetohydrodynamic mixed convection flow in a porous medium with Newtonian heating condition are obtained. Laplace transform technique is used for the problem solution. Graphs for temperature, concentration and velocity are plotted and discussed. The following main points concluded from this study are:

- Fluid velocity increases with increasing radiation parameter (R), Grashof number (Gr), modified Grashof number (Gm), porosity parameter (K) and conjugate parameter (γ).
- Skin friction behaviour is opposite to that of velocity.
- Nusselt number increases with increasing conjugate parameter and Prandtl number.
- Sherwood number increases with increasing Prandtl number, Schmidt number and conjugate parameter.

ACKNOWLEDGEMENTS

The authors gratefully acknowledge the financial support for this reasearch received from the Universiti Malaysia Pahang, Malaysia through vote numbers RDU140111 (FRGS) and RDU150101 (FRGS).

REFERENCES

1. R. A. Mohamed, S. M. A. Dahab and T. A. Nofal, “Thermal radiation and MHD effects on free convective flow of a polar fluid through a porous medium in the presence of internal heat generation and chemical reaction”, *Math. Problems Eng.*, **2010**, 2010, Art. ID 804719.
2. Seethamahalakshmi, G. V. R. Reddy and B. D. C. N. Prasad, “Unsteady MHD free convection flow and mass transfer near a moving vertical plate in the presence of thermal radiation”, *Adv. Appl. Sci. Res.*, **2011**, 2, 261-269.
3. P. Mebine and E. M. Adigio, “Effects of thermal radiation on transient MHD free convection flow over a vertical surface embedded in a porous medium with periodic boundary temperature”, *Math. Aeterna*, **2011**, 1, 245-261.
4. S. Suneetha, N. B. Reddy and V. R. Prasad, “Thermal radiation effects on MHD free convection flow past an impulsively started vertical plate with variable surface temperature and concentration”, *J. Naval Archit. Marine Eng.*, **2008**, 2, 57-70.

5. Z. Uddin and M. Kumar, "Radiation effect on unsteady MHD heat and mass transfer flow on a moving inclined porous heated plate in the presence of chemical reaction", *Int. J. Math. Model., Simulat. Appl.*, **2010**, 3, 155-163.
6. R. Muthucumaraswamy and V. Valliammal, "MHD flow past an exponentially accelerated vertical plate with variable temperature and mass diffusion in the presence of chemical reaction", *Annals Fac. Eng. Hunedoara Int. J. Eng.*, **2012**, 151-154.
7. R. Nandkeolyar, M. Das and P. Sibanda, "Exact solutions of unsteady MHD free convection in a heat absorbing fluid flow past a flat plate with ramped wall temperature", *Bound. Value Probl.*, **2013**, 2013, 247.
8. D. A. Nield and A. Bejan, "Convection in Porous Media", 2nd Edn., Springer, New York, **1999**.
9. D. B. Ingham, A. Bejan, E. Mamut and I. Pop (Eds.), "Emerging Technologies and Techniques in Porous Media", Springer, Dordrecht (Netherlands), **2004**.
10. O. A. Beg, J. Zueco, S. K. Ghosh and A. Heidari, "Unsteady MHD heat transfer in a semi-infinite porous medium with thermal radiation flux: Analytical and numerical study", *Adv. Numer. Anal.*, **2011**, 2011, Art. ID 304124.
11. T. S. Reddy, M. C. Raju and S. V. K. Varma, "Unsteady MHD free convection oscillatory couette flow through a porous medium with periodic wall temperature in presence of chemical reaction and thermal radiation", *Int. J. Sci. Adv. Technol.*, **2011**, 1, 51-58.
12. P. M. Kishore, V. Rajesh and S. V. Verma, "The effects of thermal radiation and viscous dissipation on MHD heat and mass diffusion flow past an oscillating vertical plate embedded in a porous medium with variable surface conditions", *J. Theoret. Appl. Mech.*, **2012**, 39, 99-125.
13. F. Ali, I. Khan, Samiulhaq, N. Mustapha and S. Shafie, "Unsteady magnetohydrodynamic oscillatory flow of viscoelastic fluids in a porous channel with heat and mass transfer", *J. Phys. Soc. Jpn.*, **2012**, 81, 064402-064402-8.
14. N. Ahmed and K. K. Das, "MHD mass transfer flow past a vertical porous plate embedded in a porous medium in a slip flow regime with thermal radiation and chemical reaction", *Open J. Fluid Dyn.*, **2013**, 3, 230-239.
15. E. R. G. Eckert and R. M. Drake, Jr., "Analysis of Heat and Mass Transfer", McGraw Hill, New York, **1972**.
16. N. Ahmed, "Heat and mass transfer in Hartmann flow with Soret effect in presence of a constant heat source", *Turk. J. Phys.*, **2012**, 36, 446-460.
17. M. Narayana, A. A. Khidir, P. Sibanda and P. V. S. N. Murthy, "Soret effect on the natural convection from a vertical plate in a thermally stratified porous medium saturated with non-Newtonian liquid", *J. Heat Transfer*, **2013**, 135, 032501-032510.
18. F. Ali, I. Khan, S. Shafie and N. Musthapa, "Heat and mass transfer with free convection MHD flow past a vertical plate embedded in a porous medium", *Math. Probl. Eng.*, **2013**, 2013, Art. ID 346281.
19. A. K. Jha, K. Choudhary and A. Sharma, "Influence of Soret effect on MHD mixed convection flow of visco-elastic fluid past a vertical surface with Hall effect", *Int. J. Appl. Mech. Eng.*, **2014**, 19, 79-95.
20. B. K. Sharma, S. Gupta, V. V. Krishna and R. J. Bhargavi, "Soret and Dufour effects on an unsteady MHD mixed convective flow past an infinite vertical plate with Ohmic dissipation and heat source", *Afr. Matemat.*, **2014**, 25, 799-821.

21. N. Vedavathi, K. Ramakrishna and K. J. Reddy, "Radiation and mass transfer effects on unsteady MHD convective flow past an infinite vertical plate with Dufour and Soret effects", *Ain Shams Eng. J.*, **2015**, 6, 363-371.
22. R. K. Deka and S. K. Das, "Radiation effects on free convection flow near a vertical plate with ramped wall temperature", *Engineering*, **2011**, 3, 1197-1206.
23. R. Muthukumaraswamy, "Natural convection on flow past an impulsively started vertical plate with variable surface heat flux", *Far East J. Appl. Math.*, **2004**, 14, 99-119.
24. A. A. Dare and M. O. Petinrin, "Modelling of natural convection along isothermal plates and in channels using diffusion velocity method", *Maejo Int. J. Sci. Technol.*, **2010**, 4, 43-52.
25. J. H. Merkin, "Natural-convection boundary-layer flow on a vertical surface with Newtonian heating", *Int. J. Heat Fluid Flow*, **1994**, 15, 392-398.
26. D. Lesnic, D. B. Ingham, I. Pop and C. Storr, "Free convection boundary-layer flow above a nearly horizontal surface in a porous medium with Newtonian heating", *Heat Mass Transf.*, **2004**, 40, 665-672.
27. M. Z. Salleh, R. Nazar and I. Pop, "Boundary layer flow and heat transfer over a stretching sheet with Newtonian heating", *J. Taiwan Inst. Chem. Eng.*, **2010**, 41, 651-655.
28. M. Z. Salleh, R. Nazar, N. M. Arifin and I. Pop, "Forced-convection heat transfer over a circular cylinder with Newtonian heating", *J. Eng. Math.*, **2011**, 69, 101-110.
29. S. Das, C. Mandal and R. N. Jana, "Radiation effects on unsteady free convection flow past a vertical plate with Newtonian heating", *Int. J. Comput. Appl.*, **2012**, 41, 36-41.
30. A. R. M. Kasim, N. F. Mohammad, Aurangzaib and S. Sharidan, "Natural convection boundary layer flow of a viscoelastic fluid on solid sphere with Newtonian heating", *World Acad. Sci. Eng. Technol.*, **2012**, 64, 628-633.
31. R. C. Chaudhary and P. Jain, "Unsteady free convection boundary-layer flow past an impulsively started vertical surface with Newtonian heating", *Roman. J. Phys.*, **2006**, 51, 911-925.
32. P. Mebine and E. M. Adigio, "Unsteady free convection flow with thermal radiation past a vertical porous plate with Newtonian heating", *Turk. J. Phys.*, **2009**, 33, 109-119.
33. A. Hussanan, Z. Ismail, I. Khan, A. G. Hussein and S. Shafie, "Unsteady boundary layer MHD free convection flow in a porous medium with constant mass diffusion and Newtonian heating", *Eur. Phys. J. Plus*, **2014**, 129, 46. (doi 10.1140/epjp/i2014-14046-x)
34. M. Narahari and M. Y. Nayan, "Free convection flow past an impulsively started infinite vertical plate with Newtonian heating in the presence of thermal radiation and mass diffusion", *Turk. J. Eng. Environ. Sci.*, **2011**, 35, 187-198.
35. H. Abid, M. A. Zakaria, Samiulhaq, I. Khan and S. Sharidan, "Radiation effect on unsteady magnetohydrodynamic free convection flow in a porous medium with Newtonian heating", *Int. J. Appl. Math. Stat.*, **2013**, 42, 474-480.
36. M. Narahari and A. Ishak, "Radiation effects on free convection flow near a moving vertical plate with Newtonian heating", *J. Appl. Sci.*, **2011**, 11, 1096-1104.
37. F. Ali, I. Khan, S. U. Haq and S. Shafie, "Influence of thermal radiation on unsteady free convection MHD flow of Brinkman type fluid in a porous medium with Newtonian heating", *Math. Probl. Eng.*, **2013**, 2013, Art. ID 632394.
38. A. Hussanan, I. Khan and S. Shafie, "An exact analysis of heat and mass transfer past a vertical plate with Newtonian heating", *J. Appl. Math.*, **2013**, 2013, Art. ID 434571.

39. E. M. Sparrow and J. P. Abraham, “A new buoyancy model replacing the standard pseudo-density difference for internal natural convection in gases”, *Int. J. Heat Mass Transf.*, **2003**, 46, 3583-3591.
40. E. Magyari and A. Pantokratoras, “Note on the effect of thermal radiation in the linearized Rosseland approximation on the heat transfer characteristics of various boundary layer flows”, *Int. Commun. Heat Mass Transf.*, **2011**, 38, 554-556.

© 2015 by Maejo University, San Sai, Chiang Mai, 50290 Thailand. Reproduction is permitted for noncommercial purposes.

Full Paper

An analogue of Eulerian polynomials related to L -type function

Serkan Araci^{1,*}, Mehmet Acikgoz², Roberto B. Corcino³ and Cenap Özel⁴

¹Department of Economics, Faculty of Economics, Administrative and Social Science, Hasan Kalyoncu University, TR-27410 Gaziantep, Turkey

²Department of Mathematics, Faculty of Arts and Science, University of Gaziantep, TR-27310 Gaziantep, Turkey

³Department of Mathematics, Cebu Normal University, Cebu City 6000, Philippines

⁴Department of Mathematics, Dokuz Eylül University, TR-35160 Izmir, Turkey

* Corresponding author, e-mail: mtsrxn@hotmail.com

Received: 24 April 2014 / Accepted: 27 July 2015 / Published: 25 August 2015

Abstract: We introduce Dirichlet's type of twisted Eulerian polynomials by using p -adic fermionic q -invariant integral in the p -adic integer ring and obtain some new interesting identities. Using a complex contour integral representation based on the generating function of Dirichlet's type of twisted Eulerian polynomials, we get L -type function which interpolates for Dirichlet's type of Eulerian polynomials at negative integers.

Keywords: p -adic fermionic q -integral on Z_p , Eulerian polynomials, contour integral, L -function, Dirichlet character

INTRODUCTION

The Eulerian polynomials $A_n(x)$ are given by means of the following exponential generating series:

$$\sum_{n=0}^{\infty} A_n(x) \frac{t^n}{n!} = e^{A(x)t} = \frac{1-x}{e^{t(1-x)} - x}. \quad (1)$$

In fact, the Eulerian polynomials can be generated via the following recurrence relation:

$$(A(t) + (t-1))^n - tA_n(t) = \begin{cases} 1-t & \text{if } n=0 \\ 0 & \text{if } n \neq 0, \end{cases} \quad (2)$$

where we have used $A^n(x) := A_n(x)$ symbolically [7, 22].

Let p be a fixed odd prime number. Throughout this paper we make use of the following notations: Z_p denotes the ring of p -adic rational integers, Q denotes the field of rational numbers, Q_p denotes the field of p -adic rational numbers and C_p denotes the completion of algebraic closure of Q_p . Let N be a set of natural numbers and $N^* = N \cup \{0\}$. The normalised p -adic absolute value is defined by

$$|p|_p = \frac{1}{p}.$$

When one talks of a q -extension, q can be variously considered as an indeterminate, a complex number $q \in C$, or a p -adic number $q \in C_p$. If $q \in C$, one normally assumes $|q| < 1$. If $q \in C_p$, one normally assumes $|q-1| < p^{-\frac{1}{p-1}}$. The q -integer $[x]_q$ with x in C is also defined by

$$[x]_q = \frac{1-q^x}{1-q} \quad \text{and} \quad [x]_{-q} = \frac{1-(-q)^x}{1+q}.$$

It is easy to see that $\lim_{q \rightarrow 1} [x]_q = x$ [1-26].

For a positive integer d with $(d, p) = 1$, set

$$X = X_d = \varprojlim_n Z / dp^n Z = \bigcup_{a=0}^{dp-1} (a + dpZ_p)$$

with

$$a + dp^n Z_p = \{x \in X \mid x \equiv a \pmod{dp^n}\},$$

where $a \in Z$ satisfies the condition $0 \leq a < dp^n$, and let $\sigma : X \rightarrow Z_p$ be the transformation introduced by the inverse limit of the natural transformation:

$$Z / dp^n Z \mapsto Z / p^n Z.$$

If f is a function of Z_p , then we will utilise the same notation to indicate the function $f \circ \sigma$.

Let $UD(Z_p)$ be the space of uniformly differentiable functions on Z_p . That is, for $f \in UD(Z_p)$, the p -adic q -integral on Z_p was originally defined by Kim [11-14] as follows:

$$I_q(f) = \int_{Z_p} f(v) d\mu_q(v) = \int_{Z_p} f(v) d\mu_q(v) = \lim_{n \rightarrow \infty} \frac{1}{[p^n]_q} \sum_{v=0}^{p^n-1} q^v f(v) \quad (3)$$

The bosonic integral is considered as the bosonic limit $q \rightarrow 1$, $I_1(f) = \lim_{q \rightarrow 1} I_q(f)$.

Similarly, the p -adic fermionic integration on Z_p was firstly defined by Kim [16, 18] as follows:

$$I_{-q}(f) = \lim_{q \rightarrow -q} I_q(f) = \int_{Z_p} f(v) d\mu_{-q}(v). \quad (4)$$

The above integrals are powerful tools in the studying of p -adic analogue of some special polynomials such as Bernoulli polynomials, Euler polynomials, Genocchi polynomials, Frobenius-Euler polynomials, Eulerian polynomials, Boole polynomials and their various generalisations [1-33].

By (4), we have the following integral equation:

$$q^n I_{-q}(f_n) + (-1)^{n-1} I_{-q}(f) = [2]_q \sum_{l=0}^{n-1} (-1)^{n-1-l} q^l f(l) \tag{5}$$

where $f_n(x)$ is a translation given by $f_n(x) := f(x+n)$. It follows from (5) that

$$q I_{-q}(f_1) + I_{-q}(f) = [2]_q f(0). \tag{6}$$

If we replace q by q^{-1} in (6), it becomes

$$I_{-q^{-1}}(f_1) + q I_{-q^{-1}}(f) = [2]_q f(0). \tag{7}$$

Recently, Kim et al. [22] considered the case $f(x) = e^{-x(1+q)t}$ in (7) and derived the following Witt's formula of the Eulerian polynomials for $n \in \mathbb{N}^*$:

$$I_{-q^{-1}}(x^n) = \frac{(-1)^n}{(1+q)^n} A_n(-q). \tag{8}$$

Note that Kim and Kim [23, 24] also introduced the q -analogue of Eulerian polynomials and the p -adic integral representation of the Boole polynomials.

Based on the work of Kim et al. [22], Araci et al. [7] defined the generating function of Dirichlet's type of the Eulerian polynomials as follows:

$$\sum_{n=0}^{\infty} A_{n,\chi}(-q) \frac{t^n}{n!} = [2]_q \sum_{l=0}^{d-1} (-1)^l q^{d-l+1} \chi(l) \frac{e^{-l(1+q)t}}{e^{-d(1+q)t} + q^d}. \tag{9}$$

Also, they gave the following Witt's formula for Dirichlet's type of the Eulerian polynomials:

$$I_{-q^{-1}}(\chi(x)x^n) = \frac{(-1)^n}{(1+q)^n} A_{n,\chi}(-q).$$

In this paper we construct Dirichlet's type of twisted Eulerian polynomials. By using a complex contour integral representation (or known as Mellin transformation) based on the generating function of Dirichlet type of twisted Eulerian polynomials, we define an L -type function which interpolates Dirichlet's type of twisted Eulerian polynomials at negative integers.

ON DIRICHLET'S TYPE OF TWISTED EULERIAN POLYNOMIALS

By using (5), we have

$$I_{-q^{-1}}(f_d) + q^d I_{-q^{-1}}(f) = [2]_q \sum_{l=0}^{d-1} (-1)^l q^{d-l+1} f(l). \tag{10}$$

Let $C_{p^n} = \{\zeta \mid \zeta^{p^n} = 1\}$ be the cyclic group of order p^n , and let

$$T_p = \lim_{n \rightarrow \infty} C_{p^n} = C_{p^\infty} = \bigcup_{n \geq 0} C_{p^n},$$

where T_p is locally constant space. Let χ be a Dirichlet character of conductor $d (= \text{odd})$ and $\zeta \in T_p$. Taking $f(x) = \zeta^x \chi(x) e^{-x(1+q)t}$ in (10) gives

$$\begin{aligned}
 I_{-q^{-1}} \left(\zeta^{x+d} \chi(x+d) e^{-(x+d)(1+q)t} \right) + q^d I_{-q^{-1}} \left(\zeta^x \chi(x) e^{-x(1+q)t} \right) \\
 = [2]_q \sum_{l=0}^{d-1} (-1)^l q^{d-l+1} \chi(l) e^{-l(1+q)t} \zeta^l.
 \end{aligned}$$

From this, we derive

$$I_{-q^{-1}} \left(\zeta^x \chi(x) e^{-x(1+q)t} \right) = [2]_q \sum_{l=0}^{d-1} (-1)^l q^{d-l+1} \zeta^l \chi(l) \frac{e^{-l(1+q)t}}{\zeta^d e^{-d(1+q)t} + q^d}. \quad (11)$$

Therefore, we give the following definition of the generating function for Dirichlet's type of twisted Eulerian polynomials.

Definition 1. Let $G_{q,\zeta}(t|\chi) = \sum_{n=0}^{\infty} A_{n,\chi,\zeta}(-q) \frac{t^n}{n!}$ and $\zeta \in T_p$. Then we define the twisted Dirichlet's type of Eulerian polynomials by means of the following generating function:

$$\sum_{n=0}^{\infty} A_{n,\chi,\zeta}(-q) \frac{t^n}{n!} = [2]_q \sum_{l=0}^{d-1} (-1)^l q^{d-l+1} \zeta^l \chi(l) \frac{e^{-l(1+q)t}}{\zeta^d e^{-d(1+q)t} + q^d}.$$

By this definition, we have the following corollary.

Corollary 1. For any $\zeta \in T_p$ and $n \in \mathbb{N}^*$, we have

$$A_{n,\chi,\zeta}(-q) = \left[\frac{t^n}{n!} \right] [2]_q \sum_{l=0}^{d-1} (-1)^l q^{d-l+1} \zeta^l \chi(l) \frac{e^{-l(1+q)t}}{\zeta^d e^{-d(1+q)t} + q^d}$$

where $[t^n]f(t)$ means the coefficient of t^n in $f(t)$.

Now we give an integral representation of the twisted Dirichlet's type of Eulerian polynomials.

Theorem 1. The following equalities hold:

$$I_{-q^{-1}} \left(\zeta^x \chi(x) x^n \right) = \int_{Z_p} \zeta^x \chi(x) x^n d\mu_{-q^{-1}}(x) = \frac{(-1)^n}{(1+q)^n} A_{n,\chi,\zeta}(-q) \quad (12)$$

Proof. It is evident from (11) and Definition 1.

By Definition 1, we have the following Theorem.

Theorem 2. For $\zeta \in T_p$, we have

$$G_{q,\zeta}(t|\chi) = \sum_{n=0}^{\infty} A_{n,\chi,\zeta}(-q) \frac{t^n}{n!} = [2]_q \sum_{m=0}^{\infty} \frac{(-1)^m \zeta^m \chi(m) e^{-m(1+q)t}}{q^{m-1}}. \quad (13)$$

Proof. From Definition 1, we discover:

$$\begin{aligned} \sum_{n=0}^{\infty} A_{n,\chi,\zeta}(-q) \frac{t^n}{n!} &= [2]_q \sum_{l=0}^{d-1} (-1)^l q^{d-l+1} \zeta^l \chi(l) \frac{e^{-l(1+q)t}}{\zeta^d e^{-d(1+q)t} + q^d} \\ &= [2]_q \sum_{l=0}^{d-1} (-1)^l q^{-l+1} \zeta^l \chi(l) e^{-l(1+q)t} \sum_{m=0}^{\infty} (-1)^m \zeta^{md} q^{-md} e^{-md(1+q)t} \\ &= q [2]_q \sum_{m=0}^{\infty} \sum_{l=0}^{d-1} (-1)^{l+md} \chi(l+md) q^{-(l+md)} \zeta^{l+md} e^{-(l+md)(1+q)t} \\ &= q [2]_q \sum_{m=0}^{\infty} (-1)^m \zeta^m \chi(m) q^{-m} e^{-m(1+q)t}. \end{aligned}$$

Thus, we arrive at the desired result.

Now we give the following Theorem, which is an explicit formula for twisted Dirichlet's type of Eulerian polynomials.

Theorem 3. For $\zeta \in T_p$, we have

$$\frac{(-1)^n}{q(1+q)^{n+1}} A_{n,\chi,\zeta}(-q) = \sum_{m=1}^{\infty} \frac{(-1)^m \zeta^m \chi(m) m^n}{q^m}. \tag{14}$$

Proof. By using Taylor expansion of $e^{-m(1+q)t}$ in (13), we see that

$$\sum_{n=0}^{\infty} A_{n,\chi,\zeta}(-q) \frac{t^n}{n!} = [2]_q \sum_{n=0}^{\infty} \left(\sum_{m=0}^{\infty} \frac{(-1)^m \zeta^m \chi(m) (-m)^n (1+q)^n}{q^{m-1}} \right) \frac{t^n}{n!}$$

Comparing the coefficients of $\frac{t^n}{n!}$ on both sides of the above equation, we arrive at the desired result.

From (12) and (14), we have the following corollary.

Corollary 2. For $\zeta \in T_p$ and $n \in N$, we have

$$\lim_{n \rightarrow \infty} \sum_{x=0}^{p^n-1} \frac{(-1)^x \zeta^x \chi(x) x^n}{q^x} = 2q^2 \sum_{m=1}^{\infty} \frac{(-1)^m \zeta^m \chi(m) m^n}{q^m}.$$

Now also, we give multiplication theorem for Dirichlet's type of twisted Eulerian polynomials.

Theorem 4. The following is true:

$$\frac{(-1)^n}{(1+q)^n} A_{n,\chi,\zeta}(-q) = \frac{d^n}{[d]_{-q^{-1}}} \sum_{a=0}^{d-1} (-1)^a \chi(a) \zeta^a q^{-a} \int_{Z_p} \left(\frac{a}{d} + x \right)^n \zeta^{dx} d\mu_{-q^{-d}}(x) \tag{15}$$

Proof. For each $\zeta \in T_p$ and $n \in N^*$ we see that

$$\begin{aligned}
 & I_{-q^{-1}}(\zeta^x \chi(x) x^n) \\
 &= \int_{Z_p} \zeta^x \chi(x) x^n d\mu_{-q^{-1}}(x) \\
 &= \lim_{m \rightarrow \infty} \frac{1}{[dp^m]_{-q^{-1}}} \sum_{x=0}^{dp^m-1} (-1)^x \zeta^x \chi(x) x^n q^{-x} \\
 &= \frac{d^n}{[d]_{-q^{-1}}} \sum_{a=0}^{d-1} (-1)^a \zeta^a \chi(a) q^{-a} \left(\lim_{m \rightarrow \infty} \frac{1}{[p^m]_{-q^{-d}}} \sum_{x=0}^{p^m-1} (-1)^x \zeta^{dx} \left(\frac{a}{d} + x\right)^n q^{-dx} \right) \\
 &= \frac{d^n}{[d]_{-q^{-1}}} \sum_{a=0}^{d-1} (-1)^a \chi(a) \zeta^a q^{-a} \int_{Z_p} \left(\frac{a}{d} + x\right)^n \zeta^{dx} d\mu_{-q^{-d}}(x).
 \end{aligned}$$

So we complete the proof of the theorem.

Corollary 3. For any $\zeta \in T_p$ and $n \in \mathbb{N}^*$, we have

$$A_{n,\zeta}(-1) = (-2d)^n \sum_{a=0}^{d-1} (-1)^a \chi(a) \zeta^a E_{n,\zeta^d} \left(\frac{a}{d}\right).$$

Proof. It is interesting to point out that the case $q = 1$ in (15) gives

$$\frac{(-1)^n}{2^n} A_{n,\zeta}(-1) = d^n \sum_{a=0}^{d-1} (-1)^a \chi(a) \zeta^a \int_{Z_p} \left(\frac{a}{d} + x\right)^n \zeta^{dx} d\mu_{-1}(x). \tag{16}$$

With the help of Rim and Kim's work [25], we get

$$E_{n,\zeta}(x) = \int_{Z_p} \zeta^y (x+y)^n d\mu_{-1}(y) \tag{17}$$

where $\zeta \in T_p$. Taking $x = 0$ in the above equation, we have $E_{n,\zeta}(0) := E_{n,\zeta}$, which is defined by the following generating function:

$$\sum_{n=0}^{\infty} E_{n,\zeta} \frac{t^n}{n!} = \frac{2 \sum_{l=0}^{d-1} (-1)^l \zeta^l e^{lt}}{\zeta^d e^{dt} + 1}, \quad |t| < \frac{\pi}{d}. \tag{18}$$

Combining (16), (17) and (18), we end the proof of Corollary 3.

ON L-TYPE FUNCTION IN C

We describe L -type function by applying Mellin transformation to the generating function of Dirichlet's type of twisted Eulerian polynomials (stated in Definition 1), which is an interpolated function of Dirichlet's type of twisted Eulerian polynomials at negative integers for the corresponding Cauchy-Residue theorem. Further information about these topics can be obtained elsewhere [4, 6, 7, 15, 17, 19, 25, 31-33].

By (13), for $s \in C$, we consider the following complex contour integral representation (or known as Mellin transformation):

$$L_{E,\zeta}(s, \chi) = \frac{\int_0^{\infty} t^{s-1} G_{q,\zeta}(t | \chi) dt}{\int_0^{\infty} t^{s-1} e^{-t} dt}. \tag{19}$$

It follows from (19) that

$$L_{E,\zeta}(s, \chi) = q[2]_q \sum_{m=0}^{\infty} (-1)^m \chi(m) \zeta^m q^{-m} \left\{ \frac{\int_0^{\infty} t^{s-1} e^{-m(1+q)t} dt}{\int_0^{\infty} t^{s-1} e^{-t} dt} \right\}$$

$$= \frac{q}{(1+q)^{s-1}} \sum_{m=1}^{\infty} \frac{(-1)^m \chi(m) \zeta^m}{q^m m^s}.$$

On the other hand, we see that

$$L_{E,\zeta}(s, \chi) = \sum_{n=0}^{\infty} \frac{A_{n,\chi,\zeta}(-q)}{n!} \left(\frac{\int_0^{\infty} t^{s-n+1} dt}{\int_0^{\infty} t^{s-1} e^{-t} dt} \right). \tag{20}$$

Therefore, we give the definition of twisted Eulerian L -function as follows:

Definition 2. Let $\zeta \in T_p$ and $s \in C$; we define

$$L_{E,\zeta}(s, \chi) = \frac{q}{(1+q)^{s-1}} \sum_{m=1}^{\infty} \frac{(-1)^m \chi(m) \zeta^m}{q^m m^s}.$$

By (14) and Definition 2, we derive the following Theorem.

Theorem 5. The following equality holds:

$$L_{E,\zeta}(-n, \chi) = (-1)^n A_{n,\chi,\zeta}(-q).$$

Proof. From (14):

$$\frac{(-1)^n}{q(1+q)^{n+1}} A_{n,\chi,\zeta}(-q) = \sum_{m=1}^{\infty} \frac{(-1)^m \zeta^m \chi(m) m^n}{q^m}.$$

Putting $s = -n$ in Definition 2 gives

$$L_{E,\zeta}(-n, \chi) = q(1+q)^{n+1} \sum_{m=1}^{\infty} \frac{(-1)^m \chi(m) \zeta^m m^n}{q^m}$$

from which we have

$$L_{E,\zeta}(-n, \chi) = (-1)^n A_{n,\chi,\zeta}(-q).$$

Thus, the proof of the theorem is completed.

ACKNOWLEDGEMENTS

The authors would like to thank the referees for many valuable comments and suggestions, through which we have substantially improved the presentation of the paper.

REFERENCES

1. S. Araci, "Novel identities involving Genocchi numbers and polynomials arising from applications of umbral calculus", *Appl. Math. Comput.*, **2014**, 233, 599-607.
2. S. Araci, "Novel identities for q -Genocchi numbers and polynomials", *J. Funct. Spaces Appl.*, **2012**, 2012, Article ID 214961.
3. S. Araci, M. Acikgoz and E. Sen, "On the extended Kim's p -adic q -deformed fermionic integrals in the p -adic integer ring", *J. Number Theory*, **2013**, 133, 3348-3361.

4. S. Araci, M. Acikgoz, K. H. Park and H. Jolany, "On the unification of two families of multiple twisted type polynomials by using p -adic q -integral at $q = -1$ ", *Bull. Malays. Math. Sci. Soc.*, **2014**, 37, 543-554.
5. S. Araci, E. Sen and M. Acikgoz, "Theorems on Genocchi polynomials of higher order arising from Genocchi basis", *Taiwan. J. Math.*, **2014**, 18, 473-482.
6. S. Araci, M. Acikgoz and H. Jolany, "On p -adic interpolating function associated with modified Dirichlet's type of twisted q -Euler numbers and polynomials with weight α ", *J. Class. Anal.*, **2013**, 2, 35-48.
7. S. Araci, M. Acikgoz and E. Ağyüz, "On the Dirichlet's type of Eulerian polynomials", *Math. Sci.*, **2014**, 8, 131.
8. S. Araci, A. Bagdasaryan, C. Özel and H. M. Srivastava, "New symmetric identities involving q -zeta-type functions", *Appl. Math. Inform. Sci.*, **2014**, 8, 2803-2808.
9. S. Araci, M. Acikgoz, A. Bagdasaryan and E. Sen, "The Legendre polynomials associated with Bernoulli, Euler, Hermite and Bernstein polynomials", *Turk. J. Anal. Number Theory*, **2013**, 1, 1-3.
10. S. Araci and M. Acikgoz, "A note on the Frobenius-Euler numbers and polynomials associated with Bernstein polynomials", *Adv. Stud. Contemp. Math.*, **2012**, 22, 399-406.
11. T. Kim, "On a q -analogue of the p -adic log gamma functions and related integrals", *J. Number Theory*, **1999**, 76, 320-329.
12. T. Kim, " q -Volkenborn integration", *Russian J. Math. Phys.*, **2002**, 19, 288-299.
13. T. Kim, "Non-archimedean q -integrals associated with multiple Changhee q -Bernoulli polynomials", *Russian J. Math. Phys.*, **2003**, 10, 91-98.
14. T. Kim, " p -Adic q -integrals associated with the Changhee-Barnes' q -Bernoulli polynomials", *Integr. Transf. Special Funct.*, **2004**, 15, 415-420.
15. T. Kim, "Analytic continuation of multiple q -zeta functions and their values at negative integers", *Russian J. Math. Phys.*, **2004**, 11, 71-76.
16. T. Kim, "Some identities on the q -Euler polynomials of higher order and q -stirling numbers by the fermionic p -adic integral on Z_p ", *Russian J. Math. Phys.*, **2009**, 16, 484-491.
17. T. Kim, "On the q -extension of Euler and Genocchi numbers", *J. Math. Anal. Appl.*, **2007**, 326, 1458-1465.
18. T. Kim, "On the analogs of Euler numbers and polynomials associated with p -adic q -integral on Z_p at $q = -1$ ", *J. Math. Anal. Appl.*, **2007**, 331, 779-792.
19. T. Kim, S. H. Lee, H. H. Han and C. S. Ryoo, "On the values of the weighted q -Zeta and L -functions", *Discrete Dynam. Nat. Soc.*, **2011**, 2011, Article ID 476381.
20. T. Kim, D. S. Kim, T. Mansour, S.-H. Rim and M. Schork, "Umbral calculus and Sheffer sequences of polynomials", *J. Math. Phys.*, **2013**, 54, 083504.
21. T. Kim, D. S. Kim, D. V. Dolgy and S. H. Rim, "Some identities on the Euler numbers arising from Euler basis polynomials", *Ars Combin.*, **2013**, 109, 433-446.
22. D. S. Kim, T. Kim, W. J. Kim and D. V. Dolgy, "A note on Eulerian polynomials", *Abstr. Appl. Anal.*, **2012**, 2012, Article ID 269640.
23. D. S. Kim and T. Kim, "A note on q -Eulerian polynomials", *Proc. Jangjeon Math. Soc.*, **2013**, 16, 445-450.

24. D. S. Kim and T. Kim, "A note on Boole polynomials", *Integr. Transf. Special Funct.*, **2014**, 25, 627-633.
25. S.H. Rim and T. Kim, "A note on q -Euler numbers associated with the basic q -zeta function", *Appl. Math. Lett.*, **2007**, 20, 366-369.
26. Y. He and C. Wang, "Some formulae of products of the Apostol-Bernoulli and Apostol-Euler polynomials", *Discrete Dynam. Nat. Soc.*, **2012**, 2012, Article ID 927953.
27. H. Ozden, I. N. Cangul and Y. Simsek, "Multivariate interpolation functions of higher order q -Euler numbers and their applications", *Abstr. Appl. Anal.*, **2008**, 2008, Article ID 390857.
28. I. N. Cangul, H. Ozden and Y. Simsek, "A new approach to q -Genocchi numbers and their interpolation functions", *Nonlinear Anal.*, **2009**, 71, e793-e799.
29. I. N. Cangul, H. Ozden and Y. Simsek, "Generating functions of the (h, q) extension of twisted Euler polynomials and numbers", *Acta Math. Hungar.*, **2008**, 120, 281-299.
30. B.-N. Guo and F. Qi, "Some identities and an explicit formula for Bernoulli and Stirling numbers", *J. Comput. Appl. Math.*, **2014**, 255, 568-579.
31. H. M. Srivastava, "Some formulas for the Bernoulli and Euler polynomials at rational arguments", *Math. Proc. Cambridge Philos. Soc.*, **2000**, 129, 77-84.
32. H. M. Srivastava, "Some generalizations and basic (or q -) extensions of the Bernoulli, Euler and Genocchi polynomials", *Appl. Math. Inform. Sci.*, **2011**, 5, 390-444.
33. H. M. Srivastava and J. Choi, "Zeta and q -Zeta Functions and Associated Series and Integrals", Elsevier Science Publishers, Amsterdam, **2012**.

© 2015 by Maejo University, San Sai, Chiang Mai, 50290 Thailand. Reproduction is permitted for noncommercial purposes.

Full Paper

Köthe-Toeplitz duals of some n -normed valued difference sequence spaces

Hemen Dutta*

Department of Mathematics, Gauhati University, Guwahati-781014, India

* E-mail: hemen_dutta08@rediffmail.com

Received: 12 February 2014 / Accepted: 26 August 2015 / Published: 27 August 2015

Abstract: First, a few basic results are presented that are relevant to some n -normed real linear valued difference sequence spaces. Then Köthe-Toeplitz duals of some such spaces are computed.

Keywords: n -norm, difference sequences, Köthe-Toeplitz dual

INTRODUCTION

A sequence space is a linear space whose elements are sequences chosen from another linear space. The analysis of sequence spaces primarily deals with questions related to the distance between sequences, Cauchy sequences and limits of a sequence of 'points' in the class of all sequences, where 'points' refer to a set of real or complex numbers. The theory of sequence spaces deals with different classes of sequences including those defined by the difference operator and over n (≥ 2)-normed spaces as base space.

Throughout, w , λ_∞ , ℓ_1 , c and c_0 denote the spaces of all, bounded, absolutely summable, convergent and null sequences $x = (x_k)$ with complex terms respectively.

The zero element of a normed linear space is denoted by θ . A complete normed linear space is called a Banach space. It is well known that λ_∞ is a Banach space under the norm

$$\|x\| = \sup_k |x_k|,$$

which is called the sup-norm or uniform norm. The spaces c and c_0 are complete subspaces of λ_∞ .

A BK-space, $(Z, \|\cdot\|)$, introduced by K. Zeller [1], is a Banach space of complex sequences $x = (x_k)$, in which the co-ordinate maps are continuous; that is, $|x_k^n - x_k| \rightarrow 0$, whenever $\|x^n - x\| \rightarrow 0$ as $n \rightarrow \infty$, where $x^n = (x_k^n)$, for all $n \in N$ and $x = (x_k)$.

Let $(X, \|\cdot\|)$ be a normed linear space and λ be a scalar valued sequence space; then the vector valued sequence space or X -valued sequence space $\lambda(X)$ is defined as

$$\lambda(X) = \{ (x_k) : x_k \in X \text{ for all } k \in N \text{ and } \|x_k\| \in \lambda \}$$

Clearly $\lambda(X)$ is a linear space under coordinate-wise addition and scalar multiplication over the field of scalars of X . If X is a Banach space, then the vector valued sequence spaces $c_0(X)$, $\lambda_\infty(X)$ are also Banach spaces with the norm defined by

$$\|x\| = \sup_k \|x_k\|, \text{ where } x = (x_k)$$

Investigations of spaces are often combined with those of their duals. For the duality theory, the study of sequence spaces is more useful when we consider them equipped with linear topologies. In such cases, however, it is rather cumbersome to obtain their topological duals. Even if we are successful in finding these duals, we would like to deal with only those duals whose members can be represented as sequences. Indeed such situations do not present much difficulty in the analysis. Köthe and Toeplitz [2] first recognised the problem and to overcome the situation, they introduced the notion of α -dual (known also as Köthe-Toeplitz dual), which turns out to be the same as the topological dual in quite many familiar and useful examples of sequence spaces endowed with their natural linear matrices. More details about the notion of algebraic duals can be found in the literature [3, 4].

Let X be a normed space. Then the set of all bounded linear functionals on X constitutes a normed space with norm defined by

$$\|f\| = \sup_{\substack{x \in X \\ x \neq 0}} \frac{|f(x)|}{\|x\|} = \sup_{\substack{x \in X \\ \|x\|=1}} |f(x)|,$$

which is called the dual space of X and is denoted by X' .

Let E and F be two sequence spaces. Then the F dual of E is defined as

$$E^F = \{ (x_k) \in w : (x_k y_k) \in F \text{ for all } (y_k) \in E \}$$

For $F = \ell_1$, the dual is termed as α -dual (Köthe-Toeplitz dual) of E and denoted by E^α . If $X \subset Y$, then $Y^\alpha \subset X^\alpha$.

Gähler [5-10] introduced and studied the concept of 2-normed spaces extensively at the initial stage. Then White [11], Diminnie et al. [12], Gähler et al. [13], Siddiqi [14], etc. also contributed in popularising the theory. Later on the concept was generalised to $n(>2)$ -normed space and some initial work on n -normed structures were carried out by Misiak [15, 16]. Since then, Kim and Cho [17], Malčeski [18], Gunawan [19, 20], Gunawan and Mashadi [21, 22], Dutta [23-27], Acikgöz et al. [28], Dutta and Reddy [29], and many others have studied this concept and obtained various results and links with other theories.

The notion of difference sequence space was introduced by Kizmaz [30], who studied the difference sequence spaces $\lambda_\infty(\Delta)$, $c(\Delta)$ and $c_0(\Delta)$. The notion was further generalised by Et and Colak [31] by introducing the spaces $1_\infty(\Delta^m)$, $c(\Delta^m)$ and $c_0(\Delta^m)$, where m is a fixed non-negative integer.

Let m be non-negative integers. Then for Z , a given sequence space, we have

$$Z(\Delta^m) = \{ x = (x_k) \in w : (\Delta^m x_k) \in Z \}$$

where $\Delta^m x = (\Delta^m x_k) = (\Delta^{m-1} x_k - \Delta^{m-1} x_{k+1})$ and $\Delta^0 x_k = x_k$ for all $k \in N$, which is equivalent to the following binomial representation:

$$\Delta^m x_k = \sum_{v=0}^m (-1)^v \binom{m}{v} x_{k+v}$$

Taking $m = 1$ and $Z = \lambda_\infty, c$ and c_0 , we get the spaces $\lambda_\infty(\Delta), c(\Delta)$ and $c_0(\Delta)$. For some other notions of difference sequences, one may refer to Dutta [32].

PRELIMINARIES

The definitions of n -norm and several associated preliminary notions are described below in order to make the relevant theories of this paper comprehensible. Let $n \in N$ and X be a real vector space of dimension d , where $n \leq d$. A real-valued function $\|.,. . .,.\|$ on X^n satisfying the following four conditions, viz.

- (N1) $\|x_1, x_2, . . . , x_n\| = 0$ if and only if $x_1, x_2, . . . , x_n$ are linearly dependent,
- (N2) $\|x_1, x_2, . . . , x_n\|$ is invariant under permutation,
- (N3) $\|\alpha x_1, x_2, . . . , x_n\| = |\alpha| \|x_1, x_2, . . . , x_n\|$, for any $\alpha \in R$, and
- (N4) $\|x+x', x_2, . . . , x_n\| \leq \|x, x_2, . . . , x_n\| + \|x', x_2, . . . , x_n\|$,

is called an n -norm on X and the pair $(X, \|.,. . .,.\|)$ is called an n -normed space.

A trivial example of an n -normed space is $X = R^n$, equipped with the following Euclidean n -norm:

$$\|x_1, x_2, . . . , x_n\|_E = \text{abs} \left(\begin{matrix} x_{11} & L & x_{1n} \\ MO & & M \\ x_{n1} & L & x_{nn} \end{matrix} \right), \text{ where } x_i = (x_{i1}, \dots, x_{in}) \in R^n \text{ for each } i = 1, 2, \dots, n$$

Gunawan [19] showed how we can actually define an n -inner product and accordingly an n -norm on any inner product space, provided that the dimension is sufficiently large, as follows.

Let $n \in N$ and $(X, \langle ., . \rangle)$ be a real inner product space of dimension $d \geq n$. Define the following function $\langle ., \dots, . | ., . \rangle$ on $X \times \dots \times X$ ($n+1$ factors) by

$$\langle x_1, \dots, x_{n-1} | y, z \rangle = \begin{vmatrix} \langle x_1, x_1 \rangle L \langle x_1, x_{n-1} \rangle & \langle x_1, z \rangle \\ M & O & M & M \\ \langle x_{n-1}, x_1 \rangle L \langle x_{n-1}, x_{n-1} \rangle & \langle x_{n-1}, z \rangle \\ \langle y, x_1 \rangle & L & \langle y, x_{n-1} \rangle & \langle y, z \rangle \end{vmatrix}$$

Then one may check that this function satisfies the following five properties:

- (I1) $\langle x_1, \dots, x_{n-1} | x_n, x_n \rangle \geq 0$; $\langle x_1, \dots, x_{n-1} | x_n, x_n \rangle = 0$ if and only if x_1, \dots, x_n are linearly dependent;
- (I2) $\langle x_1, \dots, x_{n-1} | x_n, x_n \rangle = \langle x_{i_1}, \dots, x_{i_{n-1}} | x_{i_n}, x_{i_n} \rangle$ for every permutation (i_1, \dots, i_n) of $(1, \dots, n)$;
- (I3) $\langle x_1, \dots, x_{n-1} | y, z \rangle = \langle x_1, \dots, x_{n-1} | z, y \rangle$;
- (I4) $\langle x_1, \dots, x_{n-1} | y, \alpha z \rangle = \alpha \langle x_1, \dots, x_{n-1} | y, z \rangle$;
- (I5) $\langle x_1, \dots, x_{n-1} | y, z + z' \rangle = \langle x_1, \dots, x_{n-1} | y, z \rangle + \langle x_1, \dots, x_{n-1} | y, z' \rangle$.

Accordingly, we can define $\|., \dots, .\|$ on $X \times \dots \times X$ (n factors) by

$$\|x_1, \dots, x_n\| = \langle x_1, \dots, x_{n-1} | x_n, x_n \rangle^{1/2};$$

that is,

$$\|x_1, \dots, x_n\| = \left| \begin{matrix} \langle x_1, x_1 \rangle & \dots & \langle x_1, x_n \rangle \\ \vdots & \dots & \vdots \\ \langle x_n, x_1 \rangle & \dots & \langle x_n, x_n \rangle \end{matrix} \right|^{1/2}$$

For $n = 1$, we know that $\|\cdot\|$ is a norm, while for $n = 2$, $\|\cdot, \cdot\|$ defines a 2-norm. Note further that for $n = 1$, $\|x_1\|$ gives the length of x_1 , while for $n = 2$, $\|x_1, x_2\|$ represents the area of the parallelogram spanned by x_1 and x_2 . For $n = 3$ and $X = R^3$, one may observe that $\|x_1, x_2, x_3\|$ is nothing but the volume of the parallelepiped spanned by x_1, x_2 and x_3 ; that is,

$$\|x_1, x_2, x_3\| = |x_1 \cdot (x_2 \times x_3)|$$

Thus, in general, $\|x_1, \dots, x_n\|$ can be interpreted as the volume of the n -dimensional parallelepiped spanned by x_1, \dots, x_n in X . Further, it satisfies the four properties (N1)-(N4) of n -norm.

Let $n \in N$ and X be a real vector space of dimension $d \geq n$. A function $\langle \cdot, \dots, \cdot | \cdot, \cdot \rangle$ on $X \times \dots \times X$ ($n+1$ factors) satisfying the five properties (I1)-(I5) listed above is called an n -inner product on X , and the pair $(X, \langle \cdot, \dots, \cdot | \cdot, \cdot \rangle)$ is called an n -inner product space. Meanwhile, a function $\|\cdot, \dots, \cdot\|$ on $X \times \dots \times X$ (n factors) satisfying the four properties (N1)-(N4) listed above is called an n -norm on X , and the pair $(X, \|\cdot, \dots, \cdot\|)$ is called an n -normed space.

The definition of n -inner product given by Gunawan [19] is slightly simpler than that by Misiak [15, 16]. To see that it is equivalent to Misiak's, one only needs to verify that

$$\langle x_1, \dots, x_{n-1} | y, z \rangle = \langle x_{i_1}, \dots, x_{i_{n-1}} | y, z \rangle$$

for every permutation (i_1, \dots, i_{n-1}) of $(1, \dots, n-1)$, but this will follow easily from property (I2) and the polarisation identity:

$$\langle x_1, \dots, x_{n-1} | y, z \rangle = \frac{1}{4} [\langle x_1, \dots, x_{n-1} | y+z, y+z \rangle - \langle x_1, \dots, x_{n-1} | y-z, y-z \rangle]$$

Moreover, the first three properties of the n -norm are easy to prove. To prove the fourth property or the triangle inequality, Cauchy-Schwartz inequality is needed. Gunawan [19] has given the Cauchy-Schwartz inequality for n -inner product spaces as follows.

Proposition 1 (Theorem 3.1 [19]). *Let $(X, \langle \cdot, \dots, \cdot | \cdot, \cdot \rangle)$ be an n -inner product space. Then we have*

$$\langle x_1, \dots, x_{n-1} | y, z \rangle^2 \leq \langle x_1, \dots, x_{n-1} | y, y \rangle \langle x_1, \dots, x_{n-1} | z, z \rangle$$

and the equality holds if and only if $x_1, \dots, x_{n-1}, y, z$ are linearly dependent.

Proposition 2 (Corollary 3.2 [19]). *On an n -inner product space $(X, \langle \cdot, \dots, \cdot | \cdot, \cdot \rangle)$, the following function,*

$$\|x_1, \dots, x_n\| = \langle x_1, \dots, x_{n-1} | x_n, x_n \rangle^{1/2},$$

defines an n -norm. In particular, the triangle inequality,

$$\|x_1, \dots, x_{n-1}, y+z\| \leq \|x_1, \dots, x_{n-1}, y\| + \|x_1, \dots, x_{n-1}, z\|,$$

holds for all $x_1, \dots, x_{n-1}, y, z \in X$.

Proposition 3 (Corollary 3.3 [19]). *Let $(X, \langle \cdot, \dots, \cdot | \cdot, \cdot \rangle)$ be an n -inner product space. If $x_1, \dots, x_{n-1}, y, z$ are linearly dependent on X , then*

$$\|x_1, \dots, x_{n-1}, y + z\| = \|x_1, \dots, x_{n-1}, y\| + \|x_1, \dots, x_{n-1}, z\|$$

or

$$\|x_1, \dots, x_{n-1}, y - z\| = \|x_1, \dots, x_{n-1}, y\| + \|x_1, \dots, x_{n-1}, z\|$$

Conversely, if one of the above two equalities holds, then $x_1, \dots, x_{n-1}, y, z$ are linearly dependent on X .

Gunawan and Mashadi [22] showed that if $(X, \|\cdot, \dots, \cdot\|)$ is an n -normed space of dimension $d \geq n \geq 2$ and $\{a_1, a_2, \dots, a_n\}$ is a linearly independent set in X , then the following function $\|\cdot, \dots, \cdot\|_\infty$ on X^{n-1} defined by

$$\|x_1, x_2, \dots, x_{n-1}\|_\infty = \max \{ \|x_1, x_2, \dots, x_{n-1}, a_i\| : i = 1, 2, \dots, n \}$$

defines an $(n-1)$ norm on X with respect to $\{a_1, a_2, \dots, a_n\}$ and this is called the derived $(n-1)$ -norm.

A sequence (x_k) in an n -normed space $(X, \|\cdot, \dots, \cdot\|)$ is said to converge to some $L \in X$ in the n -norm if

$$\lim_{k \rightarrow \infty} \|x_k - L, u_2, \dots, u_n\| = 0, \text{ for every } u_2, \dots, u_n \in X$$

A sequence (x_k) in an n -normed space $(X, \|\cdot, \dots, \cdot\|)$ is said to be Cauchy with respect to the n -norm if

$$\lim_{k, l \rightarrow \infty} \|x_k - x_l, u_2, \dots, u_n\| = 0, \text{ for every } u_2, \dots, u_n \in X$$

If every Cauchy sequence in X converges to some $L \in X$, then X is said to be complete with respect to the n -norm. Any complete n -normed space is said to be n -Banach space.

Now I state the following results as Lemmas. For details one may refer to Gunawan and Mashadi [22].

Lemma 1. Every n -normed space is an $(n-r)$ -normed space for all $r = 1, 2, \dots, n-1$. In particular, every n -normed space is a normed space.

Lemma 2. A standard n -normed space is complete if and only if it is complete with respect to the usual norm $\| \cdot \|_S = \langle \cdot, \cdot \rangle^{\frac{1}{2}}$.

Lemma 3. On a standard n -normed space X , the derived $(n-1)$ -norm $\|\cdot, \dots, \cdot\|_\infty$, defined with respect to orthonormal set $\{e_1, e_2, \dots, e_n\}$, is equivalent to the standard $(n-1)$ -norm $\|\cdot, \dots, \cdot\|_S$. Precisely, we have

$$\|x_1, \dots, x_{n-1}\|_\infty \leq \|x_1, \dots, x_{n-1}\|_S \leq \sqrt{n} \|x_1, \dots, x_{n-1}\|_\infty$$

for all x_1, \dots, x_{n-1} , where $\|x_1, \dots, x_{n-1}\|_\infty = \max \{ \|x_1, \dots, x_{n-1}, e_i\|_S : i = 1, \dots, n \}$.

Definition 1. An n -BK-space $(X, \|\cdot, \dots, \cdot\|)$ is an n -Banach space of real sequences $x = (x_k)$, in which the co-ordinate maps are continuous.

The well-known spaces c_0, c and λ_∞ can be extended to n -normed space valued difference sequences using m th order difference operator as follows.

Let $(X, \|\cdot, \dots, \cdot\|)$ be an n -normed real linear space and $w(n-X)$ denote X -valued sequence space. Let m be a non-negative integer; then we have the following sequence spaces:

$$c_0(\Delta^m, \|\cdot, \dots, \cdot\|) = \{ (x_k) \in w(n-X) : \lim_{k \rightarrow \infty, z_1, \dots, z_{n-1} \in X} \|\Delta^m x_k, z_1, \dots, z_{n-1}\| = 0 \},$$

$$c(\Delta^m, \|\cdot, \dots, \cdot\|) = \{ (x_k) \in w(n-X) : \lim_{k \rightarrow \infty, z_1, \dots, z_{n-1} \in X} \|\Delta^m x_k - L, z_1, \dots, z_{n-1}\| = 0, \text{ for some } L \text{ in } X \},$$

$$\ell_\infty(\Delta^m, \|\cdot, \dots, \cdot\|) = \{(x_k) \in w(n-X) : \sup_{\substack{k \geq 1, \\ z_1, \dots, z_{n-1} \in X}} \|\Delta^m x_k, z_1, \dots, z_{n-1}\| < \infty\}.$$

MAIN RESULTS

Throughout this section, Y is assumed to be any one of the spaces $c_0(\Delta^m, \|\cdot, \dots, \cdot\|)$, $c(\Delta^m, \|\cdot, \dots, \cdot\|)$ and $\ell_\infty(\Delta^m, \|\cdot, \dots, \cdot\|)$. First, a few basic descriptions of these spaces with certain immediate results are given. Then the algebraic dual of some of these spaces are computed.

Theorem 1. *The spaces Y are linear over the field of reals.*

Proof. The proof is omitted as it is just a routine verification.

Let us define the function $\|\cdot, \dots, \cdot\|_Y$ on $Y \times \dots \times Y$ (n -factors) by

$$\begin{aligned} \|x^1, x^2, \dots, x^n\|_Y &= 0, \text{ if } x^1, x^2, \dots, x^n \text{ are linearly dependent and} \\ \|x^1, x^2, \dots, x^n\|_Y &= \sum_{k=1}^m \|x_k^1, z_1, \dots, z_{n-1}\| + \sup_{k \geq 1} \|\Delta^m x_k^1, z_1, \dots, z_{n-1}\|, \text{ for every } z_1, \dots, z_{n-1} \in X, \\ &\text{if } x^1, x^2, \dots, x^n \text{ are linearly independent.} \end{aligned}$$

Theorem 2. *The function $\|\cdot, \dots, \cdot\|_Y$ is an n -norm on Y .*

Proof: In view of Dutta [24, 25], the proof is easy so it is omitted.

Note 1. We call $\|\cdot, \dots, \cdot\|_Y$ a non-standard n -norm [29].

For any linearly independent set $\{a_1, a_2, \dots, a_n\}$, we can define

$$\|x_k^1, z_1, z_2, \dots, z_{n-r-1}\|_\infty = \max \{ \|x_k^1, z_1, z_2, \dots, z_{n-r-1}, a_{i_1}, a_{i_2}, \dots, a_{i_r}\| \}, \{i_1, i_2, \dots, i_r\} \subseteq \{1, 2, \dots, n\}$$

Then $\|\cdot, \dots, \cdot\|_\infty$ is an $(n-r)$ -norm on X for each $k \geq 1$ and for all $r = 1, 2, \dots, n-1$.

We can define another function $\|\cdot, \dots, \cdot\|_Y$ on $Y \times \dots \times Y$ ($(n-r)$ -factors) by

$$\begin{aligned} \|x^1, x^2, \dots, x^{n-r}\|_Y^{n-r} &= 0 \text{ if } x^1, x^2, \dots, x^{n-r} \text{ are linearly dependent and} \\ \|x^1, x^2, \dots, x^{n-r}\|_Y^{n-r} &= \sum_{k=1}^m \|x_k^1, z_1, \dots, z_{n-r-1}\|_\infty + \sup_{k \geq 1} \|\Delta^m x_k^1, z_1, \dots, z_{n-r-1}\|_\infty, \text{ for every} \\ &z_1, \dots, z_{n-r-1} \in X, \text{ if } x^1, x^2, \dots, x^{n-r} \text{ are linearly independent.} \end{aligned}$$

Theorem 3. *The function $\|\cdot, \dots, \cdot\|_Y$ is a $(n-r)$ -norm on Y for all $r = 1, 2, \dots, n-1$.*

Proof. The proof is similar to that of Theorem 2.

Note 2: We call the $(n-r)$ -norm $\|\cdot, \dots, \cdot\|_Y^{n-r}$ on the spaces Y for all $r = 1, 2, \dots, n-1$ a derived norm.

Corollary 1. *The spaces Y are normed spaces.*

Theorem 4. *If the base space X is an n -Banach space, then the spaces Y are n -Banach spaces under the n -norm $\|\cdot, \dots, \cdot\|_Y$.*

Proof. The proof is easy in view of Dutta [24, 25].

The following corollary is due to Lemma 2.

Corollary 2. *If X is a Banach space under the standard n -norm, then the spaces Y are n -Banach space under the n -norm $\|\cdot, \dots, \cdot\|_Y$.*

In view of the above results, we have the following immediate consequence.

Corollary 3. *The spaces Y are n -BK spaces under the n -norm $\|\cdot, \dots, \cdot\|_Y$, provided that the base space is an n -Banach space or Banach space.*

In order to compute the Köthe-Toeplitz dual, we need the following definitions and results [27]. An n -functional is a real valued mapping with domain $A_1 \times \dots \times A_n$, where A_1, \dots, A_n are linear manifolds of a linear n -normed space.

Let F be an n -functional with domain $A_1 \times \dots \times A_n$. F is called a linear n -functional whenever for all ${}^1a_1, {}^1a_2, \dots, {}^1a_n \in A_1, {}^2a_1, {}^2a_2, \dots, {}^2a_n \in A_2, \dots, {}^na_1, {}^na_2, \dots, {}^na_n \in A_n$ and all $\alpha_1, \dots, \alpha_n \in R$, we have

- i) $F({}^1a_1 + {}^1a_2 + \dots + {}^1a_n, {}^2a_1 + {}^2a_2 + \dots + {}^2a_n, \dots, {}^na_1 + {}^na_2 + \dots + {}^na_n) = \sum_{1 \leq i_1, i_2, \dots, i_n \leq n} F({}^1a_{i_1}, {}^2a_{i_2}, \dots, {}^na_{i_n})$ and
- ii) $F(\alpha_1 a_1, \dots, \alpha_n a_n) = \alpha_1 \dots \alpha_n F(a_1, \dots, a_n)$

Let F be an n -functional with domain $D(F)$. F is called bounded if there is a real constant $K \geq 0$ such that $|F(a_1, \dots, a_n)| \leq K \|a_1, \dots, a_n\|$ for all $(a_1, \dots, a_n) \in D(F)$. If F is bounded, we define the norm of F , $\|F\|$, by

$$\|F\| = \text{glb} \left\{ K : |F(a_1, \dots, a_n)| \leq K \|a_1, \dots, a_n\| \text{ for all } (a_1, \dots, a_n) \in D(F) \right\}$$

If F is not bounded, we define $\|F\| = +\infty$.

For the following two results, one may refer to White [11] and proofs can similarly be obtained.

Theorem 5. *A linear n -functional F is continuous if and only if it is bounded.*

Theorem 6. *Let B^* be the set of bounded linear n -functionals with domain $B_1 \times \dots \times B_n$. Then B^* is an n -Banach space up to linear dependence.*

As far as is known, the theory of continuous duals for n -normed spaces has not been developed well enough. For any n -normed space E , its continuous dual will be denoted by E^* . Dutta [27] defined the Köthe-Toeplitz dual of sequence spaces, with base space an n -normed space, as follows.

Let E be an n -normed linear space, normed by $\|\cdot, \dots, \cdot\|_E$. Then the Köthe-Toeplitz dual of the sequence space $Z(E)$ whose base space is E is defined as

$$[Z(E)]^\alpha = \left\{ (y_k) : y_k \in E^*, k \in N \text{ and } \left(\|x_k, u_2, \dots, u_n\|_E \|y_k, v_2, \dots, v_n\|_{E^*} \right) \in \ell_1, \right. \\ \left. \text{for every } v_2, \dots, v_n \in E^*, u_2, \dots, u_n \in E, (x_k) \in Z(E) \right\}$$

It is easy to check that $\phi \subset X^\alpha$. If $X \subset Y$, then $Y^\alpha \subset X^\alpha$.

Lemma 4. *For every non-zero $u_2, \dots, u_n \in X$, we have:*

- (i) $x \in \ell_\infty(\Delta^m, \|\cdot, \dots, \cdot\|)$ implies $\sup_k k^{-1} \|\Delta^{m-1} x_k, u_2, \dots, u_n\| < \infty$
- (ii) $x \in \ell_\infty(\Delta^m, \|\cdot, \dots, \cdot\|)$ implies $\sup_k k^{-m} \|x_k, u_2, \dots, u_n\| < \infty$

Proof. (i) Let $x \in \ell_\infty(\Delta^m, \|\cdot, \dots, \cdot\|)$; then

$$\sup_{k \geq 1} \|\Delta^{m-1}x_k - \Delta^{m-1}x_{k+1}, z_1, \dots, z_{n-1}\| < \infty, \text{ for every non-zero } z_1, \dots, z_{n-1} \in X$$

Then there exists a $U > 0$ such that for every non-zero $z_1, \dots, z_{n-1} \in X$,

$$\|\Delta^{m-1}x_k - \Delta^{m-1}x_{k+1}, z_1, \dots, z_{n-1}\| < U \text{ for all } k \in N$$

Now for every non-zero $z_1, \dots, z_{n-1} \in X$,

$$\|\Delta^{m-1}x_1 - \Delta^{m-1}x_{k+1}, z_1, \dots, z_{n-1}\| \leq \frac{1}{k} \sum_{l=1}^k \|\Delta^{m-1}x_l - \Delta^{m-1}x_{l+1}, z_1, \dots, z_{n-1}\| < U$$

Then from the above inequality, we have the desired result using the inequality:

$$\frac{1}{k} \|\Delta^{m-1}x_{k+1}, z_1, \dots, z_{n-1}\| \leq \frac{1}{k} (\|\Delta^{m-1}x_1, z_1, \dots, z_{n-1}\| + \|\Delta^{m-1}x_1 - \Delta^{m-1}x_{k+1}, z_1, \dots, z_{n-1}\|)$$

(ii) The proof follows from part (i).

Let us set

$$D = \left\{ a = (a_k) : \sum_{k=1}^{\infty} k^m \|a_k, z_2, \dots, z_n\|_{X^*} < \infty, \text{ for every } z_2, \dots, z_n \in X^* \right\}.$$

Theorem 7. The Köthe-Toeplitz dual of the spaces $\ell_\infty(\Delta^m, \|\cdot, \dots, \cdot\|)$ and $c(\Delta^m, \|\cdot, \dots, \cdot\|)$ is D , i.e.

$$[\ell_\infty(\Delta^m, \|\cdot, \dots, \cdot\|)]^\alpha = [c(\Delta^m, \|\cdot, \dots, \cdot\|)]^\alpha = D$$

Proof. Let $a \in D$; then $\sum_{k=1}^{\infty} k^m \|a_k, z_2, \dots, z_n\|_{X^*} < \infty$ for every $z_2, \dots, z_n \in X^*$. Now for any $x \in \ell_\infty(\Delta^m, \|\cdot, \dots, \cdot\|)$, we have $\sup_k k^{-m} \|x_k, u_2, \dots, u_n\|_X < \infty$ for every $u_2, \dots, u_n \in X$. Then we have

$$\sum_{k=1}^{\infty} \|a_k, z_2, \dots, z_n\|_{X^*} \|x_k, u_2, \dots, u_n\|_X \leq \sup_k k^{-m} \|x_k, u_2, \dots, u_n\|_X \sum_{k=1}^{\infty} k^m \|a_k, z_2, \dots, z_n\|_{X^*} < \infty$$

Hence

$$\begin{aligned} a &\in [\ell_\infty(\Delta^m, \|\cdot, \dots, \cdot\|)]^\alpha \\ D &\subseteq [c(\Delta^m, \|\cdot, \dots, \cdot\|)]^\alpha \end{aligned} \quad \text{----- (1)}$$

Again, we know that

$$[\ell_\infty(\Delta^m, \|\cdot, \dots, \cdot\|)]^\alpha \subseteq [c(\Delta^m, \|\cdot, \dots, \cdot\|)]^\alpha \subseteq [c_0(\Delta^m, \|\cdot, \dots, \cdot\|)]^\alpha \quad \text{----- (2)}$$

Conversely, suppose that $a \in [c(\Delta^m, \|\cdot, \dots, \cdot\|)]^\alpha$. Then $\sum_{k=1}^{\infty} \|a_k, z_2, \dots, z_n\|_{X^*} \|x_k, u_2, \dots, u_n\|_X < \infty$ for each $x \in c(\Delta^m, \|\cdot, \dots, \cdot\|)$. So we take

$$x_k = k^m, \quad k \geq 1$$

and choose $u_2, \dots, u_n \in X$ such that

$$\|k^m, u_2, \dots, u_n\|_X = k^m \|1, u_2, \dots, u_n\|_X = k^m, \quad k \geq 1.$$

Then

$$\sum_{k=1}^{\infty} k^m \|a_k, z_2, \dots, z_n\|_{X^*} =$$

$$\sum_{k=1}^{\infty} \|k^m, u_2, \dots, u_n\|_X \|a_k, z_2, \dots, z_n\|_{X^*} = \sum_{k=1}^{\infty} \|a_k, z_2, \dots, z_n\|_{X^*} \|x_k, u_2, \dots, u_n\|_X < \infty$$

This implies that $a \in D$. Thus,

$$\left[c(\Delta^m, \|\cdot, \dots, \cdot\|)^\alpha \right] \subseteq D \quad \text{----- (3)}$$

Combining (3) with (1) and (2), it follows:

$$\left[\ell_\infty(\Delta^m, \|\cdot, \dots, \cdot\|)^\alpha \right] = \left[c(\Delta^m, \|\cdot, \dots, \cdot\|)^\alpha \right] = D$$

ACKNOWLEDGEMENTS

This research work was supported by University Grant Commission, New Delhi-110002, India as a minor research project under F. No. 39-935/2010 (SR). The author also benefited from the referees' reports and editorial assessment comments, which contributes to a better presentation of the content of this paper.

REFERENCES

1. K. Zeller, "Theorie der Limitierungsverfahren", *Springer Verlag*, Berlin, **1958**.
2. G. Köthe and O. Toeplitz, "Linear Raume mit unendlichvielen koordinaten and Ringe unenlicher Matrizen", *J. Reine Angew. Math.*, **1934**, 171, 193-226.
3. C. G. Lascarides, "A study of certain sequence spaces of Maddox and a generalization of a theorem of Iyer", *Pacific J. Math.*, **1971**, 38, 487-500.
4. I. J. Maddox, "Continuous and Köthe-Toeplitz duals of certain sequence spaces", *Proc. Camb. Philos. Soc.*, **1969**, 65, 431-435.
5. S. Gähler, "2-Metrische Räume und ihre topologische Struktur", *Math. Nachr.*, **1963**, 26, 115-148.
6. S. Gähler, "2-Normed spaces", *Math. Nachr.*, **1964**, 28, 1-43.
7. S. Gähler, "Linear 2-normierte Räume", *Math. Nachr.*, **1965**, 28, 1-43.
8. S. Gähler, "Über der Uniformisierbarkeit 2-metrische Räume", *Math. Nachr.*, **1964**, 28, 235-244.
9. S. Gähler, "Über 2-Banach Räume", *Math. Nachr.*, **1969**, 42, 335-347.
10. S. Gähler, "Untersuchungen Über verallgemeinerte m -metrische Räume II", *Math. Nachr.*, **1969**, 40, 229-264.
11. A. G. White, "2-Banach spaces", *Math. Nachr.*, **1969**, 42, 43-60.
12. C. Diminnie, S. Gähler and A. G. White, "2-Inner product spaces", *Demonstr. Math.*, **1973**, 6, 525-536.
13. S. Gähler, A. H. Siddiqi and S. C. Gupta, "Contributions to non-archimedean functional analysis", *Math. Nachr.*, **1975**, 69, 163-171.
14. A. H. Siddiqi, "2-Normed spaces", *Aligarh Bull. Math.*, **1980**, 7, 53-70.
15. A. Misiak, " n -Inner product spaces", *Math. Nachr.*, **1989**, 140, 299-319.
16. A. Misiak, "Orthogonality and orthonormality in n -inner product spaces", *Math. Nachr.*, **1989**, 143, 249-261.
17. S. S. Kim and Y. J. Cho, "Strict convexity in linear n -normed spaces", *Demonstr. Math.*, **1996**, 29, 739-744.
18. R. Malčeski, "Strong n -convex n -normed spaces", *Mat. Bilten.*, **1997**, 21, 81-102.

19. H. Gunawan, "On n -inner product, n -norms, and the Cauchy-Schwarz inequality", *Sci. Math. Jpn.*, **2002**, 55, 53-60.
20. H. Gunawan, "The space of p -summable sequences and its natural n -norm", *Bull. Aust. Math. Soc.*, **2001**, 64, 137-147.
21. H. Gunawan and M. Mashadi, "On finite dimensional 2-normed spaces", *Soochow J. Math.*, **2001**, 27, 321-329.
22. H. Gunawan and M. Mashadi, "On n -normed spaces", *Int. J. Math. Math. Sci.*, **2001**, 27, 631-639.
23. H. Dutta, "An application of lacunary summability method to n -norm", *Int. J. Appl. Math. Stat.*, **2009**, 15, 89-97.
24. H. Dutta, "On n -normed linear space valued null, convergent and bounded sequences", *Bull. Pure Appl. Math.*, **2010**, 4, 103-109.
25. H. Dutta, "On sequence spaces with elements in a sequence of real linear n -normed spaces", *Appl. Math. Lett.*, **2010**, 23, 1109-1113.
26. H. Dutta, "On some n -normed linear space valued difference sequences", *J. Franklin Inst.*, **2011**, 348, 2876-2883.
27. H. Dutta, "Some classes of Cesàro-type difference sequences over n -normed spaces", *Adv. Diff. Equ.*, **2013**, 286, doi: 10.1186/1687-1847-2013-286.
28. M. Acikgöz, N. Aslan and S. Araci, "The generalization of appollonious identity to linear n -normed spaces", *Int. J. Comtemp. Math. Sci.*, **2010**, 5, 1187-1192.
29. H. Dutta and B. S. Reddy, "On non-standard n -norm on some sequence spaces", *Int. J. Pure Appl. Math.*, **2011**, 68, 1-11.
30. H. Kizmaz, "On certain sequence spaces", *Canad. Math. Bull.*, **1981**, 24, 169-176.
31. M. Et and R. Colak, "On generalized difference sequence spaces", *Soochow J. Math.*, **1995**, 21, 377-386.
32. H. Dutta, "Characterization of certain matrix classes involving generalized difference summability spaces", *Appl. Sci.*, **2009**, 11, 60-67.

© 2015 by Maejo University, San Sai, Chiang Mai, 50290 Thailand. Reproduction is permitted for noncommercial purposes.

Full Paper

Nutritional composition, in vitro starch digestibility and estimated glycemic index of three varieties of ‘Kluai Namwa’ banana (*Musa sapientum L.*) and its products

Nednapis Vatanasuchart^{1,*}, Pisut Butsuwan² and Wassana Narasri¹

¹Department of Nutrition and Health, Institute of Food Research and Product Development, Kasetsart University, Bangkok 10900, Thailand

²Department of Processing and Preservation, Institute of Food Research and Product Development, Kasetsart University, Bangkok 10900, Thailand

* Corresponding author, e-mail: ifrnvp@ku.ac.th

Received: 10 February 2014 / Accepted: 24 August 2015 / Published: 31 August 2015

Abstract: The effects of ripening on nutritional composition, in vitro starch digestibility and estimated glycemic index (GI) of banana pulp obtained from three varieties of Kluai Namwa banana (Mali-ong, Khao-nuan and Laong-nam) were determined. The ripening stage has no significant effect on the energy and carbohydrate of the bananas. Laong-nam has the lowest energy: 390.03±0.16 kcal/100g at the ripe stage. Rapid conversion of starch into more soluble sugars, mainly glucose and fructose, with ripening was observed for all varieties. Ripe Laong-nam has the lowest total sugars of 41.61±0.05 g/100g. A reduction in total dietary fibre, mainly insoluble fibre, was found for the ripe bananas of all varieties, while soluble fibre increases with ripening; Laong-nam gives the highest of 2.84±0.23 g/100g. The GI of the bananas obtained at different ripening stages is less than 55; Laong-nam has the lowest of 46.4. Flour and extruded snack processed from green bananas show low GI, with Laong-nam having the lowest value. A slow rate of starch digestion of banana pulp, flour and snack was observed among the varieties and was associated with their GI values. This could be related to the composition of resistant starch in the bananas.

Keywords: bananas, nutritional composition, starch digestibility, glycemic index

INTRODUCTION

Bananas (*Musa* sp.) are one of the most important tropical fruits and are consumed worldwide by people of all age groups. In Thailand bananas are called 'Kluai'; species of *sapientum* L. is commonly cultivated [1] such as Kluai Hom (AAA genome group), Kluai Khai (AA), Kluai Lebmunang (AA) and Kluai Namwa (ABB), which are economically important for both domestic consumption and export [2]. In particular, Kluai Namwa is the most commercially important for fresh consumption and utilisation in several kinds of banana products. Both green and ripe Kluai Namwa provide good texture suitable for food applications due to a high flour content of 26.0% at the green stage and complexation of non-starch polysaccharides such as pectin, cellulose and hemicelluloses when ripe [3-5]. More importantly, bananas are known as a healthy food choice and consumer demand is increasing due to their nutritional composition and antioxidant properties [6]. Several researchers have reported that green banana has a high resistant starch content, which can help improve glucose regulation in diabetes and facilitate weight control for the obese through its slow rate of digestibility [7-10].

Starch is the most common carbohydrate in the human diet. The major sources of starch intake worldwide are cereals (rice, wheat and maize) and root vegetables (potatoes and cassava), which possess properties of rapid digestion and absorption. Starch digestibility is known to vary among different starchy foods depending on the nature of the starch, its physical form, protein and lipid interaction, and the presence of anti-nutrients as well as some extrinsic factors such as enzyme inhibitor and food processing method [9-11]. The rate of starch digestion and absorption is a determinant for blood glucose response to a starchy meal. There is evidence that slowly digested and absorbed carbohydrates are favourable for the dietary management in metabolic disorders such as diabetes and hyperlipidemia [9, 12]. Studies have been carried out to assess blood glucose response after intake of carbohydrates from different plant sources [13, 14].

Glycemic index (GI) is an important measure to characterise starch digestibility [12]. The GI concept of classifying foods on the basis of their postprandial blood glucose response was introduced by Jenkins et al. [12]. GI is usually obtained by dividing the incremental postprandial blood glucose response of a test food by the corresponding glucose production after ingestion of a reference food containing an equal amount of carbohydrate. Goñi et al. [15] developed a simple in vitro hydrolysis procedure using three enzymes, namely pepsin, α -amylase and amyloglucosidase, for digesting starchy foods and the rate of starch digestibility was measured. This was used to estimate the metabolic glycemic response to a food. The estimated GI can be calculated using the equation: estimated GI = $39.71 + (0.549 \times \text{hydrolysis index (HI)})$. Several studies on starchy foods for healthy consumption, such as rice and bean sprouts, have adopted this measurement for evaluation of GI values, which could differentiate their starch digestibility [16-18].

Our previous study has shown that Kluai Namwa bananas contain the highest levels of resistant starch, 77.3-81.1 g /100g, as compared with other cultivars, i.e. Kluai Hom, Kluai Khai and Kluai Lebmunang [4]. In Thailand Kluai Namwa is commonly grown in almost every province and planting areas are larger than for other bananas. There are several varieties of Kluai Namwa that can be eaten raw and are appropriate for processing into several kinds of food products such as dried banana, roasted banana, banana chips and banana desserts [2,19]. Therefore, it is of interest to acquire more knowledge about the nutritional and functional qualities of different varieties of Kluai Namwa and their suitability for processing into food products. The objective of this research is to determine the effects of ripening (green, green-to-yellow and ripe stages) on the nutrient

composition, the rate of in vitro starch digestibility, and the GI of banana pulp and processed samples obtained from three varieties of Kluai Namwa.

MATERIALS AND METHODS

Banana Samples and Their Preparation

Green (unripe) bananas, aged 90-120 days, from three varieties of Kluai Namwa (ABB genome group) [1] were collected from banana plantations. Mali-ong variety was obtained from Pathum Thani province, Khao-nuan variety from Nakhon Nayok province and Laong-nam variety from Chonburi province. Three ripening stages, i.e. green, green-to-yellow and yellow or ripe (Figure 1), were studied. Sampling of bananas at the green stage was done on harvesting day and the remaining bananas were allowed to ripen to green-to-yellow and ripe stages before sampling again.

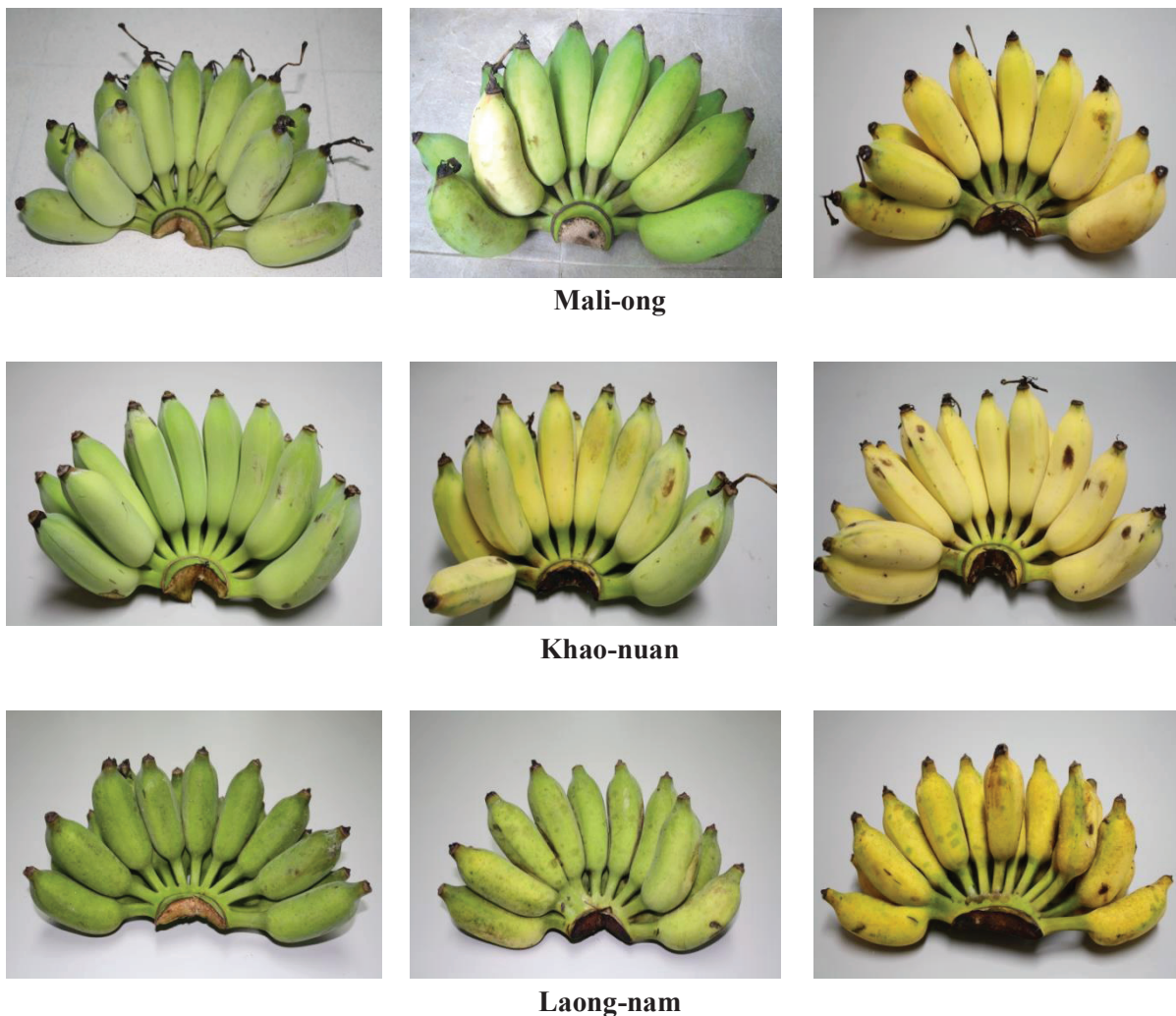


Figure 1. Three varieties of Kluai Namwa and their ripening stages

For banana pulp preparation, each variety of Kluai Namwa from each ripening stage was peeled and sliced into 1-mm-thick pieces and kept in plastic bags at -20°C until further use. For preparation of processed products (Figure 2), banana flour was prepared from green banana pulp of

each variety by drying in a hot-air oven at 50°C for 8 hr and then milling and passing through a 100-mesh sieve. Extruded banana snack was processed using a laboratory-scale cooking extruder (model ZE 25x33D co-rotating twin-screw extruder, Hermann Berstorff, Germany) with a 25-mm-diameter barrel and 3-mm-diameter die. The temperature of barrel was set at 45°, 55°, 105°, 134°, 143°, 129°, and 120° C and the screw speed was 350 rpm. Samples of banana flour with 6.6% moisture were fed at a rate of 2.07 kg/hr with a feeding moisture rate of 2.65 kg/hr. Banana starch was prepared from Mali-ong pulp at green stage according to a water/alkaline extraction process as performed in our previous study [20].



Figure 2. Kluai Namwa products

Reagents and Chemicals

Hydrolytic enzymes of pancreatic α -amylase (Sigma-Aldrich, 23 IU/mg, EC 3.2.1.1), pepsin (Merck, 2000 FIP-U/g, EC 3.4.23.1), amyloglucosidase (Boehringer, EC 3.2.1.3), and a glucose oxidase/peroxidase kit (Sigma-Aldrich) were used for in vitro starch digestibility tests and glucose determination. Other chemical agents were of analytical grade (Merck).

Nutritional Composition

Banana pulp samples from three varieties of Kluai Namwa were analysed for moisture, protein, fat and ash using AOAC standard methods [21] and carbohydrate was calculated by the difference. The energy content was determined by multiplying the protein, fat and carbohydrate contents by the factors 4, 9 and 4 respectively and then totalling [21]. Soluble sugars were collected after protein precipitation and residue filtration, and then the glucose, fructose and sucrose contents were determined by liquid chromatography [22]. An HP 1100 chromatograph (Agilent Technologies, Germany) was connected with a Prevail carbohydrate column (250 mm x 4.6 mm i.d., 5.0 μ m) and an ELSD 2000 ES detector. The mobile phase was composed of acetonitrile-water (3:1) and the flow rate was 1 mL/min. The total dietary fibre (soluble + insoluble) was determined using the enzymatic gravimetric method [23]. The banana sample was subjected to sequential enzymatic digestion by heat-stable α -amylase, protease and amyloglucosidase to remove starch and protein. Filtration of the enzyme digestate and residue washings were done before calculation of the soluble and insoluble dietary fibre values.

In Vitro Starch Digestibility Test

In vitro starch digestibility was determined following the method of Goñi et al. [15] with slight modification. Blended banana pulp or ground sample of banana flour, starch or snack (50 mg)

was mixed with 10 mL of HCl-KCl buffer (pH 1.5) in a tube. Then 0.2 mL of a solution containing pepsin (20 mg) was added and the tube was incubated for 60 min. in a shaking water bath at 40°C. The volume of the mixture was made up to 25 mL by adding Tris–maleate buffer. Five mL of a Tris–maleate solution containing α -amylase (3.3 IU) was then added and the mixture incubated at 37°C to hydrolyse digestible starch. An aliquot sample (1 mL) was taken every 30 min. between 0–180 min. and placed in a tube at 100°C to inactivate the enzyme. Then amyloglucosidase (60 μ L) was added to each aliquot sample to hydrolyse the digested starch into glucose at 60°C for 45 min. After centrifugation (15 min. at 4500 g), the glucose content in the supernatant was measured using a glucose oxidase/peroxidase kit, and the digestible starch was calculated as mg of glucose \times 0.9. The rate of starch digestibility was expressed in terms of total glucose released per 100 g of the sample hydrolysed at different times (0, 30, 60, 120, 160 and 180 min.) [24-26]. Reference glucose was determined in the same manner as the banana sample. All determinations were done in duplicate.

Determination of Estimated GI

The kinetics of starch digestion and estimated GI of the banana samples were calculated according to a non-linear model [15, 24-26]. A first-order equation [$C = C_{\infty} (1 - e^{-kt})$] was applied to describe the kinetics of starch hydrolysis, where C is the percentage of the starch hydrolysed at different times (0–180 min.), C_{∞} is the equilibrium percentage of the starch hydrolysed after 180 min., k is the kinetic constant and t is the time (min.) [16-17]. A digestibility curve from the obtained C value against hydrolysis time was plotted and the area under the curve of each banana sample as well as the reference glucose was calculated. The HI was obtained by dividing the area under the curve of each sample by the corresponding area of the reference glucose. The estimated GI was calculated using the equation [$GI = 39.71 + (0.549 \times HI)$] [15, 17, 26].

Statistical Analysis

The SPSS for Windows program, version 10 (SPSS Inc., USA) was used to analyse the results obtained from duplicate determinations. The mean \pm standard deviation for each treatment was calculated, and analysis of variance and Duncan's multiple range test were used to compare differences in the mean values at $P < 0.05$.

RESULTS AND DISCUSSION

Nutritional Composition

The nutritional composition of fresh Kluai Namwa banana pulp (Mali-ong, Khao-nuan and Laong-nam varieties) is shown in Tables 1-3 and the effects of the ripening stage are observed. The results for Mali-ong variety (Table 1) show that the ripening stage does not effect the energy value, whereas there is a significant decrease in the protein, fat and ash contents during ripening. On the other hand, total sugars, glucose and fructose significantly increase with ripening, as well as the carbohydrate content. The sugars present are glucose and fructose, with no sucrose detected. The total dietary fibre finally decreases when fully ripe. Conversely, the soluble fibre significantly increases with ripening, while for the insoluble fibre the opposite result occurs.

The nutritional composition of Khao-nuan variety is shown in Table 2. No significant change in the energy content with ripening is observed. A significant decrease is only found for the

protein content upon ripening. As in the case of Mali-ong variety, there is a significant increase in total sugars, glucose and fructose during ripening. The trend of change in fibre content is similar to that for Mali-ong variety.

Table 1. Energy, nutritional composition and moisture content of Kluai Namwa (Mali-ong variety)

	Ripening stage		
	Green	Green-to-yellow	Yellow
Energy, kcal	392.61 ± 0.75	392.92 ± 0.01	393.19 ± 0.34
Protein	1.14 ± 0.01 ^a	0.98 ± 0.02 ^b	0.50 ± 0.00 ^c
Fat	0.98 ± 0.30 ^a	0.85 ± 0.03 ^b	0.79 ± 0.01 ^b
Ash	3.07 ± 0.15 ^a	2.83 ± 0.01 ^{ab}	2.70 ± 0.12 ^b
Carbohydrate	94.81 ± 0.12 ^a	95.34 ± 0.06 ^b	96.01 ± 0.14 ^c
Total Sugar	3.49 ± 0.02 ^a	16.32 ± 0.22 ^b	55.63 ± 2.76 ^c
Glucose	1.65 ± 0.02 ^a	7.44 ± 0.17 ^b	26.56 ± 1.13 ^c
Fructose	1.85 ± 0.00 ^a	8.88 ± 0.05 ^b	29.07 ± 1.64 ^c
Sucrose,	0.00	0.00	0.00
Total dietary fibre	10.39 ± 0.01 ^a	11.23 ± 0.21 ^a	7.98 ± 0.63 ^b
Soluble fibre	1.33 ± 0.04 ^a	1.92 ± 0.22 ^b	2.13 ± 0.20 ^b
Insoluble fibre	5.12 ± 0.53 ^a	4.81 ± 0.12 ^a	3.63 ± 0.32 ^b
Moisture, %	67.22 ± 0.45	67.47 ± 0.37	67.90 ± 0.06

Note: Nutritional content is in % of dry weight. Values are means of duplicate analysis. Mean values in a row not sharing a common superscript are significantly different at $P < 0.05$ by analysis of variance and Duncan's multiple range test.

Table 2. Energy, nutritional composition and moisture content of Kluai Namwa (Khao-nuan variety)

	Ripening stage		
	Green	Green-to-yellow	Yellow
Energy, kcal	392.83 ± 0.34	392.98 ± 0.18	393.00 ± 0.54
Protein	5.56 ± 0.17 ^a	4.76 ± 0.14 ^b	4.73 ± 0.10 ^b
Fat	0.42 ± 0.02	0.41 ± 0.04	0.35 ± 0.06
Ash	2.32 ± 0.06	2.26 ± 0.01	2.19 ± 0.06
Carbohydrate	91.71 ± 0.21 ^a	92.58 ± 0.09 ^b	92.73 ± 0.11 ^b
Total Sugar	3.37 ± 0.03 ^a	25.79 ± 1.19 ^b	52.98 ± 0.22 ^c
Glucose	1.98 ± 0.01 ^a	16.37 ± 0.65 ^b	34.87 ± 0.26 ^c
Fructose	1.27 ± 0.00 ^a	9.28 ± 0.54 ^b	17.95 ± 0.04 ^c
Sucrose	0.12 ± 0.02	0.15 ± 0.00	0.15 ± 0.00
Total dietary fibre	10.39 ± 0.19 ^a	6.96 ± 0.44 ^c	9.21 ± 0.12 ^b
Soluble fibre	0.76 ± 0.23 ^a	1.37 ± 0.01 ^a	2.25 ± 0.38 ^b
Insoluble fibre	9.62 ± 0.04 ^a	5.60 ± 0.43 ^c	6.95 ± 0.26 ^b
Moisture, %	63.10 ± 0.09 ^a	65.51 ± 0.14 ^b	67.05 ± 0.20 ^c

Note: Nutritional content is in % of dry weight. Values are means of duplicate analysis. Mean values in a row not sharing a common superscript are significantly different at $P < 0.05$ by analysis of variance and Duncan's multiple range test.

Table 3. Energy, nutritional composition and moisture content of Kluai Namwa (Laong-nam variety).

	Ripening stage		
	Green	Green-to-yellow	Yellow
Energy, kcal	389.98 ± 0.47	389.29 ± 0.10	390.03 ± 0.16
Protein	1.85 ± 0.13	1.65 ± 0.07	1.91 ± 0.15
Fat	0.00	0.00	0.00
Ash	2.50 ± 0.12	2.68 ± 0.03	2.49 ± 0.04
Carbohydrate	95.65 ± 0.01	95.67 ± 0.09	95.60 ± 0.19
Total Sugar	1.37 ± 0.00 ^a	20.68 ± 1.08 ^b	41.61 ± 0.05 ^c
Glucose	0.36 ± 0.00 ^a	10.79 ± 0.55 ^b	22.20 ± 0.01 ^c
Fructose	1.01 ± 0.00 ^a	9.89 ± 0.53 ^b	19.41 ± 0.06 ^c
Sucrose	0.00	0.00	0.00
Total dietary fibre	12.70 ± 0.04 ^a	11.47 ± 0.27 ^b	8.40 ± 0.24 ^c
Soluble fibre	2.52 ± 0.11	2.36 ± 0.21	2.84 ± 0.23
Insoluble fibre	6.19 ± 0.13 ^a	2.30 ± 0.05 ^b	1.88 ± 0.11 ^c
Moisture, %	66.46 ± 0.11 ^a	66.95 ± 0.04 ^b	68.32 ± 0.05 ^c

Note: Nutritional content is in % of dry weight. Values are means of duplicate analysis. Mean values in a row not sharing a common superscript are significantly different at $P < 0.05$ by analysis of variance and Duncan's multiple range test.

The trend in energy values for the Laong-nam variety (Table 3) is similar to those for the other varieties, while the ripening stage does not affect the protein, fat, ash and carbohydrate contents. As in other varieties, significant increase in total sugars, glucose and fructose with ripening is observed. The changes in total, soluble and insoluble dietary fibre contents of Laong-nam are also similar to those for the other varieties.

A change in carbohydrates during ripening primarily involves available carbohydrates such as starch being converted into more soluble sugars such as glucose, fructose and sucrose, as well as water at the ripe stage [8]. A study on the occurrence and transformation of banana starch indicates that the disappearance of the starch reserve during banana ripening appears to be relatively rapid because several enzymes (e.g. α - and β - amylases, α -1,4- and α -1,6-glucosidase, invertase, sucrose synthase and sucrose phosphate synthase) as well as the gibberellin hormones act together via more than one pathway [8]. Likewise, the increased moisture and total sugars with ripening are found in this present study.

Of the three varieties of Kluai Namwa at the ripe stage, Laong-nam has the lowest content of total sugar (41.61 ± 0.05 g/100g) and Mali-ong the highest (55.63 ± 2.76 g/100g). Mali-ong and Laong-nam contain glucose and fructose no sucrose. However, Cordenunsi et al. [27] reported that Nanicao (AAA) and Mysore (AAB) cultivars have a predominance of sucrose over glucose and fructose. This could be due to the activity of sucrose synthase and sucrose phosphate synthase which are involved in starch synthesis and breakdown during development and ripening of the banana fruit [28], which in turn might stem from the difference in genotype from Kluai Namwa variety (ABB genome), as well as in the planting location and environmental effects.

Some studies have shown that people on diets high in dietary fibre have reduced risks of certain diseases such as cancer, coronary heart disease, obesity and possibly diabetes [29-30]. Dietary fibre consists of non-available carbohydrates or non-starch polysaccharides resistant to

digestion by human gastrointestinal enzymes. Soluble fibre can also reduce blood cholesterol levels, thus helping to reduce the risk of heart disease [29]. Pectin is the most common soluble fraction in ripe bananas [5]. Ripe Kluai Namwa contains a higher level of soluble fibre compared with green ones. The total dietary fibre content found in this study confirms that the three banana varieties are a good source of dietary fibre, in accordance with the findings of Cordenunsi et al. [27].

In Vitro Starch Digestibility and Estimated GI

The results of in vitro starch digestibility from the starch hydrolysis model of the three varieties of fresh Kluai Namwa were shown in Table 4. Mali-ong at the ripe stage has significantly lowest GI when compared with the other stages while Khao-nuan and Laong-nam show an opposite result. This seems to indicate that the ripening stage has no effect on GI values of the bananas, although when the three varieties are compared, Laong-nam exhibits the lowest value of 46.4 ± 0.1 . Figure 3 shows starch hydrolysis curves of the pulp samples at different ripening stages as compared with the reference glucose. The curves exhibit similar kinetics of starch hydrolysis among the different varieties and ripening stages, although the curve of Laong-nam variety at the green stage appears to show the slowest starch digestion. These findings confirm that bananas have a high level of resistant starch, which accounts for a slow rate of starch digestibility.

Table 4. Equilibrium concentration (C_{∞}), kinetic constant (k), hydrolysis index (HI) and estimated glycemic index (GI) of pulp samples from three varieties of Kluai Namwa at different ripening stages

Sample	C_{∞}	k	HI	Estimated GI
Mali-ong				
Green	19.5 ± 0.1^{bc}	0.043	21.1 ± 0.3^b	51.3 ± 0.2^b
Green-to-yellow	19.7 ± 0.1^{bc}	0.041	21.2 ± 0.2^b	51.3 ± 0.1^b
Ripe	14.9 ± 0.2^d	0.037	15.8 ± 0.2^e	48.4 ± 0.1^e
Khao-nuan				
Green	18.8 ± 0.2^{bc}	0.041	20.2 ± 0.1^c	50.8 ± 0.0^c
Green-to-yellow	18.1 ± 0.4^c	0.039	19.3 ± 0.2^d	50.3 ± 0.1^d
Ripe	20.2 ± 0.5^b	0.039	21.6 ± 0.8^b	51.6 ± 0.4^b
Laong-nam				
Green	11.6 ± 0.3^e	0.035	12.2 ± 0.2^g	46.4 ± 0.1^g
Green-to-yellow	15.7 ± 0.4^d	0.027	15.7 ± 0.2^e	48.3 ± 0.1^e
Ripe	12.6 ± 1.0^e	0.038	13.4 ± 0.4^f	47.1 ± 0.2^f
Reference glucose	98.2 ± 2.4^a	0.031	100 ± 0.0^a	94.6 ± 0.0^a

Note: Values are means of duplicate analysis. Mean values in a column not sharing a common superscript are significantly different at $P < 0.05$ by analysis of variance and Duncan's multiple range test.

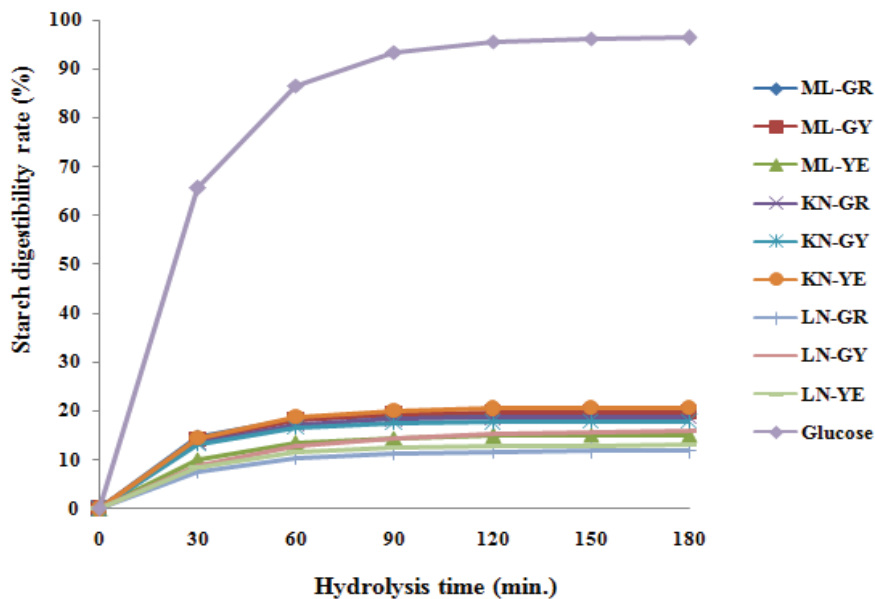


Figure 3. Rate of in vitro starch digestibility (%) of pulp samples from three varieties of Kluai Namwa (ML: Mali-ong; KN: Khao-nuan; LN: Laong-nam) at different ripening stages (GR: green; GY: green-to-yellow; YE: yellow) compared with reference glucose

For in vivo measurement, GI is usually determined by giving the subjects a test sample and reference glucose containing 25 g or 50 g of available carbohydrate and then collecting their blood samples over 2 hr. The collected blood samples are analysed for blood glucose concentrations and the incremental area under the glucose response curve is calculated for each test and the reference. The GI range is classified as low (GI = 55 or less), medium (GI = 56–69) and high (GI = 70 or more) [31]. Presently, measuring the rate at which carbohydrates in foods are digested in vitro has been increasingly used for estimating the glycemic response and is suggested as a cheaper and less time-consuming method for predicting the GI values of foods [16-18, 32]. An international table of GI and glycemic load values for 11 banana samples from different sources and at different ripening stages shows that their GI values range between 42-70, with most of the values being less than 55; hence they can be defined as a low-GI food [32]. Similarly, in the present study, the GI values found for the three varieties of fresh Kluai Namwa at any stage of ripening are less than 55. It should be noted, however, that several nutritionists consider bananas to be a medium-GI food.

Table 5 shows the results of in vitro starch digestibility analysis and GI values of flour, starch and extruded snack processed from green bananas. Clearly, the GI values of the flour are much lower than that of the starch, which exhibits the highest GI value of 70.7. The GI values of the extruded snack are similar to those of the flour used as the main ingredient for snack production. The high GI value of banana starch is reflected by its rapid rate of digestion, whereas the flour and snack samples with lower GI both show a slower digestion rate (Figure 4). This can be explained by the complexation between starch and dietary fibres or non-starch polysaccharides such as pectin, cellulose and hemicelluloses, which can help resist digestion better than starch alone [5, 20, 33].

Table 5. Equilibrium concentration (C_{∞}), kinetic constant (k), hydrolysis index (HI) and estimated glycemic index (GI) of processed samples from three varieties of Kluai Namwa

Sample	C_{∞}	k	HI	Estimated GI
Banana flour				
Mali-ong	23.9 ± 0.4^c	0.026	23.7 ± 0.3^d	52.7 ± 0.2^d
Khao-nuan	26.8 ± 0.6^b	0.048	29.3 ± 0.1^b	55.8 ± 0.1^b
Laong-nam	19.5 ± 0.2^f	0.043	21.1 ± 0.3^c	51.3 ± 0.2^e
Extruded snack				
Mali-ong	19.5 ± 0.2^f	0.041	20.8 ± 0.6^e	51.1 ± 0.4^e
Khao-nuan	22.4 ± 0.0^d	0.048	26.0 ± 2.0^c	54.0 ± 1.1^c
Laong-nam	20.2 ± 0.2^e	0.043	21.8 ± 0.3^{de}	51.7 ± 0.2^{de}
Banana starch				
Mali-ong	51.7 ± 0.0^a	0.046	56.5 ± 0.3^a	70.7 ± 0.2^a

Note: Values are means of duplicate analysis. Mean values in a column not sharing a common superscript are significantly different at $P < 0.05$ by analysis of variance and Duncan's multiple range test.

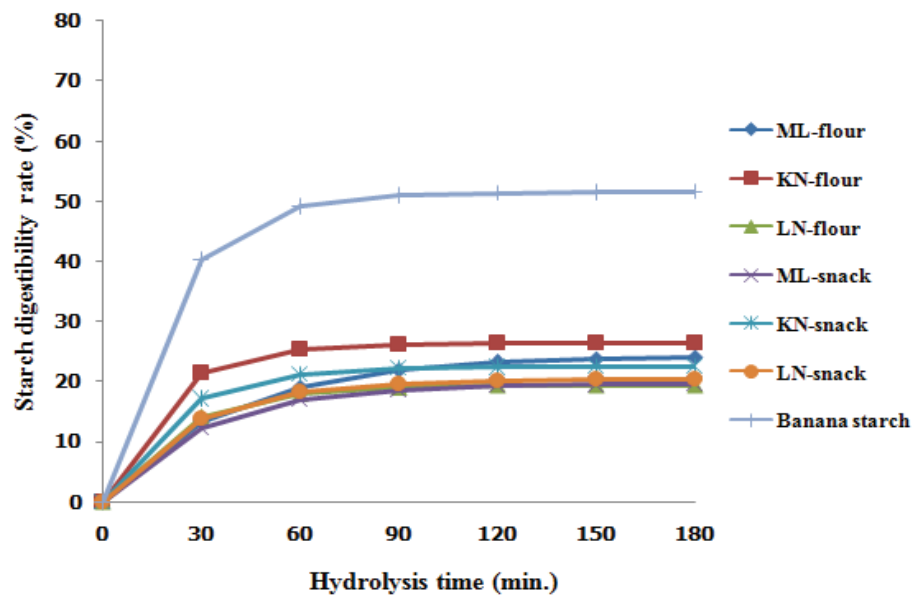


Figure 4. Rate of in vitro starch digestibility (%) of processed samples from three varieties of Kluai Namwa (ML: Mali-ong; KN: Khao-nuan; LN: Laong-nam)

Foster-Powell et al. [32] indicated that the variation in GI may be due to differences in variety, stage of ripeness, cooking and processing methods, and length of storage. Rice and potatoes are notable examples, ranging from moderate to very high GI even within the same variety. The present study, however, shows similarly low GI values for Kluai Namwa from three different varieties and maturation periods. Similar results were also obtained when the bananas were processed into flour and snack product.

CONCLUSIONS

Starch in Kluai Namwa banana is degraded during ripening almost entirely into soluble sugars, viz. glucose and fructose. The total dietary fibre decreases with ripening while soluble fibre content increases. The Laong-nam variety has the lowest energy (390.03 ± 0.16 kcal/100g), the lowest total sugar (41.61 ± 0.05 g/100g) and the highest soluble fibre (2.84 ± 0.23 g/100g) when ripe. The GI values of pulp samples from Kluai Namwa of all varieties are less than 55, the green Laong-nam variety exhibiting the lowest GI (46.4 ± 0.1). All fresh bananas, as well as the flour and extruded snack processed from green bananas, exhibit similar kinetics of slow starch digestion, with Laong-nam at the green stage showing the slowest rate of digestion.

ACKNOWLEDGEMENTS

The authors thank the National Research Council of Thailand for research funding and Kasetsart University for constant support.

REFERENCES

1. N. Chomchaloa, "Words for Banana", Thailand Network for the Conservation and Enhancement of Landraces of Cultivated Plants, Bangkok, **2008**, pp.92-99 (In Thai).
2. S. Achavachajchuan and C. Maksumpun, "Thai Bananas", Platapean Publishing, Bangkok, **2007**, pp.6-24 (in Thai).
3. Editorial Board for Matichon Technology-ChaoBan, "Kluai Namwa for Thai Economic and Income Earning", **2013**, <http://www.matichonbook.com/index.php/occupation/978-974-02-1214-0.html> (Accessed: January 2014) (In Thai).
4. N. Vatanasuchart, B. Niyomwit and W. Narasri, "Resistant starch, physicochemical and structural properties of bananas from different cultivars with an effect of ripening and processing", *Kasetsart J. Nat. Sci.*, **2012**, 46, 461-472.
5. X. Duan, G. Cheng, E. Yang, C. Yi, N. Ruenroengklin, W. Lu, Y. Luo and Y. Jiang, "Modification of pectin polysaccharides during ripening of postharvest banana fruit", *Food Chem.*, **2008**, 111, 144-149.
6. G. Aurore, B. Parfait and L. Fährasmane, "Bananas, raw materials for making processed food products", *Trends Food Sci. Technol.*, **2009**, 20, 78-91.
7. N. Faisant, A. Buléon, P. Colonna, C. Molis, S. Lartigue, J. P. Galmiche and M. Champ, "Digestion of raw banana starch in the small intestine of healthy humans: Structural features of resistant starch", *Br. J. Nutr.*, **1995**, 73, 111-123.
8. P. Zhang, R. L. Whistler, J. N. BeMiller and B. R. Hamaker, "Banana starch: Production, physicochemical properties, and digestibility—A review", *Carbohydr. Polym.*, **2005**, 59, 443-458.
9. U. Lehmann and F. Robin, "Slowly digestible starch – its structure and health implications: A review", *Trends Food Sci. Technol.*, **2007**, 18, 346-355.
10. P. Zhang and B. R. Hamaker, "Banana starch structure and digestibility", *Carbohydr. Polym.*, **2012**, 87, 1552-1558.
11. R. L. Whistler and J. R. Daniel, "Molecular structure of starch", in "Starch: Chemistry and Technology", 2nd Edn. (Ed. R. L. Whistler, J. N. BeMiller and E. F. Paschall), Academic Press, Orlando (FL), **1984**, pp.153-182.

12. D. J. Jenkins, C. W. Kendall, L. S. Augustin, S. Franceschi, M. Hamidi, A. Marchie, A. L. Jenkins and M. Axelsen, "Glycemic index: Overview of implications in health and disease", *Am. J. Clin. Nutr.*, **2002**, 76, 266S-273S.
13. H. N. Englyst, J. Veenstra and G. J. Hudson, "Measurement of rapidly available glucose (RAG) in plant foods: A potential in vitro predictor of the glycaemic response", *Br. J. Nutr.*, **1996**, 75, 327-337.
14. K. N. Englyst, H. N. Englyst, G. J. Hudson, T. J. Cole and J. H. Cummings, "Rapidly available glucose in foods: An in vitro measurement that reflects the glycemic response", *Am. J. Clin. Nutr.*, **1999**, 69, 448-454.
15. I. Goñi, A. Garcia-Alonso and F. Saura-Calixto, "A starch hydrolysis procedure to estimate glycemic index", *Nutr. Res.*, **1997**, 17, 427-437.
16. M. Frei, P. Siddhuraju and K. Becker, "Studies on the in vitro starch digestibility and the glycemic index of six different indigenous rice cultivars from the Philippines", *Food Chem.*, **2003**, 83, 395-402.
17. P. Hu, H. Zhao, Z. Duan, Z. Linlin and D. Wu, "Starch digestibility and the estimated glycemic score of different types of rice differing in amylose contents", *J. Cereal Sci.*, **2004**, 40, 231-237.
18. M. Swieca, B. Baraniak and U. Gawlik-Dziki, "In vitro digestibility and starch content, predicted glycemic index and potential in vitro antidiabetic effect of lentil sprouts obtained by different germination techniques", *Food Chem.*, **2013**, 138, 1414-1420.
19. Anonymous, "Banana: Thai fruit that should be rapidly developed for industrial products", **2009**, <http://positioningmag.com/prnews/prnews.aspx?id=82319> (Accessed: January 2014).
20. N. Vatanasuchart, B. Niyomwit and K. Wongkrajang, "Resistant starch content, in vitro starch digestibility and physico-chemical properties of flour and starch from Thai bananas", *Maejo Int. J. Sci. Technol.*, **2012**, 6, 259-271.
21. W. Horwitz (Ed.), "Official Methods of Analysis of AOAC International", 17th Edn., AOAC International, Gaithersburg (MD), **2000**, Methods 925.45, 938.08, 989.05 and 992.23.
22. W. Horwitz (Ed.), "Official Methods of Analysis of AOAC International", 18th Edn., AOAC International, Gaithersburg (MD), **2006**, Ch.33.
23. G. W. Latimer (Ed.), "Official Methods of Analysis of AOAC International", 19th Edn., AOAC International, Gaithersburg (MD), **2012**, Ch.45.
24. Y. Granfeldt, I. Björck, A. Drews and J. Tovar, "An in vitro procedure based on chewing to predict metabolic response to starch in cereal and legume products", *Eur. J. Clin. Nutr.*, **1992**, 46, 649-660.
25. K. S. Sandhu and S. T. Lim, "Digestibility of legume starches as influenced by their physical and structural properties", *Carbohydr. Polym.*, **2008**, 71, 245-252.
26. K. Srikaeo and J. Sangkhiaw, "Effects of amylose and resistant starch on glycaemic index of rice noodles", *LWT - Food Sci. Technol.*, **2014**, 59, 1129-1135.
27. B. R. Cordenunsi, T. M. Shiga and F. Lajolo, "Non-starch polysaccharide composition of two cultivars of banana (*Musa acuminata* L.: cvs. Mysore and Nanicão)", *Carbohydr. Polym.*, **2008**, 71, 26-31.
28. J. R. O. do Nascimento, B. R. Cordenunsi and F. Lajolo, "Sucrose synthase activity and expression during development and ripening in bananas", *J. Plant Physiol.*, **2000**, 156, 605-611.

29. J. L. Buttriss and C. S. Stokes, “Dietary fibre and health: An overview”, *Nutr. Bull.*, **2008**, 33, 186-200.
30. L. M. Ohr, “Fortifying with fiber”, *Food Technol. Aust.*, **2004**, 58, 71-75.
31. J. C. Brand-Miller, K. Stockmann, F. Atkinson, P. Petocz and G. Denyer, “Glycemic index, postprandial glycemia, and the shape of the curve in healthy subjects: Analysis of a database of more than 1,000 foods”, *Am. J. Clin. Nutr.*, **2009**, 89, 97-105.
32. K. Foster-Powell, S. H. Holt and J. C. Brand-Miller, “International table of glycemic index and glycemic load values: 2002”, *Am. J. Clin. Nutr.*, **2002**, 76, 5-56.
33. R. V. da Mota, F. M. Lajolo, B. R. Cordenunsi and C. Ciacco “Composition and functional properties of banana flour from different varieties”, *Starch/Stärke*, **2000**, 52, 63-68.

© 2015 by Maejo University, San Sai, Chiang Mai, 50290 Thailand. Reproduction is permitted for noncommercial purposes.

Full Paper

Genetic mapping of leaf blast resistance gene in landrace rice cultivar ‘GS19769’

Nonglak Parinthawong^{1,*}, Pennapar Tansian^{1,2} and Tanee Sreewongchai³

¹ Faculty of Agricultural Technology, King Mongkut’s Institute of Technology Ladkrabang, Bangkok10520, Thailand

² Centre of Excellence on Agricultural Biotechnology, Bangkok 10900, Thailand

³ Department of Agronomy, Faculty of Agriculture, Kasetsart University, Bangkok 10900, Thailand

* Corresponding author, e-mail: kpnongla@kmitl.ac.th; tel.: +66 2 3298513; fax: +66 2 3298513

Received: 19 March 2014 / Accepted: 23 July 2015 / Published: 31 August 2015

ABSTRACT: The rice blast fungus, *Magnaporthe oryzae*, is highly varied and therefore overcomes resistance in a few years. Rice cultivars with the ability to resist different blast races are therefore required. In this study, a resistance gene of landrace rice cultivar ‘GS19769’ is identified using a mix of 19 blast isolates collected from several epidemic areas in Thailand. The selected cultivar was fertilised with the blast susceptible variety, Khao Dok Mali 105 (KDML105), to generate the mapping population. Segregation analysis in the F₂ population shows that ‘GS19769’ contains more than 1 resistance gene, as the Chi-square test for segregation of resistance and susceptibility does not fit the ratio of 3:1. The bulk segregant analysis by simple sequence repeat (SSR) markers shows that the identified resistance gene is linked to the SSR markers RM224 and RM144 on chromosome 11. Analysis of 15 F₂ plants susceptible to the blast was conducted. The gene was mapped to RM224 and RM144 at the same distance of 20 cM.

Key words: genetic mapping, rice blast, landrace rice, *Magnaporthe oryzae*, SSR markers

INTRODUCTION

Rice blast is one of the most devastating diseases for rice-growing countries worldwide. The causal fungal pathogen, *Magnaporthe oryzae*, has the ability to infect several parts of the plant at all 3 growth stages, i.e. seedling, tillering and panicle stages. The fungus can survive over seasons on many gramineous hosts other than rice. Moreover, the diversity of the fungus occurs as it easily adapts to different environmental conditions across seasons [1]. In Thailand, a high diversity has

been confirmed by the determination of 623 pathotypes collected during 2002-2005 on 18 near isogenic lines [2]. The disease dispersal in 1992 damaged over 650,000 tons or 60% of the total yield of rice in Thailand [3].

Developing blast-resistant rice cultivars is an effective approach to controlling the blast disease. The blast resistance in rice is controlled by a resistance (R) gene corresponding to an avirulence gene in blast fungal isolates and its reaction follows the gene-for-gene hypothesis [4]. Many blast-resistant cultivars have been generated by molecular-assisted breeding programmes, where an identified resistance gene was introduced to the cultivars. However, the new cultivars developed often lost their resistance after a few years. Blast isolates could break resistant cultivars, especially when a single resistance gene is present. The goal of the rice breeder is to develop a rice cultivar with a broad-spectrum-resistance phenotype against the infection of several blast isolates [5]. This type of resistant cultivar consists of a resistance (R) gene obtained from disease-resistant varieties. A number of broad-spectrum R genes have been identified from resistance genes in non-cultivated varieties. As summarised by Yang et al. [6], over 80 resistance genes have been identified and are distributed on 11 rice chromosomes, with the exception of chromosome 3. Among these, *Pi2*, *Pi9*, *Piz-t*, *Pigm* and *Pi50(t)* from the *Pi2/9* locus on chromosome 6 confer broad-spectrum resistance to blast isolates [5, 7-11].

Generally, R genes are identified in landraces, cultivars or wild rice collections [12]. Recent work on the identification of blast-resistant varieties from landrace rice using 29 blast isolates revealed that 4 out of 263 landrace rice varieties showed broad-spectrum resistance with no symptoms of disease after inoculation with a mix of blast isolates collected from disease outbreak areas in Thailand [13]. The objectives of this study are to locate the resistance gene and identify simple sequence repeats (SSR) markers closely linked to a broad-spectrum blast resistance gene of a landrace rice cultivar 'GS19769'. The marker obtained, linked to the resistant phenotype, would be useful for the marker-assisted selection of a blast-resistance trait in a rice breeding programme.

MATERIALS AND METHODS

Rice Variety

The landrace rice cultivar 'GS19769' used in this study was derived from screening of the landrace rice cultivars for a blast-resistant phenotype using 29 blast isolates collected from the disease epidemic areas in Thailand, as described in Salih et al. [13]. The F₁ obtained from the crossing between GS19769 and Khao Dok Mali 105 (KDML105, obtained from Rice Department, Ministry of Agriculture and Cooperatives, Thailand), a well-known aromatic rice variety which is susceptible to leaf and neck blast diseases, were grown for F₂ seed production. The resistant Jao Hom Nin (JHN) and susceptible KDML105 were used as standard check varieties in all experiments.

Pathogen Isolates

The 19 blast isolates were collected from disease epidemic areas across the rice planting region of Thailand (Table 1). The fungi (a single spore each) isolated from leaf or neck with blast symptoms were cultured on rice-flour agar medium (20 g/L rice flour, 20 g/L agar, 2 g/L yeast extract and 40 mg/L streptomycin) at 25°C and stored as dried mycelium on filter paper at -20°C, as described by Sirithunya et al. [14]. These were used for further experiments.

Table 1. Nineteen isolates of *M. oryzae* used in this phenotypic analysis and their collection locations

Area	Province	Number of fungal isolates
North	Chiang Rai, Phitsanulok	5
North-east	Chaiyaphum, Khon Kaen, Nong Khai, Ubon Ratchathani, Surin	8
Middle	Bangkok, Chachoengsao, Ratchaburi	5
South	Phatthalung	1

Inoculation and Disease Assessment

F₂ seeds obtained from F₁ plants were sown individually in plastic trays (33 x 11 x 11 cm) half-filled with soil and fertilised with ammonium sulphate (5 g). JHN and KDML105 were planted at both sides of the end rows as resistant and susceptible check varieties respectively. Ammonium sulphate (1 g) was added to each tray 3 days prior to inoculation. Inoculation of the blast isolates was performed following the method described by Sreewongchai et al. [15]. All 29 isolates were grown on rice-flour agar medium and incubated at 25°C. Sporulation was induced by scraping 8- to 10-day-old mycelium from each plate and allowing growth for another 2 days. Spores were harvested and the concentration of spores was adjusted to 10⁵ spores/mL in 0.5% gelatine. Inocula were sprayed onto 14-day-old seedlings using an air-brush pressure pump. The inoculated seedlings were placed in a high-humidity chamber for 18 hr at 25°C and were then transferred to a greenhouse. The degree of infection of each seedling was evaluated 7 days after inoculation by a standard reference scale for rice blast, scoring 0 (resistant) to 6 (susceptible) [16].

DNA Preparation, Amplification and Bulk Segregant Analysis

Genomic DNA of ten F₂ plants from each resistant group, susceptible group and two parental lines was extracted from leaves of seedlings by the cetyltrimethylammonium bromide method described by Doyle and Doyle [17]. The DNA quality was compared with known concentrations of DNA by electrophoresis on 0.8% agarose gel and staining with ethidium bromide.

The parents were used to screen the 270 SSR markers with known position and wide distribution on 12 rice chromosomes for polymorphism and possible association with blast resistance. These markers are reported online [18]. The polymerase chain reaction (PCR) mixture (10 µL) contained 5.9 µL of sterile distilled water, 1 µL of 10xPCR buffer, 1 µL of MgCl₂ (25 mM), 0.5 µL of dNTPs solution mix (2.5 mM), 0.1 µL of *Taq* DNA polymerase (5 units/µL) (Fermentas, USA), 0.5 µL of SSR primer pair (0.25 µM each) and 1 µL of rice genomic DNA (10 ng). The PCR was conducted in a thermal cycler as follows: initial denaturation step at 95°C for 10 min., followed by 40 cycles of 95°C for 20 sec., 57°C for 15 sec., 72°C for 30 sec., and a final extension at 72°C for 5 min. PCR products were observed by 6% polyacrylamide gel electrophoresis and made visible by silver staining [19].

The bulk segregant analysis (BSA) was arranged into 2 bulk sets according to the two F₁ plants obtained. The analysis resulted in a number of SSR markers that sufficiently distinguished the genotype of the two bulks. Two resistant bulk sets (B1) were comprised of 8 resistant F₂ plants from F₁ plant no. 1 (B1-1) and 7 resistant F₂ plants from F₁ plant no. 2 (B1-2), while 2 susceptible

bulk sets (B2) were comprised of 8 susceptible F₂ plants from F₁ plant no. 1 (B2-1) and 7 susceptible F₂ plants from F₁ plant no. 2 (B2-2). The DNA from each plant was extracted and the DNA pool was prepared for each bulk by mixing DNA of the respective F₂ DNA samples in equal quantity. The bulks were used to analyse the SSR markers obtained from parental screening (Table 4). The PCR profile was conducted and the PCR products were analysed as mentioned above.

The SSR markers found to be polymorphic among the bulks were used for the co-segregation study of F₂ progenies. Leaves of each F₂ plant and its parents were excised to give pieces 0.5 mm in diameter and 5 pieces were added into the PCR plate containing 10 µL of KAPA plant PCR mix (KAPA Biosystems, USA) for genetic analysis. The PCR products were analysed by electrophoresis as described previously.

Data Analysis

The clearly detected amplicons of SSR were scored manually as A for the susceptible parent allele, B for the resistant parent allele and H for alleles from both parents. The data sheet was generated and scored. A Chi-square (X^2) test for goodness of fit of the F₂ population for the phenotype and marker data was performed by CropStat 7.2 computer software [20]. The SSR markers surrounding the resistance gene on the specific region of the chromosome were identified. The phenotype and SSR data were combined for linkage analysis by using MAPMAKER/EXP3.0 program [21]. In addition, the frequency of recombination was calculated using the genotype of markers and the resistant phenotype of F₂ plants that showed susceptible phenotype to fungal infection.

RESULTS AND DISCUSSION

Phenotype Distributions and Correlation

A population of 250 F₂ seedlings plus two check varieties were inoculated with a mix of 19 blast isolates. The blast fungi were isolated from naturally infected rice leaf and leaf sheath from different regions of a paddy field in Thailand. They were found to be highly genetically diverse when analysed using *M. grisea* microsatellite markers, as described in Tansian et al. [22]. The score of each seedling was evaluated after inoculation and used for further analysis. Among the 250 seedlings tested, 235 were characterised as resistant while only 15 were found to be susceptible to fungal isolates (Table 2). Chi-square tests of the data obtained from the segregation of resistance are shown in Tables 2 and 3. Analysis of a two-independent-gene model or two loci interactions shows that the expected number of resistant and susceptible plants in the segregation ratio for the model of more than one dominant gene is in accordance with the 9:3:3:1 segregation ratio at the $0.90 < p < 0.95$ level of significance. The one-dominant-gene model (3:1) is also considered. However, the Chi-square data obtained is 48.13, with a p value of less than 0.0005 ($p < 0.0005$) (Table 2). The Chi-square data on the segregation analysis suggest that the resistant phenotype of the GS19769 cultivar against blast disease is controlled by more than one gene.

Table 2. Segregation of F₂ population obtained from the cross between KDML105 and GS19769 rice cultivars and inoculated with 19 isolates of *M. oryzae*

Total no. of seedlings	Resistant (R)	Susceptible (S)	Expected ratio	χ^2	<i>p</i> value
250	235	15	3:1	48.133	0.000

Note: $X^2(0.05, 1) = 3.84$, $df=1.0$

Table 3. Chi-square tests of two independent genes (9:3:3:1) and epistatic effect (15:1) for blast resistance in F₂ population derived from the cross between KDML105 and GS19769 rice cultivars inoculated with 19 isolates of *M. oryzae*

Gene model	Total no. of F ₂ seedlings	Observed ratio				Expected ratio	χ^2	<i>p</i> value
		R	MR	MS	S			
Independent genes ^a	250	134	59	42	15	9:3:3:1	3.980	0.264
Epistatic effect ^b	250	235	-	-	15	15:1	0.027	0.870

^a $\chi^2 0.5, 3 = 2.38$, $df=3$; $\chi^2 0.25, 3 = 4.11$, $df=3$

^b $\chi^2 0.75, 1 = 0.10$, $df=1$; $\chi^2 0.90, 1 = 0.02$, $df=1$

R = resistant; MR = moderately resistant; MS = moderately susceptible; S = susceptible

Molecular Marker Analysis

Two hundred and seventy SSR markers were screened for polymorphism between the parents KDML105 and GS19769. The 66 markers which showed polymorphism between the parents and were widely distributed along 12 rice chromosomes were then used in the BSA. Markers with polymorphic bands that showed distinct alleles between resistant and susceptible plants, either A:B:B:A or A:B:H:A for KDML105: GS19769: B1: B2, were selected (Table 4). In this experiment, SSR markers that scored H (heterozygous) for the resistant phenotype were also considered as this indicated that the resistant phenotype in this BSA might be controlled by a dominant allele. Out of the 66 SSR markers, 4 markers that fit the genotype patterns were selected and used in the analysis of the individual F₂ population. These markers were: RM125 (Chr.7), RM201 (Chr.9), RM144 (Chr.11) and RM247 (Chr.12). Their genotype patterns (KDML105: GS19769: B1-1: B2-1: B1-2: B2-2, where B1-1 and B2-1 were progenies from F₁ plant number 1, and B1-2 and B2-2 were from F₁ plant number 2) were ABAABA, ABAAHA, ABHAHA and ABAAHA respectively (Figure 1). The segregation analysis of F₂ plants revealed that the resistant allele(s) associated with markers RM125 and RM144 had the Chi-square results of 1.20 (1:2:1 at $p = 0.549$, where $df = 2$) and 6.02 ($p = 0.049$, where $df = 2$) respectively (Table 5). These Chi-square data confirmed that the analysis of the F₂ population according to marker RM125 and RM144 fitted Mendel's segregation theory of 1:2:1. Moreover, the data indicated that the population segregation was normal. The results suggest that the resistant allele(s) might link either to RM125 on chromosome 7 or to RM144 on chromosome 11. Interestingly, marker RM144 is the only one that provides a distinguishable genotype between resistance and susceptibility in the BSA. However, the segregation analysis of RM125 in individual F₂ plants results in over 50 per cent recombination (Table 6), suggesting that the position of RM125 is not linked to the resistant allele.

In order to define the location of the blast resistant allele, additional markers from chromosomes 7, 9, 11 and 12 were selected to define which chromosome harbours the resistant allele (Table 4). Among these, RM224 and RM287, located 3.1 and 54.6 cM respectively above RM144 on chromosome 11, were found in the same F₂ population. RM224 has a Chi-square of 3.91 with $p = 0.14$, while the value for RM287 is 1.60 with $p = 0.44$, which fits the 1:2:1 segregation and represent the normal segregation of this population. Thus, the results confirm the location of the resistant allele on chromosome 11 and link its location to those 3 markers.

Table 4. List of SSR markers used in BSA

Marker	Forward primer (5'-3')	Reverse primer (5'-3')	Chromosome no.	Product size (bp)
RM125	ATCAGCAGCCATGGCAGCGACC	AGGGGATCATGTGCCGAAGGCC	7	127
RM11	TCTCCTCTTCCCCGATC	ATAGCGGGCGAGGCTTAG	7	140
RM1132	ATCACCTGAGAAACATCCGG	CTCCTCCCACGTCAAGGTC	7	93
RM5122	CTCGCAATTTATACGTAATC	CTCACGAAATAAAAATGAGTG	9	161
RM201	CTCGTTTATTACCTACAGTACC	CTACCTCCTTTCTAGACCGATA	9	158
RM205	CTGGTTCTGTATGGGAGCAG	CTGGCCCTTCACGTTTCAGTG	9	122
RM287	TTCCCTGTAAAGAGAGAAAATC	GTGTATTTGGTGAAAGCAAC	11	118
RM224	ATCGATCGATCTTCACGAGG	TGCTATAAAAGGCATTCGGG	11	157
RM144	TGCCCTGGCGCAAATTTGATCC	GCTAGAGGAGATCAGATGGTAGTGCATG	11	237
RM247	TAGTGCCGATCGATGTAACG	CATATGGTTTTGACAAAGCG	12	131
RM1261	GTCCATGCCCAAGACACAAC	GTTACATCATGGGTGACCCC	12	168
RM235	AGAAGCTAGGGCTAACGAAC	TCACCTGGTCAGCCTCTTTC	12	124

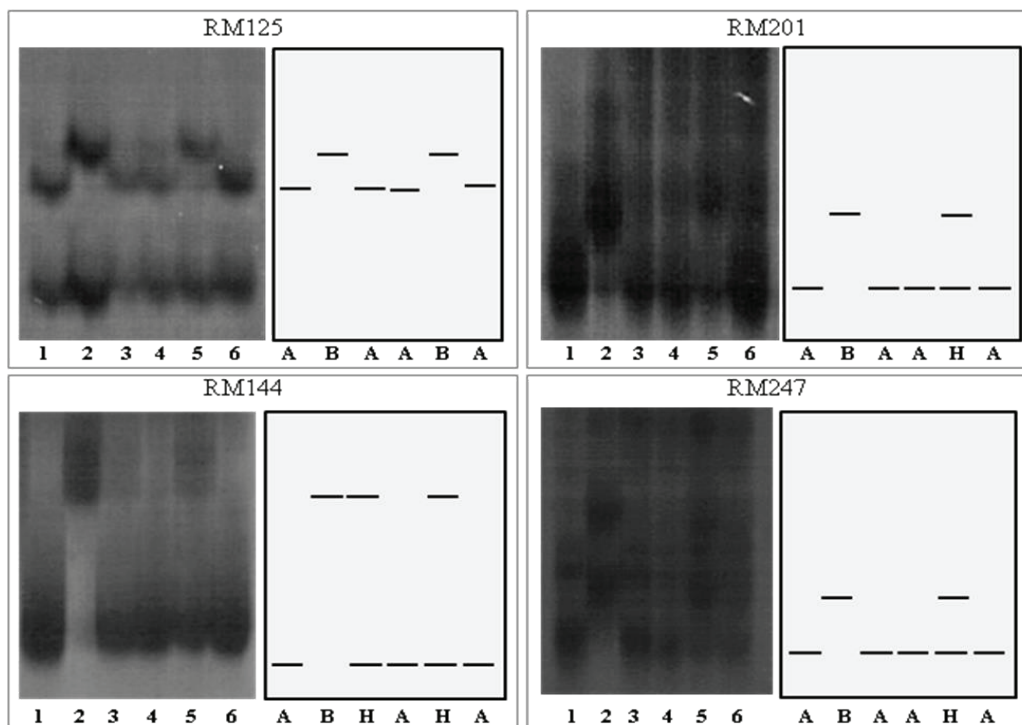


Figure 1. Results BSA by using susceptible parent KDML105 (1) and resistant parent GS19769 (2) and their respective bulks: resistant bulks B1-1 (3) and B1-2 (5); susceptible bulks B2-1 (4) and B2-2 (6), with SSR markers RM125, RM201, RM144 and RM 247

Table 5. Markers analysed in F₂ population derived from the cross between KDML105 and GS19769 cultivars

Marker	Marker segregation analysis (no. of lines observed)			χ^2 (1:2:1)	p value
	A	AB=SG	B		
RM144	46	133	71	6.024	0.049
RM224	49	135	66	3.912	0.141
RM287	54	129	67	1.608	0.448
RM125	55	130	65	1.200	0.549

Note: df=2, χ^2 0.025=7.38, χ^2 0.05= 5.99, χ^2 0.1=4.61, χ^2 0.25=2.77, χ^2 0.5=1.39

A = resistant; B = susceptible; AB or SG = segregant, according to model with single dominant gene

Table 6. Resistant genotype and phenotype of markers showing frequency of recombination occurring in F₂ plants that appear to be phenotypes susceptible to *M. oryzae* infection

Chr.	Marker	Genotype																% Recombination		
		Parents		F2 population																
		P1	P2	1	2	3	4	5	6	7	8	9	10	11	12	13	14		15	
7	RM125	A	B	H	H	A	H	A	H	A	H	H	A	A	H	H	A	H	60	
7	RM11	A	B	H	B	A	B	A	H	B	H	H	A	H	H	H	A	H	73.33	
7	RM1132	A	B	H	B	A	H	A	B	H	H	H	H	H	H	H	A	B	80	
9	RM5122	A	B	H	H	A	H	H	H	A	B	A	H	H	H	H	A	H	73.33	
9	RM201	A	B	H	A	A	H	B	H	A	B	H	H	B	A	H	A	H	66.66	
9	RM205	A	B	H	A	A	H	B	B	H	B	H	A	B	A	H	A	A	60	
11	RM287	A	B	A	A	B	B	A	H	H	B	B	A	B	A	H	H	A	60	
11	RM224	A	B	A	B	A	A	A	A	H	H	A	A	A	A	A	A	A	20	
11	RM144	A	B	A	B	A	A	A	A	H	H	A	A	A	A	A	A	A	20	
12	RM247	A	B	A	H	A	H	H	H	H	B	H	B	H	A	B	H	A	73.33	
12	RM1261	A	B	A	A	A	A	A	A	H	B	H	H	A	H	B	H	H	53.33	
12	RM235	A	B	A	B	A	A	B	B	B	B	B	B	A	B	B	B	A	66.66	
		Phenotype																		
		5	0	5	5	5	5	5	5	5	5	5	5	5	6	5	5	5	6	

Note: A = susceptible parent allele, B = resistant parent allele, H = alleles from both parents

Mapping of Resistant Allele

The localisation of the gene of interest is useful for further operations such as map-based cloning, identification of a resistance gene and breeding of a disease-resistant variety. The determination of the frequency of recombination on rice chromosomes would provide an estimated position of the resistant allele. Chromosome 11 was speculated for gene location and was analysed by SSR and additional markers. Fifteen F₂ plants that showed a susceptible phenotype (score 5 and 6) to blast fungi were analysed. As they were phenotypically confirmed, using 15 susceptible plants was sufficient and enabled the percentage of recombination on the chromosome of those plants to be analysed. As shown in Table 6, markers RM224 and RM144 have a similar recombination of 20%. This can be explained by a map of SSR markers [18] as shown on Figure 2, which shows a close proximity of both markers, with a distance of 3.1 cM. RM287 shows 60% recombination, thus indicating that the marker is not linked to the resistant allele. In addition, SSR markers on other

chromosomes such as 7, 9 and 12 were also analysed to clarify the gene location. The results show that the recombination percentage of each detected marker is higher than 50% (Table 5).

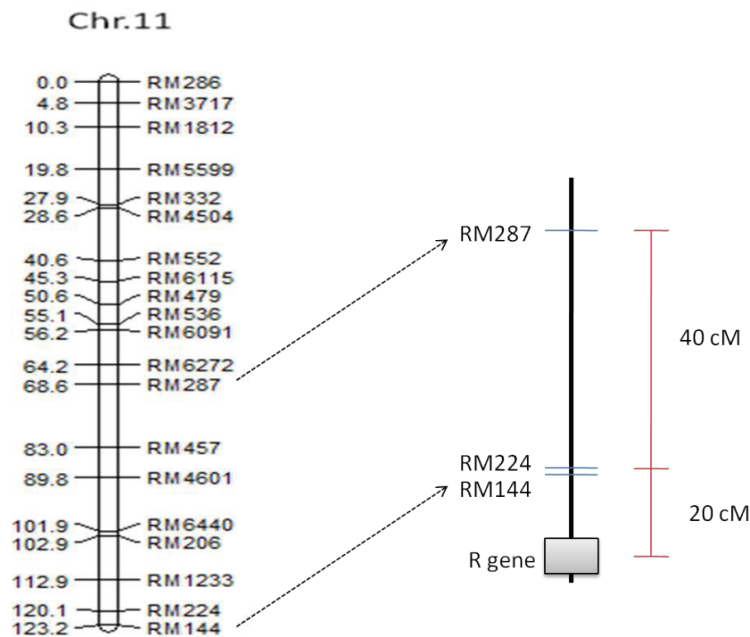


Figure 2. SSR map of resistance gene on rice chromosome 11. The linkage map was obtained from analysis using a KDML105 x GS19769 F₂ population. Location and distance in cM of known SSR markers are shown according to the comparative map available online [18]. The resistance gene is located close to RM224 and RM144.

A number of resistance genes have been identified by SSR markers on chromosome 11, including *Pi34^b*, *Pi38*, *PiCO39*, *Pik-h*, *Pik-s* and *Pi-l* [5, 23-24]. Among these, the *Pik-h*, *Pik-s* and *Pi-l* genes were reported to link with RM224 at the distance of 0.0 cM. A previous study mapped *Pi-l* gene at a distance of 6.8 cM away from RM144 [23]. However, the resistance gene identified in this study is mapped downstream of RM224 and RM144 with a distance of 20 cM. Therefore, it is possible that it is a new blast-resistance gene candidate.

CONCLUSIONS

Analysis of leaf blast resistance genes reveals a dominant inheritance pattern controlling the resistant phenotype in the landrace rice cultivar GS19769. The identified resistance gene is found to be a broad-spectrum blast resistance gene as it is resistant to a mixture of 19 blast isolates. From the segregation analysis, the GS19769 cultivar contains more than 1 resistance gene loci. From bulk segregant analysis, the gene is found to be on chromosome 11 and is tightly linked to the SSR markers RM144, being mapped downstream of the markers at a distance of 20 cM. Locating of the resistance gene and the linked SSR markers should help to narrow down the position of the resistance gene in this landrace cultivar.

ACKNOWLEDGEMENTS

The authors thank Fisseha Worede Kirkos, Chatchawan Jantasuriyarat and Antony Buchala for their critical reading of the manuscript. We are grateful to the National Science and Technology Development Agency for the blast isolates used in this study. This research was supported by King

Mongkut's Institute of Technology Ladkrabang Research Fund and the Centre of Excellence on Agricultural Biotechnology, Science and Technology Postgraduate Education and Research Development Office, Office of Higher Education Commission, Ministry of Education (AG-BIO/PERDO-CHE).

REFERENCES

1. S. H. Ou, "Rice Disease I", 2nd Edn., Commonwealth Mycological Institute, Kew, **1985**, pp.109-201.
2. P. Mekwatanakarn, P. Cobelli, A. N. L. Noenplab, T. Rithmontree, K. Ketsuwan, C. Klinmanee and S. T. Deerith, "Determination of pathotype diversity of rice blast fungal population in Thailand", *Thai Rice Res. J.*, **2007**, *1*, 52-64.
3. S. Disthaporn, "Current rice blast epidemics and their management in Thailand", in "Rice Blast Disease" (Ed. R. S. Zeigler, S. A., Leong and P. S. Teng), CAB International, Wallingford, **1994**, pp.333-342.
4. H. H. Flor, "Current status of the gene-for-gene concept", *Ann. Rev. Phytopathol.*, **1971**, *9*, 275-296.
5. G. Liu, G. Lu, L. Zeng and G. L. Wang, "Two broad-spectrum blast resistance genes, *Pi9(t)* and *Pi2(t)*, are physically linked on rice chromosome 6", *Mol. Genet. Genom.*, **2002**, *267*, 472-480.
6. Q. Z. Yang, F. Lin, S. J. Feng, L. Wang and Q. H. Pan, "Recent progress on molecular mapping and cloning of blast resistance genes in rice (*Oryza sativa* L.)", *Sci. Agric. Sin.*, **2009**, *42*, 1601-1615.
7. D. H. Chen, M. dela Vina, T. Inukai, D. J. Mackill, P. C. Ronald and R. J. Nelson, "Molecular mapping of the blast resistance gene, *Pi44(t)*, in a line derived from a durably resistant rice cultivar", *Theor. Appl. Genet.*, **1999**, *98*, 1046-1053.
8. Y. Shen, H. Adreit, X. D. Zhu, J. Milazzo, H. Q. Chen and D. Tharreau, "Resistance evaluation of some hybrid rice, conventional early *indica* and late *japonica* rice to *Magnaporthe grisea* in China", *Sci. Agric. Sin.*, **2004**, *37*, 362-369.
9. N. Jiang, Z. Li, J. Wu, Y. Wang, L. Wu, S. Wang, D. Wang, T. Wen, Y. Liang, P. Sun, J. Liu, L. Dai, Z. Wang, C. Wang, M. Luo, X. Liu and G. L. Wang, "Molecular mapping of the *Pi2/9* allelic gene *Pi2-2* conferring broad-spectrum resistance to *Magnaporthe oryzae* in the rice cultivar Jefferson", *Rice*, **2012**, *5*, 29.
10. X. Zhu, S. Chen, J. Yang, S. Zhou, L. Zeng, J. Han, J. Su, L. Wang and Q. Pan, "The identification of *Pi50(t)*, a new member of the rice blast resistance *Pi2/Pi9* multigene family", *Theor. Appl. Genet.*, **2012**, *124*, 1295-1304.
11. J. Imam, S. Alam, M. Variar and P. Shukla, "Identification of rice blast resistance gene *Pi9* from Indian rice land races with STS marker and its verification by virulence analysis", *Proc. Natl. Acad. Sci. India B: Biol. Sci.*, **2013**, *83*, 499-504.
12. S. D. Tanksley and S. R. McCouch, "Seed banks and molecular maps: Unlocking genetic potential from the wild", *Science*, **1997**, *277*, 1063-1066.
13. A. Salih, T. Sreewongchai, P. Sripichitt and N. Parinthawong, "Identification of blast-resistant varieties from landrace, improved and wild species of rice", *Kasetsart J. Nat. Sci.*, **2013**, *47*, 1-7.

14. P. Sirithunya, S. Tragoonrung, A. Vanavichit, N. Pa-In, C. Vongsaprom and T. Toojinda, "Quantitative trait loci associated with leaf and neck blast resistance in recombinant inbred line population of rice (*Oryza sativa*)", *DNA Res.*, **2002**, *9*, 79-88.
15. T. Sreewongchai, S. Sriprakhon, C. Wongsaprom, A. Vanavichit, T. Toojinda, D. Tharreau and P. Sirithunya, "Genetic mapping of *Magnaporthe grisea* avirulence gene corresponding to leaf and panicle blast resistant QTLs in Jao Hom Nin rice cultivar", *J. Phytopathol.*, **2009**, *157*, 338-343.
16. E. Roumen, M. Levy and J. L. Nottegham, "Characterisation of the European pathogen population of *Magnaporthe grisea* by DNA fingerprinting and pathotype analysis", *Eur. J. Plant Pathol.*, **1997**, *103*, 363-371.
17. J. J. Doyle and J. L. Doyle, "A rapid total DNA preparation procedure for fresh plant tissue", *Focus*, **1990**, *12*, 13-15.
18. M. K. Monaco, J. Stein, S. Naithani, S. Wei, P. Dharmawardhana, S. Kumari, V. Amarasinghe, K. Youens-Clark, J. Thomason, J. Preece, S. Pasternak, A. Olson, Y. Jiao, Z. Lu, D. Bolser, A. Kerhornou, D. Staines, B. Walts, G. Wu, P. D'Eustachio, R. Haw, D. Croft, P. J. Kersey, L. Stein, P. Jaiswal and D. Ware, "Gramene 2013: Comparative plant genomics resources", *Nucleic Acids Res.*, **2014**, *42* (Database issue), D1193-D1199.
19. H. Benbouza, J.-M. Jacquemin, J.-P. Baudoin and G. Mergeai, "Optimization of a reliable, fast, cheap and sensitive silver staining method to detect SSR markers in polyacrylamide gels", *Biotechnol. Agron. Soc. Environ.*, **2006**, *10*, 77-81.
20. "CropStat for Windows 7.2", International Rice Research Institute, Dapo, Metro Manila, Philippines, **2007**.
21. E. S. Lander, P. Green, J. Abrahamson, A. Barlow, M. J. Daly, S. E. Lincoln and L. A. Newburg, "Mapmaker: An interactive computer package for constructing primary genetic linkage maps of experimental and natural populations", *Genomics*, **1987**, *1*, 174-181.
22. P. Tansian, T. Sreewongchai and N. Parinthawong, "Genetic diversity analysis of rice blast pathogen in Thailand using *Magnaporthe grisea* microsatellite (MGM) markers", Proceedings of 52nd Kasetsart University Annual Conference on "Agriculture Sciences: Leading Thailand to World Class Standards", **2014**, Bangkok, Thailand, pp.400-406.
23. S. P. Liu and Y. H. Xue, "Locating rice blast resistance gene by DNA microsatellite markers", *J. Chi. Three Gorges Univ. (Nat. Sci.)*, **2003**, *25*, 574-576.
24. M. S. Prasad, B. A. Kanthi, S. M. Balachandran, M. Seshumadhav, K. M. Mohan and B. C. Viraktamath, "Molecular mapping of rice blast resistance gene *Pi-1(t)* in the elite *indica* variety Samba mahsuri", *World J. Microbiol. Biotechnol.*, **2009**, *25*, 1765-1769.